UNITED STATES DEPARTMENT OF COMMERCE
HARRY L. HOPKINS, Secretary
NATIONAL BUREAU OF STANDARDS
Lyman J. Briggs, Director

✦

Journal of Research

of the

National Bureau of Standards

✦

Volume 23, Number 1
July 1939

[Published with approval of the Director of the Budget]

UNITED STATES
GOVERNMENT PRINTING OFFICE
WASHINGTON : 1939

For sale by the Superintendent of Documents, Washington, D. C. - - - - - Price 30 cents
$3.50 per year on subscription

The prices of the separate Research Papers appearing in this JOURNAL are given on the front cover page. If 100 or more copies of any separate are ordered, a discount of 25 percent is allowed. Those who desire copies of separate Research Papers should send their orders and remittances without delay to the Superintendent of Documents, U. S. Government Printing Office, Washington, D. C. This will aid him to determine the number of copies to be printed for sale. Research Papers are not printed from electrotypes, and usually no more reprints can be had when the first and only printing is exhausted.

U. S. DEPARTMENT OF COMMERCE NATIONAL BUREAU OF STANDARDS

RESEARCH PAPER RP1218

Part of Journal of Research of the National Bureau of Standards, Volume 23, July 1939

X-RAY DIFFRACTION PATTERNS OF HEVEA, MANIHOT, AND OTHER RUBBERS

By George L. Clark,[1] Siegfried T. Gross,[2] and W. Harold Smith

ABSTRACT

When rubber from *Hevea brasiliensis* is stretched quickly and exposed to a beam of X-rays, a crystal fiber diffraction pattern is obtained. During previous work, done jointly by the National Bureau of Standards and the University of Illinois on sol and gel fractions of this rubber, no pattern was produced by the stretched sol fraction. With the stretched gel fraction, however, the pattern was sharp and intense. Rubber from *Manihot glaziovii* also may be separated into sol and gel fractions, and in recent work they, too, have been stretched and examined by X-rays. With the stretched Manihot sol, a few interferences were obtained, but many more resulted with the stretched gel. When crystallized by "freezing" at low temperatures for 24 hours, the interferences from the gel again outnumbered those from the sol. The X-ray measurements of Manihot rubber agree with those of Hevea rubber and indicate that the same structure exists in each. Rubbers obtained from latices of *Funtumia elastica*, *Cryptostegia grandiflora*, and *Castilla elastica* were also examined. Their structures, too, were like that of Hevea rubber, and the similarity confirms earlier observations made when X-ray technique was less highly developed. In crystallized specimens, the crystals melted within the range of temperatures previously observed with Hevea rubber.

In earlier work a large spacing was observed in a specimen of unstretched Hevea gel rubber. This spacing has been observed also in a new specimen of stretched Hevea gel rubber, together with a second spacing approximately twice as large.

CONTENTS

	Page
I. Introduction	1
II. Purification of the rubbers	2
III. Melting temperatures of frozen specimens	3
IV. X-ray patterns	3

I. INTRODUCTION

The preparation of ether sol and gel fractions of rubber from *Hevea brasiliensis* was described in a previous publication.[3] When fractions prepared by that method are stretched, the sol fraction does not produce the X-ray diffraction pattern characteristic of a crystal fiber,[4] but such a pattern is formed by stretched total rubber. The stretched gel fraction produces a pattern at approximately 100-percent elongation, and at 200-percent elongation the pattern is quite sharp and intense. Ether sol and gel fractions have not been reported to occur in all crude rubbers. They may be obtained, however, from the rubber of *Manihot glaziovii*, a tree closely related

[1] Professor, University of Illinois.
[2] Instructor, University of Illinois.
[3] W. Harold Smith, Charles Proffer Saylor, and Henry J. Wing, BS J. Research **10**, 479 (1933) RP544.
[4] George L. Clark, Enno Wolthuis, and W. Harold Smith, J. Research NBS **19**, 479 (1937) RP1039.

to *Hevea brasiliensis*. The ether sol and gel of *Manihot* rubber, when stretched, have been examined by X-rays for comparison with the behavior of the corresponding fractions of Hevea rubber.

Some years ago it was reported by Hauser [5] that 20 rubbers from different sources were found by X-ray examination to be alike. Since that time X-ray measurements have been refined. Three rubbers, other than Hevea, were examined by modern equipment to check Hauser's observations. In our earlier work a large spacing was noted in a specimen of unstretched Hevea gel rubber, and, for comparison with it, a new specimen of this fraction has been investigated in the stretched condition.

II. PURIFICATION OF THE RUBBERS

The rubbers used in the present work were obtained as latices from the nursery of the Department of Agriculture at Coconut Grove, Fla., through the courtesy of the Office of Plant Exploration and Introduction. They represented *Hevea brasiliensis*, *Manihot glaziovii*, *Funtumia elastica*, *Cryptostegia grandiflora*, and *Castilla elastica*. Their purification was undertaken by a method which had been developed with Hevea latex. As originally described, it was used successfully with Castilla latex, and the resulting rubber contained 0.04 percent of nitrogen. With the other latices some modification of the original method was necessary, because natural latices have differing characteristics.

Manihot glaziovii, the rubber of which is known in commerce as Ceara or Manicoba, belongs to the same family, *Euphorbiaceae*, as *Hevea brasiliensis* and has some marked resemblances to it. For example, the trees of each species may be subjected to suitable repeated tappings without a diminishing yield of latex. The latex of *Manihot glaziovii*, however, is less stable than that of *Hevea brasiliensis*, and may coagulate during tapping.[6] The Manihot latex as received always was coagulated. The loose coagulum was washed with successive portions of distilled water to remove serum constituents, then cut into pieces about 1 mm^3 and again washed with water. As much protein as possible was removed by digestion with a solution of trypsin, but since the solution could not penetrate the coagulated rubber, some protein remained. The residual rubber was washed with a 1-percent solution of sodium hydroxide at room temperature, and then with distilled water until all alkali was removed. The extracted total rubber contained 0.09 percent of nitrogen (determined by the Kjeldahl method). Part of the nitrogen is doubtless accounted for by protein, which does not affect the diffraction pattern of stretched rubber. Finally, the rubber was extracted with acetone for 18 hours in an apparatus through which nitrogen was passed, and then extracted with ether to separate the sol form from the gel form. As an additional precaution against oxidation, some of the natural antioxidant extracted from pale crepe Hevea rubber was dissolved in the acetone and in the ether.

[5] E. A. Hauser, Naturwissenschaften **15**, 100 (1927).

[6] Although Manihot latex contains spherical particles like those of Hevea latex, most of the rubber consists of tiny rods, which, according to Zimmermann (A. Zimmerman, Der Manihot Kautschuk, G. Fischer, Jena, 1913) are less than 1 μ wide and approximately 10μ long. Freundlich and Hauser (H. Freundlich and E. A. Hauser, Kolloid- Z. **36** (Supplement), 29 (1925)) found no adsorption layer around the rods, and its absence probably accounts for the instability of the latex. They noted that the rods of rubber consist of very tough, tacky, homogeneous material.

The latex of *Funtumia elastica* contains an effective stabilizing agent which inhibits coagulation. After treatment with trypsin, the latex was dialyzed to remove as many of the impurities as possible, and coagulated with acetone. The rubber was dissolved in benzene, the impurities were allowed to settle, and from the clear solution in benzene the rubber was precipitated with acetone. When benzene, acetone, and moisture were removed, the rubber contained 0.07 percent of nitrogen.

When the latex of *Cryptostegia grandiflora* was treated with trypsin, a black solid material slowly collected on the surface. It was removed and discarded. Subsequently, the latex was dialyzed, and most of the residual colored material was removed, but the rubber slowly coagulated. The coagulum was collected, washed with hot water, dried, and as much of it as possible was dissolved in benzene. When the impurities had settled, the dissolved rubber was precipitated by acetone. It contained 0.02 percent of nitrogen. When treated with benzene or with ethyl ether, this rubber did not dissolve completely. Some undissolved gel and impurities remained.

III. MELTING TEMPERATURES OF FROZEN SPECIMENS

The melting temperatures of crystalline material in specimens of Hevea rubber, crystallized by "freezing" at suitable low temperatures, have already been reported in this journal.[7] The temperatures within which melting occurred were not the same for all the specimens, but all melted between $-5°$ and $+16°$ C. This range was similar to that previously observed with discrete crystals prepared from ethereal solutions. For comparison with these observations, the melting ranges were determined of frozen specimens prepared from the other latices used in this work. As was observed with Hevea rubber, the temperatures of melting with different specimens of the same rubber were not alike, but specimens of all the rubbers melted within the range $-5°$ to $+16°$ C.

IV. X-RAY PATTERNS

Except when otherwise indicated, the technique used for X-ray measurement is the same as that which was described in a previous publication.[8]

The specimens of Manihot sol and gel with which patterns were obtained were stretched quickly, almost to the breaking point. In figure 1 (*A*) that of the sol is reproduced and in figure 1 (*B*) that of the gel. Each pattern was made with filtered $K\alpha$ radiation from copper. The pattern of the sol definitely shows less perfect fibering. A monochromatic fiber pattern of stretched Manihot gel is shown in figure 1 (*C*). The monochromatic beam was obtained by diffracting the X radiation from copper from the ground surface of a crystal of pentaerythritol, according to the technique described by I. Fankuchen.[9]

A list of the more important measurements obtained with stretched Manihot gel is given in table 1. The deviations of spacing from the corresponding measurements with Hevea gel rubber are doubtless caused by an uncertainty in estimating the center of the stretched sample. The distance from specimen to film was about 6.9 cm.

[7] W. Harold Smith and Charles Proffer Saylor, J. Research NBS **21**, 257 (1938) RP1129.
[8] J. Research NBS **19**, 479 (1937) RP1039.
[9] I. Fankuchen, Nature **139**, 193-94 (1937).

TABLE 1.—*Measurements from stretched Manihot gel rubber*

[In the tables, d is the distance between the set of planes making an angle θ with the incident beam, R is the radius of the diffraction spot or ring as measured on a flat film, and the letter i indicates an intense interference]

Designation of lines	*Radius, R*	*d*
	cm	*A*
Equatorial layer line:		
A1	1.69*i*	6.28
A2	2.62*i*	4.26
A3	3.70	3.16
First layer line:		
B1	2.20*i*	5.02
B2	2.99*i*	3.79
B3	3.31	3.49
Second layer line:		
C0	2.72	4.12
C1	3.32*i*	3.46
C2	3.86	3.05

Specimens of unstretched Manihot sol and gel were kept simultaneously at −20° C for 24 hours. Two interferences were observed with the sol fraction, corresponding to spacings of 6.18 A and 4.25 A.

The pattern shown in figure 1 (*D*) is that of the frozen Manihot gel. It was made in a low-temperature camera very similar to that used by Wolthuis,[10] but with less distance, approximately 3 cm, between specimen and film. The exact distance was determined by calibration with sodium chloride. Unfiltered $K\alpha$ radiation from copper was used. Measurements of the pattern are given in table 2 with the computed interplanar distances, which are compared with those previously found for frozen Hevea gel rubber.[11]

TABLE 2.—*Measurements from frozen Manihot gel rubber and those previously obtained from frozen Hevea gel rubber*

Manihot gel			Hevea gel
Lines	Radius	*d*	*d*
	cm	*A*	*A*
1	0.67	6.30	6.20
2	.86	5.02	4.99
3	1.04	4.21	4.20
4	1.18	3.76	3.74
5	1.25	3.58	3.48
6	1.31	3.44	----
7	1.37	3.31	----
8	1.42	3.21	----
9	1.53	3.02	3.02
10	1.61	2.89	2.82
11	2.58	2.07	2.07
12	2.69	2.02	----

Hauser [12] examined with X-rays rubbers from 20 different sources. The rubbers represented different botanical classifications and came from different geographical origins. The lattice spacings and intensitives were the same in all. Since that work was done the methods of producing X-ray diffraction patterns have been much improved and, at present, measurements of rubber by different investigators agree within a few hundredths of an angstrom unit.

[10] J. Research NBS **19**, 479 (1937) RP1039.
[11] See footnote 10.
[12] E. A. Hauser, Naturwissenschaften **15**, 100 (1927).

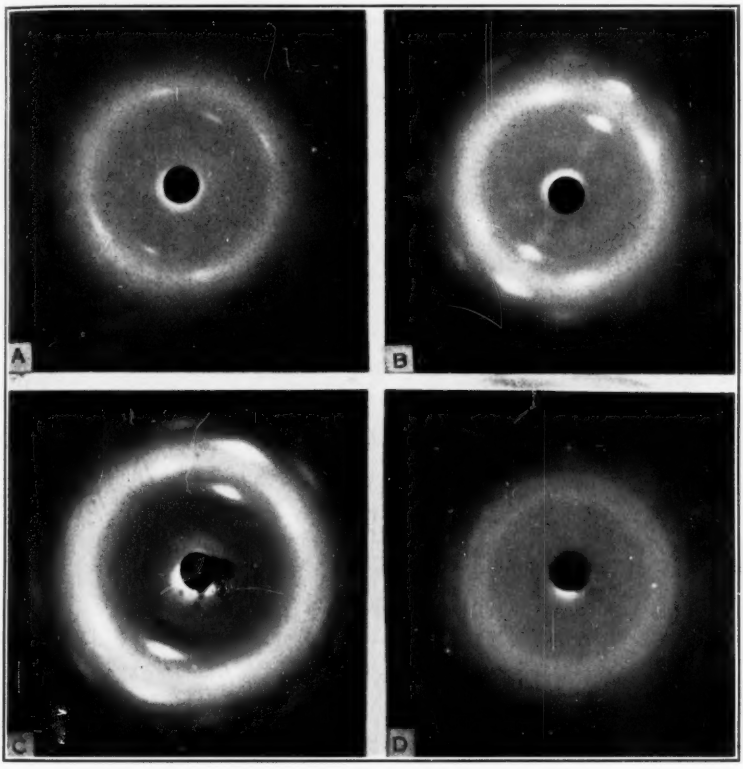

FIGURE 1.—*X-ray diffraction patterns.*

A and *B* were obtained with stretched Manihot sol and gel rubbers, respectively, made with filtered $K\alpha$ radiation from copper; *C* is a monochromatic fiber pattern of stretched Manihot gel; and *D* is a pattern of frozen Manihot gel.

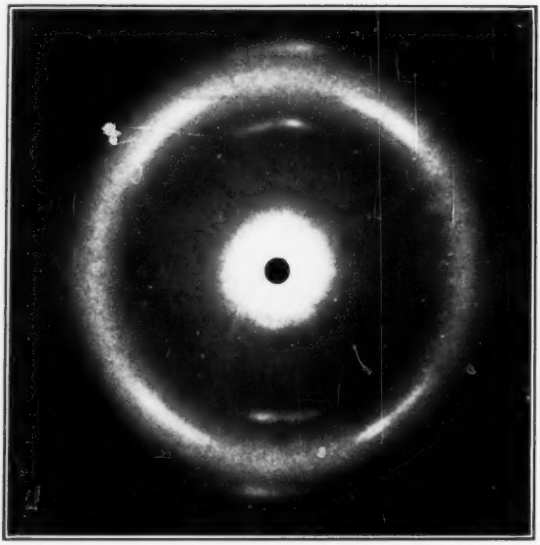

FIGURE 2.—*X-ray diffraction fiber pattern of stretched Hevea gel rubber, showing two large interplanar spacings.*

X-ray measurements were also made on frozen specimens of *Funtumia elastica*, *Cryptostegia grandiflora*, and *Castilla elastica*. The values of interferences obtained with each rubber agreed and were the same as those reported by Lotmar and Meyer,[13] by Clark, Wolthuis, and Smith,[14] and by Barnes,[15] within 0.05 A. These results confirm the earlier observations of Hauser.

In a previous publication [16] there was an illustration of a long spacing of 54 A, which was observed in a specimen of unstretched ether gel of Hevea rubber. The spacing was absent from the corresponding sol. The gel from which the specimen was taken was stored in contact with ether and in darkness at temperatures between 2° and 6° C to suppress oxidation. It was hoped that during storage, any residual soluble material would be dissolved, leaving undissolved the molecules of greatest weight. Under the conditions of storage, however, less than 2 percent of the gel became soluble. After 18 months a specimen was freed of ether and it was examined by X-rays. The diffraction pattern of the stretched material, using filtered $K\alpha$ radiation from copper, is reproduced in figure 2. The same long spacing appears at the position observed before, 54 A. The long-spacing arcs on the equator of the pattern are clearly visible. In addition there is faint but definite evidence of a second still longer spacing which corresponds to about 108 A. On the film this ring appears as a darkened area around the central spot.

The material used in this work was obtained from the Department of Agriculture through L. G. Polhamus, Bureau of Plant Industry, Washington, D. C., and H. F. Loomis, U. S. Plant Introduction Garden, Coconut Grove, Fla. Their cooperation is appreciated.

WASHINGTON, March 14, 1939.

[13] W. Lotmar and K. H. Meyer, Monatsh. **69**, 115 (1936).
[14] J. Research NBS **19**, 479 (1937) RP1039.
[15] William H. Barnes, Can. J. Research **15**, 156 (1937).
[16] See footnote 14.

U. S. DEPARTMENT OF COMMERCE NATIONAL BUREAU OF STANDARDS

RESEARCH PAPER RP1219

Part of Journal of Research of the National Bureau of Standards, Volume 23, July 1939

PROPERTIES OF AIR-SETTING REFRACTORY-BONDING MORTARS OF THE WET TYPE

By Raymond A. Heindl and William L. Pendergast

ABSTRACT

Twenty brands of refractory mortars were studied with regard to their tendency to segregate and harden, their water content, fineness, alkali content, pyrometric cone equivalent, suitability for troweling and dipping, drying properties, and strength after heating at various temperatures and cooling. The setting time, strength, types of failure of assemblages of two half-brick and mortar, and tendency of the mortar to shrink, crack, and flow when exposed to high temperatures, both in fusion blocks and in units of three brick each, were also studied.

The results of the tests show a wide range in the properties of refractory mortars of the air-setting type. In general, neat mortars having a high air-setting strength will show good strength after heating and cooling. Although not all mortars reached their lowest strength after heating at 750°C and cooling, that strength was, in general, close to the lowest obtained, after heating over a fairly wide range of temperatures. The materials were all finely ground, very little being retained on a No. 40 sieve. A preliminary calcining of the mortars did not affect the pyrometric cone equivalent but greatly facilitated obtaining the end points. Some of the mortars could be troweled satisfactorily under all of four different conditions of a mechanical-troweling test; others were satisfactory in only some of these tests. If curling occurred with drying of the mortar, it was usually accompanied by cracking. The results of the fusion-block tests correlated well with observations made on the three-brick units in the heat-soaking tests.

CONTENTS

	Page
I. Introduction	8
II. Materials	9
III. Preparation of specimens and methods of testing	9
1. Mortar	9
(a) Segregation, condition, and consistency	9
(b) Water loss at 105° C	9
(c) Alkali content	9
(d) Sieve analysis	10
(e) Pyrometric cone equivalent	10
(f) Fusion block	10
(g) Troweling	10
(1) Appearance before drying	11
(2) Appearance after drying	11
(h) Transverse strength and linear shrinkage	11
(1) Heated and cooled specimens	12
(2) Specimens tested at 750° C	12
(i) Porosity and solubility	12
2. Assemblage of two half-brick and mortar	12
(a) Setting time of mortar	13
(b) Transverse strength	13
3. Pier of three brick and mortar	14

Page
IV. Results and discussion 14
1. Mortar 14
(a) Segregation, condition, and consistency 14
(b) Water loss at 105° C 17
(c) Alkali content 18
(d) Sieve analysis 18
(e) Pyrometric cone equivalent 18
(f) Troweling 18
(1) Appearance before drying 18
(2) Appearance after drying 19
(g) Transverse strength and linear shrinkage 22
(1) Heated and cooled specimens 22
(2) Specimens tested at 750° C 24
(h) Porosity and solubility 25
2. Assemblage of two half-brick and mortar 26
(a) Setting time of mortar 26
(b) Transverse strength 27
(c) Types of failure 29
(d) Resistance to weathering 29
3. Three-brick pier and fusion-block test 29
4. Strength tests of single and duplicate shipments of mortars 35
V. Summary and conclusions 36

I. INTRODUCTION

The number of new brands of air-setting refractory-bonding mortars marketed in the wet condition in recent years, as well as production statistics, indicate an increasing popularity of this product. This popularity may be attributed to the fact that these mortars usually develop a high strength at ordinary temperatures, and retain a goodly proportion of that strength throughout the lower ranges of moderately high temperatures. At still higher temperatures a strength is developed through partial vitrification of some of the constituents of the mortar. A high strength of the mortar joints is thereby assured over a wide range of temperature. This is in contrast to a mortar prepared from only ground fire clay and water. In most cases very little strength is attained by such a mortar until it has been heated to a sufficiently high temperature to cause some vitrification of the clay. The air-setting mortar, therefore, may advantageously be used in installations where the temperatures reached are moderately high, but not high enough to cause any vitrification of the clay, and also in installations where the range in temperature may vary from close to ordinary temperatures in certain parts of the installation to high temperatures (for example, approximately 1,300° C) in other parts.

Refractory mortars of widely varying properties are on the market, and it is to be expected that certain of these mortars will prove to be more suitable in one type of service than in another, whereas others may prove satisfactory in nearly all types. It is, therefore, essential to evaluate the properties of these mortars by means of laboratory tests [1] as an aid in their selection for specific services. The National Bureau of Standards has been requested to prepare a Federal specification for this commodity; therefore, a study of the properties of a group of such mortars was undertaken.

Air-setting mortars are marketed in both the wet and the dry condition; those of the wet type were studied first, and the results are reported in this paper. It is planned to report the results of a study of mortars marketed in the dry condition in a future paper.

[1] Laboratory tests for evaluating the properties of air-setting mortars have been proposed, among others, by J. F. McMahon, J. Can. Ceram. Soc. **6**, 55 (1937); and also by S. M. Phelps, Am. Refractories Inst. Tech. Bul. 60 (September 1935).

II. MATERIALS

Twenty-three [2] air-setting refractory mortars were obtained from 20 manufacturers rather widely distributed throughout the United States. In all cases the mortar was furnished in air-tight containers, and in all but six cases it was furnished in several small (5- or 10-lb.) containers.

III. PREPARATION OF SPECIMENS AND METHODS OF TESTING

1. MORTAR

(a) SEGREGATION, CONDITION, AND CONSISTENCY

Since all the mortars could not be tested simultaneously, and since the different tests were made over a fairly long period, the containers were opened at varying intervals of time after their receipt. Observations were made at the time of opening the container as to whether the solids and the liquid had segregated, and also, whether the condition of the mortar was such that it could be easily removed from the container and remixed without much difficulty. The mortar was churned or kneaded mechanically for 15 minutes before it was used for test purposes. After removing the mortar from the sealed container, it was kept in a pan covered with a wet cloth to retard loss of moisture while the specimens were being made.

Each mortar was classified according to the ease with which it could be spread with a mason's trowel. This property, designated "consistency for troweling", was based solely on the judgment of the investigators.

A joint 1/16 in. or "thinner," obtained by dipping the brick in a slurry of mortar, is usually recommended by the manufacturers when mortars of this type are used for laying brick. Consequently, the desirability of making some observations as to the ease with which mortars, as received from the manufacturers, may be changed to a dipping consistency was important. A quantity of the mortar was placed in a pan and mixed by hand with measured amounts of water until the desired dipping consistency was obtained.

(b) WATER LOSS AT 105°C

The loss in weight, assumed to indicate the water content, was obtained on 200-g samples by drying them to constant weight at about 105°C. The loss was determined at the end of 72 hours, and again at the end of 96 hours, on the mortars as received, and also after changing them to a dipping consistency. If there was a loss in weight during the last 24-hour period, the mortar was dried for another 24-hour period.

(c) ALKALI CONTENT [3]

The alkali content of the mortars was determined on bars 1 in. wide and 1/4 in. thick which were initially dried with the top or finishing surface uppermost, at least until set had occurred. After drying the samples to constant weight at 105°C, three of them were taken for test: One (5 g) representing the entire cross section of the sample,

[2] Because of delayed receipt of 3 mortars, they were subjected to only a limited number of tests. It is specifically stated in the text when the information discussed covers all 23 mortars.
[3] Determined by E. H. Hamilton, of the Bureau staff.

one (1.5 to 3 g) the upper surface, and one (1.5 to 3 g) the lower surface. The object was to determine the content of free alkali and its approximate degree of migration. The dried sample in each case was digested with 200 ml of water on a steam bath overnight, filtered, and the residue leached a second time overnight with the same quantity of water. The filtrate from the two leachings was titrated with 0.1 *N* hydrochloric acid.

(d) SIEVE ANALYSIS

The sieve analysis was made by the wet method [4] on a sample of approximately 200 g of each mortar. United States Standard Sieves Nos. 20, 40, 60, and 100 were used. Sieving of the dried residue was accomplished with a machine.

(e) PYROMETRIC CONE EQUIVALENT

The pyrometric cone equivalents (softening points) were determined according to ASTM standard method, serial designation C 24–35.[5] Cones were made from the mortars both before and after calcining at approximately 1,200° C. In either case, after placing the cones in plaques, they were heated to about 1,200° C and cooled before testing.

(f) FUSION BLOCK

The blocks were of a refractory composition (pyrometric cone equivalent 32). The compartment for holding the test material was made approximately ½ in. deep in some blocks and ⅛ in. deep in others. The mortar was dried, then ground to pass a No. 70 United States Standard Sieve, and wetted slightly with a solution of gum tragacanth before being placed in the compartments. One set of blocks filled with mortar to a depth of ½ in. was heated at 1,425° C for 5 hours and a second set at 1,500° C for 5 hours. One series of blocks filled with mortar ⅛ in. deep was heated at 1,500° C for 5 hours. After the mortars cooled, they were examined for shrinkage, bubbles, glassiness, and flow.

(g) TROWELING

In order to eliminate the personal factor, a machine was built to simulate the motion of the mason's trowel while spreading the mortar on a brick. The machine is shown in figure 1. The brick was fixed in position in the machine, and the mechanical trowel moved backward and forward lengthwise over the brick. The trowel was actuated by two pistons driven by water pressure. A constant speed of travel of the trowel throughout the stroke was assured by a constant head of water acting on the pistons, which were directly connected to the trowel. The machine automatically provided for the two-way motion of the trowel and the thickness of the prospective mortar joint. The minimum automatic reduction in thickness of layer of mortar with each stroke of the trowel was 0.005 in. The trowel, in the form of a trough, was made from $\frac{1}{16}$-in. sheet iron and was 6.5 in. long and 1 in. wide. The sides of the trough had an angle of 120° between them. The outside corner of the trowel was nearest the 9- by 4½-in. face of the brick, and the two sides made equal angles (30°) with the face. The trowel was placed so that its axis made an

[4] The manner of conducting the test was in general similar to method C 92-36, p. 31, American Society for Testing Materials, Manual of ASTM Standards on Refractory Materials, 1937.

[5] Described in American Society for Testing Materials Manual of ASTM Standards on Refractory Materials, 1937, p. 53.

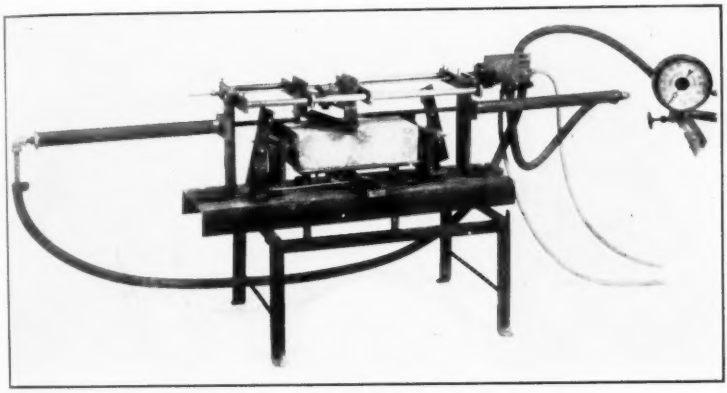

FIGURE 1.—*Machine used for simulating the motion of the mason's trowel while spreading mortar on a brick.*

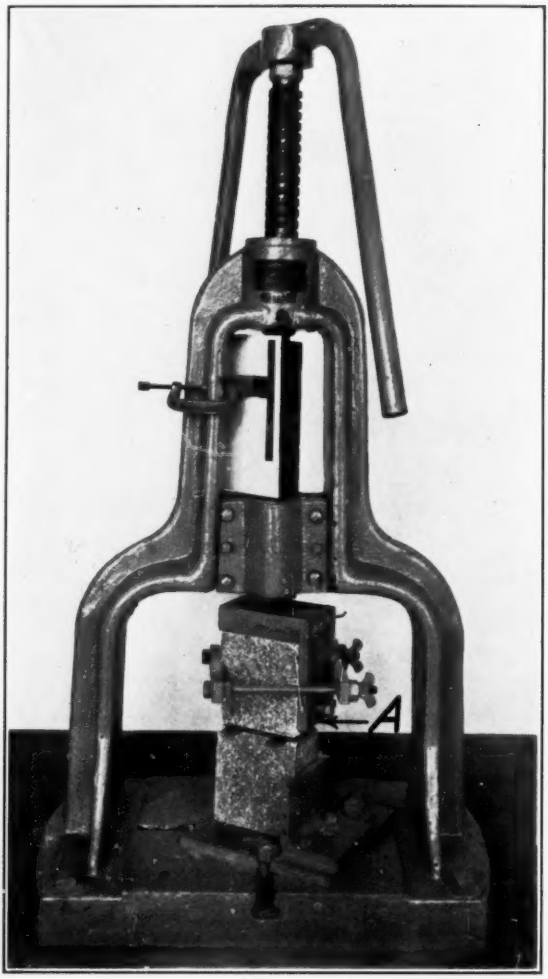

FIGURE 2.—*Screw-press with two half-brick in position, showing the manner in which a brick-and-mortar assemblage was made.*

angle of 10° with the plane of the 2½- by 4½-in. face of the brick. This angle has no special significance as far as the troweling operation is concerned. The trowel operated at a speed of 24 strokes per minute, and the water pressure was maintained at 5 ± 1 lb/in.^{2} during the troweling operation.

Four troweling tests were made of each mortar, as follows: The brick was first placed in a wooden frame, the inside dimensions of which corresponded to the outside dimensions of the brick, except that it was 2¾ in. high. The mortar was spread evenly by hand troweling on the upper 9- by 4½-in. face of the brick and also flush with the edge of the frame, thus forming a uniform ¼-in. coating over that face. The mortar-covered brick was removed from the frame and immediately placed in the machine, preparatory to making the troweling tests. From 2 to 3 minutes were required for placing the mortar on the brick and fastening the brick in the machine. The first test consisted in reducing the ¼-in. layer to a ⅛-in. layer in one stroke. The second test consisted in reducing the ¼-in. layer to a ⅛-in. layer in 25 strokes. The third test reduced a ¼-in. layer to a 1/16-in. layer in one stroke. The fourth test reduced the ¼-in. layer to a 1/16-in. layer in 37 strokes.

(1) *Appearance before drying.*—On completion of the troweling tests, observations were made in each case on the appearance of the layer of mortar, as an indication of whether it had satisfactory or unsatisfactory troweling properties.

(2) *Appearance after drying.*—The mortar-covered brick thus treated were set aside for drying at room temperature under ordinary atmospheric conditions. After drying, the mortar was examined to determine whether it had dried free of shrinkage cracks, had curled, and whether it had separated from the brick.

(h) TRANSVERSE STRENGTH AND LINEAR SHRINKAGE

The transverse strength (modulus of rupture) was determined on bars 6 by 1 by ¼ in., over a 5-in. span. The bars were made in brass molds, which rested on slips of newspaper; these in turn rested on glass plates. The newspaper was used because it adjusted itself more readily than other types of paper to the movements of the specimen during shrinkage. Because of the different consistencies of the mortars as taken from the containers it was necessary to use three different methods for preparing specimens, namely:

1. Casting the mortar into the mold, jolting the mold slightly to level the mortar, and not smoothing it with a spatula.
2. Pressing the mortar into the mold and smoothing it with a spatula on top side only.
3. Pressing the mortar into the mold and smoothing it with a spatula from both top and bottom.

After filling the mold, the specimen in the mold and the attached paper were placed on a fire-clay brick with paper side down. Within a few minutes an initial set would take place, and the mold was then removed from the specimen. A safety-razor blade was used to separate the mold from the specimen. The specimens were covered with a damp cloth until placed in a constant humidity room for the routine drying treatment. To prevent excessive warping during drying, the following drying schedule was followed for each mortar: 48 hours at approxi-

mately 60- to 65-percent humidity [6] and at 20 to 22° C; 18 hours (overnight) at ordinary laboratory temperature and humidity; and 27 hours in a drying oven at approximately 105 to 110° C. In several cases it was necessary to heat the specimens slowly up to 105° C to prevent bloating of the specimens. The paper was removed while the specimens were still in the constant-humidity room, but not until they had become sufficiently hard to permit handling without breakage. The side of the specimen originally next to the paper was identified as the "bottom" of the specimen, even though the bars were turned over a number of times to prevent warpage after the removal of the paper. Five specimens were tested with the original bottom on the bottom during the breaking of the specimen, and a second set of five with the original bottom on top during this test.

(1) *Heated and cooled specimens.*—To determine whether any changes in strength took place because of heating and cooling the mortars, the modulus of rupture of the bar specimens was determined after drying and also after heating them for 24 hours at different temperatures and cooling. Different lots of specimens of all mortars were heated for 24 hours at 500, 750, and 1,000° C, and for 1 hour at 1,310 and 1,350° C; specimens of mortars Nos. 1 to 5, inclusive, also received heat treatments for 24 hours at 250, 625, and 850° C. No lot of specimens received more than one heat treatment.

The over-all linear shrinkage of the specimens was measured before they were tested for transverse strength.

(2) *Specimens tested at 750° C.*—Specimens 10 by 1 by ¼ in. were prepared from six mortars for modulus of rupture tests at 750° C. After drying, each test specimen was heated to 750° C and maintained at approximately that temperature for one hour before it was broken in bending over an 8-in. span. After cooling, the two portions of the broken specimen were tested at room temperature for breaking strength over a 3-in. span.

(i) POROSITY AND SOLUBILITY

Specimens of mortars Nos. 1 to 5, inclusive, heated at several different temperatures and cooled, were tested for porosity. The determinations were made in accordance with the test method adopted by the American Ceramic Society.[7]

The relative water solubility of the alkali salts in the specimens tested for porosity was obtained by titrating the liquid (distilled water), in which the porosity specimens had been boiled, against a 0.1 *N* solution of hydrochloric acid.

2. ASSEMBLAGE OF TWO HALF-BRICK AND MORTAR

The standard size [8] (9-inch) brick used in the tests for the determination of strength of bond and time of set of the various mortars were of the stiff-mud type and had a moderately coarse texture and an absorption of 8.6 percent. They were cut by means of an abrasive wheel into two equal parts and parallel to the 2½- by 4½-in. faces. They were then placed overnight in a drier maintained at approximately 90° C. A laboratory screw press (fig. 2) was slightly changed

[6] These humidity and temperature ranges were conveniently available at all times in one of the rooms at the Bureau, and use was made of those facilities.

[7] J. Am. Ceram. Soc. **11**, 456 (1928).

[8] The effect of strength and total absorption of bricks on the strength of mortar joints was discussed by R. A. Heindl and W. L. Pendergast in the Bul. Am. Ceram. Soc. **15**, 182 (1936).

to accommodate a 9-in. brick on end. A jig, or aligning guide, *A*, and clamp were attached to the frame of the press to prevent lateral motion of the two halves of the brick when they were forced together with the mortar between them. The operation of bonding was as follows: After clamping the two halves of the brick in place with the molded faces in contact,[9] two spacers were placed on the lower half of the brick and the upper half was then brought in contact. These spacers were 1/16 in. thick when joints for bonding strength of mortars were being prepared, and 1/4 in. thick when joints for "time of set" tests were being prepared. With the two half-brick in contact, the reading indicated on a scale was noted, the upper section of the brick was then raised about 3/4 in., and the spacers were removed. Approximately double the amount of mortar required for the joint was placed between the two half-brick, and the upper portion was again lowered until the scale reading corresponded to that first noted. The excess material forced from the joint was then removed and the specimen released from the clamp. The entire operation consumed about 3/4 minute.

A series of specimens was also prepared for the purpose of determining the bonding strength of the mortars when used in a dipping consistency. The end surface of the half-brick was dipped in the mortar and two 1/16-in. spacers placed on it before the dipped end of the second half of the brick was brought in contact. A *C*-clamp was used to squeeze out the excess mortar by forcing the two half-brick together.

(a) SETTING TIME OF MORTAR

The bonded specimen, prepared with the 1/4-in. joint of mortar, after removal from the press was set on end on the floor. After the lapse of 3 minutes from the time the mortar first touched the brick, a 50-lb. weight [10] was gently set on the end of the brick, and it was noted whether the mortar was squeezed from the joint. If the mortar gave no indication of flowing from the joint, a second specimen was tested, the elapsed time between the application of the mortar and load being but 2 minutes. If the result was still negative, then the elaspsed time was reduced to 1 minute for a third specimen. If, on the other hand, the mortar flowed from the joint at the end of the 3-minute period, additional tests on newly prepared specimens were made after longer periods, increasing by 3-minute increments, up to 15 minutes. If the mortar still flowed, the increment was lengthened to as much as 10 minutes, depending on the fluidity of the mortar. When a sufficiently long interval was reached so that no flow was observed, then this period would be reduced by 1-minute decrements until the point was determined to the nearest minute when the mortar ceased to flow. The time elapsing between placing the mortar on the bricks and the attainment of sufficient stiffness to prevent flow when loaded is designated "time of set."

(b) TRANSVERSE STRENGTH

After bonding the two half-brick, the assemblages intended for testing the strength of the mortar joint were stored on end, care being

[9] The original surfaces of the brick were bonded to simulate service conditions.

[10] The decision to use a 50-lb. load and a 1/4-in. mortar joint was reached after experiments with 25-, 50-, and 100-lb. loads and 1/16-, 1/8-, and 1/4-in. joints. The behavior of the chosen combination, with the particular brick used in these experiments, indicated that a reasonably good spread in time-of-set values between the different mortars would be obtained.

taken not to jar them while the mortar was still damp. Those which were to be tested without heat treatment, other than a final drying at 105° C, were stored in the constant-humidity room and given the same drying treatment as that of the bar specimens already described. Those which were to be tested, after having been heated at different temperatures and cooled, were stored in the laboratory. In all cases brick-and-mortar assemblages were heated simultaneously and in the same furnace with the bar specimens from the corresponding mortar. The modulus of rupture of the mortar joint was determined over an 8-in. span.

3. PIER OF THREE BRICK AND MORTAR

A second type of brick-and-mortar assemblage was made which consisted of a pier of two standard size brick and two half-brick. Three of these piers were laid up with a $\frac{1}{16}$-in. dipped joint and three with a $\frac{1}{8}$-in. troweled joint. The two half-brick with the two original end surfaces toward one another were laid flat between the two full-sized brick. Each pier, therefore, had two horizontal joints and one vertical joint. For the dipped joint, $\frac{1}{16}$-in. drill rods were used as spacers, and for the larger joint $\frac{1}{8}$-in. spacers. The troweled joint was made entirely with mortar of a troweling consistency.

The piers were examined for defects of the mortar and mortar joint after curing and drying as previously described, again after heating at 750° C for 24 hours, again after heating at 1,425° C for 24 hours, and lastly after heating at 1,500° C for 5 hours. Two piers of each thickness of joint were heated at each temperature. Since three piers only were made, it was necessary to heat some piers at successively higher temperatures.

IV. RESULTS AND DISCUSSION

1. MORTAR

(a) SEGREGATION, CONDITION, AND CONSISTENCY

The difficulty of preventing segregation of the solid material from the liquid in a mortar is indicated by the information on supernatant liquid given in table 1, column 2. Fifteen of the twenty mortars showed an appreciable layer of liquid, one just a trace, and four no liquid on top of the solid material, when the container was opened. The containers had been in storage from 9 to 33 months.

The length of time that a mortar had been in storage would, in some cases, affect its working properties.[11] Not only was it very difficult to remove some of the mortars from the containers, but it would have been practically impossible to recombine the liquid and solids of these mortars by mixing them in a mortar box in the usual manner. However, in the laboratory the kneading machine recombined the liquids and solids within the allotted time. Table 1, column 3, gives the months of storage of various mortars before the containers were opened, and shows that 5 of the 20 mortars were rated as difficult to work [12] after being in storage from 9 to 17 months. Information obtained on 3 of the 5 mortars indicated that they were workable after shorter periods in storage. For the remaining 15 mortars, all of which were

[11] Silicate of Soda Cements (Philadelphia Quartz Co. Bul. 241, p. 4, 1936).

[12] This rating, based solely on the judgment of the investigators, classified these mortars as being commercially unsatisfactory as far as this property is concerned.

rated as workable, the maximum period of storage for any one mortar was 33 months.

As taken from the container, the consistency of each mortar for troweling purposes is given in table 1, column 4. Ten of the mortars were rated good, nine fair, and one poor. A word or two in explanation of the fair or poor classification is given for some mortars. Two ratings are given for mortars 2, 11, and 16, because of variation between containers. The addition of water would undoubtedly have improved the working consistency of some of the mortars rated other than "good," but as will be shown later, this might have been to the disadvantage of other properties. Furthermore, unless the producer specifies the quantity of water which is to be added, it cannot be expected that the properties obtained after the addition of water will correspond to those claimed by the producer for the mortar in a troweling consistency.

Information on the ease of changing the mortar from the as-received condition to a consistency suitable for dipping, and the workability of the latter mixture is given in table 1, column 7. The majority of the mortars could be brought to a satisfactory dipping consistency with less than 15 minutes of mixing. Such mortars were considered as having "mixed readily." Mortars 10, 14, 16, and 18 required approximately one-half hour of mixing, and 3 and 15 approximately 1 hour, to bring these mortars to a dipping consistency. The time required to bring them to a dipping consistency was considered excessive; therefore, it was reported in the table that they "did not mix readily."

The workability of the dipping mixture was considered "good" if the mortar remained in suspension, the excess mortar could readily be forced from between the brick, and the brick had no tendency to slip out of position after laying. It was considered "poor" if the mixture dried so quickly after dipping the brick that it was very difficult to force the excess mortar from between the brick as soon as they were laid. The rapid loss of water in some cases (mortars 3 and 15) may have been due to the presence of the large percentage of material retained on a No. 60 sieve. Mortars 10 and 16 failed to stay in suspension after mixing, but could be used if constantly agitated. Mortar 21 was different from the others in that most of it would slip from the brick as it was withdrawn from the dipping mixture.

152687—39——2

TABLE 1.—*Some properties of air-setting refractory mortars marketed in the wet condition*

Mortar number	Supernatant liquid	Condition after months [1] in storage	Consistency [2] (troweling) after mixing	Loss of water at 105° C. Based on dry weight [3]		(a) Ease of changing consistency; (b) workability of dipping mixture	Alkali as Na_2O			Sieve analysis		
				As received	For dipping		Upper surface	Lower surface	Cross section	Retained on No. 40	Passed No. 40; retained on No. 60	Passed No. 60; retained on No. 100
(1)	(2)	(3)	(4)	(5)	(6)	(7)	(8)	(9)	(10)	(11)	(12)	(13)
				%	%		%	%	%	%	%	%
1	Yes	Workable; 16.	Fair	26.5	42.5	(a) Mixed readily (b) Good	2.85	2.71	2.79	1.0	1.8	6.2
2	do	Workable; 17.	Good Too liquid	28.2 32.8	51.0	(a) Mixed readily (b) Good	2.64	2.33	2.48	1.2	1.3	27.6
3	do	Workable; 16.	Fair (short, stiff).	23.1	41.0	(a) Did not mix readily. (b) Dried too fast	1.95	1.94	1.94	.1	13.0	21.2
4	do	Workable; 12.	Good	25.5	38.7	(a) Mixed readily (b) Good	3.14	2.97	3.08	0	.5	6.6
5	No	Difficult to work; 9.	do	28.5	30.7	(a) Mixed readily (b) Good	2.08	1.55	1.75	0	.6	4.7
6	do	Workable; 20.	Fair (short)	23.7	36.2	(a) Mixed readily (b) Fair	2.26	1.78	2.02	.1	7.3	24.8
8	Yes	Difficult to work; 13.	Good	32.3	34.7	(a) Mixed readily (b) Dried too fast	1.60	.99	1.22	5.7	7.8	10.2
9	do	Workable; 16.	do	24.4	37.9	(a) Mixed readily (b) Good	3.00	2.71	2.94	.2	2.2	13.2
10	do	do	Good (sticky)	23.7	28.5	(a) Did not mix readily. (b) Did not stay in suspension.	3.54	3.25	3.40	.1	.4	2.2
11	No	Workable; 23.	Fair Good	20.6 25.3	28.5	(a) Mixed readily (b) Good	2.24	1.67	1.88	1.0	6.4	14.9
12	Yes	Workable; 33.	Fair (thin)	26.9	26.9	(a) Not changed (b) Slightly thick	2.93	2.52	2.73	0	0	0
13	do	Workable; 16.	Poor (short, stiff).	23.9	30.8	(a) Mixed readily (b) Poor	2.75	2.32	2.55	2.6	5.8	12.2
14	Trace	Difficult to work; 17.	Fair (fatty, stiff).	24.3	41.4	(a) Did not mix readily. (b) Good	2.13	1.97	2.03	.1	3.8	10.2
15	Yes	do	Fair (short, stiff).	23.4	42.5	(a) Did not mix readily. (b) Poor	1.64	1.18	1.32	.8	14.6	17.3
16	do	Difficult to work; 16.	Good Poor	29.6 22.9	40.2	(a) Did not mix readily. (b) Did not stay in suspension.	2.61	2.31	2.34	1.7	14.5	19.8
17	do	Workable; 17.	Good	20.2	30.7	(a) Mixed readily (b) Good	2.50	2.40	2.45	.3	6.0	9.4
18	do	do	do	21.6	34.6	(a) Did not mix readily. (b) Good	2.60	2.40	2.43	1.4	4.9	20.9
19	do	do	do	20.1	35.4	(a) Mixed readily (b) Good	2.47	2.25	2.37	.3	5.5	13.4
20	do	do	Fair (stiff, fatty).	21.5	34.7	(a) Mixed readily (b) Fair	2.65	2.43	2.52	.1	10.2	19.2
21	No	Workable; 20.	Fair (stiff, short).	22.7	39.6	(a) Mixed readily (b) Fair	3.25	2.87	2.99	.6	5.5	6.8

[1] Numerals represent number of months in storage. First containers of mortars 14, 15, and 16 opened after 1, 8, and 2 months, respectively, at which time they were satisfactory for working.

[2] Directions on container implied that most mortars were of a trowelling consistency ready for use. Considerable differences in water content between original and later shipments of mortars 2, 11, and 16 were noted; therefore, the two conclusions are given.

[3] Mortars 22, 23, and 24 were received late; consequently, they were not subjected to all tests. The water content for these "as received" was 20.5, 29.9, and 17.9 percent and for "dipping" 47.2, 31.6, and 36.0 percent, respectively. All three mixed readily to a dipping consistency.

TABLE 1.—*Some properties of air-setting refractory mortars marketed in the wet condition*—Continued

Pyrometric cone equivalent		Troweling. Spreading and reducing layer from—				Appearance after troweling and drying		Time of set (minutes)
Raw	Calcined	¼" to 1/16" in 1 stroke	¼" to 1/16" in 25 strokes	¼" to 1/16" in 1 stroke	¼" to 1/16" in 37 strokes	Curled	Cracked	
(14)	(15)	(16)	(17)	(18)	(19)	(20)	(21)	(22)
Cone	Cone							*min*
23	23	Fair	Good	Fair	Fair	No	Slightly	2
20	20	Very good	Very good	Very good	Very good	Moderately	do	60
32	32	Good	Good	Poor	Fair	do	Badly	1
34	34	Very good	Very good	Very good	Very good	Slightly	Slightly	60
33	33	Good	Good	Good	Good	Moderately	Badly	2
32-33	32-33	Fair	Poor	do	Poor	Slightly	Slightly	1
29	29	Good	Good	do	do	do	do	2
30	30	Very good	Very good	Very good	Very good	No	No	48
20	19	do	do	do	do	do	do	90
37	37	Good	Good	Good	do	Slightly	Slightly	1
27-28	28	Very good	Very good	Very good	Very good	No	No	24
32-33	32-33	Poor	Poor	Poor	Fair	do	do	60
28	27	Good	do	Good	Poor	Moderately	Moderately	1
30	30	do	do	do	do	Badly	do	1
26-27	26-27	do	do	do	do	Moderately	Badly	1
31	31	do	Fair	do	Good	Slightly	No	3
18	18	Very good	Good	Very good	do	do	Slightly	2
27	27	do	Very good	do	Very good	No	No	3
14	15	Fair	Poor	Poor	Poor	Slightly	Slightly	1
[1] 29	23-26	Good	do	do	Fair	Badly	Moderately	1

[1] Very difficult to obtain satisfactory end point.

(b) WATER LOSS AT 105° C

Based on the dry weight, the loss of moisture at 105° C of the 23 mortars "as received" ranged from 17.9 to 32.8 percent, and for the material in a dipping consistency the range was from 26.9 to 51.0 percent. The values are given in table 1, columns 5 and 6. The relative water content of the mortars as received was not an indication of their troweling consistency (table 1, column 4). A second shipment of mortar 2 contained 2.6 percent more water than the first, which

changed it from a good troweling consistency to a consistency that was considered too fluid, since it would not support the brick. A second shipment of mortar 11, which contained approximately 5 percent more water than the first, was rated "good" compared with a rating of "fair" for the first shipment. The second shipment of mortar 16 was rated "good." It contained about 7 percent more water than the first which was rated "poor." There was a great deal of difference in the quantity of water necessary to change the various mortars from a troweling consistency to a dipping consistency.

(c) ALKALI CONTENT

The total alkali content of the mortars, in terms of sodium oxide, ranged from 1.22 to 3.40 percent (table 1, column 10). The alkali content near the upper surface and that near the lower surface of the dried specimens are given in columns 8 and 9, respectively. The migration of the alkali salts, which it is assumed takes place during the drying of the mortar specimens, varied greatly. For example, in mortars 3 and 17 the migration was negligible, but in mortars 8, 11, and 15 the migration was pronounced. On the whole there appeared to be no relation between migration and water loss when all the mortars were considered. However, a very good direct relation is indicated for all the four mortars (5, 8, 10, and 12) whose consistency was such that the test specimens were made by casting. Since only four mortars are included in this class, the relation may result from chance, even though the range in both water content and migration was great.

(d) SIEVE ANALYSIS

The results obtained in the sieve analyses are given in table 1, columns 11, 12, and 13. The residue on a No. 20 sieve is not given, because 15 of the 20 mortars showed 0.1 percent or less retained on this sieve. Only one mortar (8) showed as much as 1 percent retained. Furthermore, 15 of the mortars showed 1 percent or less residue retained on a No. 40 sieve. The material which would not pass a No. 100 sieve ranged from 0 to 35 percent.

(e) PYROMETRIC CONE EQUIVALENT

The pyrometric cone equivalent (pce, or softening point) of the mortars given in table 1, columns 14 and 15, ranged from 14 to 37 for the uncalcined material, and from 15 to 37 for the calcined mortars. These results indicate that very little difference in pyrometric cone equivalents may be expected between calcined and uncalcined material. However, in a number of cases the end points of the uncalcined materials were much more difficult to obtain than when calcined materials were used, because of the tendency of the cones to twist and curl.

(f) TROWELING

(1) *Appearance before drying.*—The results of the troweling tests are given in table 1, columns 16 to 19, inclusive. The ratings, very good, good, fair, and poor, are used to designate the comparative ease with which the mortars spread with the mechanical trowel, and their appearance on the brick immediately after each of the four tests was completed. As examples (see fig. 3), mortar 12 was rated "very good" and mortars 13 and 21 both rated "poor." A rating of "very

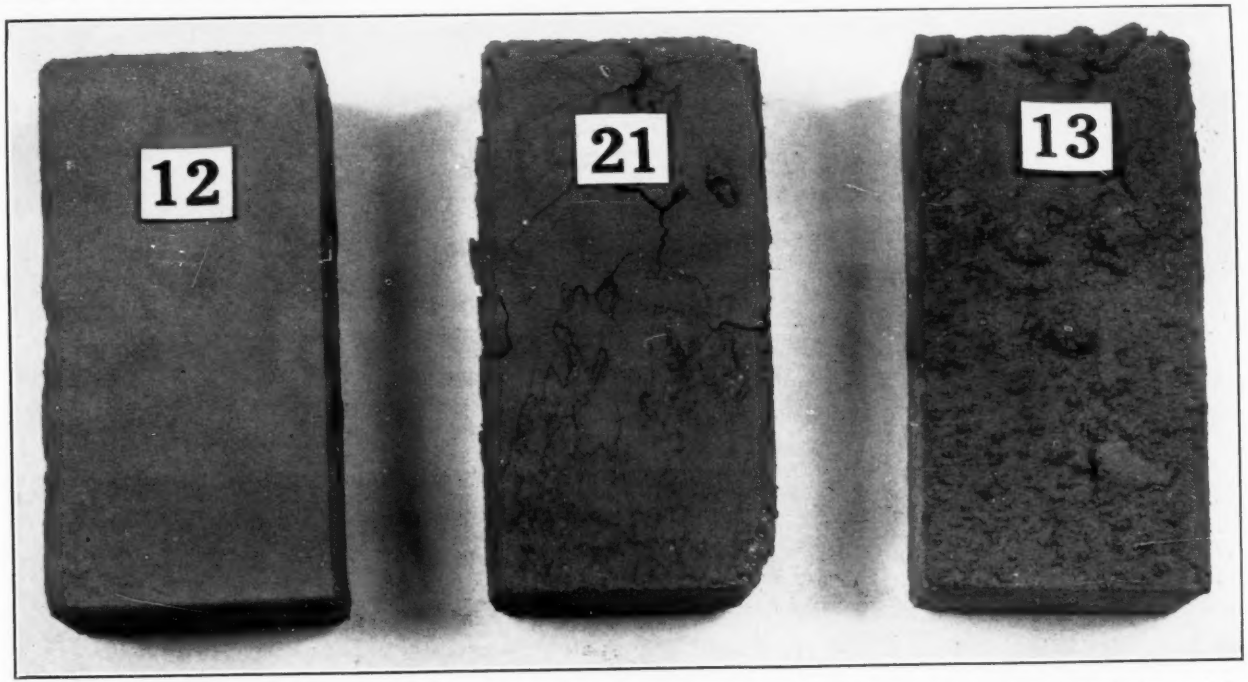

FIGURE 3.—*Appearance of three mortars after having been spread on firebrick, by means of a mechanical troweling device, and dried.*

Mortar 12 spread smoothly and easily; mortar 21 had a tendency to stick to the trowel and consequently pulled from the brick in spots; mortar 13, although sticking to the brick, was so "short" and stiff that it would not spread

FIGURE 4.—*A case of cracking and curling is illustrated by mortar 21.*
The entire layer of mortar after drying could be easily removed from the brick.

good" was given if the mortar spread easily and uniformly, without the least indication of pulling from the brick as the trowel traveled over the mortar, and if the surface had a smooth texture. A rating of "good" was given if the mortar spread satisfactorily although the texture was coarse or rough, possibly because of the lack of plastic material or of a sufficiently high percentage of fines. A rating of "fair" indicated that some of the mortar actually pulled from the brick, leaving bare spots, and the mortar showed some tendency to spread unsatisfactorily. A rating of "poor" was given if these conditions were accentuated so that from one-third to one-half of the brick was pulled bare of mortar, or if a very rough surface remained which was apparently caused by the mortar being too stiff or short, so that it would not spread to the desired thinness.

Six mortars (2, 4, 9, 10, 12, and 19) rated "very good" and only one (5) rated "good" in all the troweling tests. Not one of the 20 mortars was rated "poor" in all four tests, although several were given that rating in either two or three of the four tests. Mortar 3 was satisfactory when the layer of mortar was held at ⅛ in., but was unsatisfactory when reduced to a 1/16-in. layer. Other mortars, for example 14, 15, and 16, rated "good" in the 1-stroke test but were unsatisfactory in the 25- and the 37-stroke tests.

The ratings of mortars 13 and 15 were changed from poor to very good in the 37-stroke test by the addition of water to the mortar. These were the only mortars whose consistency was changed. The 37-stroke test was the only one made with the changed consistency.[13]

(2) *Appearance after drying.*—The following ratings, based on the appearance of the mortar after drying on the brick, were given to differentiate the several degrees to which the mortars were curled or cracked: no, slightly, moderately, and badly. The tendency of the mortar to curl, resulting in the pulling of the mortar from the brick, is given in table 1, column 20, and the tendency to crack, which developed with the drying, is given in column 21. The ratings were based upon the appearance of the mortar on all four brick used in the mechanical troweling tests. The degrees of curling and cracking were not entirely independent.

Four of the mortars which rated "very good" in all the troweling tests showed neither curling nor cracking on drying. Mortar 12, shown in figure 3, comes within that category. None of the mortars were both badly cracked and curled, but five were so rated in either one or the other respect (3, 5, 15, 16, and 21). Mortar 21, shown in figures 3 and 4, curled badly, cracked moderately, and lacked adhesiveness, so that practically the entire top of the brick could easily be brushed free from the dried mortar.

Mortar 13 showed no indication of curling or cracking when the material as received was tested, nor after the consistency was changed, as described in the preceding section. On the other hand, mortar 15 cracked moderately on drying, both with the original and with changed consistency.

[13] The effect of change of consistency on some other properties of these two mortars will be discussed under the section on transverse strength and linear shrinkage.

TABLE 2.—*Transverse strength of neat-mortar bars and two half-brick-and-mortar assemblages, and shrinkage of mortars*

Mortar and molding[1] method	Transverse strength,[2] neat-mortar bars after heating at ° C									Transverse strength, two half-brick-and-mortar assemblage after heating at ° C and manner of failure[3]									Length changes after heating[4] at ° C			
	105	250	500	625	750	850	1,000	1,310	1,350	105	250	500	625	750	850	1,000	1,310	1,350	105	750	1,000	1,350
	lb/in.[2]	*lb/in.*[2]	*lb/in.*[2]	*lb/in.*[2]	*lb/in.*[2]	*lb/in.*[2]	*lb/in.*[2]	*lb/in.*[2]	*lb/in.*[2]	*lb/in.*[2]	*lb/in.*[2]	*lb/in.*[2]	*lb/in.*[2]	*lb/in.*[2]	*lb/in.*[2]	*lb/in.*[2]	*lb/in.*[2]	*lb/in.*[2]	%	%	%	%
1-*X*	5,165	3,175	2,185	2,350	1,725	1,820	1,865	Bloated	Bloated	505 *B*	285 *B & J*	375 *B & J*	290 *B & J*	310 *B*	330 *B & J*	350 *B*	295 *B & M*	300 *B & M*	4.5	+0.7	2.7	-----
	5,800	4,350	2,075	2,275	2,115	1,925	2,040	Bloated	Bloated													
	5,455	3,760	2,360	2,310	1,920	1,870	1,960	Bloated	Bloated													
2-*Y*	1,100	990	610	355	360	335	190	Bloated	Bloated	115 *J & M*	95 *J*	30 *J*	10 *J*	5 *J*	30 *J*	15 *J*	320 *B, J, & M*	315 *M*[4]	6.1	+.7	+1.2	-----
	1,465	950	755	370	620	520	245	Bloated	Bloated													
	1,265	975	670	365	490	430	215	Bloated	Bloated													
3-*Y*	2,850	2,795	1,930	2,175	2,010	1,965	1,805	2,810	3,065	430 *B & J*	295 *B & J*	225 *J & M*	285 *J & M*	230 *J & M*	285 *B, M, & J*	315 *B, M, & J*	370 *B, M, & J*	310 *B, M, & J*	2.2	0	2.7	1.1
	3,430	2,760	2,300	2,515	2,240	2,110	2,030	2,925	3,125													
	3,140	2,780	2,115	2,345	2,125	2,030	1,915	2,870	3,095													
4-*X*	6,105	5,665	3,670	2,955	2,705	2,850	3,700	Bloated	Bloated	540 *B*	365 *B & J*	445 *B*	365 *B*	415 *B & M*	375 *B & J*	400 *B*	290 *B & J*	300 *B & M*	4.5	+2.1	0.4	-----
	6,830	6,890	4,340	3,490	2,645	2,750	3,575	Bloated	Bloated													
	6,470	6,270	4,005	3,220	2,675	2,800	3,635	Bloated	Bloated													
5-*Z*	1,280	1,275	1,185	1,080	995	1,310	2,020	1,330	1,560	245 *J & M*	240 *M*	215 *M*	145 *M*	105 *M*	205 *M*	245 *M & J*	300 *B, M, & J*	300 *B, M, & J*	3.9	.1	.7	1.3
	1,070	1,435	1,410	1,310	1,255	1,670	1,820	1,635	1,565													
	1,155	1,330	1,300	1,215	1,115	1,490	1,990	1,480	1,565													
6-*Y*	2,150	-----	970	-----	920	-----	1,255	1,910	2,600	415 *M & J*	-----	320 *M*	-----	285 *M*	-----	390 *B & M*	405 *B & M*	245 *M*	4.6	.8	+.1	3.7
	2,200	-----	1,370	-----	1,235	-----	1,435	2,155	2,780													
	2,175	-----	1,190	-----	1,070	-----	1,345	2,030	2,695													
8-*Z*	580	-----	455	-----	445	-----	920	1,650	1,555	50 *M*	-----	95 *M & J*	-----	90 *M & J*	-----	70 *M & J*	175 *M & J*	205 *M & J*	4.5	.2	1.3	4.0
	790	-----	665	-----	520	-----	960	1,510	1,455													
	685	-----	560	-----	485	-----	940	1,585	1,505													
9-*X*	3,910	-----	1,960	-----	1,850	-----	1,870	1,770	2,160	460 *B*	-----	390 *B*	-----	395 *B*	-----	360 *B*	330 *B & M*	300 *B & M*	3.8	+1.8	+1.2	.8
	5,000	-----	2,530	-----	2,400	-----	2,405	2,480	2,455													
	4,455	-----	2,245	-----	2,100	-----	2,140	2,165	2,350													
10-*Z*	3,485	-----	2,565	-----	2,945	-----	2,555	-----	1,995	245 *J*	-----	175 *J*	-----	140 *J*	-----	185 *J*	190 *J*	225 *M*	2.7	.8	.2	+3.1
	4,545	-----	2,315	-----	3,630	-----	3,130	-----	2,400													
	4,065	-----	2,440	-----	3,290	-----	2,840	-----	2,195													
11-*X*	1,670	-----	1,600	-----	1,375	-----	2,020	2,640	2,510	335 *B, M, & J*	-----	220 *J*	-----	310 *J*	-----	315 *B & J*	280 *B, M, & J*	270 *B & M*	2.0	.5	.1	.8
	2,050	-----	1,750	-----	1,910	-----	2,370	2,500	2,210													
	1,815	-----	1,675	-----	1,530	-----	2,195	2,560	2,360													
12-*Z*	2,700	-----	2,025	-----	1,430	-----	2,405	Bloated	Bloated	440 *B*	-----	240 *M*	-----	240 *M*	-----	310 *B & J*	410 *B & J*	360 *B & J*	5.8	+.2	+.1	-----
	2,725	-----	2,470	-----	1,915	-----	2,435	Bloated	Bloated													
	2,710	-----	2,275	-----	1,675	-----	2,420	Bloated	Bloated													
13-*X*	2,185	-----	1,720	-----	1,225	-----	1,385	1,555	1,835	475 *B*	-----	370 *B*	-----	395 *B*	-----	375 *B*	330 *B & M*	330 *B & M*	1.8	+.2	.2	2.9
	3,090	-----	2,260	-----	1,910	-----	2,365	2,580	2,755													
	2,640	-----	2,045	-----	1,465	-----	1,875	2,295	2,255													

14-*Y*	2,425	2,445	2,165	2,150	3,155	2,375	120	M & J	75	J	65	J	135	J	140	J	85	J	8.3	.2	1.3	2.4
	2,980	2,720	1,975	2,670	3,260	2,735																
	2,705	2,580	2,080	2,410	3,210	2,520																
15-*Y*	740	650	650	1,245	1,620	1,410	75	M & J	85	M & J	50	M & J	125	M & J	105	M & J	95	M	5.3	.3	1.5	2.6
	910	780	730	1,125	1,780	1,815																
	830	715	690	1,185	1,700	1,595																
16-*X*	1,565	900	780	880	1,585	1,575	340	M	85	M & J	100	M & J	240	M & J	235	M & J	240	M & J	6.8	.9	+.2	2.2
	2,455	1,205	945	1,440	1,470	1,470																
	2,010	1,070	880	1,160	1,520	1,520																
17-*X*	3,640	1,795	1,065	1,315	2,125	2,020	360	B	340	B	390	B	400	B	355	B	300	B	4.2	.4	+.4	1.5
	4,615	1,590	1,540	2,010	2,340	2,250																
	4,130	1,690	1,305	1,690	2,220	2,110																
18-*X*	1,875	1,410	775	380	695	Fused	215	J	110	J	115	M & J	105	J	290	M & J	325	M	6.0	.4	+.9	-----
	2,705	1,565	680	455	695	Fused																
	2,290	1,490	730	415	695	Fused																
19-*X*	2,715	1,350	880	955	765	-----	365	B	300	J	200	M & J	210	M & J	375	M	380	M	6.1	.3	+.4	-----
	3,905	1,340	1,175	1,245	670	-----																
	3,310	1,345	950	1,085	720	-----																
20-*X*	4,775	2,100	1,105	940	1,000	Bloated	305	J	135	J	170	J	135	J	365	B & M	340	B & M	7.6	.7	+1.1	-----
	4,845	2,565	1,315	1,085	1,080	Bloated																
	4,510	2,335	1,210	1,010	1,040	Bloated																
21-*Y*	2,810	1,780	1,840	2,520	3,430	Bloated	335	J	160	J	195	J	210	M & J	345	B & J	370	B & J	8.3	1.0	1.7	-----
	2,970	2,190	2,200	2,740	2,810	Bloated																
	2,890	1,990	2,020	2,630	3,125	Bloated																

[1] Neat-mortar specimens molded, (*X*) from 1 side only, (*Y*) from 2 sides, (*Z*) by pouring or casting. Method of molding depended on consistency which varied in some cases with different shipments.

[2] The three values for each mortar at the various temperatures represent, in the order given: (1) The average of 5 specimens broken with the surface on top that was uppermost during drying; (2) the same number of specimens with that surface on the bottom; (3) the average of all specimens.

[3] *B*, *J*, and *M* indicate failure occurred in brick, joint, or mortar, respectively.

[4] Mortar ran from joint.

[5] Except the values for 105° C, which represent the drying shrinkage, the length changes given represent changes between the dry length and the length after heating. "+" indicates expansion.

(g) TRANSVERSE STRENGTH AND LINEAR SHRINKAGE

(1) *Heated and cooled specimens.*—In table 2 are given the transverse strengths (moduli of rupture) of the mortars after they were heated to various temperatures and cooled. In each case three sets of values are given: First, the average for not less than five specimens broken, with the surface that was originally at the bottom on top (hence, in compression); second, a similar average but for specimens with this surface at the bottom (hence, in tension); and third, the average for both positions. It will be noted that with comparatively few exceptions the strength was greater, and in many instances decidedly so, when the original top surface was in tension during the breaking of the specimen. This difference in strength is probably related to the differences in concentration of the alkali salts near the two surfaces (table 1, columns 8 and 9). A few tests of the transverse strength of specimens made of fire clay to which no silicate of soda had been added failed to show a similar difference in strength. Some mortars, however, for example, 1, 3, 14, and 17, showed comparatively little migration of the salts in comparison with some of the other mortars, yet all showed as great a difference in strengths as those in which the migration of the salts was much greater. Since only one specimen of each mortar was tested for alkali content, and since it was quite difficult in many cases to prepare equally thin sections for test in all mortars, it is quite probable that at best the values for the alkali content represent only an approximation of the migration of the salts.

The strengths of the mortar specimens dried at 105° C covered a very wide range, the lowest average for the two positions of test being 685 lb/in.^{2} and the highest 6,470 lb/in.^{2} The change in strength of the mortars heated at higher temperatures and then cooled to room temperature varied with the materials. Such variations in strength between three mortars are illustrated in figure 5. The mortars, in general, may be classed according to loss or gain in strength into three groups, illustrated by the types in figure 5, namely:

1. Those with high initial or air-setting strength which was lowered by heating at intermediate temperatures. The strength increased again, probably because of vitrification, by heating at the highest temperatures.

2. Those of high initial or air-setting strength which was lowered by heating at intermediate temperatures and was not further changed, even after heating at the highest temperature.

3. Those of comparatively low initial strength which changed very little with heating at the lower temperatures but increased progressively with heating at moderately higher and the highest temperatures.

Nine mortars (3, 4, 5, 6, 12, 13, 14, 16, and 21) were of the first type, eight (1, 2, 9, 10, 17, 18, 19, and 20) of the second type, and three (8, 11, and 15) of the third type.

Strength tests could not be made of mortars 1, 2, 4, and 12 after heating them at 1,310° or 1,350° C, because the specimens bloated badly. Although bloating due to overfiring might have been expected in the cases of mortars 1 and 2 because of their low pce, it was rather unexpected in the cases of mortars 4 and 12, which had higher pyrometric cone equivalents. It is somewhat puzzling why mortar 4 should have bloated, since it has a pce of 34. Although it was among the highest in alkali content, the others with comparable alkali con-

tent and lower pyrometric cone equivalents did not have the same tendency to bloat.

Fifteen of the twenty mortars had an air-setting strength of over 2,000 lb/in.^{2}, and 12 had a strength of over 2,500 lb/in.^{2} Those mortars having an initial air-setting strength exceeding 2,500 lb/in.^{2} continued to have a satisfactory strength after being heated at all

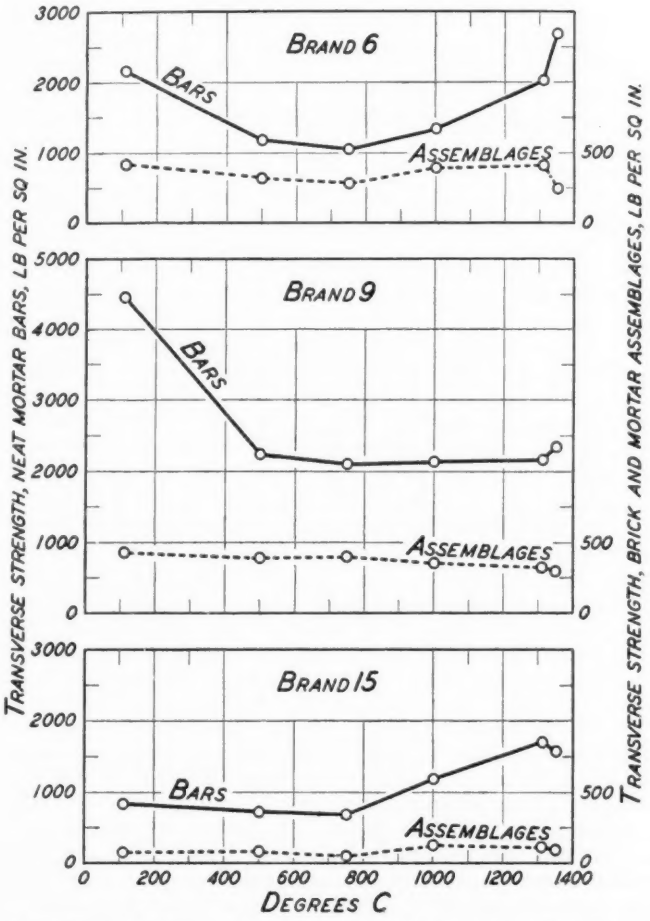

FIGURE 5.—*Changes in transverse strengths with temperatures of heating for bars and two-half-brick-and-mortar assemblages made with mortars 6, 9, and 15, representing three different types of trends.*

succeeding higher temperatures and cooled. Mortars 5 and 11 were exceptions; although they had a rather low initial strength, they retained a satisfactory strength after heating them at all higher temperatures and subsequent cooling. Because of these exceptions, it would appear necessary to test mortars after air-setting, and also after heating at 750° C and cooling. Although not all mortars reached their lowest strength after heating at 750° C and cooling, the values

obtained after such treatment are in general close to the lowest obtained after the various heat treatments.

After the mortars were heated at 1,350° C, much glass was observed by a visual inspection of the test specimens. This glass, which in many cases was concentrated near the surfaces, apparently was the result of the large quantities of sodium silicate, which the mortars contain.

Changing the water content of mortar 13 from 21.3 to 24.9 and then 26.6 percent caused the transverse strength to change, respectively, from 4,170 to 4,035 and then to 3,270 lb/in.^{2} For mortar 15, changing the water content from 24.9 to 27.5 and then to 38.5 percent caused the strength to change from 735 to 685 and then to 485 lb/in.^{2}, respectively.

The coefficients of variation were computed for the transverse strengths of those neat mortar specimens heated at 105° and 1,000° C and tested in the manner described. The range in coefficients for the mortar specimens heated to 105° C was from 3.5 to 47.1 percent, the latter being an exceptionally high value. The mean coefficient was 13.6 percent. The range in coefficients for the specimens heated to 1,000° C was from 3.7 to 25.7, with the mean 11.9 percent.

The linear shrinkages and expansions, after heating the mortars at several different temperatures, are given in table 2. The values for the mortars cured at 105° C represent the average of five specimens, those for the heated mortars the average of three specimens. The shrinkage of the mortars after drying overnight at approximately 105° C ranged from 1.8 to 8.3 percent. In most cases very little additional shrinkage took place with heating at either 500° or 750° C; in fact, a slight expansion was noted in several cases, but heating at 1,000° C and above caused appreciable length changes in most mortars. Heating at 1,000° C caused expansion in nine mortars, but heating them at the highest temperature caused shrinkage in all but one of those for which data could be obtained. The values for changes in length were also of particular interest, because they showed the very low shrinkage from the wet condition caused by heating at 1,350° C, as noted in a number of mortars.

(2) *Specimens tested at 750° C.*—Although specimens were prepared from six mortars for test at 750° C, over an 8-in. span, the deformation of two of them (4 and 9) under their own weight was so great at this temperature that satisfactory strength tests could not be made. The values for the four mortars tested are given in table 3. The first column gives the strength of the material after air-setting, the second column the strength at 750° C, the third column the strength at approximately 20° C of the two 5-in. sections that resulted from rupturing the 10-in. specimens at 750° C, the fourth column gives the values for specimens also tested at 750° C, but which had been first heated at 750° C for an hour and cooled to room temperature before testing at 750° C.

The results, based on a limited number of specimens, indicate that at room temperature the modulus of rupture of mortar 18 was somewhat lower than it was at 750° C, and that of each of the other three mortars was somewhat greater. However, a decided decrease in strength was obtained for all four mortars when tested at room temperature after being heated for a short time at 750° C. After heating the mortars to 750° C and cooling to room temperature and then

testing at 750° C, the strengths for mortars 19, 20, and 21 (no data available for mortar 18) follow approximately the same trend as those obtained on specimens tested at 750° C without the preliminary heating at 750° C.

TABLE 3.—*Modulus of rupture of mortars tested after different heat treatments*

Mortar number	Tested at			
	20° C, after drying at 105° C[a]	750° C, after drying at 105° C[a]	20° C, after heating at 750° C[b]	750° C, after heating at 750° C and cooling [a]
	lb/in.[2]	*lb/in.*[2]	*lb/in.*[2]	*lb/in.*[2]
18	2,955	3,660	870	
19	4,880	2,925	1,315	2,995
20	4,890	3,456	1,385	3,500
21	4,640	4,535	3,190	3,880

[a] Average of 3 specimens (6 for mortar 19) over an 8-in. span.
[b] Average of 6 specimens (12 for mortar 19) over a 3-in. span.

No explanation for the decrease in strength due to the heating at a comparatively low temperature and cooling is offered. The high strength obtained at 750° C may be explained on the basis of the presence of crystalline silica as shown by the results of studies,[14] reported by R. A. Heindl and W. L. Pendergast.

(h) POROSITY AND SOLUBILITY

The porosities, obtained only for mortars 1 to 5, inclusive, are given in table 4. Each value represents the average of five determinations. It is rather doubtful that the porosity values for the materials heated to 105° C are correct, because of the possibility of partial disintegration of the specimens during their contact with water. As indicated in the table, mortars 1 and 4 disintegrated. Values are given for all five mortars after they were heated at 250° C, but it is doubtful also that any are correct because of partial dissolution of the specimens. The values for mortars 1 and 4 give some indication that this is true.

The values in table 4 are of some interest in that they give an indication of the action of the salts in the different mortars. In this group the highest alkali content was shown by mortars 1 and 4 (see table 1). These two show the greatest changes in porosity after the various heat treatments through 1,000° C. The porosity of mortar 4 was greatest after being heated at 750° C, except after it was heated at 1,310° C, when it showed definite signs of bloating.

Figure 6 shows the relation between porosity and strength of mortar 3 and shows also the effect of heating on these properties.

Solution of the salts, as evidenced by a simple titration test, occurred with all five mortars after they were heated at 250° C, but in no case was solubility evident after the mortars had been heated at 500° C. No attempt was made to determine the relative amount of soluble material of the five mortars after the 250° C heating. Also, it is not known whether contact with water for a longer time than in these tests would cause solution of salts in specimens which had been heated at 500° C.

[14] *Fire clays; some fundamental properties at several temperatures*, BS J. Research **5**, 213 (1930) RP194. *Young's modulus of elasticity at several temperatures for some refractories of varying silica content*, J. Research NBS **13**, 851 (1924) RP747.

TABLE 4.—*Porosity of mortars 1 to 5 after being heated at various temperatures and cooled*

Mortar number	Porosity after heating at °C								
	105	250	500	625	750	850	1,000	1,310	1,350
	%	%	%	%	%	%	%	%	%
1	(a)	11.5	17.5	22.3	22.8	21.9	24.4	(b)	(b)
2	18.2	20.1	25.3	26.5	23.0	24.1	26.3	(b)	(b)
3	19.5	18.3	24.1	22.2	23.8	22.8	19.0	13.6	12.7
4	(a)	10.3	21.6	28.7	35.8	29.3	29.3	43.8	(b)
5	27.9	31.0	33.1	34.1	34.2	35.2	33.5	28.6	29.2

(a) Specimens disintegrated.

(b) Specimens bloated badly, no determinations made.

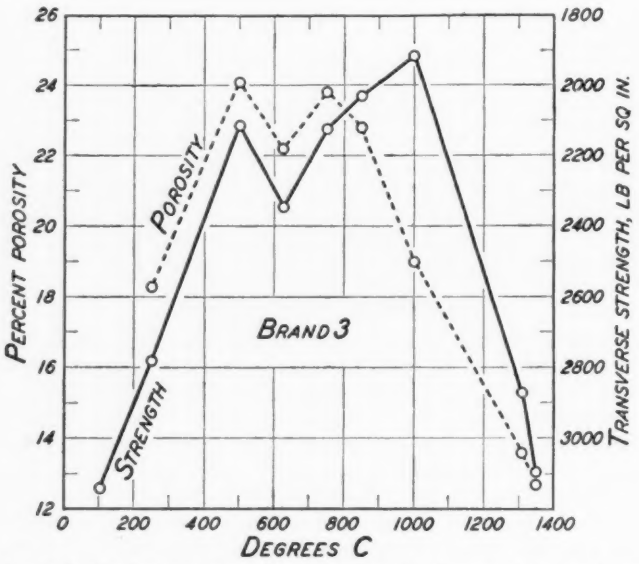

FIGURE 6.—*Relation between porosity and strength of mortar 3 after it was heated at various temperatures.*

2. ASSEMBLAGE OF TWO HALF-BRICK AND MORTAR

(a) SETTING TIME OF MORTAR

The time required for each of the mortars to air-set, or stop flowing under loads when placed between firebrick, is given in table 1, column 22. Figure 7 illustrates the two extremes in time of set as represented by mortars 10 and 11. Sixty minutes had elapsed before the 50-lb. weight was placed on assemblage 10, but, as shown in the figure, the flow of the mortar was still quite high. The time required for this mortar to set under the conditions of the test was 90 minutes. On the other hand, only 1 minute had elapsed before the weight was placed on assemblage 11. A total of eight mortars set within 1 minute and only six had failed to set after 3 minutes. These 6 mortars ranged in time of set from 24 to 90 minutes, leaving a rather wide gap between

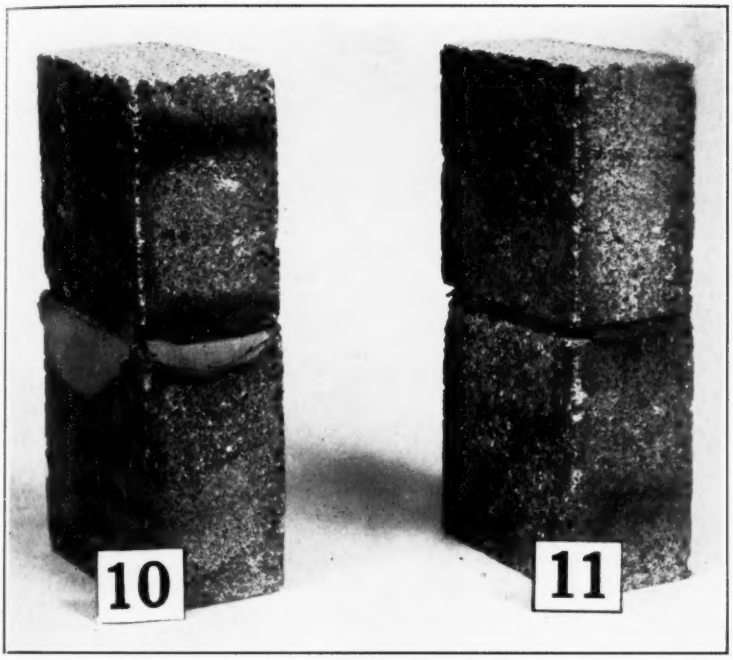

FIGURE 7.—*Appearance of brick-and-mortar assemblages after test for determining the time for mortars to air-set or stop flowing under load.*

Brick-and-mortar assemblage 10 showed high flow of the mortar even after 60 minutes had elapsed before application of the load. Brick-and-mortar assemblage 11 showed no flow after 1 minute under the same conditions.

UNIV. OF MICH.

these and the other 14 mortars, which showed no flow within 3 minutes or less.[15]

No relation between the time of set and the other properties of the mortars is apparent. It is true that the alkali content of all the mortars which require considerable time to air-set is quite high, as is also the air-setting strength. Furthermore, all these mortars, with the exception of mortar 13, were classed "very good" in the mechanical troweling test.

(b) TRANSVERSE STRENGTH

The transverse strengths of the two half-brick-and-mortar assemblages, tested after being heated in the same furnace as, and simultaneously with bar specimens of the neat mortar, are given in table 2. They ranged from 5 lb/in.^{2} (mortar 2) to 540 lb/in.^{2} (mortar 4). The values of strength of assemblage for mortars 6, 9, and 15 are plotted in figure 5 with the strengths of the neat mortars at the corresponding temperatures. On the average, the trends of the cross-breaking strengths of the assemblages, after having been heated at various temperatures and cooled, resembled those of the neat mortars considerably more than the examples shown in figure 5. However, the trends for the assemblages varied considerably more among themselves than did the trends for the bars. Some of the probable reasons for such variations are discussed in the following paragraph.

It was reported by Heindl and Pendergast [16] that the modulus of rupture of the brick (stiff-mud type) used in this study was 745 lb/in.^{2} It was found that in no case did the modulus of rupture of the assemblage of brick and mortar approach this value, though in many cases the brick failed rather than the mortar or the joint. However, as already pointed out, the assemblage was made by joining the two outside end surfaces of the brick. A difference in physical characteristics between the central portion of this particular type of brick and the ends may be a partial explanation for the discrepancy. Some weight can be given this supposition, because tests made by Heindl and Mong [17] showed that considerable differences may exist between specimens cut from different parts of the same brick. There is also the possibility that the silicate of soda, which migrates to the pores of the brick, weakens the structure. With a 20-power binocular it was possible to distinguish in some cases white opaque particles of similar appearance in both the mortar and the brick surface adhering to the mortar. Migration of the liquid from the mortar joint to the brick was also indicated by a dye added to mortar 4.

In general, a high air-setting strength of the neat mortar presages a satisfactory strength of the brick-and-mortar assemblage. Mortar

[15] The porosity of the brick has apparently a considerable effect on the rate at which the mortar with which it comes in contact loses its water. For example, bricks of 1.5- and 8.6-percent absorption when bonded with mortars 3 and 5 and loaded as described, but using a 100- instead of a 50-lb. weight, gave the following information:

Mortar number	Absorption of brick (percent)	Setting time (minutes)
3	1.5	45
3	8.6	2
5	1.5	30
5	8.6	2

[16] *Bonding strength of cold-setting refractory cements*, Bul. Am. Ceram. Soc. **15**, 182 (1936).
[17] *Young's modulus of elasticity, strength, and extensibility of refractories in tension*, J. Research NBS **13**, 851 (1934) RP747.

14 is the only exception; the neat mortar not only has a fairly high air-setting strength, but maintains a high strength after being heated at the various temperatures, yet the assemblage shows only a low strength. This mortar has a shrinkage (see table 2) equal to the highest in the group of 20 mortars. Brands 2, 8, and 15 would be considered as having low assemblage-joint strengths, but all three show the neat mortar to have low air-setting strengths. A high strength of the assemblage of brick and mortar after air-setting usually, but not always, presages a good assembly strength after heating at moderately high temperatures. The assemblage for mortar 16 was one of the exceptions (table 2; assemblages heated at 500 and 750° C).

A brick-and-mortar assemblage for each mortar, except mortar 4, was heated at 1,500° C for 1 hour. After the mortars cooled, the strength was found to range from 345 to 765 lb/in.^{2} The values are not tabulated, because they represent only one specimen in each case.

To obtain an indication of the effect of long-time heating at a low temperature on the strength of the bond in the assemblage of two half-brick and mortar the following test was made: Five assemblages of each of three air-setting refractory mortars selected at random, and, for comparison, five of one high-alumina hydraulic mortar (1 cement, 2 sand) were heated continuously at 260° C for 9 months, cooled, and then tested for transverse strength. The results are given in table 5.

TABLE 5.—*Effect of long-time heating on strength of assemblage*

Mortar number	Strength [a] after heating 18 hours at 105° C	Strength after heating 9 months at 260° C	Loss in strength
	lb/in.^{2}	*lb/in.*^{2}	*Percent*
1	505	275	45.5
2	115	30	74.0
5	245	260	[c] −6.0
Hydraulic	[b] 220	65	70.5

[a] Taken from table 2. [b] Tested after curing (laboratory air) for 9 months. [c] Increase.

The two-half-brick assemblages prepared with the mortar in a dipping consistency were cured and then dried at 105° C. The results of transverse-strength tests on these assemblages are given in table 6.

TABLE 6.—*Modulus of rupture of assemblage of two half-brick and mortar used in a dipping consistency*

Mortar number [1]	Specimens	Modulus of rupture	Failed [2] in	Mortar number [1]	Specimens	Modulus of rupture	Failed [2] in
		lb/in.^{2}				*lb/in.*^{2}	
1	7	205	*J*	13	10	450	*B*
2	10	40	*J*	14	6	50	*J*
3	5	140	*M*	15	10	40	*J*
4	10	320	*B* & *J*	17	10	235	*J*
5	10	140	*J* & *M*	18	10	5	*J*
6	10	270	*J* & *M*	19	8	220	*J*
10	5	430	*B*	20	8	140	*J*
11	8	245	*J*	21	10	25	*J*

[1] Mortars 8, 9, 12, and 16 not tested.
[2] *B*, *J*, and *M* indicate that failure occurred in brick, joint, or mortar, respectively.

All of these values, with the exception of those for mortars 10 and 13, are considerably below those obtained when the mortar was applied in a troweling consistency (see table 2).

The coefficients of variation for the cross-breaking strengths of the assemblages (table 2) heated at 105° C varied from 7.9 to 38.5 percent, and the mean value was 20.2 percent. Information was not obtained on the variation for the assemblages heated at other temperatures.

(c) TYPES OF FAILURE

The four types of failure which occurred in the tests of the cross-breaking strength of the assemblages of two half-brick and mortar were as follows:

1. The brick failed.
2. The assemblage failed in the joint.
3. The mortar failed.
4. Some combination of the foregoing types.

The manner in which the bonded brick specimens failed when the mortar was used as received is indicated in table 2. Considered collectively, no particular type of failure predominates, except that at the highest temperature the partial or complete failure of the brick structure appeared to occur. For any one mortar the type of failure was, in general, the same, regardless of the heat treatment, except as noted above. This was especially true for the heat treatments ranging from 105 to 1,000° C, inclusive.

Of the four types, the failure of the assembly in the joint varied over the widest ranges, namely, from 5 lb/in.^{2} (mortar 2, 750° C heating) to 335 lb/in.^{2} (mortar 21, 105° C heating).

(d) RESISTANCE TO WEATHERING

An approximate indication of the weathering resistance of the two-half-brick-and-mortar assemblages was obtained by exposing one specimen of each to the weather. The specimens were so placed on a parapet that one-half of the assemblage extended over the edge and would drop of its own weight as soon as the mortar bond could no longer support the half-brick. At the end of 16 months' exposure to the rain, snow, and sunshine in Washington, D. C., 10 specimens had failed. The first failure occurred at the end of 17 days (mortar 5) and for all mortars there was, in general, a direct relation between the strength of bond (see table 1) and the number of days before rupture occurred.

3. THREE-BRICK PIER AND FUSION-BLOCK TEST

In table 7 a summary is given of the observations made of the three-brick (two whole and two half) assemblages or piers after being dried, after being heated at 750° C for 24 hours, again after being heated at 1,425° C for 24 hours, and lastly after being heated at 1,500° C for 5 hours. The appearance of the mortars after having been heated at 1,425° and 1,500° C in the fusion blocks is also noted. The conclusions drawn from the appearance of the mortar in the fusion-block tests correlate well with those drawn from an examination of the piers.

Cracks occurring in the horizontal joints are designated "$\parallel$"; those in the vertical joints "$\perp$." No differentiation was made as to the direction of the cracks themselves within the joints. Only those cracks designated as "bad" would be considered as affecting the quality of the mortar.

TABLE 7.—*Appearance of mortar in fusion block and*

Mortar No.	Appearance [1] of dry mortar in joint		Appearance [1] of mortar in joint after heating 24 hours at 750° C		Appearance [1] of mortar in joint after heating 24 hours at 1,425° C		Appearance [1] of mortar in joint after heating 5 hours at 1,500° C	
	1/16"	1/8"	1/16"	1/8"	1/16"	1/8"	1/16"	1/8"
1	Good	∥ cracks	⊥ and ∥ cracks.	∥ cracks.	∥ cracks	Good	⊥ and ∥ thermal cracks.	⊥ and ∥ thermal cracks.
2	∥ cracks	Good	∥ cracks.	Bad ⊥ and ∥ cracks.	Very glassy. Lower joint flowed.	Very glassy. Lower joint flowed.	Bulged. Full of large bubbles. Bricks slipped out of place. Glassy.	Bulged. Full of large bubbles. Bricks slipped out of place. Glassy.
3	Good	do	do	⊥ and ∥ cracks.	Good	Good	⊥ cracks	⊥ shrinkage and thermal cracks.
4	do	do	⊥ and ∥ cracks.	do	do	Good. ∥ thermal cracks. Bulged.	⊥ and ∥ cracks.	Bulged
5	do	do	Bad ⊥ and ∥ cracks.	⊥ cracks in ∥ joint.	do	Good. ∥ thermal cracks.	⊥ shrinkage and ∥ thermal cracks.	⊥ and ∥ shrinkage cracks.
6	∥ cracks	do	⊥ and ∥ cracks.	Good	do	Good	⊥ thermal cracks. Glassy.	⊥ and ∥ shrinkage cracks. Glassy.
8	do	∥ cracks.	do	⊥ and ∥ cracks.	Shrinkage cracks mostly healed. ∥ thermal cracks.	Shrinkage cracks mostly healed. ∥ thermal cracks.	Glassy	Glassy; bulged.
9	do	Good	do	Good	Good	Good	Good	Good
10	Good	do	Good	⊥ cracks.	No bond with brick. All joints badly cracked.	No bond with brick. All joints badly cracked.	Mortar cracked and pulled from brick.	Mortar cracked and pulled from brick.
11	do	do	do	Good	Good	Good	⊥ cracks	⊥ cracks
12	do	⊥ and ∥ cracks.	⊥ and ∥ cracks.	⊥ and ∥ cracks.	do	do	Bulged	Mortar flowed from ⊥ joint.
13	do	Good	Good	⊥ cracks.	∥ thermal cracks.	∥ cracks	∥ and ⊥ shrinkage and ⊥ thermal cracks.	⊥ cracks
14	∥ cracks	do	⊥ and ∥ cracks.	⊥ and ∥ cracks.	⊥ cracks	∥ thermal cracks.	Good	Good. Bulged.
15	⊥ cracks	do	do	⊥ cracks.	∥ thermal cracks.	∥ thermal and shrinkage cracks.	⊥ thermal and shrinkage cracks.	⊥ cracks
16	do	⊥ cracks	Bad ⊥ and ∥ cracks.	⊥ cracks in ∥ joint.	Bad ⊥ and ∥ cracks.	Bad ⊥ cracks.	⊥ cracks	Bulged. Bubbles.
17	Good	Good	Good	Good	Good	⊥ thermal cracks.	Good	∥ thermal and ⊥ shrinkage cracks.
18	do	do	do	do	∥ thermal cracks.	∥ thermal cracks.	Very glassy. Bricks slipped. Flowed.	Very glassy. Bricks slipped. Flowed.
19	do	do	do	do	Good	Good	do	do
20	do	∥ cracks	do	Bad ∥ cracks.	do	do	Very glassy. Bulged. Flowed from joint.	Very glassy. Bulged. Flowed from joint.
21	⊥ cracks	Good	⊥ and ∥ cracks.	⊥ and ∥ cracks.	⊥ and ∥ cracks.	⊥ and ∥ thermal cracks. Bulged.	∥ thermal and ⊥ shrinkage cracks.	⊥ and ∥ thermal cracks. Bulged.

See footnotes at end of table.

in joints of three brick-and-mortar assemblages or piers

Remarks on general appearance after heating at 1,500° C	Appearance of mortar in fusion block [2] after heating for 5 hours at			Appearance [1] of cap of mortar on brick after heating [4]
	1,425° C (7/16" thick)	1,500° C (7/16" thick)	1,500° C (1/2" thick)	
Good	Bubbles on surface. Fused and flowed to 1. High shrinkage.	Bubbles on surface. Fused and flowed to 1. High shrinkage.	Flow 0. Bubbles. High shrinkage.	Moderately cracked.
Very poor	Flow 1½. Glass	Flow 6. Glass	Flow 2. Glass	Fused [3] and crawled.
Very good	Flow 0. High shrinkage.	Flow 0. High shrinkage.	Flow 0. High shrinkage.	Slightly [3] cracked.
1/16", good. 1/8", poor.	Flow ¾. Bloated. Glassy surface.	Flow ¾. Bloated. Glassy surface.	Flow 0. Bubbles and glassy surface. Shrinkage 0.	
Good	Flow 0. Slight shrinkage. No bubbles.	Flow 0. Slight shrinkage. No bubbles.	Flow 0. Slight shrinkage. No bubbles.	Moderately cracked.
do	Flow ¾. Bloated. Glassy surface.	Flow ¾. Bloated. Glassy surface.	Flow 0. Bubbles. Glassy surface.	
Fair	Flow 0. Few bubbles. High shrinkage.	Flow 0. Few bubbles. High shrinkage.	Flow 0. Few bubbles. High shrinkage.	Badly [3] cracked.
Very good	Bubbles on surface. Fused and flowed to 1.	Bubbles on surface. Fused and flowed to 1.	Flow 0. Bubbles. High shrinkage.	Almost no defects.
Poor	Flow 0. Glassy surface and chalky body.	Flow 0. Glassy surface and chalky body.	Flow 0.	
Very good	Flow 0. Little shrinkage and no glass.	Flow 0. Little shrinkage and no glass.	do	No defects.
Poor exterior. Very good interior.	Flow 1. Bubbles on surface fused to glass.	Flow 1. Bubbles on surface fused to glass.	Flow 0. Bubbles. High shrinkage.	
Fair	Flow 0. Bubbles on surface are glassy. High shrinkage.	Flow 0. Bubbles on surface are glassy. High shrinkage.	Flow 0. No bubbles. Moderate shrinkage.	
1/16", good. 1/8", fair.	Flow 0. High shrinkage. Bubbles on surface are glassy.	Flow 0. High shrinkage. Bubbles on surface are glassy.	Flow 0. High shrinkage. No bubbles.	
Good	Flow 0. High shrinkage. No bubbles.	Flow 0. High shrinkage. No bubbles.	do	Moderately cracked.
1/16", fair. 1/8", exterior poor, interior good.	Flow 0. High shrinkage. Bubbles on surface.	Flow 0. High shrinkage. Bubbles on surface.	Flow 0. High shrinkage. No bubbles.	
Good	Flow ¼. Bloated and glassy surface.	Flow ½. Bloated and glassy surface.	Flow 0. Bubbles. Moderate shrinkage.	Slightly cracked.
Very poor	Flow ¾. Glass	Flow 4. Glass	Flow ¾. Glass	Fused [3] and crawled.
do	Flow 1. Glass	Flow 2. Glass	Flow ½. Glass	Fused to glass.
1/16", fair. 1/8", poor.	do	Flow 6. Glass	do	Fused and crawled.
1/16", fair. 1/8", poor.	Flow 1. High shrinkage. Bubbles and glassy.	Flow 1. High shrinkage. Bubbles and glassy.	Flow 0. High shrinkage. Bubbles and glassy.	Badly cracked and curled.

TABLE 7.—*Appearance of mortar in fusion block and in*

Mortar No.	Apperance[1] of dry mortar in joint		Appearance[1] of mortar in joint after heating 24 hours at 750° C		Apperance[1] of mortar in joint after heating 24 hours at 1,425° C		Appearance[1] of mortar in joint after heating 5 hours at 1,500° C	
	1/16"	1/8"	1/16"	1/8"	1/16"	1/8"	1/16"	1/8"
22	do	do	Bad ⊥ cracks.	do	∥ cracks. Glassy.	∥thermal cracks. Bulged.	do	∥ and ⊥ thermal cracks. Bulged. Flowed from ⊥ joint.
23	do	do	∥ cracks.	do	∥ thermal cracks.	do	⊥ and ∥ thermal cracks.	⊥ and ∥ thermal cracks.
24	Good	do			Good	Good	Good	∥thermal cracks. Slightly glassy.

[1] When cracks carry no identification as to cause, it is intended to be understood that they are shrinkage cracks. Those occurring in the horizontal joint are labeled "∥," in the vertical joint "⊥."
[2] Each division on the fusion block is equal to ¼ inch.
[3] Heated at 1,425° C for 24 hours; the others were heated at 1,500° C for 5 hours.
[4] No information was obtained where no comment is made.

joints of three brick-and-mortar assemblages or piers—Continued

Remarks on general appearance after heating at 1,500° C	Appearance of mortar in fusion block [2] after heating for 5 hours at			Appearance [1] of cap of mortar on brick after heating [4]
	1,425° C (7/16" thick)	1,500° C (7/16" thick)	1,500° C (3/8" thick)	
1/16", fair. 1/8", poor.	Flow 0. Bloated and glassy. High shrinkage.	Flow ½. Bloated and glassy. High shrinkage.	Flow 0. Bloated and glassy. High shrinkage.	Moderately cracked.
Good	Flow 0. Moderate shrinkage. No bubbles. Glazed.	Flow 0. Moderate shrinkage. No bubbles. Glazed.	Flow 0. Moderate shrinkage. No bubbles. Glazed.	Do.
Very good	Flow 0. No bubbles. Glazed. Slight shrinkage.	Flow 0. No bubbles. Glazed. Slight shrinkage.	Flow 0. No bubbles. Glazed. Slight shrinkage.	Almost no defects.

After drying the piers, neither the 1/16-in. nor the 1/8-in. joints had cracked seriously. There was a slightly greater tendency for cracks to occur in the thinner than in the thicker joints. After heating the piers at 750° C, the mortar joints in many units had developed cracks, which were not visible after drying, although only four mortars were classified as having cracked badly. Four mortars did not have cracks after the treatment at 750° C.

One effect of heating at 1,425° C was that many of the cracks visible after the treatment at 750° C had apparently healed in many cases (for examples, see mortars 3, 6, 9, 12, etc.). A number of the units had, however, developed cracks which have been designated "thermal cracks" (for examples, see mortars 4, 5, 8, 15, etc.). In such cases the mortar had become glassy or had reacted with the brick and during cooling had cracked because of stresses which developed. Mortar 2 had become very glassy and full of bubbles, and the mortar in the lower joint of the piers, whether 1/8 or 1/16 in. thick, showed a slight indication of flow. Mortar 10 also appeared to be unsatisfactory for use at high temperatures. The mortar was badly cracked and pulled from the brick in many places, and consequently the bond of this mortar was very weak.

After the soaking at 1,500° C, many changes for the worse had taken place. In three cases (piers 2, 18, and 19) the brick had slipped out of alignment, even though the pier was apparently resting vertically, that is, on a 9- by 4½-in. face. An example of this slippage is illustrated in figure 8, which shows a pier bonded with mortar 2. The photograph was so taken that the extent of the slippage could be readily seen. The apparently glazed appearance of the surface of the brick was caused by shadows. Table 1 shows the pyrometric cone equivalent of this mortar to be only 20. The mortar had apparently become quite liquid at 1,500° C, since very little of it remained in the 7/16-in. deep compartment of the fusion block (see fig. 8), and the flow was quite high also from the compartment 1/8-in. deep.

Mortars 4, 14, 16, 20, 21, and 22 when used in a 1/16-in. joint had a better appearance than when used in the 1/8-in. joint. In none of these cases, however, was even the 1/16-in. mortar joint given the highest rating. On the other hand, mortars 3, 9, 11, and 24 may apparently be used successfully in either 1/16- or 1/8-in. joints, since in either case they are practically free from defects. In figure 9 may be seen the appearance of mortar 11 after being heated at 1,425° C (1/16-in. joint) and at 1,500° C (1/8-in. joint). No defects are visible in the joints, and the excellent appearance of the mortar in the fusion blocks is a good indication that the joints should be of a high quality. Although table 7 indicates that some mortars have cracks in the vertical joints, these cracks were few in number and of hairline magnitude and have no significance.

An example of a somewhat different type of mortar (12) from that just discussed is shown in figure 10 in the pier in which a 1/8-in. joint was used. The mortar had a pce of 28, but, as may be seen, the edges of the joints have bulged badly. The appearance of the mortar after heating in the fusion block was indicative of what might be expected

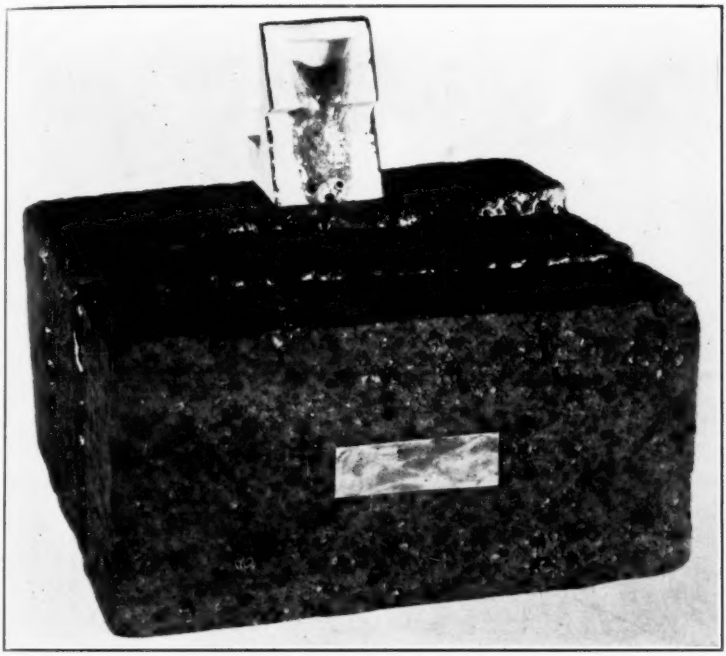

FIGURE 8.—*Mortar 2 had become so fusible at 1,500° C that the bricks laid with a ⅛-in. joint slipped out of position when built into a pier.*

During heating, the pier was approximately vertical, that is, a 4½-by 9-in. face was the bottom. The fusibility of the mortar is illustrated by the extent of the flow from the vertical (2½-in.) joint in the pier as well as the compartment in the fusion block heated simultaneously with the pier.

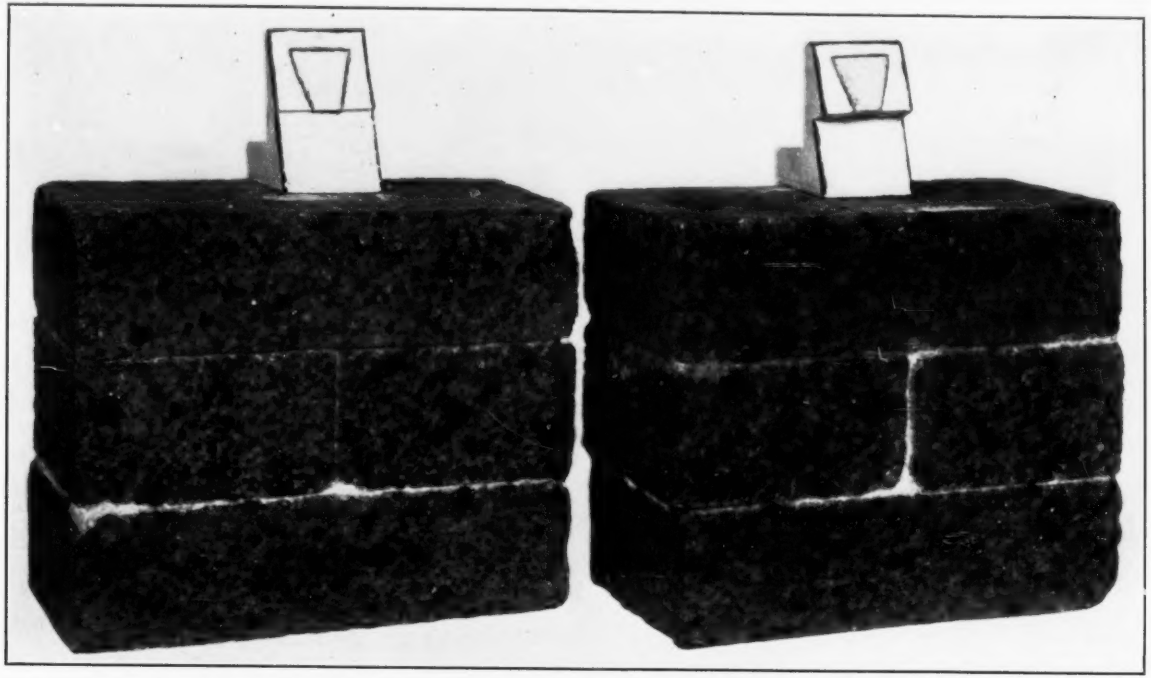

FIGURE 9.—*Mortar 11 gave excellent results in piers regardless of whether a* $\frac{1}{16}$*-in. dipped joint (heated at 1,425° C) or a* $\frac{1}{8}$*-in. troweled joint (heated at 1,500° C) was used.*

The excellent properties of the mortar are further illustrated by its appearance after it was heated in the fusion test blocks. Shrinkage is very low and signs of cracking, curling, or flow are entirely absent.

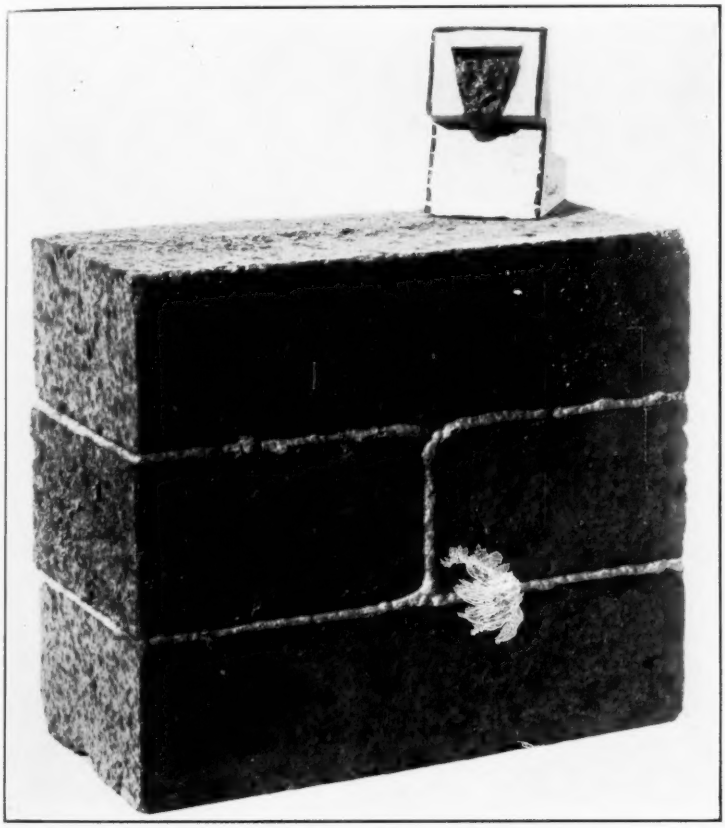

FIGURE 10.—*Mortar 12 used in a pier with ⅛-in. joints and heated at 1,500° C showed bulging.*

The pyrometric cone equivalent of this mortar was 32. However, because the migration of the sodium silicate was high, as was evident both from the edges of the mortar joints and the surface of the mortar in the fusion test blocks, bulging occurred at the edges of the joints.

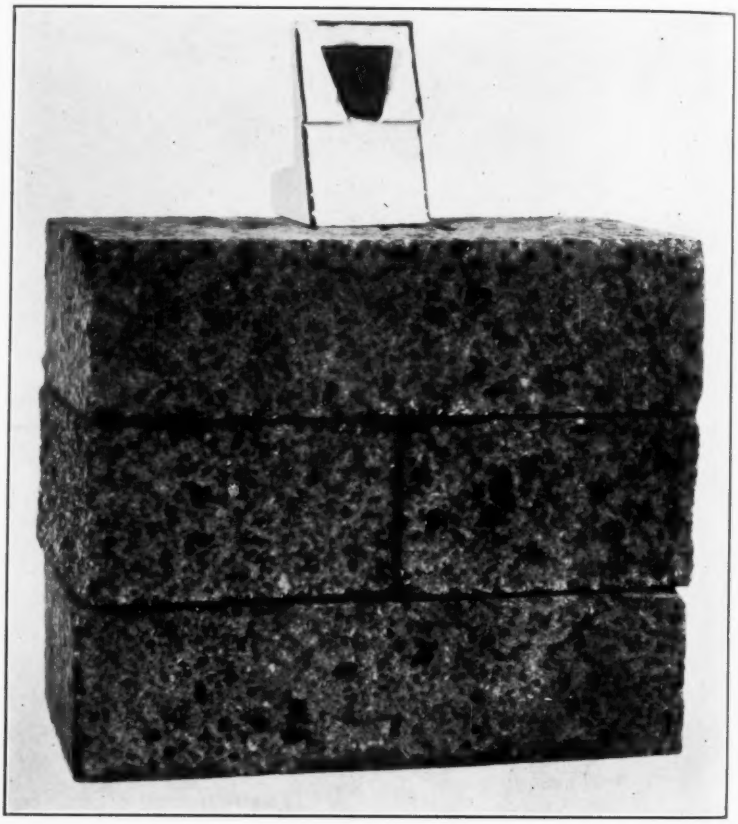

FIGURE 11.—*Mortar 16 showed high shrinkage and cracking after it was heated at 1,500° C in the fusion test block having a ⅛-in. deep compartment.*

The vertical joint in the pier also showed excessive cracking, as did the horizontal joints, although in the latter they are not so apparent.

when it was heated at 1,500° C in a mortar-and-brick assemblage. There is apparently a high degree of migration of the sodium silicate, since there was little indication of fusion below the surface of the mortar in the fusion block. Also, when the brick were separated, the mortar in the interior of the layer showed no visible signs of glassiness. Although the mortar did not flow from the ⅛-in. fusion-block compartment, it did flow as far as the first division from the 7/16-in. compartment in the soaking tests at 1,425° and 1,500° C.

An example of high shrinkage is illustrated by mortar 16 (see fig. 11), in both fusion block (compartment ⅛ in. in depth) and pier, after heating to 1,500° C. In the block the mortar showed both high shrinkage and cracks. A close inspection of the vertical 1/16-in. joint of the pier in the figure will disclose that it is also cracked badly. The ⅛-in. joint was bulged and full of bubbles around the outside of the brick, but the interior of the joint appeared satisfactory.

In some cases a layer or cap of mortar approximately ⅛-in. thick was placed on the outside face of the upper brick to observe the effect of temperature on the exposed mortar. The last column of table 7 describes briefly the appearance of this cap of mortar after the heat treatment. In general, the conclusions reached were in accord with those arrived at regarding the mortars in the piers and in the fusion blocks.

In the fusion-block test, some flow was shown by mortars 4, 9, 12, and 17, the pyrometric cone equivalents of which (see table 1) were 34, 30, 28, and 31, respectively. The flow in these highly refractory mortars was apparently caused by the migration of the silicate of soda to the surface of the mortar, where it reacted with the clay, forming a low-fusing mixture. This surface mixture flowed, but the portion below this surface layer showed very little sign of fusion.

4. STRENGTH TESTS OF SINGLE AND DUPLICATE SHIPMENTS OF MORTARS

It was impracticable to prepare at one time the large number of specimens required for test purposes. Not only were specimens prepared from mortars coming from different containers in the same shipment, but also in some cases, specimens were prepared from shipments of the same mortar received as much as 18 months apart. Since length of storage is generally considered to influence the properties of this type of mortar, it was of considerable interest to learn the extent of the variation in strength between specimens prepared under these conditions. The results of strength tests on such specimens after having been heated at 105° C are given in table 8.

In general, the results are fairly constant for any one brand of mortar, but those of high alkali content appear to show more variation than those of low alkali content. Mortar 21 was especially variable, a considerable difference existing between groups of specimens prepared from the different small containers of the same shipment.

TABLE 8.—*Results of strength tests of the same and duplicate shipments of mortars*

Mortar number	Shipment number	Transverse strength (dried at 105° C)
		lb/in.²
1	1	6,100
1	2	5,125
1	2	5,455
4	1	8,910
4	2	6,470
5	1	1,030
5	1	1,155
6	1	2,260
6	1	2,175
8	1	650
8	2	685
9	1	4,650
9	2	4,455
10	1	4,690
10	1	4,065
13	1	2,640
13		2,700
13		2,960
17	1	4,130
17	1	3,945
19	1	3,440
19	2	3,310
21	1	4,660
21	1	2,890

V. SUMMARY AND CONCLUSIONS

Twenty-three air-setting refractory mortars, marketed in the wet condition and furnished by 20 manufacturers, were subjected to a series of tests, both without the addition of water (troweling consistency) and with the addition of water (dipping consistency), in order to obtain information suitable for preparing a Federal specification covering this commodity. Three of the mortars, received late, were not tested as completely as the other 20, and the summary which follows omits any reference to them.

The condition of the different mortars, after having been in storage for varying periods up to 33 months, was judged by the relative ease with which they could be removed from the container, and with which the segregated liquid and solids could be recombined. Five of the twenty mortars, after having been in storage from 9 to 17 months, had settled to such an extent that remixing them in a mortar box would not have been feasible. After they were remixed, the troweling consistency of 12 mortars was good, 7 fair, and 1 poor. The loss of moisture at 105° C, based on the dry weight of the mortar, ranged from 20.6 to 32.8 percent. The amount of water in the mortars when in a dipping consistency ranged from 26.9 to 51.0 percent. Fifteen of the twenty mortars showed 1 percent or less of residue retained on a No. 40 United States Standard Sieve, and for all the mortars the residue on a No. 100 sieve ranged from 0 to 35 percent. The alkali content, expressed as sodium oxide, ranged from 1.22 to 3.40 percent. The pyrometric cone equivalents of the mortars ranged from 14 to 37. There was very little difference in pyrometric cone equivalents between the calcined and uncalcined mortars, although in some cases the end points of the uncalcined materials were much more difficult to obtain.

A mechanical device was used to classify the mortars as to the comparative ease with which they could be spread or troweled on fire-clay brick. Four tests were made in which both the number of strokes of the trowel and the final thickness of the mortar layer were varied. Six mortars were rated as "very good" in all tests, one "good" in all tests, and the remainder from "very good" through "fair" and "poor," the ratings varying with the individual tests. After drying on the brick, the mortars were rated on their tendency to curl and to crack as follows: "no," "slightly," "moderately," or "badly." Four of the six mortars which rated "very good" in the troweling test showed no cracking or curling on drying. None of the mortars were rated "badly" in both respects, but five rated as such in either one or the other.

The average transverse strengths of the air-set neat mortars ranged from 685 to 6,470 lb/in.^{2} The strength of the test bars was greater in many cases when the surface uppermost during drying was in tension in the breaking test. This effect was caused probably by the concentration of alkali salts (due to migration) near this surface. The change in strengths of the mortars resulting from heating at various temperatures up to 1,350° C and cooling varied with the materials. According to such change in strengths the mortars could be classed as follows: (1) Those of high air-setting strength, which was lowered by heating at intermediate temperatures but raised again, probably because of vitrification, when heated at the highest temperatures; (2) those of high air-setting strength, which was lowered by heating at intermediate temperatures and not further changed by heating, even at the highest temperatures; (3) those of comparatively low air-setting strength, which changed very little with heating at the lower range of temperatures, but increased progressively with heating at moderately higher and the highest temperatures. Most of the mortars were of the first two types. Although not all mortars reached their lowest strengths after being heated at 750° C and cooled, such strengths were, in general, close to the lowest obtained after they were heated over a fairly wide range of temperatures.

The time required for the mortars to air-set, as indicated by their resistance to flow under load, ranged from 1 to 90 minutes when used to bond firebrick of 8.6-percent absorption. Eight mortars set within 1 minute and an additional six set within 3 minutes.

The bonding strength of the mortars in assemblages of two half-brick and mortar was obtained. These assemblages were heated at the same temperatures at which specimens from the neat mortars had been heated. The lowest strength was 5 lb/in.^{2} and the highest 540 lb/in.^{2} In general, a high air-setting strength of the neat mortar presages a satisfactory strength of a brick-and-mortar assembly in cross bending. Failure of the assembly occurred either in the brick, in the mortar, in the joint, or in some combination of these.

Piers of two standard-size brick and two half-brick (making two horizontal and one vertical joint) were made up with ⅛-in. and 1/16-in. joints. After drying, none of the joints showed serious cracking, but after they were heated at 750° C, four were found to have cracked badly. During the heating at 1,425° C many of the cracks visible before the heat treatment healed, but numerous cases of thermal cracking occurred. Heating at 1,500° C caused slippage of the brick in the case of three mortars. The appearance of five mortars was

much better in units made with the 1/16-in. joint than with the 1/8-in. one. Four mortars were practically free from defects in either size of joint.

Examination of the mortars after heating at 1,425° C and 1,500° C in fusion-test blocks gave information relative to shrinkage, cracking, migration of salts and flow because of fusion. This information was in good agreement with observations made of piers of two whole and two half-brick and mortar heated similarly.

The results of this study lead to the conclusion that a specification governing air-setting refractory mortars may be prepared with the assurance that a satisfactory commercial product may be obtained readily in the open market.

WASHINGTON, January 15, 1939.

U. S. DEPARTMENT OF COMMERCE NATIONAL BUREAU OF STANDARDS

RESEARCH PAPER RP1220

Part of Journal of Research of the National Bureau of Standards, Volume 23, July 1939

A SENSITIVE PYRAMIDAL-DIAMOND TOOL FOR INDENTATION MEASUREMENTS

By Frederick Knoop, Chauncey G. Peters, and Walter B. Emerson

ABSTRACT

A sensitive diamond indenting tool was developed which gives indentations of accurately measurable length in the most resistant steels with loads of less than 1 kg. It was found that the use of these light loads permits extension of indentation tests to small specimens and to tests of brittle materials, such as glasses, which shatter under the heavy loads required by present indenters.

The indenter is pyramidal in form, giving a diamond-shaped (rhomb) indentation of which the diagonals have an approximate ratio of 7 to 1 instead of 1 to 1 for the square-based pyramid. Such indenters were duplicated to the required accuracy and showed no discernible wear with use.

Elastic recovery of indentations with this indenter takes place in a transverse rather than a longitudinal direction, and, consequently, from the measured length of the long diagonal and the constants of the indenter, unrecovered dimensions of an indentation are obtained. Results of tests are expressed as indentation numbers which relate the applied load in kilograms to the unrecovered projected area in square millimeters.

Recovered projected areas also, may be determined with an added measurement of the short diagonal. Since knowledge of both recovered and unrecovered dimensions may be obtained, the indenter offers possibilities for study of the fundamentals involved in indentation testing that are not afforded by ball, cone, and square-based pyramidal indenters, which, because of their symmetrical form, yield recovered dimensions only.

The performance of seven indenters of different angular formation was investigated to determine their relative sensitivity and adaptability for use in different materials and to determine also the effect of load and of different dimensional bases of computation on indentation number. Consideration of the results led to the selection of an indenter which gives excellent performance in many materials. Comparison is made of indentation numbers given by this indenter and corresponding Brinell and Vickers numbers for the same specimens.

CONTENTS

	Page
I. Introduction	40
1. Indentation testing	40
2. Forms of indenters	41
(a) Indenters in common use	41
(b) Development of the diamond-based pyramid indenter	41
3. Purpose of this investigation	41
II. Diamond-based indenting tool	42
1. Description	42
2. Production, duplication, and wear	43
III. Preliminary considerations for the indentation tests	43
1. Various indenters used	43
2. Indenting and measuring apparatus	44
(a) Mechanisms for applying loads	44
(b) Apparatus for measuring indentations	44
3. Specimens	45
(a) Materials and specimens selected	45
(b) Size	45
(c) Preparation	45

III. Preliminary considerations for the indentation tests—Con. Page
4. Notes on indenting procedure ... 45
(a) Setting the indenter ... 45
(b) Rate of descent of the indenter ... 45
(c) Contact period ... 45
5. Computation of indentation numbers ... 46
IV. Experimental observations ... 46
1. Types of indentations ... 46
2. Indentation tests of a stainless steel with indenters 4 and 5 under the same load ... 47
3. Effect of load upon indentation number ... 49
4. Indentation tests with elongated pyramidal indenters having different included angles ... 49
(a) Indentation numbers with different indenters, using penetration and unrecovered volume ... 51
(b) Indentation numbers with different indenters, using unrecovered lateral area ... 51
(1) Results with various indenters ... 51
(2) Effect of ridge upon indentation numbers ... 53
(c) Indentation numbers with different indenters, using unrecovered projected area ... 54
(d) Indentation numbers with different indenters, using recovered projected area ... 55
(e) Relation between (c) and (d); w_1/w ratio ... 56
V. Selection of dimensional basis for computation ... 57
VI. Selection of an indenter for general use ... 58
VII. Comparison of the indentation scale of indenter 8 with Brinell and Vickers scales ... 59
VIII. Field of application of the indenter ... 60

I. INTRODUCTION

1. INDENTATION TESTING

The merits of indentation tests which account for their universal application are concisely stated in a recent National Bureau of Standards paper:[1] "The chief value * * * of an indentation test lies in its simplicity, in the fact that it measures a combination of properties that has proved significant in the choice of metals, and that it can be used to check the uniformity of a given product by making and measuring a few indentations in that product." The result of a test is usually expressed as an indentation number, commonly called a "hardness" number, in which the load applied to the indenting tool is related to the lateral area, projected area, depth, or volume of the indentation after the indenter has been removed. Results thus obtained are interpreted as a measure of "hardness," which is defined by Osmond[2] as "the resistance to permanent deformation." However, because of the elastic properties of materials, the dimensions of an indentation may change appreciably upon removal of the loaded indenter. Consequently, it appears somewhat more logical to associate the applied load with dimensions under load, or "unrecovered" dimensions, rather than with those of the final indentation. This is the view favored by O'Neil,[3] since "in this way both the elastic and plastic deformation are incorporated in the test."

[1] Serge N. Petrenko, Walter Ramberg, and Bruce Wilson, *Determination of the Brinell number of metals*, J. Research NBS **17**, 59 (1936) RP903.
[2] M. F. Osmond. Comm. des Méthodes d'Essai des Matériaux de Construction (1895), **3A**, 279.
[3] Hugh O'Neil, The Hardness of Metals and Its Measurement (The Sherwood Press, Cleveland, Ohio, 1934). The development of indentation testing, a description of the various methods, and an extensive bibliography are given.

2. FORMS OF INDENTERS

(a) INDENTERS IN COMMON USE

In the development of indentation methods, many shapes of indenting tools have received attention, and of these the ball, cone, and square-based pyramidal forms, which because of their symmetry yield dimensions of the final indentations only, have come into general use. These indenters have proved applicable to specimens of sufficient size and have the inherent characteristics to withstand the heavy loads required to produce indentations of the magnitude necessary for accurate measurements, but they are of little value in testing brittle materials like glass and small specimens, including thin metal films.

(b) DEVELOPMENT OF THE DIAMOND-BASED PYRAMID INDENTER

One shape of indenting tool which has not been used extensively is the regular pyramid with diamond-shaped (rhomb) base. Earliest use of this sensitive indenter appears to have been by Major W. Wade [4] in 1850–51 for testing the hardness of cast iron. Later, at his suggestion, its use was extended to measurement of the pressure of gas in the bore of a gun by an indentation method devised by Captain T. J. Rodman.[5] In each case the indenter was made of steel. Martel [6] used similar steel tools to determine the hardness of metals by a dynamic indentation method. Restricted dissemination of the excellent results obtained by Wade and Rodman may account for the failure of other investigators to develop further the elongated pyramidal indenter. The indenting diamond, ground to the form of a square-based pyramid by Smith and Sandland,[7] which is, of course, a special case of the elongated pyramidal indenter, seems to be the only later application. Results obtained with diamond indenting tools of the elongated pyramidal shape [8] indicate that this indenter deserves greater recognition in that (1) it makes possible accurate measurements of unrecovered indentations, (2) it extends the application of indentation tests to glass and other brittle materials as well as to specimens of small size, and (3) it permits a better understanding and possible evaluation of elastic recovery and other physical properties which are involved in indentation measurements. Later developments indicate that this indenter may find application in testing fields other than that of hardness. In addition to its use by Rodman for the measurement of gas pressures within guns, its use by H. C. Dickinson and S. A. McKee of the Lubrication and Liquid Fuels Section of the National Bureau of Standards for measuring wear of airplane-engine cylinder walls has increased the measuring accuracy appreciably. These applications may in turn suggest to other workers added uses for these indenting tools.

3. PURPOSE OF THIS INVESTIGATION

The excellent performance of the diamond-based pyramid indenting tool from the standpoint of sensitivity, well-defined indentations, and reproducibility of results, in testing glass and crystals of the Mohs

[4] Reports of experiments on metals for cannon by officers of the U. S. Ordnance Dept., 1856 (Henry Carey Baird, Philadelphia, Pa.).
[5] Reports of experiments on metal for cannon and cannon powder. U. S. Ordnance Dept., 1861. (Chas. H. Crosby, Boston, Mass.).
[6] Martel. Comm. des Méthodes d'Essai des Matériaux de Construction **3A**, 261 (1895).
[7] Smith and Sandland, Proc. Inst. Mech. Eng. **1,** 623 (1922). Smith and Sandland, J. Iron and Steel Inst. **61,** 285 (1925).
[8] Hardness testing device. U. S. Patent 2091995 issued to Frederick Knoop and assigned by him to the U. S. Government.

scale [9] and dental plastics and enamels,[10] appeared to warrant a more extensive consideration of this indenter. The authors believed that its general characteristics could be best developed by the use of indenters with different pyramidal angles in specimens which present the fewest testing complications and which could also be tested with the usual forms of indenters, thus giving the added advantage of direct comparison with other indentation scales. The results of such tests are presented with the hope that they will prove of value to those who require an indenter which is more sensitive than the ball, cone, or square-based pyramid, and one which also yields reliable quantitative indentation measurements with applied loads of less than 1 kg.

II. DIAMOND-BASED INDENTING TOOL

1. DESCRIPTION

The indenting tool consists of a diamond crystal of 0.25 to 1.5 carats rigidly mounted in a metal holder for cutting and use. Figure 1 shows, schematically, one of the shapes used in the present work, together

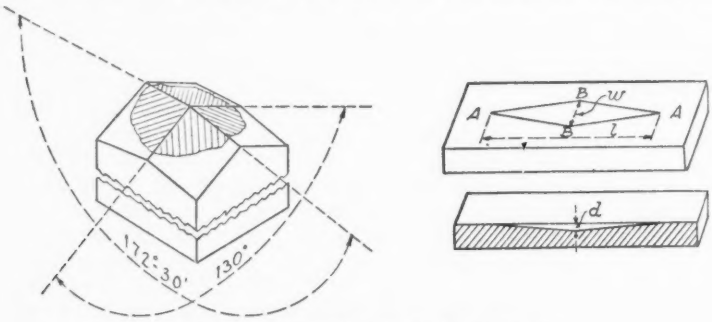

FIGURE 1.—*The diamond indenting tool.*

with its resulting indentation. The sensitivity of this indenter results from its elongated shape, which, for this tool, gives an indentation of length, l, that is about 7 times the width, w, and 30 times the depth, d. From consideration of displacement, it is evident that a specimen under load will be greatly strained at BB and relatively unstrained beyond A, A. This is substantiated by examination of indentations in transparent materials in polarized light and, also, by the appearances of indentations in brittle materials under excessive loads, which show decreasing rupture of the specimens from a maximum at B to none at A. These considerations indicate that the major part of the elastic recovery of an indentation upon removal of the indenter will take place crosswise rather than lengthwise of the indentation. Further, although only the modulus of cubic compressibility of the diamond has been measured, its high value (5.5×10^{12} dynes/cm^2) makes it certain that the relative deformation of a diamond indenter will be small in comparison with the deformation of the indented material. Consequently, from the measurement of a single dimension, l, and

[9] C. G. Peters and Frederick Knoop, *Measurements of relative hardness of glasses*, Glass Ind. **17**, 153 (1936).

[10] George C. Paffenberger, Irl C. Schoonover, and Wilmer Souder, *Dental silicate cements: Physical and chemical properties and a specification*, J. Am. Dental Assn. and the Dental Cosmos **25**, 32-87 (Jan. 1938).

from the indenter constants in terms of l, a close approximation to the unrecovered width, lateral or contact area, projected area, penetration, and volume becomes known; and with an added measurement of the width, w, of the final indentation, the recovered projected area may likewise be determined.

2. PRODUCTION, DUPLICATION, AND WEAR

Previous to this investigation, apparatus had been devised and the necessary technique developed by one of the authors for cutting diamonds to the angular shapes required for indenting tools. These cut diamonds have plane faces which intersect in edges that appear straight and free from the most minute nicks when viewed under a magnification of 75. The angles of these diamonds can be readily measured to the required accuracy, and indenters can be duplicated with an exactness sufficient to give the same results on a given material within the experimental errors. Cut diamonds seem to show little wear when used for indenting purposes; in fact, no wear was discernible in the indenters used in the present work after 2 years' service. The manufacturers of Vickers testing machines find that diamond indenters in continual service require relapping at intervals varying from 6 months to 2 years.

III. PRELIMINARY CONSIDERATIONS FOR THE INDENTATION TESTS

1. VARIOUS INDENTERS USED

In a preliminary endeavor to select a suitable indenting tool for microindentation testing, indenters 1, 2, 3, and 4 were cut with the angles given in table 1, and, of these, indenter 4 was selected for general use. Quarter-carat diamonds were used for these tools, and although they were sufficiently large for microindentation testing, larger diamonds were necessary to meet the requirements of the extended investigation. Indenter 5 is a larger diamond cut to duplicate and to extend the measuring range of 4, and a comparison of the measured angles of the two indenters shows the exactness with which indenter 4 has been duplicated. Indenters 6 and 7 were designed to give added investigational information, and indenter 8 approximates the shape selected on the basis of this study as probably the most suitable for general indentation testing. Constants for these indenters and also for the Vickers indenter of Smith and Sandland are given in the table.

TABLE 1.—*Constants of the indenters*

A_P=projected area.
A_L=lateral or contact area.
p=penetration.
V=volume.
l=length of longitudinal diagonal.
w=length of transverse diagonal.

Indenter	Included angle between edges				Constants, C, relating dimensions with length, l				Ratios		
	Transverse		Longitudinal		$C_P \times 10^3$ $(A_P = C_P l^2)$	$C_L \times 10^3$ $(A_L = C_L l^2)$	$C_p \times 10^3$ $(p = C_p l)$	$C_V \times 10^4$ $(V = C_V l^3)$	Length (l) / Width (w)	Length (l) / Penetration (p)	Lat. area (A_L) / Proj. area (A_P)
	deg	*min*	*deg*	*min*							
1	118	36	175	20	3.43	3.99	2.04	2.33	14.57	49.1	1.164
2	134	15	174	53	5.29	5.75	2.23	3.94	9.44	44.8	1.086
3	126	36	171	42	7.21	8.09	3.63	8.72	6.93	27.6	1.121
4	126	12	173	52	5.28	5.93	2.68	4.72	9.47	37.3	1.123
5	126	6	173	52	5.27	5.92	2.68	4.70	9.49	37.3	1.123
6	136	0	170	44	10.03	10.85	4.05	13.55	4.99	24.7	1.082
7	100	36	170	0	5.27	6.86	4.38	7.68	9.49	22.9	1.303
8	129	40	172	32	6.94	7.69	3.26	7.55	7.20	30.6	1.107
Vickers	148	*7	148	*7	50.00	53.93	14.29	238.2	1.00	7.0	1.079

* The angles between opposite faces of Vickers indenters are 136°.

2. INDENTING AND MEASURING APPARATUS

In making indentation tests, apparatus is required (a) to apply a known load to an indenter at a constant rate of speed and for a definite contact period and (b) to measure the resulting indentations. The devices for making and measuring indentations are frequently incorporated in a single unit to facilitate and expedite the testing. Since in the present case the limiting requirements of these indenters were undetermined, a simple exploratory device for applying loads was constructed for microindentation testing, and advantage was taken of existing commercial testers for applying large loads.

(a) MECHANISMS FOR APPLYING LOADS

The instrument for applying loads up to 0.5 kg to an indenter is shown in figure 2. A calibrated lever arm carries a sliding weight, W. The arm is provided with pivot points near one end and carries indenter, I, at its other extremity. A sliding and elevating specimen holder is shown at H. The indenter is raised to its correct position above the specimen by a cam-and-lever arrangement which lifts piston rod, R, of dashpot, P. The rate of uniform descent of I is controlled by a valve in P. The whole assembly is mounted on a base provided with levels and levelling screws.

Loads of 10 to 45 kg were applied by means of commercial dead-weight machines made available through the courtesy of the Engineering Mechanics Section of the National Bureau of Standards; and to span the range 0.5 to 10 kg, the arm of the small instrument was heavily weighted to give fixed loads of 1, 2, and 4 kg.

(b) APPARATUS FOR MEASURING INDENTATIONS

Lengths and widths of indentations were measured by means of a micrometer microscope. Its sensitivity was such that one to six divisions (depending upon the microscope objective) on the screw head

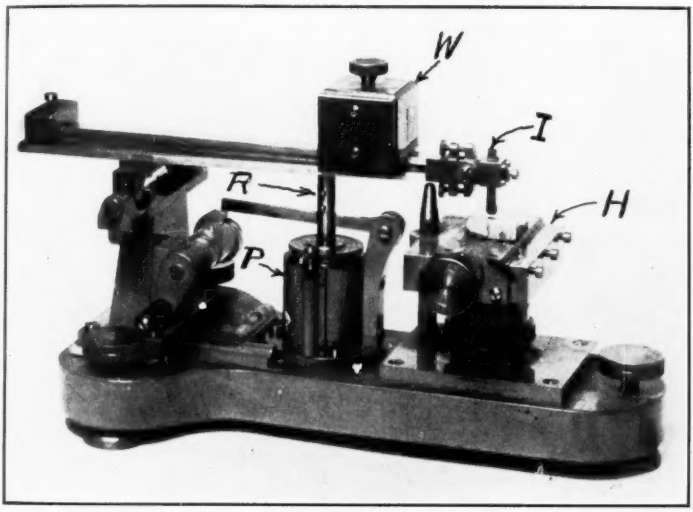

FIGURE 2.—*Indenting apparatus for light loads.*

UNIV. OF MICH.

were equivalent to 1 μ. The micrometer screw was calibrated with a steel line standard ruled by light waves. A green filter within the vertical illuminator eliminated eyestrain.

3. SPECIMENS

(a) MATERIALS AND SPECIMENS SELECTED

The following materials and specimens were originally selected for test:

Material	Specimen
Steel	Rockwell test blocks *C 25, C 47, C 65–67.* NBS, gage blocks 1 and 2.
Brass	Rockwell test block *B 7–9.*
Copper	Rolled.

Specimens of medium flint glass, cast and electrolytic copper, cast and rolled platinum, cast and rolled gold,[11] cast aluminum, cast tin, and stainless steel were also used during the investigation. Since interest lay in the performance of the indenters rather than in a study of materials, the chemical composition of the specimens was not determined.

(b) SIZE

All specimens were sufficiently large so that differences in indentations could not be attributed to the size of the specimens.

(c) PREPARATION

Surfaces were lapped and polished plane and free from scratches to increase the accuracy of measurement and to avoid differences in indentation determinations which might result from surface irregularities with the light loads and small resulting penetrations in some of the tests.

4. NOTES ON INDENTING PROCEDURE

(a) SETTING THE INDENTER

The direction of motion of the indenter was made normal to the surface of the specimen by means of suitable adjustments. The symmetry of an indentation is a critical indication of the proper setting when regular indenters and plane specimens are used. Some lack of symmetry may be in evidence without affecting appreciably the indentation numbers.

(b) RATE OF DESCENT OF THE INDENTER

The rate of descent of the indenter was varied from 36 mm/min to 1 mm/min for each material. Indentation results were the same for rates not exceeding 18 mm/min (which for the mechanism used was equivalent to a descent of 3 mm in 10 sec); therefore, this 18 mm/min rate was adopted for all tests.

(c) CONTACT PERIOD

The time that indenter and specimen remained in contact was varied from 10 sec to 4 min. This type of indenter appears to reach static equilibrium quite rapidly, and no change in indentation number occurred in the more resistant materials after 20 sec; the decrease for

[11] These specimens were actually rolled from gold castings. "Rolled gold" has a somewhat different meaning in the jewelry trade.

rolled gold was about 1 percent when the contact time was increased from 20 sec to 120 sec, and was less than 4 percent for cast copper when the time was increased from 20 sec to 4 min. A contact period of 20 sec was selected as standard for testing all materials.

5. COMPUTATION OF INDENTATION NUMBERS

Indentation results are expressed in the form of numbers which relate the unrecovered projected areas to the loads applied to the indenters. Or

$$I=\frac{L}{A_P}=\frac{L}{l^2C_P},$$

in which:

I=indentation number.
L=load (in kilograms) applied to the indenter.
A_P=unrecovered projected area of the indentation (in square millimeters).
l=measured length of the long diagonal of the indentation (in millimeters).
C_P=constant relating l to the projected area.

The indentation number corresponding to a measured length, l, for a given load and a given indenter may be read from a chart.

Reasons for selecting the unrecovered projected area for computational purposes and consideration of some of the factors which may affect the indentation numbers are developed in succeeding pages.

IV. EXPERIMENTAL OBSERVATIONS

1. TYPES OF INDENTATIONS

In general, the types of indentations for various materials may be classified according to the contour of the surface adjacent to the ends of the transverse diagonal; namely, type *A*, those having a definite ridge; type *B*, those having no visible disturbance of the original surface level; and type *C*, those in which the surface level appears depressed.

Type *A* is shown in figure 3 (*A*). Height, h, of the ridge decreases from a maximum at the ends of the transverse diagonal to zero as it approaches the ends of the longitudinal diagonal. Lateral boundaries of the elevated surfaces are shown for rolled copper and for *C 25* steel in figure 4. Optical tests show that the greatest height of the ridge is at the immediate edge of an indentation.

Although no disturbance of the surface surrounding a *B*-type indentation is visible by microscopic inspection, interferometric examination shows a slight uniform elevation extending over a considerable area as in figure 3 (*B*). A slight sinking of the surface at the immediate edge of the indentation is indicated in some materials. The height of the raised surface is small compared to the penetration of the diamond for this class of indentation. The general outline of the disturbed surface of a specimen of tin can be seen in the upper photograph of figure 5. The fine scratches at 45° to the long diagonal show the original lapped surface. After the indentation had been made, the surface was again lightly lapped at right angles to the indentation. The fine lap marks in this direction show the outline of the raised area. This (shown more definitely at the left of the indentation)

corresponds approximately with the outline of the strain patterns of indentations in glass when viewed in polarized light, and, also, with the shape which fractures tend to take when a brittle specimen is shattered by a heavily loaded indenter.

In type-*C* indentation the surface for a considerable distance beyond the ends of the short diagonal is depressed as in figure 3 (*C*). This type is recognized in the microscope by the inability of an observer to obtain a sharp focus for width measurements and may be illustrated by the lower photograph, figure 5, for cast gold. Here again the diagonal scratches represent the original surface. These scratches remain in the sunken-in material adjacent to the indentation, whereas the raised surrounding area shows the lap marks at right angles to the indentation.

It seems well to call attention to the marked decrease in width relative to length of indentations in elastic materials. With one exception, all indentations in figure 6 were made with the same indenter, and by comparing the indentations in glass and hardened steel with those in the less elastic stainless steel, narrowing of the indentation is readily seen.

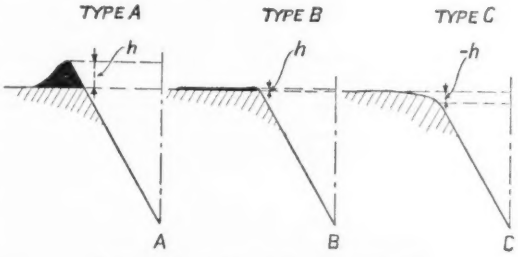

FIGURE 3.—*Types of indentations.*

The appearance of indentations obtained with several types of indenters by the application of light loads is shown in figure 7. The faint circular mark at the extreme right of the lower photograph (glass) results from the application of 2 kg to a Brale indenter. All indentations in steel were made by indenters under the same load (1 kg); consequently, the photograph illustrates the relative sensitivity of the various indenting tools.

Indentations with ball, cone, and square-based pyramidal indenters are usually classified as "ridging" and "sinking-in" types, and the type of indentation is commonly associated with the capacity of a specimen to be work-hardened. With the present indenter the demarcation of types is not distinct for metals, and cold-working of such materials as cast gold, platinum, and copper changes the indentations from a nonridging or sinking-in type to a ridged indentation.

2. INDENTATION TESTS OF A STAINLESS STEEL WITH INDENTERS 4 AND 5 UNDER THE SAME LOAD

Measurements of the included angles of indenters 4 and 5 showed them to be alike in a longitudinal direction and to differ by 6 min in a transverse direction. Tests were made to determine the differences in indentation numbers that would result from the substitution of one indenting tool for the other, to show the uniformity in length of indentations produced by a given indenter, and to show, also, the spread in length measurements of an indentation by the same and by different observers. The tests were made on an inclusion-free 14-percent-chromium stainless-steel specimen which was carefully heat-treated and polished to a plane optical surface. Five indentations

were made with each indenter under a 4-kg load, and four measurements of the length of an indentation were made by each of two observers.

The results of the test are presented in table 2. Observer *A* obtained an indentation number with indenter 4 that was 0.3 percent greater than that obtained with indenter 5, whereas observer *B* obtained a number with indenter 4 which differed from that obtained with indenter 5 by less than 0.05 percent. The values by *A* were 0.4 percent greater than those by *B* using indenter 4, and 0.2 percent greater using indenter 5. The spread of readings by these two observers is of approximately the same magnitude as that of a larger group on another steel specimen. The individual indentations with a given indenter appear to be uniform in size within the limits of measurement. The data indicate that the difference, if any, in indentation numbers with indenters 4 and 5 is small and is masked by the uncertainties of measurement by the same or by different observers.

TABLE 2.—*Indentation tests of a stainless-steel specimen*

[Indenters 4 (C_P=0.05280) and 5 (C_P=0.05268); applied load, 4 kg; l=measured length of an indentation I=indentation number]

Values with indenter 4					Values with indenter 5				
Indentation measured	Observer *A*		Observer *B*		Indentation measured	Observer *A*		Observer *B*	
	l	*I*	*l*	*I*		*l*	*I*	*l*	*I*
	μ		μ			μ		μ	
First	391.6	494.0	391.6	494.0	First	393.7	489.9	393.4	490.6
	391.6	494.0	392.0	493.0		393.7	489.9	393.0	491.6
	391.6	494.0	391.6	494.0		394.1	488.9	393.0	491.6
	391.6	494.0	391.6	494.0		393.7	489.9	393.4	490.6
Mean		494.0		493.8	Mean		489.7		491.1
Second	391.6	494.0	393.0	490.5	Second	391.6	495.1	392.0	494.1
	391.6	494.0	392.3	492.3		391.3	495.9	392.3	493.4
	391.6	494.0	392.7	491.3		392.0	494.1	392.3	493.4
	392.0	493.0	392.3	492.3		392.3	493.4	392.0	494.1
Mean		493.8		491.6	Mean		494.6		493.8
Third	391.6	494.0	393.0	490.5	Third	392.7	492.4	392.3	493.4
	392.0	493.0	392.3	492.3		393.0	491.6	393.0	491.6
	391.3	494.8	392.7	491.3		393.7	489.9	393.4	490.6
	392.7	491.3	393.0	490.5		393.0	491.6	393.0	491.6
Mean		493.3		491.2	Mean		491.4		491.8
Fourth	391.3	494.8	393.0	490.5	Fourth	391.6	495.1	393.4	490.6
	392.3	492.3	392.3	492.3		392.3	493.4	393.0	491.6
	391.3	494.8	392.3	492.3		391.6	495.1	392.7	492.4
	392.3	492.3	393.0	490.5		392.3	493.4	393.0	491.6
Mean		493.6		491.4	Mean		494.3		491.6
Fifth	391.3	494.8	393.0	490.5	Fifth	392.3	493.4	393.4	490.6
	391.6	494.0	393.0	490.5		392.0	494.1	393.4	490.6
	391.3	494.8	392.7	491.3		393.0	491.6	393.4	490.6
	390.9	495.8	393.0	490.5		392.3	493.4	393.0	491.6
Mean		494.9		490.7	Mean		493.1		490.9
Average of means		493.9		491.7	Average of means		492.6		491.8

Observer	*I* (indenter 4)	*I* (indenter 5)	*Difference* (percent)
A	493.9	492.6	0.3
B	491.7	491.8	.0
Mean	492.8	492.2	0.1

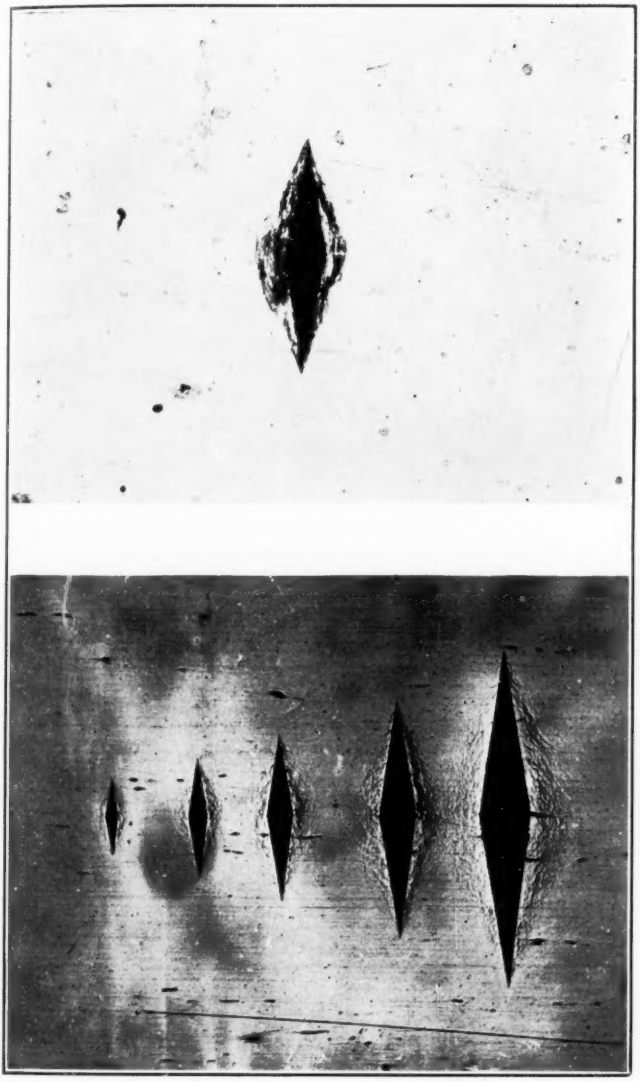

FIGURE 4.—*Type A indentations.*

Upper, rolled copper; indenter 8; load, 4 kg; magnification, ×50. Lower, *C25* steel; indenter 8; loads—0.2, 0.5, 1.0, 2.0, and 4.0 kg; magnification, ×100.

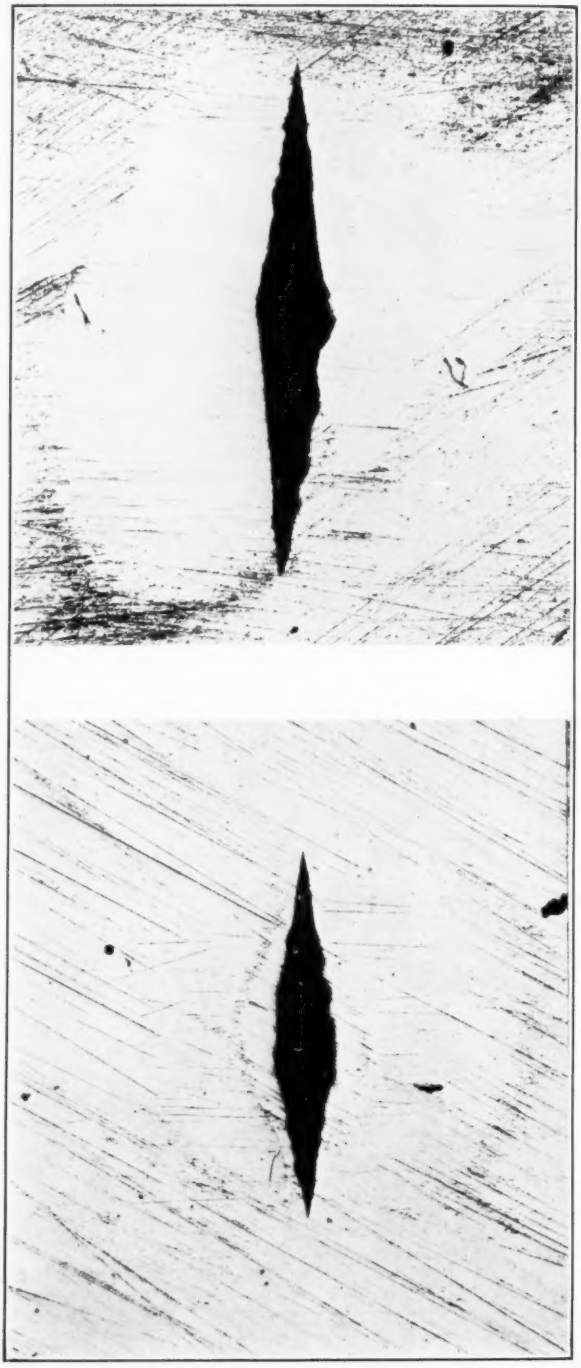

FIGURE 5.—*Type B and type C indentations.*

Upper, tin; type *B*, magnification, ×35. Lower, cast gold; type *C*, magnification, ×35.

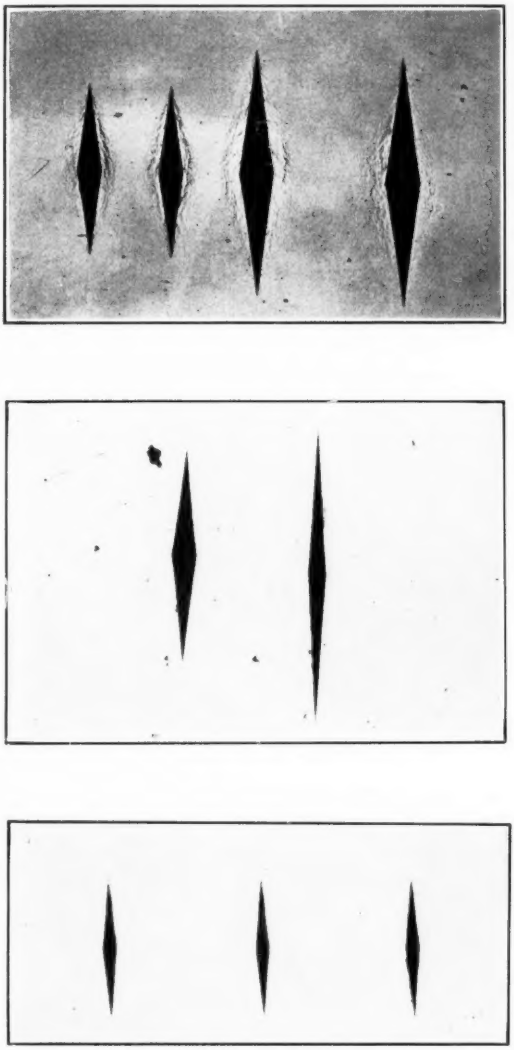

FIGURE 6.—*Indentations in specimens having different elasticities.*

Upper, stainless steel; indenter 8; loads, 2 and 4 kg; magnification, ×100. Central, *C65–67* steel; left, indenter 8; right, indenter 1; load, 4 kg; magnification ×110. (Although the indentation on the right shows indenter 1 to be extremely sensitive, its use in elastic materials is to be avoided. Because of the transverse recovery, the end sof indentations are not sufficiently abrupt to be fully resolved. Greater measuring accuracy may be obtained with a less sensitive indenter having a smaller l/w ratio.) Lower, medium flint glass; indenter 8; load, 1 kg; magnification, ×100.

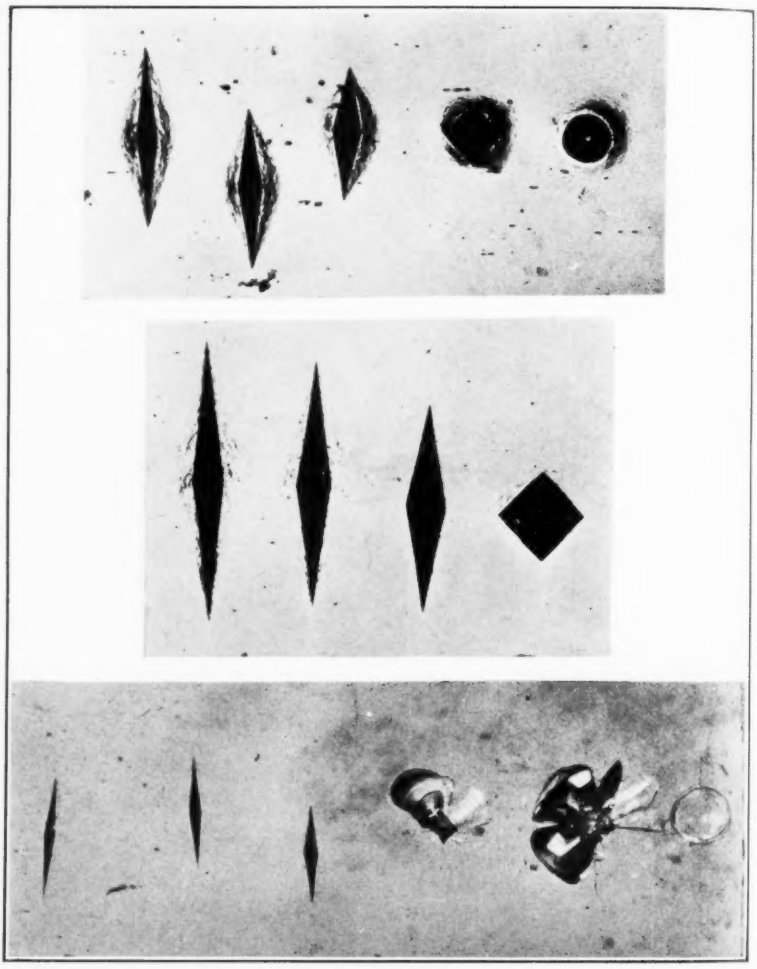

FIGURE 7.—*Indentations with different indenters.*

Upper, *C25* steel; indenters 4, 8, 6, Vickers, and Brale; load, 1 kg; magnification, ×50. Central, stainless steel; indenters 4, 8, 6, and Vickers; load, 1 kg; magnification, ×100. Lower, medium flint glass; indenters 4, 8, 6 (1 kg), Vickers (0.5 and 1.0 kg), and Brale (2 kg); magnification, ×90.

3. EFFECT OF LOAD UPON INDENTATION NUMBER

Indentation numbers were determined for specimens of steel, copper, and glass with loads of 0.1 to 4.0 kg, using indenter 4 with an 18 mm/min rate of descent and a 20-sec contact period. Five indentations were made for each load and the mean value was used for computing. All indentations were sharply defined at the ends of the long diagonals. Length readings by the same or by different observers usually agreed to 1 μ, and adjacent marks gave the same uniformity; but indentations scattered over the surface indicated a lack of homogeneity of 2 or 3 percent for some specimens. To extend the range of the tests, loads up to 45 kg were applied to specimens by indenter 5, which was inserted in Rockwell and Vickers testing machines.

The results of the tests, table 3, appear to give either a decrease in indentation number with load or a surface hardness effect for light loads in several specimens. However, more uniform results were obtained from lengths measured with a microscope having greater

TABLE 3.—*Variation of Indentation Number with Applied Load*

[Indenter 4, 0.1 to 4.0 kg; indenter 5, 15.0 to 45.0 kg]

Applied load	Lengths of indentations and indentation numbers													
	Rolled copper		Steel *C 25*		Glass, med. flint		Steel *C 47*		Steel gage 1		Steel gage 2		Steel *C 65–67*	
	l	*I*	*l*	*I*	*l*	*I*	*l*	*I*	*l*	*I*	*l*	*I*	*l*	*I*
kg	μ		μ		μ		μ		μ		μ		μ	
0.1	124.5	122	82.5	278	69.2	395	62.5	485	51.7	708	47.6	835	46.6	872
0.2	176.0	122	117.4	275	100.2	377	88.1	488	74.3	686	66.9	846	67.4	834
0.3	214	125	143.7	275	123.6	372	108.0	487	90.8	689	82.5	834	82.6	833
0.4	248	124	163.9	282	142.4	373	124.8	486	104.6	693	95.5	831	95.8	825
0.5	276	125	184.6	278	160.4	368	139.4	487	117.9	681	107.6	818	107.7	816
1.0	393	126	263	282	231	365	198.8	494	171.5	663	155.8	804	155.1	811
2.0	550	126	367	282			276	497	240	659	218	797	216	812
4.0	783	124	524	276			392	493	342	649	311	782	307	804
15.0	1,513	125	1,005	282			759	494	669	635	606	775	597	800
30.0			1,425	281			1,077	491	944	639	857	775	846	795
45.0							1,321	490			1,054	768	1,037	795

magnification, thus indicating that ends of the indentations may not have been fully resolved even with the higher power. This effect was noticeable only in materials, such as hard steel and glass, in which elastic recovery (and hence, transverse contraction) of indentations was large. Inability to resolve the final micron ending of a 100 μ-indentation would cause an apparent increase in indentation number of 4 percent, and this error would be increased for shorter indentations. To minimize the end effect, it is desirable to use loads (for example: 0.1 kg for rolled copper and 0.5 kg for *C 65–67*) which will give indentations of at least 100 μ, length. Minute nicks in an early indenter gave a similar false effect of surface hardness. The curves, figure 8, which are based upon measured lengths greater than 100 μ, show that indentation numbers do not vary appreciably with load. The small differences shown by some specimens may be attributed either to a variation with load or to a slight surface hardness.

4. INDENTATION TESTS WITH ELONGATED PYRAMIDAL INDENTERS HAVING DIFFERENT INCLUDED ANGLES

Indentation tests were made on the selected specimens with the different indenting tools to determine the variation in indentation number for indenters of different angular shape, and, at the same

time, to give additional observational data on the characteristics of the tools in various materials. Tests were made with loads of 1 and 4 kg using indenters 1, 2, 3, and 4, and with loads of 4, 15, 30, and 45 kg, using indenters 5, 6, 7, and 8 whenever the size of the diamond and the resistance of the specimen permitted the use of large loads. (Results with indenter 5 will be recorded as extensions of measurements with indenter 4, since the two indenters yield the

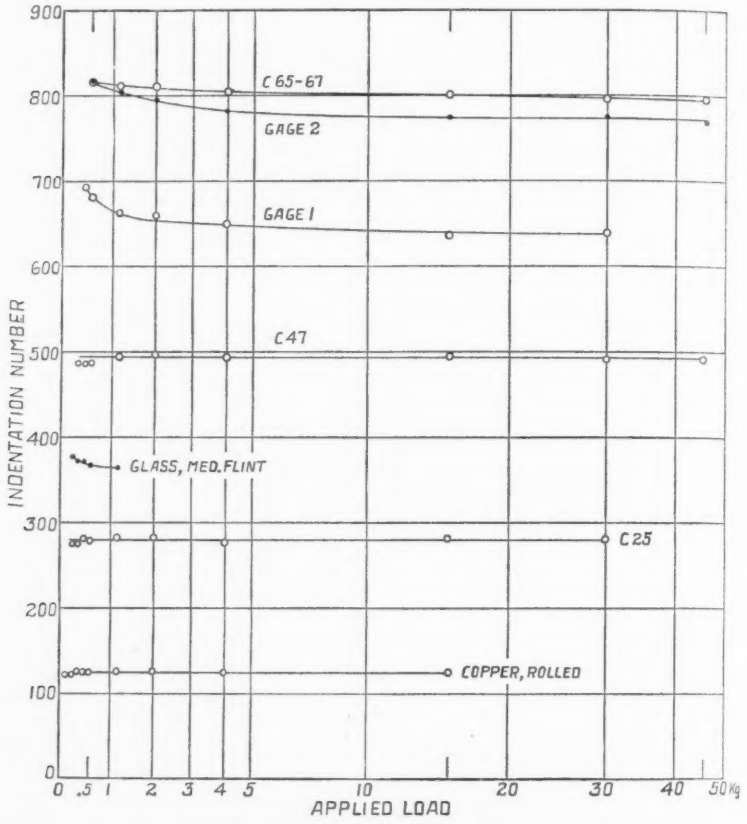

FIGURE 8.—*Effect of load on indentation number.*

Indenter 4, to 4 kg; indenter 5, from 15 to 45 kg.

same indentation numbers.) Indentation numbers with a given indenter and specimen were found to change but slightly with loads which exceeded 4 kg, yet, for consistency, comparison of results with different indenters was based upon tests with a 4-kg load whenever possible.

There seems to be no unanimity of opinion as to which dimension of an indentation should be used for computing indentation numbers. Present tests were computed on each of several bases which are available with elongated pyramidal indenters: namely, volume of material displaced by the indenter; penetration of the indenter; lateral area (contact area of indenter and specimen); unrecovered projected area;

and recovered projected area. The results of the tests were compiled in the form of curves that show the change in indentation number with angular shape of the indenter, using different bases of computation—the purpose being that data so presented might aid in establishing a dimensional basis for calculating indentation numbers.

(a) INDENTATION NUMBERS WITH DIFFERENT INDENTERS, USING PENETRATION AND UNRECOVERED VOLUME

Various formulas were used for computing indentation numbers on the basis of penetration of the indenter and of volume of material displaced. Relations $I=kg/p^2$(in mm) and $I=\sqrt{kg}/p$ for penetration computations and $I=kg/V$ (in $mm^3)^{2/3}$ and $I=(kg)^{3/2}/V$ for volume computations gave indentation numbers which remain constant for different loads with a given indenter. Figures 9 and 10 give the difference in percentage of numbers obtained with a given indenter from those with indenter 4, which was selected as a reference standard. The abscissas have no meaning except to show the spacing of the various specimens in the indentation scale of indenter 4. Actual indentation numbers for a given indenter may be obtained by increasing the value for 4 by the percentage difference given by the ordinates.

The differences in indentation numbers (fig. 9) result from the rela-

FIGURE 9.—*Indentation numbers based on penetration* ($I=\sqrt{load}/penetration$).

Ordinates are the percentage differences in indentation number with other indenters from those with indenter 4.

tive differences in penetration of the various indenters for a given load. The effect of these differences in penetration is reflected, also (fig. 10) in the volume computations, giving greater volumes and smaller numbers for indenters which penetrate deeply. Vickers numbers were determined by the Mechanical Metallurgy Section of the National

Bureau of Standards, and, from these, penetrations and volumes were computed. Since there was evidence of strain in the specimens at the ends of the diagonals of the Vickers indentations, and, hence, possible elastic recovery, the Vickers numbers may not be strictly unrecovered values and, therefore, not truly comparable with those computed on the basis of unrecovered dimensions for elongated pyramidal indenters.

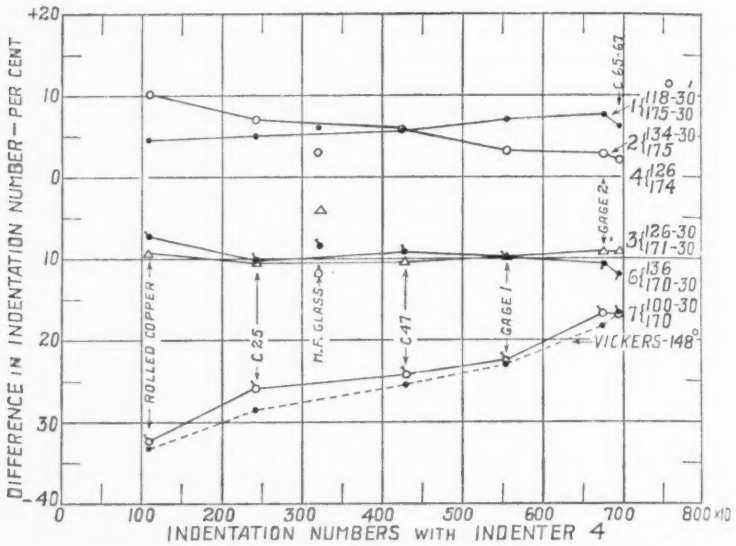

FIGURE 10.—*Indentation numbers based on volume* ($I = load/(volume)^{2/3}$).

Ordinates are the percentage differences in indentation number with other indenters from those with indenter 4.

The authors were unable to correlate the large differences in indentation number obtained with the different indenters with differences in the angles of the indenters using these methods of computation. *Areas* appear to be more directly related to applied loads in static indentation tests than either penetration or volume.

(b) INDENTATION NUMBERS WITH DIFFERENT INDENTERS, USING UNRECOVERED LATERAL AREA

(1) *Results with various indenters.*—On the basis of unrecovered lateral area (fig. 11) indenters 3, 4, and 6 give the same values within the errors of measurement and the homogeneity of the specimens in the range of rolled copper to *C 65–67* steel. "Flat" indenter 2 tends to give the same numbers in the lower range and lower numbers in the upper range, whereas the opposite is true of acute indenters 1 and 7. Tests of rolled gold and rolled platinum were made to show the general trend in the lower range, but, because of the nonuniformity of the specimens, the results are not considered reliable to several percent. Later tests on the original specimens gave about the same values for indenter 8 that were obtained with indenters 3, 4, and 6. Vickers values are also included.

Indentation numbers were also determined for specimens of cast tin, aluminum, gold, platinum, and soft brass which yielded nonridging and sinking-in indentations. These specimens gave evidence of surface hardness, probably caused by cold-working during the preparation of the specimens, that confused the results. Better comparative determinations must await the preparation of more uniform specimens. The mean results with these cast materials gave the arrangement for the various indenters which is shown by the dotted lines, but because of the inhomogeneity of the materials no great credence should be given to the values for these cast materials.

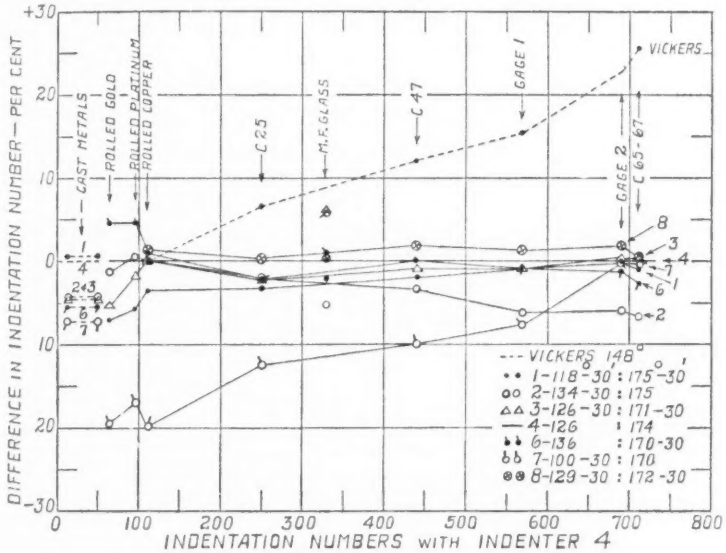

FIGURE 11.—*Indentation numbers based on unrecovered lateral area.*

Ordinates are the percentage differences in indentation number with other indenters from those with indenter 4.

(2) *Effect of ridge upon indentation numbers.*—The rolled gold, platinum, copper, and steel specimens gave ridged indentations, and it was considered probable that indentation numbers might be greatly affected by the support the indenter received from the ridged material, which, for the rolled copper specimen, gave an added supporting area of 30 percent for indenter 7. Examination of the ridge showed it to be of ruptured material which was easily removed by light polishing. The following tests were made to determine the amount of support which indenter 8 received from the ridge in a specimen of rolled sheet copper. Preliminary measurements showed that the copper was of uniform hardness; that no measurable change in indentation lengths occurred with contacts exceeding 20 sec; and that reinsertion of the indenter in the welted indentation gave no increase in length. Lengths and widths of the indentations were measured and the maximum height of the ridge was determined interferometrically. From these, the area of contact of indenter and elevated material was determined to be 18 percent of the unrecovered

lateral area as computed from the length measurements. Next, another indentation was made; the elevated material was removed by light polishing in place; and the load was applied to the ridgeless indentation. Repeated trials showed that the increase in length after removal of the ridge did not exceed 0.5 percent. Thus, while the elevated material added 18 percent to the lateral area, it actually supported less than 1 percent of the load. The same disproportionate effect of excess area and supporting force was found for steel gage 1. Since the required correction was less than the differences in uniformity of most of the specimens, no corrections for ridge were applied to the computed lateral areas.

(c) INDENTATION NUMBERS WITH DIFFERENT INDENTERS, USING UNRECOVERED PROJECTED AREA

Figure 12 presents the results of the same experimental data computed on the basis of unrecovered projected area. Indentation num-

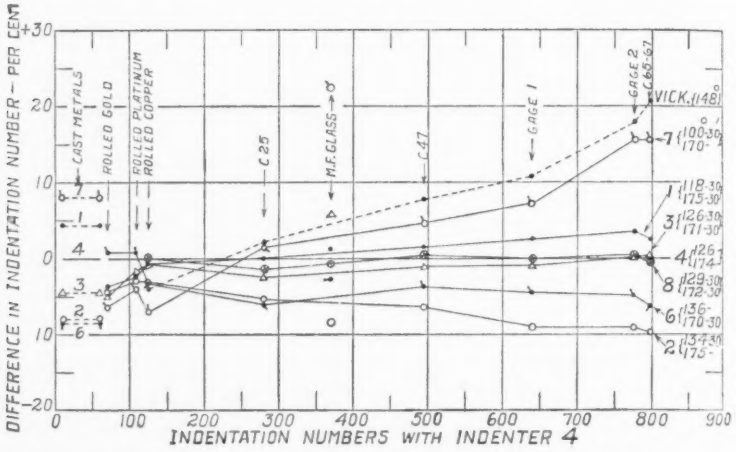

FIGURE 12.—*Indentation numbers based on unrecovered projected area.*

Ordinates are the percentage differences in indentation number with other indenters from those with indenter 4.

bers with the different indenters tend to approach the same values for inelastic materials, giving type-*A* indentations, and to depart for the more elastic materials, differences in elasticity being indicated by the transverse recovery of indentations. This departure seems to be definitely related to the indenter shape, with acute indenters giving progressively greater numbers for the more elastic materials. The transverse angle appears to be the effective angle to be related to difference in indentation number, although its action may be modified by the longitudinal angle, as shown by indenters 2 and 6. Values for the Vickers indenter are included, although, in view of the increasingly greater elastic recovery for specimens in the upper range, it is quite possible that the curve for the square-based pyramid might fall below that of indenter 7 if actual unrecovered areas were used. An orderly arrangement appears even in the questionable results (broken lines) with cast materials. The resistance to indentation of these cast materials increases greatly with mechanical working, and to what extent the difference in strain-hardening of the present specimens

by the various indenters contributes to the orderly arrangement shown in figure 12 has not been determined.

The results appear to indicate that some factor or combination of factors based upon angular shape might be applied which would bring the results of all indenters into agreement.

(d) INDENTATION NUMBERS WITH DIFFERENT INDENTERS, USING RECOVERED PROJECTED AREA

Indentation numbers based on recovered projected areas were determined from the measured lengths and the measured widths of the indentations which were used in previous computations. The percentage differences in indentation numbers with the various indenters are plotted (fig. 13) relative to indenter 4. No comparative data are

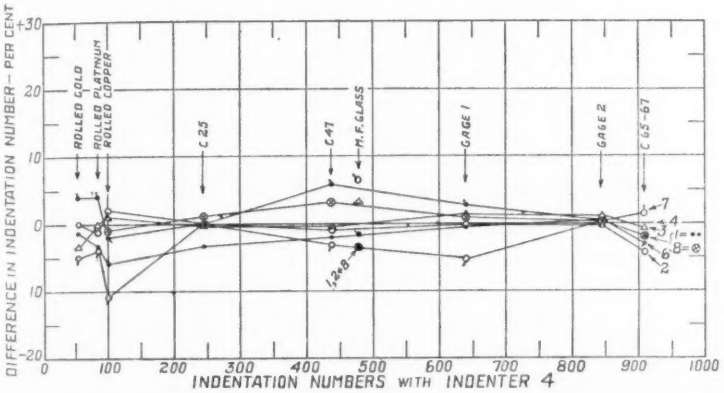

FIGURE 13.—*Indentation numbers based on recovered projected area.*

Ordinates are the percentage differences in indentation number with other indenters from those with indenter 4.

available for the Vickers indenter. The curves indicate a better agreement of indentation numbers for the different indenters in the more elastic specimens on this basis than on the basis of unrecovered projected area. The errors of measurement are greater, however, because of the small magnitude of the widths and because of the greater uncertainty in measuring diagonals which end in disrupted surfaces. For rolled copper, on which exceedingly high ridges were raised by indenters 1 and 7, the width of the indentations could not be measured with great exactness. Because of doubt as to the comparable accuracy of the indentation measurements for medium flint glass, which were obtained with an applied load of only 1.0 kg, with those of other specimens, values for flint glass were plotted but not included in the curves (figs. 11 and 12). It is of interest to note, however (fig. 13), the closer agreement of numbers with the several indenters for the glass on the basis of recovered projected area than on the basis of unrecovered projected area, and to note, also, the relative position of the glass in this indentation scale. Because of its great elastic return, the glass appears "harder" than *C 47* steel on the basis of recovered dimensions, whereas the latter was the more resistant on the basis of unrecovered dimensions.

(e) RELATION BETWEEN (c) AND (d): w_1/w RATIO

The authors would like to call the attention of those interested in theoretical considerations involved in indentation measurements to certain data collected during the investigation: namely, the ratio of the measured width, w_1, of the recovered indentation to the width, w, of the unrecovered indentation as calculated from the measured length and the indenter constants. The w_1/w ratios for the different materials and indenters are arranged in table 4 in the order of the acuteness of indenters, indenter 7 being the most acute. These are the factors which relate the indentation values of figure 13 with those of figure 12. The interesting facts brought out in table 4 are that (1) the ratios for a given indenter decrease for the more elastic materials, (2) the difference in ratio for different indenters is small, for a given material like rolled gold, and (3) the ratios decrease (the apparent elastic recovery is greater) for the more elastic materials with obtuse indenters. It must be noted that w_1/w is not a direct measure of the elastic return across the transverse diagonal of indentations of the ridged and sinking-in types. In order to determine the actual recovery at surface level of a ridged indentation in soft-rolled copper, the recovered width was measured after removal of the ridge. This gave a ratio of recovered width to calculated width of 1.00 (no recovery) instead of a determined w_1/w value of 1.14. Also, the height of the ridge of an indentation by indenter 5 in steel gage 1 was measured by an interference method and the unrecovered width at the top of the ridge was calculated, giving a ratio of recovered to unrecovered width at that level of 0.87 (13-percent recovery) instead of a w_1/w ratio of 0.98. Although these tests were not extended to other specimens, they show the practicability of obtaining the actual transverse recovery of indentations—a factor which appears to greatly influence the w_1/w values.

TABLE 4.—*Ratio of measured width to calculated width w_1/w with different indenters in various specimens*

Indenter	w_1/w for different specimens								
	Rolled gold	Rolled platinum	Rolled copper	Steel *C 25*	Steel *C 47*	Steel gage 1	Steel gage 2	Steel *C 65–67*	Glass med. flint
7	1.32	1.28	1.31	1.17	1.22	1.13	1.06	1.00	0.90
1	1.31	1.30	1.31	1.19	1.17	1.03	0.95	0.92	.82
8	1.34	1.28	1.25	1.12	1.10	0.99	.92	.89	.80
4	1.34	1.29	1.24	1.15	1.13	1.00	.92	.88	.78
3	1.32	1.27	1.22	1.13	1.12	0.99	.91	.88	.80
6	1.30	1.25	1.22	1.08	1.03	.93	.87	.85	.77
2	1.29	1.27	1.17	1.09	1.07	.91	.84	.83	.74

Heyer[12] offers an explanation for the differences commonly observed in the contours of Brinell indentations which is based upon the relative strengths in shear and compression of the specimens. With indenters having different angles, the applied stresses will doubtlessly be distributed to give differences in the effective frictional forces, in the deformation of the diamonds, in the strain-hardening of the specimens, in the amount of material disrupted, and in the elastic recovery of the indentions. The integration of the forces acting results in the final form and size of the indentations, and it is conceivable that the w_1/w ratio may have physical significance in relating

[12] Robert H. Heyer, Proc. Am. Soc. Testing Materials **37**, pt. 2, 119 (1937).

angular shapes of the indenters to the distribution of stresses in indenters and specimens, which produces the final indentations.

The authors are impressed with the orderly arrangement of the w_1/w values in table 4 and believe that further study with carefully selected and more uniform materials will lead to a better understanding of the factors involved in correlating the indentation numbers obtained on the basis of unrecovered projected area for the different indenters. The possibility of associating these w_1/w ratios with the work-hardening capacity of a material also presents a field for investigation.

V. SELECTION OF DIMENSIONAL BASIS FOR COMPUTATION

From preceding considerations it is evident that, with a given indenter, indentation scales can be derived which are based upon the ratio of applied load to any dimension (linear, surface, or volume) of recovered or unrecovered indentations. The authors prefer to define the indentation number as the ratio of the applied load to the *unrecovered* projected area, thereby incorporating both elastic and plastic deformation in the test.

Linear dimensions and volumes of indentations were rejected as bases of computation because, although these gave agreement for a given indenter under varying loads when the square of linear dimensions or the 2/3 power of volumes was used, the results with different indenters could not be correlated. Areas (lateral or projected) appear to be more directly related to applied loads than either penetrations or volumes.

It should be understood that indenters which produce circular or square-based indentations furnish measurements of recovered (permanent) deformation only. With the elongated pyramidal indenters all dimensions of an unrecovered indentation can be obtained from the shape of the diamond and the measured length of an indentation. An added measurement of the width, combined with the measured length, yields the recovered projected area but no dimension which requires knowledge of the recovered depth. The ratio of the recovered and unrecovered widths or projected areas gives an estimate of the magnitude of the elastic deformation; and, when investigating elastic materials, it seems instructive to state this ratio in addition to the indentation number. The use of areas which depend upon the elastic recovery of a material is rejected as a method of expressing the results of indentation tests because this associates an applied load with an area other than that involved at the time the load was applied. Furthermore, an unrecovered area is chosen to express the indentation number because it seems to afford the most rational interpretation of the results, placing as it does vastly different materials such as rubber, copper, glass, and hardened steel in some logical order; whereas no reasonable sequence results from the use of recovered areas.

For expressing the results of indentation tests in terms of areas, the load may be related to either the lateral or the projected area, which for a pyramidal indenter differ merely by a factor, namely the cosine of the angle between them. Of these two areas, the projected is favored here because the measured load is applied normal to that area,

and that load is equal to the vertical component of the unknown forces reacting on the lateral faces. With lateral area the unknown force normal to the faces of the indenter would seem to be the one to use. For those materials in which the resultant of the reacting forces is normal to the faces of the indenter, the normal force will, of course, be greater than its vertical component; for materials in which the resultant of the reacting forces is not perpendicular to the indenter faces, the normal component may be greater or, conceivably, even less than the vertical component. Consequently, indentation numbers which are obtained by dividing the applied load by the lateral area will not be a true measure of resistance to indentation.

Tests based upon the unrecovered projected area (fig. 12) show that indentation numbers obtained with all the pyramidal indenters used have about the same value for materials like rolled gold and copper, which have little if any elastic recovery; whereas greater numbers are obtained for more elastic materials with acute indenters than with obtuse indenters—the latter giving the greater transverse elastic recovery. Figure 12 shows that the spread in indentation number with indenters having different angles is greatest for the materials which exhibit the greatest elastic recovery. Any attempt to analyze theoretically these divergences requires exact knowledge of the distribution of stresses within the specimens, and this distribution is, in turn, affected by the strength properties of the materials. Such analysis is beyond the scope of this investigation.

VI. SELECTION OF AN INDENTER FOR GENERAL USE

Results of the experimental work with elongated pyramidal indenters of various angular shapes indicated that an indenter might be selected that would be satisfactory for testing all materials to which indentation tests are applicable. The advantage of adopting a standard indenter for all tests is that it eliminates troublesome conversions of indentation numbers from one scale to those of some other scale. Since indentation numbers with the same indenter were found to be quite independent of the load applied, then, by adopting a standard indenter and by varying the load on this indentor to suit test conditions, all materials and specimens are placed in a single indentation scale.

In selecting the angles of an indenter for general use, consideration was given to sensitivity, definition of the indentation, possibility of longitudinal elastic recovery, and adaptability for use in different materials. The most sensitive indenters, table 5, column 6, are those which give narrow, shallow indentations. Sensitivity, however, is necessarily limited by two considerations: First, that results with such tools are greatly affected by surface irregularities, thus requiring excellent surface finish and great care in the preparation of specimens to avoid surface hardening; and, second, that lateral contraction of indentations for l/w ratios exceeding 10 gives terminations of the longitudinal diagonals (right central photograph, fig. 6) for highly elastic materials which are not fully resolved in the microscope. The definition is greatly improved by increasing the width relative to the length. For a constant transverse angle this may be accomplished by decreasing the included longitudinal angle, giving increased penetration. However, the reduction in sensitivity and the possibility of elastic recovery in a longitudinal direction makes it advisable

to use l/w ratios greater than 5. Of great practical importance in the selection of an indenting tool is its adaptability for use in different

TABLE 5.—*Relationship of indenter constants and measured lengths and calculated penetrations for different indenters with a 4-kg load in steel C 25*

Indenter	Included angles				Length / Width	Length / Penetration	Values with 4 kg for C 25	
	Longitudinal		Transverse				Length (measured)	Penetration (calculated)
(1)	(2)		(3)		(4)	(5)	(6)	(7)
	deg	*min*	*deg*	*min*			*μ*	*μ*
1	175	20	118	36	14.6	49.1	645	13.1
2	174	53	134	15	9.4	44.8	535	11.9
4	173	52	126	12	9.5	37.3	525	14.1
7	170	0	100	36	9.5	22.9	515	22.5
8	172	32	129	40	7.2	30.6	455	14.9
3	171	42	126	36	6.9	27.6	450	16.3
6	170	44	136	0	5.0	24.7	390	15.8
Vickers	148	7	148	7	1.0	7.0	• 167	• 23.9

• Computed from Vickers number = 265 for steel *C 25*.

materials. To illustrate: Indenter 2 (134° transverse angle) gave less shattering in glass with a load of 2 kg than did indenter 7 (100° lateral angle) with 0.2 kg; yet, although a broad angle gives better results in brittle materials, it is not suitable for materials which can not be readily polished to the degree of refinement obtainable with glass. From these considerations, the following shape was selected to give the best weighted performance:

Included longitudinal angle	172°30′
Included transverse angle	130°0′
Constant for projected area	7.03×10^{-2}
Constant for lateral area	7.77×10^{-2}
Ratio of length to width	7.11
Ratio of length to penetration	30.5

If from the standpoint of simplicity and accuracy of production and calibration it is better to define the shape of the standard indenter in terms of face angles, then dihedral angles of 130° between opposite faces and azimuthal angles of 16° and 164° between adjacent faces are recommended. For this shape the edge angles become 172°34′25″ and 130°25′40″, which differ but slightly from the first specification.

VII. COMPARISON OF THE INDENTATION SCALE OF INDENTER 8 WITH BRINELL AND VICKERS SCALES

Indentation numbers were determined for the standard specimens with indenter 8, which approximates the selected shape very closely. Brinell and Vickers numbers were obtained for the same specimens through the courtesy of the Engineering Mechanics and the Mechanical Metallurgy Sections of the National Bureau of Standards. The results are given in table 6. Indentation numbers, I, with indenter 8 are 20 percent greater than corresponding Brinell numbers for rolled copper and agree with the Brinell numbers for steel, *C 65–67*. Numbers with indenter 8 are 13 percent greater for rolled copper and 12 percent less for steel, *C 65–67*, than the corresponding Vickers numbers. In view of the differences in the shapes of the indenters and

in the bases of computation, greater differences in indentation numbers could well be expected.

Indentation numbers were determined with indenter 8 for many materials which are not commonly tested by indentation methods. Numbers for several widely different materials are listed in table 6. Where a single indentation number is given, the number is the average of several determinations on one or more specimens which in some cases differed appreciably. The corresponding Mohs hardness numbers for some of the specimens are given in brackets.

TABLE 6.—*Comparison of indentation numbers with indenter 8 and Brinell and Vickers numbers for the same specimens*

Specimen	Brinell test			Vickers number	Indenter 8. Indentation number, *I*
	Conditions of test		Brinell number		
	Ball	Load (30 sec)			
		kg			
Rockwell *C* 65–67	10 mm, Carboloy	3,000	780	894	791
Gage 2	do	3,000	745	848	779
Gage 1	do	3,000	611	655	637
Rockwell *C* 47	10 mm, steel	3,000	456	493	496
Rockwell *C* 25	do	3,000	241	265	276
Rolled copper	1/16 inch, steel	15	104	111	125
Rockwell *B* 7–9	10 mm, steel	500	52.8	58.2	59.2

	Specimen	*I* (indenter 8)
	Pitch (for optical polishers)	1–22
[2]	Gypsum	32
[3]	Calcite	135
[4]	Fluorite	163
	Flint glass	180–390
[5]	Apatite (parallel to axis)	360
	Apatite (perpendicular to axis)	430
	Crown glass	420–470
	Fused quartz	471
[6]	Albite	490
[6]	Orthoclase	560
[7]	Crystaline quartz (parallel to axis)	710
[7]	Crystaline quartz (perpendicular to axis)	790
	Nitrided annealed high-speed steel	800
	Chromium plate	850–900
	Carboloy	1,050
	Nitrided hardened high-speed steel	1,100
[8]	Topaz	1,250
	Alundum	1,635
	Silicon carbide	2,000
	Boron carbide (molded)	2,230
[10]	Diamond	8,000–8,500

VIII. FIELD OF APPLICATION OF THE INDENTER

In considering the performance of the diamond-based pyramid indenter, the chief characteristic which warrants its introduction among other indenters is its sensitivity. Although its use is not restricted to small loads, loads of 0.5 kg are sufficient to give indentation lengths of 100 μ in the hardest steel tested; and, with indentations of this length, differences in indentation numbers greater than 2 percent in well-surfaced specimens may be attributed to nonuniformity of the specimen. The use of light loads permits the satisfactory testing of many brittle materials which could not be tested satisfactorily by other indentation methods, and the resulting indentation numbers for these materials fall within the range of present indentation scales for metals. In view of the generally satisfactory results

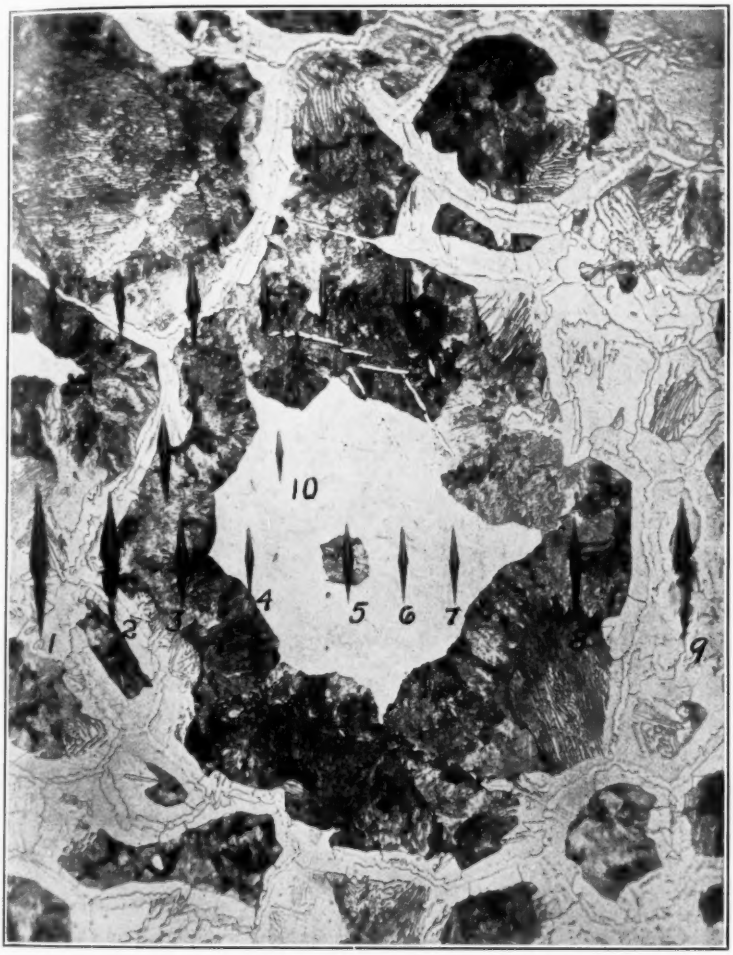

FIGURE 14.—*Indentations in a quenched, high-purity iron—1.1¼-percent-carbon alloy (magnification, ×250).*

For indentations 1 to 9 a load of 100 g was used. Nos. 1, 2, and 9 are in areas where ferrite, pearlite, and cementite predominate. Nos. 3 and 8 are in troostite (fine pearlite). Nos. 4, 6, and 7 are in martensite. No. 5 shows an indentation in an area of troostite about 25 μ in diameter entirely surrounded by martenite. No. 10 was made in martensite with a 50-g load. The indentation numbers ranged from 190 for the soft constituents to 720 for the martensite.

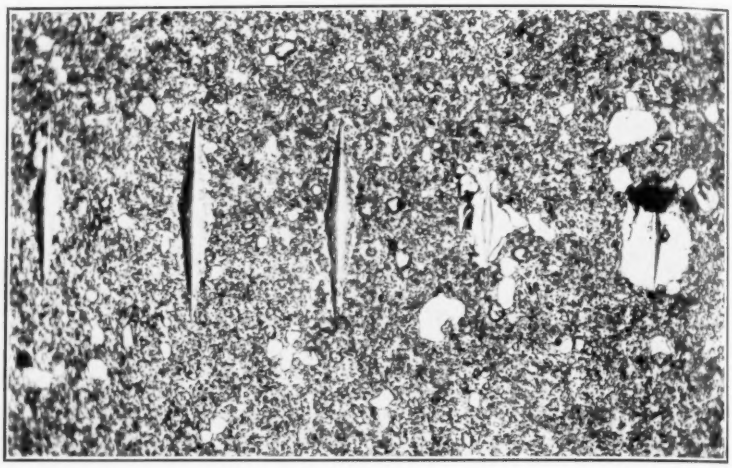

FIGURE 15.—*Indentations in a molybdenum-tungsten-cobalt steel containing large carbide particles (magnification, ×500).*

The indentation numbers were about 230 for the matrix and 1 430 for the carbide particles.

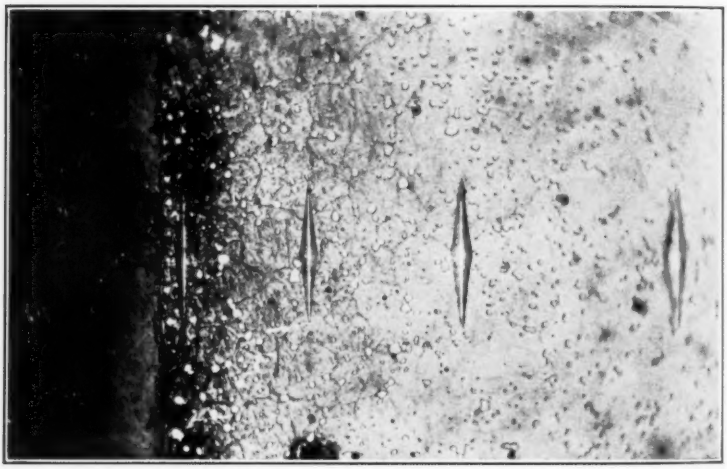

FIGURE 16.—*Indentations in a specimen of nitrided hardened molybdenum-tungsten high-speed steel cut perpendicular to the nitrided surface (magnification, ×500).*

Indentations made at positions 4 μ to 7 μ from the edge of the material partially cracked out. At distances from 10 μ to 25 μ from the edge, the indentation numbers were about 1,100, which agrees with measurements made normal to the nitrided surfaces of similar specimens. For greater distances the numbers decreased progressively until 780 (that of the original matrix) was reached at positions more than 60 μ from the edge.

obtained with present forms of indenters in testing large specimens of materials which do not shatter under heavy loads, it would appear that the immediate field of application for the diamond-based pyramid indenter would be the testing of small specimens and materials which shatter under heavy loads but will withstand application of the light loads required for this tool. Glasses, dental plastics, enamels, and porcelains have been tested satisfactorily with this indenter; and it seems equally well adapted to the testing of electrodeposits and thin sheet metal. Although no extensive study has yet been made of minimum thicknesses which may be tested, useful information was obtained from tests of layers 0.0005 in. thick.

The indenter has recently been applied to the microtesting of different areas of a quenched, high-purity iron—1.14-percent-carbon alloy (fig. 14)—furnished by T. G. Digges of the Metallurgical Division;[13] to a molybdenum-tungsten-cobalt steel (fig. 15) which contains large particles of carbide; and to a section of a nitrided specimen of hardened molybdenum-tungsten steel (fig. 16). The last two specimens were furnished by Ralph G. Kennedy, Jr., Cleveland Twist Drill Co.

In the light of the experience gained in the use of the elongated pyramidal indenter, more specific knowledge of the load requirements for accurate testing has been obtained. A range of 0.1 to 2.0 kg appears satisfactory for testing materials within the indentation range of 5 to 2,000 on this scale when the size of the specimens permits the use of these loads. For microindentation testing of exceedingly small or thin specimens, it seems desirable to have a sensitive mechanism that will apply light loads to the indenter, either progressively or in steps of 0.02 kg from 0.0 to 0.1 kg, and in larger steps from 0.1 to 0.5 kg. The use of loads exceeding a few kilograms with this indenter would appear advantageous only in testing resistant materials in which the surface finish of the specimens may not be commensurate with accurate testing with light loads and in integrating the mass hardness of heterogeneous materials.

The authors express their appreciation to W. H. Swanger, Chief of the Mechanical Metallurgy Section of the National Bureau of Standards for his invaluable information, suggestions, and encouragement, and for the practical aid so freely given throughout the investigation; to G. W. Quick for the excellent photographs of the indentations; to R. D. France for the Brinell and Vickers tests of the specimens as well as for the help given in obtaining indentation numbers with the present indenter in commercial testing devices; and to L. B. Tuckerman and B. Wilson for assistance in presenting the material.

WASHINGTON, September 17, 1938.

[13] J. Research NBS **20**, 571 (1938) RP1092.

U. S. DEPARTMENT OF COMMERCE NATIONAL BUREAU OF STANDARDS

RESEARCH PAPER RP1221

Part of Journal of Research of the National Bureau of Standards, Volume 23, July 1939

RATE OF OXIDATION OF STEELS AS DETERMINED FROM INTERFERENCE COLORS OF OXIDE FILMS

By Dunlap J. McAdam, Jr., and Glenn W. Geil

ABSTRACT

By use of interference colors, investigation has been made of the variation of thickness of the oxide film on steels with temperature and time. The rate of oxidation varies as a high power of the absolute temperature. If, over short intervals, the oxidation time at constant temperature is assumed to vary as a power of the film thickness, the exponent decreases from 100 or more for thin films to about 2 for thick films.

The film thickness, for constant oxidation time, increases rapidly with the absolute temperature. If, over short intervals, the thickness is assumed to vary as a power of the absolute temperature, the exponent increases with increase in film thickness, from 1 or less to about 20 or 25. The accelerating influence of temperature thus predominates over the retarding influence of increase in film thickness.

Various steels are compared, with reference to resistance to oxidation, and the influence of alloying elements is discussed.

CONTENTS

	Page
I. Introduction	64
II. Review of literature on the variation of the thickness of the oxide layer with temperature and time	67
1. Variation of film thickness with time, at constant temperature	67
2. Influence of temperature on oxidation time, for constant film thickness	69
3. Variation of film thickness with temperature, for constant oxidation time	70
III. Materials and methods	72
IV. Influence of temperature on oxidation time, for constant film thickness	73
1. General description of diagrams	73
2. Iron and carbon steels	75
3. Alloy tool steels and nickel steels	76
4. Chromium steels	76
5. Chromium-silicon and chromium-nickel steels	79
6. An equation to represent the influence of temperature on oxidation time, for constant film thickness	81
V. Variation of film thickness with time, at constant temperature	82
1. Derivation of diagrams	82
2. General description of diagrams	84
3. Form of the curves of variation of film thickness with time, at constant temperature	85
4. Comparison of typical diagrams	87
VI. Variation of film thickness with temperature, for constant oxidation time	90
1. General description of diagrams	90
2. Form of the curves of variation of film thickness with temperature, for constant oxidation time	90
3. Comparison of typical diagrams, representing the variation of film thickness with temperature	92
VII. Summary	92
VIII. References	93

152687—39——5

I. INTRODUCTION

The practical importance of the resistance of metals to oxidation at elevated temperatures has led to various investigations of the rate of oxidation as affected by composition, temperature, and film thickness. In most of these investigations, the temperatures have been relatively high; oxidation, therefore, has been rapid and the oxide layers have been so thick that they should be considered as scales rather than as films. A few investigations have been made with slower rates of oxidation, and with oxide films thin enough to cause interference colors. As a study of thin continuous films appeared to be well adapted to give information of theoretical as well as practical importance, this method was chosen for the investigation herewith described. This investigation, therefore, has involved a study, by means of interference colors, of the rates of formation of thin continuous oxide films.

Interference colors do not appear until the film thickness reaches about 3×10^{-6} cm. The first stage of film formation is invisible to ordinary observation. A polarimetric study of the light reflected from the metal, however, reveals the presence of a film and gives a means of determining its thickness. At ordinary temperatures, in absence of moisture, oxide films on many metals do not increase in thickness beyond the invisible stage. On most metals at elevated temperatures and on some metals at room temperature, however, the films increase in thickness until eventually they cause interference colors.

These colors, sometimes called "temper" colors or "heat" colors, are caused by interference between rays of light reflected from the inner and outer surfaces of the oxide film. The coincidence of two waves differing in phase by 180° causes light of a certain wave length to disappear; if the incident light is "white," therefore, the reflected light is of the corresponding complementary color. Interference occurs when the film thickness is an odd multiple [1] of one-fourth the wave length of a component of the incident light. Interference, however, is determined by the wave length in the oxide film, not by the wave length in air. As the wave length in the film depends on the index of refraction of the oxide, the index of refraction is a factor involved in the relationship between wave length, film thickness, and interference color.

In this paper, attention is confined to oxidation of metals in the absence of liquid moisture. Oxidation of metals in air or oxygen at temperatures above the dew point was formerly considered to be a process of direct chemical combination, thus distinguished from ordinary corrosion. However, the investigations of Joffé and coworkers [15] [2] on electrical conductivity of dielectrics, and the later investigations of Wagner and coworkers [40, 25] on diffusion of metal ions, oxygen ions, and electrons through the oxide film, have shown that the oxidation of metals, even in the absence of moisture, is an electrochemical process.

The behavior of a metal in contact with air or oxygen is greatly influenced by temperature, and by the dissociation pressure of the oxide. The dissociation pressure, which varies with the temperature,

[1] The colors corresponding to multiples 1, 3, and 5 are known as colors of the first, second, and third order, respectively.

[2] Figures in brackets indicate the literature references at the end of this paper.

is the pressure of oxygen in equilibrium with the metal and its oxide. When the pressure of oxygen is less than the dissociation pressure, oxide does not form, and any oxide already formed decomposes. Oxides of "noble" metals have dissociation pressures greater than the partial pressure of oxygen in air. Oxides of base metals, however, have very low dissociation pressures at room temperature. The dissociation pressure of Cu_2O at 225° C, for example, is only 0.56×10^{-30} atmosphere; even at 1,725° C, the dissociation pressure is only 0.44 atmosphere. In air at atmospheric pressure, therefore, such metals tend to form oxide films even at room temperature.

The rate of oxidation of metals in air or oxygen depends not only on the composition, but also on temperature, and on the concentration (pressure) of oxygen in the gaseous phase. The rate of oxidation of most metals, moreover, varies with the thickness of the oxide layer. The thickness of this layer, however, has no appreciable effect on the rate of oxidation of some metals. This difference in behavior, as shown by Pilling and Bedworth [22], depends on the relationship between the volume of the oxide and the volume of metal from which the oxide was formed. When the volume of the oxide is less than the corresponding volume of metal, the oxide generally is porous, and thus does not prevent direct access of oxygen to the metal. As the rate of oxidation of such a metal (at constant temperature) is practically unaffected by the thickness of the layer of oxide, the thickness of this layer increases uniformly with time. When the volume of the oxide is greater than the volume of the metal from which the oxide is formed, the oxide film is under lateral pressure and tends to be nonporous. Such a film prevents direct access of oxygen to the underlying metal. To reach the metal, oxygen must enter the film and traverse it by diffusion [15, 40, 25]. The rate of oxidation, consequently, decreases with increase in the film thickness. In the first group of metals are most of the light metals, excepting aluminum. In the second group, which includes all other metals, are most of the metals in common use.

In the investigation described in this paper, attention was confined to rates of oxidation of steel in air at atmospheric pressure. The partial pressure of the oxygen surrounding the metal, therefore, varied only slightly. The concentration of the oxygen, however, obviously varied inversely with the absolute temperature used in an experiment. As the concentration of an element or compound taking part in a chemical reaction may greatly affect the velocity of reaction, consideration must now be given to the importance of the variable oxygen concentration.

The effect of oxygen concentration on the rate of oxidation has not been thoroughly investigated. Variation of the rate of oxidation with the pressure of oxygen, however, apparently is slight for all pressures above the dissociation pressure. Results of the investigation of oxidation of steels [22, 34, 35] at 800° to 1,100° C appear to indicate that the rate of oxidation is about twice as great in oxygen as in air. If the variation is assumed to follow a power law, this would indicate that the average rate of oxidation varies as about the two-fifths power of the oxygen concentration. For copper [41] and nickel [41] at about 1,000° C, however, the oxidation rate was reported to vary as the seventh and sixth roots of the oxygen concentration. At these high temperatures, conditions were such that the oxide layers

were relatively thick; they were scales rather than continuous films. Investigations with steel at lower temperatures [27, 31] with films thin enough to cause interference colors, led the investigators to the view that variation of oxygen pressure between about 0.5 mm (of mercury) and atmospheric pressure has no discernible effect on the rate of oxidation. Oxygen concentration has also been reported to have no discernible effect on the rate of oxidation of zinc at 400° C [41]. The available evidence thus appears to indicate that the rate of oxidation in air is not appreciably affected by variation in oxygen concentration due to variation in temperature.

In the investigation described in this paper, the extreme temperature range for any one graph was sufficient to cause only about 50-percent variation in oxygen concentration. For an entire temperature-time-thickness diagram, however, the extreme range of oxygen concentration was sometimes as high as 3 to 1. Nevertheless, as the oxidation rate probably varied only as a small fractional power of the oxygen concentration, the effect of even the extreme range of oxygen concentration on the form of the diagram probably was small in comparison with the effects of temperature and film thickness.

The effect of water vapor in air or in oxygen, on the rate of oxidation, probably is negligible. Pilling and Bedworth [22] compared the effects of dry oxygen and of oxygen saturated with water vapor, on the rate of oxidation of copper; they found no discernible influence of the water vapor. Evans [6], in discussing the paper of Pilling and Bedworth, said that he had found dehydration of air to have no important effect on the rate of oxidation of iron. The rate of oxidation of metals in air at temperatures above the dew point, therefore, probably is not appreciably affected by variations in humidity.

The rate of oxidation of a metal may be expressed in terms of the rate of increase of film thickness with time. The rate of oxidation is not easily measurable; it is more convenient to measure the time interval from the beginning of exposure of the specimen to the attainment of any specified thickness. This time interval will be termed the oxidation time. (The mean rate of oxidation for this time interval is inversely proportional to the oxidation time.) The important factors to be considered in a study of the rates of oxidation of a given metal, therefore, are temperature, oxidation time, and film thickness. The thickness of the oxide layer has been investigated by a number of methods. In these methods, the variables observed (as indices of variation of film thickness) have included the weight change; the amount of oxygen combining with the metal; the change in electrical conductivity of the specimen; the quantity of electricity used in the reduction of the oxide film; and interference colors. To give a complete picture for any metal, however, such investigation should consider the interrelationship between all three important variables—temperature, oxidation time, and film thickness. Far-reaching conclusions have been formed and generally accepted, as a result of investigation of the relationship between only two of the variables throughout a narrow range of values. Such conclusions, as will be seen, may not be generally correct.

In obtaining a three-dimensional picture for any metal, it is necessary to obtain three complementary views, each based on a study of the relationship between two of the variables, with the third variable held constant. One of these two-dimensional views is based on

the relationship between temperature and time for constant interference color (constant film thickness). Results of such an investigation are given in Section IV. Another two-dimensional view has been obtained by investigating the relationship between oxidation time and film thickness (as determined from the entire range of temper colors), with temperature held constant. Results of this investigation are given in section V. From any pair of these views, it is possible to derive a third view, representing the relationship between temperature and film thickness, for constant oxidation time. Diagrams representing this relationship are discussed in section VI.

II. REVIEW OF LITERATURE ON THE VARIATION OF THE THICKNESS OF THE OXIDE LAYER WITH TEMPERATURE AND TIME

1. VARIATION OF FILM THICKNESS WITH TIME, AT CONSTANT TEMPERATURE

In discussing the literature dealing with the relationship between temperature, time, and film thickness, it is convenient to consider successively all the two-dimensional views of this three-dimensional relationship. These views represent the variation of film thickness with time at constant temperature; the influence of temperature on oxidation time, for constant film thickness; and the variation of film thickness with temperature, for constant oxidation time. The first of these two-dimensional views will now be considered.

When the volume of an oxide is greater than the volume of the metal from which it is formed, the rate of oxidation decreases with increase in the thickness of the oxide film. The oxidation time, therefore, increases more than in proportion to the film thickness. Several equations have been suggested to represent this variation of film thickness with time. The most widely accepted of these equations is based on theoretical considerations, which were stated first by Pilling and Bedworth [22]. According to this theory, the rate of oxidation depends on the steepness of the concentration gradient of oxygen between the outer and inner surfaces of the film. At the inner surface the equilibrium concentration would be about that corresponding to the dissociation pressure of the oxide in contact with the metal. At the outer surface of the film, the equilibrium concentration of dissolved oxygen would be the saturation value at that temperature. On the tacit assumption that the range of oxygen concentration is constant, the theory would imply that the steepness of the gradient, and hence the instantaneous rate of oxidation, varies inversely as the film thickness. The equation representing this relationship, for constant temperature, is

$$dy/dt = K/y \tag{1}$$

In this equation, y represents film thickness, t represents time, and K is a constant. Integration of this equation gives the equation for a quadratic parabola

$$y^2 = 2Kt + C \tag{2}$$

In this equation, C is a constant of integration and represents the square of the initial film thickness.

According to this theory, therefore, the film thickness (at constant temperature) increases as the square root of the time, if the time is

measured from the instant that the thickness is zero. Experimental investigation by Pilling and Bedworth [22] led them to the view that the results substantiated the theory, which they thereafter called the "quadratic law." Numerous other investigators [5, 12, 14, 16, 21, 23, 24, 26, 29, 34, 35, 36, 37, 38, 39, 42] have reported that their results substantiate this relationship, which has been frequently called the "parabolic law." In all these investigations, however, temperatures were relatively high and oxidation times were sufficient to cause relatively thick scale. Experiments with thinner layers of oxide have led some investigators to report deviations from the parabolic relationship. Such deviations in the early stages of oxidation were reported by Portevin, Prétet, and Jolivet [23, 24] and by Feitknecht [10], as a result of their investigations with electrolytic iron and copper, respectively. Vernon [39] reported that the oxidation of iron did not conform to the parabolic relationship at temperatures below 200° C. An investigation of single crystals of low-carbon iron by means of interference colors led Mehl and McCandless [17] to the view that the oxidation did not conform to the parabolic relationship. Miley [18] and Miley and Evans [19], as a result of electrometric studies of oxide films, reported that the oxidation of iron and copper (at 350° C and below) did not conform to the parabolic relationship, except for a short initial period of heating. Their conclusions thus appear to be the opposite of those reached by several investigators previously mentioned. As shown in section V, the apparently contradictory views reached by investigators of this subject are due largely to the attempt to draw general conclusions from too narrow ranges of the variables.

A very different representation of the variation of film thickness with time was obtained by Tammann and coworkers [27, 31, 32]. By use of interference colors they investigated the oxidation of iron, copper, nickel, zinc, cadmium, tin, lead, cobalt, and manganese. They reported that the variation of film thickness with time was in accordance with an exponential equation

$$t = ae^{by} - a \tag{3}$$

In this equation, t and y have the same significance as in eq 1 and 2, and the other letters represent constants. One of these constants, a, was said to be independent of temperature; the other constant, b, was said to be dependent on temperature in accordance with another exponential equation. In developing eq 3, however, Tammann and Koster assumed that the film thickness for second-order colors is only twice the thickness for first-order colors. As pointed out by Evans [7] and Dunn [4], this assumption is incorrect, and the equation of Tammann and Koster is not in accordance with the data. In a later paper, Tammann and Bochow [30] reported that the exponential relationship was followed exactly in the oxidation of nickel, but not exactly in the oxidation of copper. They did not indicate, however, whether or not their calculations were based on their original incorrect assumption as to the relationship between interference colors and film thickness. Confirmation of the Tammann and Koster exponential equation was reported by Schwarze [28], who used interference colors in studying the oxidation of fourteen steels in the temperature range 300° to 380° C.

An exponential relationship and a parabolic relationship could not both be correct as a general representation of the variation of film

thickness with time. As shown in section V, these relationships are not generally correct, nor is any other single formula generally correct.

2. INFLUENCE OF TEMPERATURE ON OXIDATION TIME, FOR CONSTANT FILM THICKNESS

Very few investigators have studied the variation of oxidation time or of its reciprocal, the mean oxidation rate, with temperature, for constant film thickness. In most investigations of oxidation of metals at elevated temperatures, increases of weight (or other indices of film thickness) have been compared, for constant oxidation time. Results of such investigations are considered in section II (3).

A study of the influence of temperature on the oxidation time, for constant film thickness, may be readily made by means of interference colors. Constancy of interference color, for the same metal, means approximate constancy of film thickness. The previously mentioned investigations of Tammann and coworkers dealt with the relationship between film thickness and both time and temperature. In their exponential equation representing the variation of film thickness with time, constant b was said to vary with temperature in accordance with another exponential equation. Although their equations were based on an incorrect assumption as to the relationship between film thickness and interference colors, Schwarze [28] reported that both equations were substantiated by results of his investigation. Entirely different equations have been reported by other investigators.

In practically all other investigations, however, much higher temperatures were used, and the oxide layers were from ten to a thousand times as thick as those obtained in investigations by means of interference colors. As a result of an investigation of this kind, Pilling and Bedworth [22] suggested the equation

$$K=aT^n \tag{4}$$

In this equation, T represents absolute temperature, K is an "oxidation rate constant", and a and n are other constants. The oxidation rate represented by K is neither the instantaneous rate, dependent on film thickness, nor the average rate. It is derived from eq 1, based on the previously mentioned theory of Pilling and Bedworth. According to this theory, the "rate constant", K, is independent of film thickness and is characteristic of the metal at the given temperature. As shown in section V, however, the relationship represented by eq 1 is not generally correct, although it may be approximately correct as applied to relatively thick, rapidly formed oxide layers.

In a theoretical discussion of the influence of temperature on the oxidation rate, Dunn [5] reasoned that the rate of oxidation is determined by the rate of diffusion through the oxide film, and that "an oxygen molecule can only pass a structural unit, provided that it possesses at the moment energy greater than a critical value causing a loosening of the oxide structure at that point." He thus arrived at the relation

$$K=Ae^{-b/T} \tag{5}$$

In this equation, T represents absolute temperature, K is the "oxidation rate constant" derived from eq 1, and A and b are constants. From this equation may be derived the equation

$$\log K=-b/T+\text{constant} \tag{6}$$

Dunn reported that results of his experiments with brasses in the temperature range 580° to 880° C., and also the results obtained by Pilling and Bedworth on the oxidation of copper, iron, and nickel, conform closely to this relationship.

The same equation was developed by Heindlhofer and Larsen [12] on reasoning (similar to that of Pilling and Bedworth) that the rate of oxidation depends on the concentration-gradient of dissolved oxygen and on the specific diffusivity of the oxygen in the oxide film. Their experimental results on the scaling of commercially pure iron between 600° and 1,100° C, and also pure copper between 600° and 1,100° C, were said to conform to this relationship. They concluded that the relationship is satisfactorily represented by eq 6, provided that the instantaneous rate of oxidation is not so high that it is affected by the rate of diffusion of oxygen in the gaseous phase, and provided that there is no blistering or discontinuity in the oxide layer. They also discussed the possible difference in diffusion in layers of different oxides of the same metal.

Confirmation of the exponential relationship represented by eq 5 and 6 has also been reported by Portevin, Prétet, and Jolivet [23, 24], as a result of their experiments with electrolytic iron in the temperature range 800° to 1,000° C. When log K was plotted against the reciprocal of the absolute temperature, they obtained two straight lines intersecting at an angle of nearly 180°, at about 900° C. They considered the apparent change of direction at this point to be due to the transition from alpha to gamma iron. With some allowance for scatter of experimental points, however, the relationship could be represented nearly as well by a single straight line, but could be represented even better by a slightly curved line. A practically straight line would be obtained also by plotting log K against log T, thus indicating a relationship similar to that shown (for much thinner films) in section IV.

Linear relationship between log K and $1/T$ has also been reported by Krupkowski and Jaszczurowski [16], as a result of their experiments with nickel and iron in the temperature range 500° to 1,200° C.

Hudson and Rooney [13], after studying the results obtained by previous investigators on the scaling of iron and carbon steels, concluded that the results conform equally well to eq 4, which gives a linear relationship with log K plotted against log T, or to eq 5, which gives a linear relationship with log K plotted against $1/T$. All the results on which these conclusions were based, however, were obtained with relatively high rates of oxidation and with relatively thick layers of oxide. For slower rates and for thin films, the only formula hitherto available has been the previously mentioned complex exponential equation suggested by Tammann and coworkers [27, 31, 32]. As shown in section IV, this formula is not generally correct.

3. VARIATION OF FILM THICKNESS WITH TEMPERATURE, FOR CONSTANT OXIDATION TIME

A number of investigators have studied the variation of thickness of the oxide layer with temperature, for constant oxidation time. In most of these investigations, increase in weight has been used as a measure of the increase in thickness.

Dickenson [3] compared the increase in weight of various carbon steels and alloy steels, in 5 hours at various temperatures within the

range 550° to 1,100° C. Practically straight lines were said to be obtained by plotting the logarithms of the average oxidation rates (for the 5-hour period) against either the absolute temperatures or the logarithms of these temperatures. The latter relationship would give an equation of the same form as eq 4, developed by Pilling and Bedworth [22]. The two equations, however, do not involve the same variables. The equation derived from Dickenson's data represents the variation of the average rate of oxidation (increase of thickness), for constant time. The equation derived from the data of Pilling and Bedworth represents the influence of temperature on an "oxidation rate constant," assumed to be independent of thickness. Although the two equations could be of the same form, therefore, the derived constants representing the slopes of the straight lines (plotted with logarithmic coordinates) would be very different. As shown in section VI, however, an equation of this form is not a generally correct representation of the variation of thickness with temperature, for constant oxidation time.

A quite different relationship between film thickness and temperature has been reported by Hudson, Herbert, Ball, and Bucknall [14], and by Vernon [39]. Both investigations, the former with copper and the latter with iron, determined the gains in weight during 1 hour at various temperatures. Results of both investigations were said to indicate that the logarithm of the gain of weight (thickness) is proportional to the reciprocal of the absolute temperature. The equation representing this relationship, therefore, is similar in form to eq 6, developed by Dunn. In eq 6, however, one of the variables is an assumed "oxidation rate constant"; in the equation based on data of Hudson, Herbert, Ball, and Bucknall [14], the corresponding variable is the increase in thickness (weight) for constant oxidation time. Although the two equations could be of the same form, therefore, the derived constants would be very different. As shown in section VI, however, an equation of this form is not a generally correct representation of the variation of film thickness with temperature, for constant oxidation time.

A still different relationship has been reported by Rickett and Wood [26], who determined the gains in weight of some chromium steels (0 to 30 percent of chromium) for constant time at various temperatures. They reported a linear relationship between the logarithm of the gain in weight and the absolute temperature. An equation of this form, as shown in section VI, cannot be considered generally correct.

Murphy, Wood, and Jominy [21] have reported that the scaling of steel in the temperature range 1,093° to 1,315° C can be represented by a linear relationship between the gain in weight and the absolute temperature. Upthegrove and coworkers [29, 34, 35], who studied the scaling of SAE 1015 and 1020 steels in the temperature range 900° to 1,150° C found no simple relationship between oxidation and temperature. Graphs of weight change, for constant oxidation time, were said to show an abrupt change at 980° C for scaling in oxygen. For scaling in air, they reported a maximum and minimum at about 980° and 1,100° C, respectively.

The various investigations on this subject, therefore, have led to contradictory conclusions. As shown in sections IV, V, and VI, many of these apparent discrepancies probably are due to deductions based on narrow ranges of only two of the three important variables.

III. MATERIALS AND METHODS

The steels used in this investigation may be classified as follows: carbon steels; tool steels; nickel steels; steels containing up to 5 percent of chromium; high-chromium steels; chromium-silicon steels; medium-chromium, high-nickel steels; high-chromium steels containing nickel. The compositions of these steels are given in table 1.

The specimens used for heat coloring were about 1 cm^2 in area and 1 mm thick. One surface was polished by the method used for metallographic specimens. The most suitable method of polishing was determined by trying various grades of abrasive and various polishing methods. The most uniform and brilliant coloring was obtained with specimens that had been polished dry by a series of emery papers (Nos. 1*G*, 0, 00, and 000), and then polished wet with levigated alumina. Additional polishing with magnesium oxide produced no significant effect on the subsequent coloring. The specimens were washed in alcohol, then with carbon tetrachloride, and were allowed to dry in air. To avoid nonuniform coloring, the surface was not afterward touched. The specimens were kept in desiccators, at room temperature, until ready for use.

At temperatures above 220° C, heat coloring was done in a small electric resistance furnace of the muffle type. A chromel-alumel thermocouple was used for measuring temperatures. The temperature was maintained, by controllers of the automatic potentiometer type, within 0.5 percent of the desired absolute temperature. To provide slow continuous change of the air inside the furnace, and thus to prevent depletion of the supply of oxygen, the opening in the top of the furnace was kept only partially covered.

At temperatures of 220° C and less, heat coloring was done in small electric ovens with automatic temperature control. Air circulation was provided by a fan and by two small openings in the furnace, one in the top and one in the side near the bottom. No difference in results (at 200° C) however, was observed when the fan was not operating and when the openings were closed. Although the speed of air flow across the heated surface (as shown by Upthegrove [34] and others) affects the scaling rate at 1,000° C or higher, at lower temperatures the effect of ordinary variations in air velocity is small.

The specimens, with the polished surface upward, were placed in the furnaces and ovens on stainless-steel plates. Such a plate served two purposes; it increased the thermal capacity of the furnace and hence was an aid in keeping the temperature constant, and it hastened the approach of the temperature of the specimen to the temperature of the furnace. Some tests with a silver plate instead of the steel plate gave unsatisfactory results; the coloring rate, especially of steels with chromium present, was accelerated by contact with the silver, although the polished surface of the specimen was not in contact with the silver. Analysis of the colored oxide film gave no indication of silver or silver compounds. Use of silver, for supporting the specimens, however, was discontinued.

There is no sharp demarcation between succeeding colors in the interference color scale. The colors change through the following sequence: Straw color, light yellow or gold, golden brown, brown with reddish or purple tint, brownish purple, light purple, dark purple,

dark blue, light blue,[3] very light greenish blue with a silvery gray appearance. The color sequence is then repeated with the colors less brilliant and less easily distinguishable.

The most easily distinguishable colors were selected for this time-temperature study. One of these is the first visible color, a very light straw color, another is brown with the first tinge of red or purple, and another is dark blue. The brown color could not be distinguished as sharply as the dark-blue color. The second-order colors selected were essentially the same. The colors of the second order were somewhat masked by the specific color of the oxide itself; on most of the specimens higher orders of color were not distinguishable.

For the tests at temperatures above 220° C, the coloring of the specimens was followed by frequent observation through the opening in the top of the furnace. For the tests at 220° C and below, observation of the coloring was made through the door of the oven, which was opened for each observation. Before inserting the specimen, the furnace or oven was allowed to attain the desired temperature. The oxidation time was reckoned from the instant the specimen was placed upon the steel plate. As about 1½ minutes' time was required for the specimen to attain the temperature of the oven, however, some correction was necessary in estimating the equivalent oxidation time at the desired temperature. This correction is important for short oxidation times, but usually unimportant for oxidation times greater than about 20 minutes.

The relationship between temperature, time, and film thickness has been studied by means of plan views, front views and side elevations of three-dimensional diagrams. Plan views, in which the coordinates represent temperature and oxidation time, are discussed in section IV. Front views, in which the coordinates represent time and temperature, are discussed in section V. Side elevations, in which the coordinates represent temperature and film thickness, are discussed in section VI.

IV. INFLUENCE OF TEMPERATURE ON OXIDATION TIME, FOR CONSTANT FILM THICKNESS

1. GENERAL DESCRIPTION OF DIAGRAMS

In a study of the variation of film thickness with temperature and time, the first relationship to be considered is the relationship between temperature and time, for constant film thickness (constant interference color). Diagrams (see footnote 4) representing this relationship for a variety of steels are shown in figures 1 to 15, inclusive, and diagrams comparing the results obtained with typical steels are shown in figures 16 to 19, inclusive. Each steel is designated by a letter, which is used also to identify it in the table of chemical compositions, table 1.

After trying various methods of plotting the results, logarithmic coordinates were chosen, because each graph[4] so plotted was found to be practically straight throughout most of its length. Abscissas represent time in minutes; at the top of each figure is an additional scale representing days. As ordinates, an attempt was made to use

[3] This is not in accordance with the statements of several investigators, who have reported that light blue appears before dark blue.

[4] The word "graph" is used to designate a single representative straight line or curve. The word "diagram" is used to designate a series or family of graphs.

the first power of the absolute temperatures. The slopes of the graphs, however, were so slight that they could not be determined with sufficient accuracy. By plotting a power of the absolute temperature, as ordinates, it is possible to increase the slope of a graph (drawn with logarithmic coordinates) without distortion. In figures 1 to 19, ordinates represent the tenth power of the absolute temperatures. By this means, the slope (tangent of the angle) has been multiplied by 10. Each figure also contains a scale in degrees centigrade.

Preceding the series of diagrams is a general legend, giving the symbols and their significance. A special legend is also included in each figure.

In each diagram of figures 1 to 15, are graphs representing the temperature-time relationship for straw color, reddish brown, and blue. Two of the diagrams, figures 8 and 12, include only the graphs for colors of the first order. The other diagrams include graphs for colors of both the first and second order, and the diagrams of figures 1, 10, and 14 include also the graphs for third-order blue. Each line is designated by letter (X, Y, or Z) representing straw color, reddish brown, or blue, respectively. For second- and third-order colors, this letter is followed by a numeral (2 or 3) to designate the order of the color.

Second-order colors are less distinct than first-order colors, and third-order colors are much less distinct than second-order colors. The distinctness of the colors varies with the composition of the steel. The 5-percent-chromium steel and the 46-percent-nickel steel gave second-order colors too indistinct to be used in studying the influence of temperature and time on film thickness. The only materials that gave third-order colors distinct enough to be used were electrolytic iron, 24-percent-chromium steel, and 25:20 chromium-nickel steel. No fourth-order colors could be distinguished on any of the steels. The indistinctness of the second- and third-order colors probably is not due entirely to decrease in transparency of the film with increase in thickness, but is due largely to coincidence of different colors of different orders. Third-order straw color probably appears before second-order blue; second-order blue thus probably coincides with some third-order color between straw and reddish brown. Third-order blue probably coincides with different colors of the fourth and fifth orders.

The experimental points in these figures represent the observed total oxidation times, with no correction for the time required for heating the specimen to the temperature of the furnace, nor for the effect of temporary lowering of the temperature each time the furnace was opened to facilitate observation of the colors. The number of such observations for any one specimen, however, generally was relatively small, except for second- and third-order colors. Because of the indistinctness of second- and third-order colors, more frequent observations were necessary in order to determine the time at which such a color reached its maximum.

The time required for this rise of temperature of the specimen varied with the temperature of the furnace. The periods necessary to heat a specimen to 650°, 530°, 355°, and 220° C, were 1.57, 1.52, 1.47, and 1.44 minutes, respectively. As the time probably is nearly proportional to the logarithm of the range of temperature through which the specimen is heated, the time required for heating the speci-

men to a furnace temperature of 950° C, the highest temperature used on these experiments, probably was about 1.65 minutes. Correction of the observed oxidation time, therefore, evidently is important when the total time is less than about 20 minutes.

The solid-line graphs in figures 1 to 15 are based on the uncorrected positions of the experimental points. Each line is based not only on the experimental points belonging to that line, but also on the probable ideal interrelationship (in form and position) between all the lines of the diagram. In determining the form of such a diagram, moreover, consideration was given to the complementary diagrams of two other types, which are illustrated in figures 21 to 28, inclusive, and discussed in sections V and VI. Each diagram of the type shown in figures 1 to 15 thus represents a plan view of a three-dimensional diagram in which the graphs are contour lines.

2. IRON AND CARBON STEELS

Diagrams for iron and pearlitic carbon steels, ranging in carbon content from 0.008 to 1.29 percent, are shown in figures 1, 2, and 3. The experimentally determined parts of the diagrams extend to temperatures as low as 100° C.[5] The solid lines representing the various interference colors are nearly straight throughout most of their extent, but are curved throughout the portions representing short oxidation time. These lines, however, are not corrected to allow for the time required to heat the specimen to the temperature of the furnace. The relative amount of such correction increases with decrease in the total oxidation time.

The lines representing the first-order colors, if correction were applied for the time of initial heating, evidently would become straight throughout the entire range of experiment. Such straightening is indicated by the broken lines diverging from some of the solid lines. The lines representing second- and third-order colors could be straightened only by applying a somewhat larger correction. A larger correction for these lines, however, is justifiable, because the indistinctness of the second- and third-order colors made it necessary to open the furnace frequently to examine the specimen. Complete correction of the oxidation time for second- and third-order colors, therefore, probably would straighten these lines throughout the entire represented range of time.

In all the diagrams of figures 1, 2, and 3, the slope is greatest for the line representing first-order straw color and is least for the highest [6] line in each diagram. The slope, therefore, evidently decreases with increase in the corresponding film thickness; the corrected lines, consequently, converge toward the top of the diagram. The difference in slope between two adjacent lines moreover, evidently decreases with increase in the corresponding film thickness.

The relative heights of these and following diagrams may be determined by comparing not only the figures containing the entire diagrams, but also by comparing corresponding single lines reproduced and assembled in figures 16 to 19. Each of these figures contains lines representing the same interference color for various steels.

[5] This is not in accordance with results reported by Vernon [39] and by Miley and Evans [20], who stated that interference colors could not be obtained below 200° C.

[6] The higher of two points in the two-dimensional diagram is the point whose ordinate is greatest.

The diagrams in figures 1, 2, and 3 differ little in position. The diagrams for 0.46-percent-carbon steel, *D*, and 0.83-percent-carbon steel, *E*, however, are somewhat higher than the diagrams for steels of either lower or higher carbon content, with the exception of the lines representing first-order straw color. This relationship is illustrated in figures 16 to 19 by the relative positions of line *A*, representing electrolytic iron, and line *E*, representing 0.83-percent-carbon steel. For first-order straw color, as shown in figure 16, lines *A* and *E* coincide. For the other interference colors, as shown in figures 17, 18, and 19, line *E* is above line *A*. At the right end, the difference in height is small, but the difference increases as the lines extend to the left.

The steels represented in figures 1, 2, and 3 are pearlitic steels. Consideration was given, however, to the influence of variation of microstructure due to heat treatment. Specimens of the 0.83-percent-carbon steel were heated to 1,450° F and cooled at various rates. Some specimens were quenched in water, others were cooled in air, and others in the furnace. Although these differences in heat treatment caused great differences in microstructure, the specimens showed no significant differences in the temperature-time relationship for interference colors.

3. ALLOY TOOL STEELS AND NICKEL STEELS

The diagrams representing alloy steels, in figures 4 to 15, are qualitatively similar to the diagrams for carbon steels. The corrected graphs are approximately straight, and the lines in each diagram diverge as they extend to the right. The divergence, however, is greater in some diagrams than in others, and the lines in some diagrams are generally steeper than in others. The relative heights and widths (range of coordinates) of the diagrams, moreover, are influenced by the alloying elements.

In figures 4 and 5 are typical diagrams for alloy tool steels, one of them a high-speed steel. In form and position these diagrams do not differ appreciably from the diagrams for carbon steels. Neither the small percentages of alloying elements in steels *G* and *H* nor the larger percentage of chromium and the large percentage of tungsten in high-speed steel have had any apparent effect on the height of the diagram.

In figure 6 are diagrams representing two nickel steels. The diagram for 3.35-percent-nickel steel, *J*, almost coincides with the diagram for 0.83-percent-carbon steel, *E*. The diagram for the 32-percent-nickel steel, *K* (as shown in figs. 16 to 19, inclusive) is somewhat higher than the diagrams for carbon steels. The large percentage of nickel in steel *K*, in absence of chromium, apparently had little effect in increasing the resistance of steel to oxidation.

4. CHROMIUM STEELS

In figures 7 to 10 are diagrams representing chromium steels, with percentages of chromium ranging between 1.38 and 24.4. The diagrams in figure 7 represent steels with small percentages of chromium. The width (vertical range) of each of these diagrams is greater than the width of a diagram representing carbon steel. This is illustrated, in each of the diagrams of figures 16 to 19, by the

relative position of line *M*, representing 2.18-percent-chromium steel. (Lines for the 1.38-percent-chromium steel, *L*, if drawn in these diagrams, would practically coincide with line *M*).

For first-order straw color (fig. 16), line *M* is below the lines (*A* and *E*) representing carbon steels. For first-order brown and blue (figs. 17 and 18), line *M* is between lines *A* and *E*. For second-order blue (fig. 19), line *M* is considerably above the lines representing carbon steels. Resistance to oxidation of steels with small percentages of chromium, therefore, evidently is less than that of carbon steels until the film thickness exceeds a value corresponding to first-order straw color. With further increase in film thickness, the apparent accelerating effect of the chromium on oxidation wanes; a retarding effect begins when the film thickness reaches a value corresponding to some second-order color.

In figure 8 the diagram for steel *N*, represented by the solid lines, shows the influence of about 5 percent of chromium. The second-order colors obtained with this steel were too indistinct to be used to establish lines. For the first-order colors, the experimental points show little scatter and the lines appear to be well established. The width of the first-order portion of the diagram for this steel is much greater than the widths of the corresponding portions of the diagrams representing carbon steels and low-chromium steels. This portion of the diagram for 5-percent-chromium steel extends below and above the corresponding portions of the diagrams for the steels previously discussed. For first-order straw color (fig. 16), line *N*, representing 5-percent-chromium steel, is below the lines representing carbon steels. For a large part of its length, moreover, line *N* is below line *M*, representing 2.18-percent-chromium steel. For first-order brown (fig. 17), line *N* is above line *M*, and (throughout most of its length) is above line *E*, representing 0.83-percent-carbon steel. For first-order blue (fig. 18), line *N* is considerably above line *E*, and almost coincides with line *K*, representing 32-percent-nickel steel. If lines could be established to represent second-order colors, they probably would show still further improvement in relative height of the diagram for 5-percent-chromium steel, corresponding with the further increase in film thickness.

The influence of 5 percent of chromium evidently is qualitatively similar to the previously described influence of smaller percentages of chromium. Resistance to oxidation is less for these steels than for carbon steels until the film thickness exceeds a value corresponding to first-order straw color. With further increase in film thickness, the apparent accelerating effect of chromium on oxidation disappears; a retarding effect then begins and increases with further increase in film thickness, at least to values corresponding to second-order colors.

In figure 9 is a diagram representing 13.6-percent-chromium steel. The scatter of experimental points is such that this diagram is less exactly established than are the diagrams previously described. The line for first-order brown may be somewhat too low. The lines, moreover, possibly should diverge more as they extend to the right. The diagram as drawn to represent the probable interrelationship of the lines, however, is considered approximately correct.

The curvature of the uncorrected upper lines in this figure extends further to the right than in any of the diagrams previously described. The greater extent of the curvature probably is connected with the

range of relatively high temperature represented by the upper part of this diagram. Whereas no diagram previously described extends above about 450° C, this diagram extends to 950° C. The curved portions of the lines representing second- and third-order colors, therefore, are based on observations with the specimen at red heat. To observe the interference colors, it was necessary either to remove these specimens from the furnace long enough for the temperature to drop below red heat, or to observe the colors by reflected light, with the specimen at red heat. The former procedure would necessitate a relatively large correction to allow for the times of repeated cooling and reheating. The latter procedure, which was generally used, caused mixture of the interference color with the red light emanating from the specimen. The admixture of red would tend to delay the observed appearance of second- and third-order blue, and thus would tend to increase the curvature of the corresponding lines. Complete correction of these lines, therefore, probably would make them practically straight.

The width of this diagram is about twice as great as the width of the diagrams for carbon steels. As shown in figure 8 (in which the lines for the 13.6-percent-chromium steel are reproduced for comparison), moreover, the diagram for 13.6-percent-chromium steel is much wider than the diagram for the 5-percent-chromium steel. The lower limit of the diagram for 13.6-percent-chromium steel, however, is above the lower limit of the diagram for 5-percent-chromium steel. Whereas chromium in percentages up to at least 5 evidently tends to lower the line representing first-order straw color, 13.6 percent of chromium raises this line considerably.

The beneficial effect of 13.6 percent of chromium evidently increases with increase in the film thickness, at least up to values represented by second-order blue. This is illustrated by the relative position of line *O* in figures 16 to 19, inclusive. For film thicknesses corresponding to first- and second-order blue, as shown in figures 18 and 19, line *O* is in the group of lines representing alloys with high resistance to oxidation.

In figure 10 is a diagram for steel *P* containing 24.4 percent of chromium. The width of this diagram is somewhat less than the width of the diagram representing 13.6-percent-chromium steel. The smaller width of the diagram for 24.4-percent chromium steel, however, is due almost entirely to the relatively high positions of the lines representing first-order straw color and brown. The line representing first-order straw color, as shown in figure 16, is considerably higher for the 24.4-percent-chromium steel than for the 13.6-percent-chromium steel. In figure 17, line *P* is far above line *O*. As previously stated, however, line *O* may be slightly too low. In figure 18, line *P* is slightly higher than line *O*. For second-order blue (fig. 19), however, line *P* is slightly below line *O*. In view of the previously mentioned uncertainty as to the exact position of some of the lines representing the 13.6-percent-chromium steel, it appears probable that the upper boundaries of the diagrams for 13.6- and 24.4-percent-chromium steels practically coincide.

The beneficial influence of increase in the chromium content beyond about 13 percent, therefore, applies chiefly to the initial stage of oxidation, represented by the growth of the film to a thickness

corresponding to first-order blue. In this stage, 24-percent-chromium steel appears to be definitely superior to 13-percent-chromium steel.

5. CHROMIUM-SILICON AND CHROMIUM-NICKEL STEELS

In figure 11 is a diagram representing steel *Q*, containing 8.8 percent of chromium and 2.8 percent of silicon. The uppermost line of this diagram is in about the same position as the corresponding lines representing 13.6- and 24.4-percent-chromium steels. The line representing first-order straw color (line *Q* of fig. 16), however, is far below the corresponding lines representing 13.6- and 24.4-percent-chromium steels, and is about as low as the lines representing 2.18- and 5-percent-chromium steels. The vertical range of the diagram for steel *Q* thus spans the vertical ranges of all the other diagrams investigated.

With increase in the film thickness from a value represented by first-order straw color to a value represented by first-order brown, the relative position of line *Q* (figs. 16 and 17) is greatly improved; line *Q* is thus raised above line *O*, representing 13.6-percent-chromium steel. With further increase in film thickness to values represented by first- and second-order blue, the relative position of line *Q* is still further improved. For first-order blue, line *Q* almost coincides with line *P*, representing 24.4-percent-chromium steel; for second-order blue, line *Q* is slightly above line *P*.

Resistance to oxidation of the steel containing 8.8 percent of chromium and 2.8 percent of silicon, therefore, was inferior to the resistance of steel containing 13.6 percent of chromium until the film thickness exceeded a value corresponding to the first interference colors. With further increase in film thickness, the resistance of the chromium-silicon steel became superior to that of the 13.6-percent-chromium steel.

In figure 12 is a diagram representing steel *R*, containing 8.8 percent of chromium, 46.8 percent of nickel, 3.6 percent of cobalt, and 1.5 percent of silicon. The steel was made at this Bureau some years ago for use in experiments on creep of metals at elevated temperatures. In its effect on resistance to oxidation, the 3.6-percent of cobalt (in steel of this composition) probably is about equivalent to the same percentage of nickel. The resistance of this steel to oxidation, therefore, probably is about that of a steel containing 8.8 percent of chromium, 1.5 percent of silicon, and about 50 percent of nickel.

The line representing first-order straw color, if plotted in figure 16, would almost coincide with line *M*, representing 5-percent-chromium steel; it would thus be below the lines representing carbon steels. The lines for brown and blue in figure 12 are unusually steep. The line for brown, if plotted in figure 17, would be between lines *E* and *K* at the right end and between lines *K* and *O* at the left end. It would thus be far above the lines for carbon steels. The line for first-order blue, if plotted in figure 18, would be considerably above the lower group of lines, but far below the line for 13.6-percent-chromium steel and the line for the steel containing 8.8 percent of chromium and 2.8 percent of silicon. The second-order colors were too indistinct to be used in establishing lines.

Steel *R*, therefore, has much less resistance to oxidation than steel *Q*, which has the same percentage of chromium but no nickel. The large amount of nickel in steel *R*, in conjunction with the 8.8 percent

of chromium, evidently was less effective in retarding oxidation, than the 2.8 percent of silicon in steel *Q*. Comparison of the diagram for steel *R* with the diagram (fig. 6) for steel *K*, containing 32 percent of nickel but no chromium, indicates that the 8.8 percent of chromium in steel *R* had considerable effect in increasing resistance to oxidation.

In figures 13 and 14 are diagrams representing two chromium-nickel steels with high percentages of chromium. The diagram (fig. 13) for steel *S*, containing 18.2 percent of chromium and 8.6 percent of nickel, differs little in form and position from the diagram for the 24.4-percent-chromium steel, *P* (fig. 10). The lines representing first-order colors in the two diagrams are at about the same height at the right end; at the left end, the line for first-order straw color is lower for steel *S* than for steel *P*. The lines for first-order brown and blue, however, are higher for steel *S* than for steel *P*. The lines representing second-order colors are higher, throughout their whole extent, for steel *S* than for steel *P*. The rates of oxidation of the two alloys, therefore, were at first about the same. With increasing film thickness, however, the rate of oxidation became less for the 18:8 chromium-nickel steel than for the 24.4-percent-chromium steel.

The diagram for the 25:20 chromium-nickel steel, *T*, (fig. 14), is lower than the diagram for the 18:8 chromium-nickel steel, *S*, except at the lower boundary and the upper-right corner. The lines for first-order straw color in the two diagrams, in view of the scatter of experimental points in figure 13, show no significant difference in height. The lines for first-order brown and blue and for second-order straw color, however, are distinctly lower for steel *T* than for steel *S*. The lines for second-order brown and blue also are lower for steel *T* than for steel *S*, except at the right end, where the corresponding lines in the two diagrams practically coincide.

The diagram for 25:20 chromium-nickel steel, *T* (fig. 14) is lower than the diagram for 24.4-percent-chromium steel, *P*, (fig. 10), except at the upper-right corner. At this corner, the diagram for the chromium-nickel steel is slightly higher than that for the chromium steel. The evidence presented in figure 14, therefore, appears to confirm the evidence in figure 13, that the presence of nickel did not increase resistance to oxidation, except for film thicknesses greater than those corresponding to first-order colors. The larger percentages of nickel and chromium in the 25:20 alloy, have not made the resistance to oxidation greater than that of the 18:8 alloy; the 25:20 alloy was actually somewhat inferior to the 18:8 alloy. Whether such relationship is typical for steels of these compositions, however, could be determined only by additional experiments with other samples.

In figure 15 is a diagram representing an alloy containing 13.4 percent of chromium and 78.6 percent of nickel. As the iron in this alloy amounted to only about 7 percent, the alloy cannot be classed as a steel. Alloys consisting chiefly of chromium and nickel, however, are much used in services requiring resistance to oxidation at elevated temperatures. It may be of interest, therefore, to compare alloy *U* with the high-chromium steels and chromium-nickel steels. Because of the scatter of experimental points in figure 15, the diagram is less exactly established than are most of the diagrams previously discussed; it may, however, be considered approximately correct.

The diagram for alloy *U* (fig. 15) differs little in form and position from the diagrams for the 24.4-percent-chromium steel, *P* (fig. 10),

and the 18:8 chromium-nickel steel, *S* (fig. 13). Line *U* in figure 16, representing first order-straw color, is somewhat higher than line *S*; it is also higher than line *P*, except at the left end. Lines *U* in figures 17 and 18, representing first-order brown and blue, are considerably lower than lines *S* and *P*. Line *U* in figure 19, representing second-order blue, is higher than line *S*, and much higher than line *P*. Although the evidence is not entirely consistent, it appears to confirm the evidence obtained with chromium-nickel steel, *S*, that nickel in conjunction with high percentages of chromium tends to increase the resistance to oxidation after the film has grown to thicknesses corresponding to second-order colors. This subject, however, needs further investigation.

6. AN EQUATION TO REPRESENT THE INFLUENCE OF TEMPERATURE ON OXIDATION TIME, FOR CONSTANT FILM THICKNESS

The linear relationship represented by the corrected graphs in figures 1 to 15, inclusive, means that the oxidation time varies inversely, and that the mean rate of oxidation varies directly, as a power of the absolute temperature. This relationship may be represented by the equation:

$$\log t_2 - \log t_1 = n\ (\log T_1 - \log T_2). \tag{7}$$

In this equation, $\log t_1$, $\log T_1$, $\log T_2$, and $\log T_2$ represent the coordinates of two points on a straight-line graph, and n represents the cotangent of the angle of slope, when the coordinates represent the first power of each variable. Because the tenth powers of the absolute temperatures are used as ordinates in figures 1 to 15, the cotangents of the angles of slope in these figures must be multiplied by 10 to obtain the corresponding values of n.

Equation 7 may be changed to the form

$$t_2/t_1 = (T_1/T_2)^n, \tag{8}$$

which shows that the oxidation time (for constant film thickness) varies inversely as nth power of the absolute temperature. The mean rate of oxidation, because it is proportional to the reciprocal of the oxidation time, varies directly as the nth power of the absolute temperature.

Values for "n" obtained from the slopes of the graphs of figures 1 to 15, have been assembled in table 2. For each alloy represented in the table, "n" increases with the progression of interference colors from first-order straw color to the last discernible color. The range of values of "n" varies with the amount of divergence of the lines in the corresponding diagram. The 0.46- and 0.83-percent carbon steels, *D* and *E*, whose diagrams are higher than those of steels with smaller or larger percentages of carbon, gave much wider ranges of "n" than those of the other steels. The average values for the carbon steels, with the exception of steels *D* and *E*, differ little from the corresponding averages for alloy tool steels, low-chromium steels, and stainless chromium-nickel alloys, *S*, *T*, and *U*. They also differ little from the values for chromium-silicon steel, *Q*, and from all the values for the 24.4-percent-chromium steel, *P*, except the low value for first-order straw color.

Considerably greater ranges of values, comparable with the ranges for steels *D* and *E*, were obtained with nickel steels, *J* and *K*. A smaller range of values was obtained with 13.6-percent-chromium steel, *O*. As previously stated, however, the diagram for this steel is less exactly established than the diagrams for most of the other steels. Low values for "*n*" were also obtained with the complex alloy, *R*. With the exceptions that have been mentioned, the steels show little difference in corresponding values for "*n*." The significance of the exceptions could be determined only by experiments with samples from other heats of these compositions.

Pilling and Bedworth [22], as stated in section II (2), obtained a linear logarithmic relationship between the absolute temperature and an "oxidation rate constant" estimated on the assumption of a parabolic relationship between oxidation time and the thickness of the oxide layer. In their experiments, however, the oxide layers were 10 to 1,000 times as thick as films giving interference colors. The value of "*n*" for iron, obtained from their data, is 19.3, which is much smaller than the value (39.7) listed in table 2 for iron with film thickness corresponding to third-order blue. Because "*n*" increases with film thickness, for all the steels listed in table 2, a higher rather than a lower value would be expected for the relatively thick oxide layers obtained by Pilling and Bedworth [22]. Further discussion of the relationship between values obtained with thin films and with relatively thick layers is given in sections V and VI.

V. VARIATION OF FILM THICKNESS WITH TIME, AT CONSTANT TEMPERATURE

1. DERIVATION OF DIAGRAMS

Each diagram of figures 1 to 15 represents a plan view of a three-dimensional diagram, in which the vertical dimension represents film thickness. The graphs in each diagram of these figures, therefore, may be viewed as contour lines. The film thickness corresponding to a contour line, which represents a constant interference color, increases with the progression of interference colors from first-order straw color to third-order blue. A plan view, therefore, gives qualitative information about the form of the three-dimensional diagram. For more definite information, both qualitative and quantitative, it is necessary to consider not only the plan view, but also the front view and side elevation. The front view gives direct information about the variation of film thickness with time at constant temperature. Diagrams of front views, derived from typical diagrams of figures 1 to 15, are shown in figures 21 to 24 and figure 26, and typical curves taken from these diagrams are compared in figure 25.

For construction of diagrams of this type, it is necessary to have information about the relationship between film thickness and interference color. The relationship between film thickness (y), wave length (λ), index of refraction (μ), and the order (b) of the interference color, is expressed by the equation

$$2y=\frac{(2b-1)\lambda}{2\mu}. \tag{9}$$

According to this equation, the film thicknesses for the same color of the first three orders are in the ratio 1:3:5. This equation is based

on the assumption that a change of 180° in phase occurs in the light reflected from both the air-oxide interface and the oxide-metal interface. Some investigators, however, have concluded that the 180° change of phase occurs only in the light reflected from the outer surface of the oxide film. On this assumption, light interference would occur when the film thickness is an even multiple of half the wave length, and the ratio of film thicknesses for the same color of the first three orders would be 1:2:3. There is strong evidence, however, in favor of the assumption involved in eq 9. Evans [8] has reported that the color of an oxide film, stripped from the metal and viewed by reflected light, is complementary to the color observed when the film was on the metal. Such a relationship is in accordance with the assumption that light reflected from the oxide-metal interface undergoes a 180° change in phase. Evidence in favor of the 1:3:5 relationship between film thicknesses for the same color of the first three orders has been reported by Dunn [4] on the basis of measurement of electrical conductivity of oxide films. Similar evidence based on weight measurements was obtained by Constable [1], by Vernon [39], by Evans and Miley [9], and by Miley and Evans [20]. Estimated film thicknesses in figures 21 to 26, therefore, are based on the assumption involved in eq 9.

The absolute thickness of the oxide film cannot be determined accurately by means of interference colors, because of lack of exact information about the index of refraction. The index of refraction varies with the composition of the oxide film and with the wave length of the incident light.[7] The influence of variations of composition on the index of refraction probably is slight for the oxide films on iron or steel. If the index of refraction did not vary with wave length, therefore, approximate relative values of film thickness could be obtained by using a constant value (such as 1.0) for "μ" in eq 9. The phenomena of dispersion of light, however, show that the index of refraction generally varies with the wave length. Even approximate relative values of film thickness, therefore, cannot be obtained without making allowance for the influence of wave length on the index of refraction.

Conclusive evidence is lacking as to the influence of wave length on the index of refraction of the oxide film on iron or steel. Results of investigation applicable to this problem were obtained by Constable [2], with oxide formed by ignition of iron in air. His results indicate that the index of refraction is about 15 percent greater for brown interference color, and 25 to 30 percent greater for straw color, than for blue. It is not certain, however, that these values represent the approximate variation of the index of refraction of the oxide film on iron or steel.

Extrapolation of values of the index of refraction of hematite, recorded in the International Critical Tables for a range of wave length from 5890 to 7600 A (angstrom units), gives a much smaller variation with wave length, about 15 percent for the range from straw color to blue. To avoid overcorrection in estimating the relative values of film thickness for use in figures 21 to 26, therefore, it has been assumed that the variation of the index of refraction with variation of the interference color from straw color to blue is 15 percent.

[7] In a recent circular referring to an investigation (not yet published) at Carnegie Institute of Technology, it is said that the index of refraction varies appreciably with the temperature. If so, the film thickness represented by a graph in figures 1 to 15 is not quite constant. The variation, however, probably is slight.

In estimating thicknesses for use in these diagrams, consequently, an uncorrected value for each interference color was obtained by using a value of 1.0 for μ in eq 9. To allow for the variation of μ with wave length, different corrections were then applied for the different interference colors. No correction was applied to the values for blue, of the three orders, but deductions of 7½ percent and 15 percent were made from the uncorrected values for brown and straw color, respectively.

The wave length corresponding to each interference color used in calculations of film thickness was determined by spectrophotometric measurements. Eighteen specimens, six for each of the interference colors used, were submitted to the Optical Division of the Bureau for examination by means of a recording spectrophotometer. Six spectral reflectance curves were thus obtained for each of the three colors. The agreement in form and position of these six curves was so close that the relationship for each color has been represented by a single curve of mean values in figure 20. The results of these measurements thus indicate that the interference colors can be distinguished accurately by use of the unaided eye.

The wave lengths for minimum reflectance may be readily estimated from the curves (fig. 20) obtained with the blue and brown interference colors. Although no minimum appears in the curve for straw color, the curve apparently is approaching a minimum, which would be at a wave length somewhat below the limit of the recording spectrophotometer (4000 A). A value of 3500 A has been assumed for this minimum. For brown and blue, the corresponding values are 4410 and 6330 A, respectively. By use of these values, corresponding values for film thickness have been calculated by means eq 9. These values, corrected as previously indicated, have been used in constructing the ordinate scales for figures 21 to 26.[8]

2. GENERAL DESCRIPTION OF DIAGRAMS

Abscissas in these front views of three-dimensional diagrams, like abscissas in the plan views (figs. 1 to 15), represent the logarithms of the first powers of the oxidation times. The scale of abscissas, however, is more condensed in the front views than in the plan views. The ordinates, for convenient representation of the slight slope of the curves at the left, represent the logarithms of the tenth powers of the thicknesses. The interference colors, from first-order straw color to third-order blue, are indicated at the right of each figure. The letters used to designate these colors have the significance indicated in the general legend, the same significance as in figures 1 to 15.

The diagrams of figures 21 to 24 are derived from typical diagrams of figures 1 to 15. Each small open circle in figures 21 to 24 corresponds to a point on one of the straight graphs of the plan view; each black circle corresponds to a point obtained by extrapolation of one of these straight graphs. Each curve of figures 21 to 24 is based not only on the corresponding small circles, but also on the interrelationship between all the curves of the diagram, and on the interrelationship between the front view, plan view, and side elevation (figs. 27 and 28, and section VI) of the three-dimensional diagram.

The eight diagrams in figures 21 to 24 are similar in form, but differ in position on the coordinate scales. Each curve represents the vari-

[8] The same values have been used in constructing diagrams of a different type, figures 27 and 28.

ation of film thickness with time at the indicated constant temperature. All the curves are qualitatively similar, and are very different in form from the contour lines shown in the plan views.

3. FORM OF THE CURVES OF VARIATION OF FILM THICKNESS WITH TIME, AT CONSTANT TEMPERATURE

The slope of a logarithmic curve of variation of film thickness with oxidation time, is slight at the left, but increases gradually as the curve extends to the right. At the upper boundary of the diagram, each curve appears to be approaching a sloping asymptote. The slope of the logarithmic curve at any point may be represented by the equation

$$\frac{d \log y}{d \log t} = dy/dt \cdot t/y = m. \tag{10}$$

In this equation, y and t have the same significance as in previous equations, and m represents the tangent of the angle of slope at any point, when the coordinates represent the first powers of the two variables. When the tenth power of the thickness is plotted against the first power of the time, as in figures 22 to 24, m is one-tenth the tangent of the angle of slope.

At film thicknesses corresponding to third-order blue, the upper curves in each diagram are nearly straight, and evidently differ little in slope from the corresponding asymptotes. The slopes of the asymptotes of the uppermost curves (represented by a broken line), moreover, are about the same in each diagram. The tangent of the angle of this slope is about 5, thus indicating that m is about 0.5. For any except the upper curves in each diagram, the slopes of the asymptotes cannot be determined even approximately. Probably, however, the asymptotes of all the curves in all the diagrams have about the same slope, corresponding to a value of about 0.5 m. A straight line with this slope represents a quadratic parabola. As each curve extends to the left, m decreases, and eventually becomes very small, probably less than 0.01.

In the experiments on which figures 21 to 24 are based, the initial film thickness was not zero. As stated in section III, the specimens after polishing were kept in dry air at room temperature until needed for experiment. Under such conditions each specimen acquired an invisible oxide film. The few experiments made to determine the thickness of such invisible oxide films, have led to widely differing conclusions. Freundlich, Patscheke, and Zocher [11], who used polarimetric methods, reported that iron mirrors, prepared by thermal decomposition of iron carbonyl in a vacuum and then exposed to air for 10 seconds or less, acquired an oxide film about 10 Angstrom units thick. Tronstad and Höverstad [33], who also used polarization methods, reported that the oxide film on polished iron surfaces in air was about 20 A thick. The accuracy obtainable by the polarization method, however, is somewhat doubtful. Much greater thickness of the oxide film formed at room temperature was reported by Miley [18]. The thickness of the film formed on iron, in 1 day in a desiccator at 18° C, was reported to be 230 A. Assuming the index of refraction to be about 2, the equivalent air thickness (for comparison with the scale of thickness used in figs. 21 to 24) would be about 450 A, which is more than half the estimated value for first-order straw color.

Even on the assumption that the relatively high value reported by Miley is correct, it can be shown that the correction to be applied to the observed oxidation time, to make allowance for the time required to form the initial film, is negligible. The amount of such correction is indicated by the equation

$$t_1/t=(y_1/y)^{1/m}. \tag{11}$$

In this equation, t represents the total correct time, t_1 represents the time necessary to form the initial film, y represents the final film thickness, and y_1 represents the initial thickness. Even assuming a value of 0.5 for y_1/y at first straw color, the corresponding value of $1/m$ is so large (10 or more) that the correction to be applied to the observed oxidation time would be only about 0.1 percent. Such correction would make no appreciable change in any of the curves of figures 21 to 24.

The increase in slope of each curve in figures 21 to 24, as it extends to the right, does not necessarily mean that the rate of oxidation (rate of increase of film thickness with time, dy/dt) increases with increase in film thickness. A curve with downward convexity when drawn with logarithmic coordinates, may become a curve with upward convexity when drawn with Cartesian coordinates, provided that m is less than 1.0, and that the curvature of the logarithmic graph is not too great. As m never exceeds 0.5, the former condition exists. That the latter condition exists can be determined only by plotting the curves with Cartesian coordinates. This has been done in the diagrams of figure 26.

Film thickness, in figure 26, is plotted against the square root of the oxidation time. This method of plotting was chosen to increase the practicable range of oxidation time that can be represented, and also because the asymptotic value of m for the logarithmic curves corresponds to a quadratic parabola. A straight line passing through the origin in a diagram such as those of figure 26, would represent a quadratic parabola, and thus would represent continuous decrease of oxidation rate with increase in film thickness. The upward convexity of the graphs, therefore, indicates that the decrease in velocity of oxidation with increase in film thickness is more rapid than that corresponding to a quadratic parabola. The strong initial curvature of these graphs, the gradual decrease in curvature, and the approach to approximate straightness, are in accordance with the corresponding variation of m (figs. 21 to 24) from less than 0.01 to about 0.5. The initial rate of oxidation, as shown in figure 26, is so great that the first part of each curve appears vertical, up to a film thickness (air equivalent) of about 600 A. At and near the origin, the slope of each curve is governed largely by the rate of chemical combination of iron and oxygen (in absence of an impeding film). With the formation and increase in thickness of the film, the rate of oxidation decreases. At first this decrease in velocity is extremely rapid, in accordance with a parabola of high degree. The rate of decrease of velocity, however, rapidly decreases, and eventually reaches a value represented approximately by a quadratic parabola, which would correspond to an approximately linear relationship in figure 26. (The approach to a quadratic parabola is indicated only qualitatively by the approach to straightness of the graphs in fig. 26, because the approximately quad-

ratic portion of each curve does not pass through the origin of coordinates.)

As shown in section II (1), Pilling and Bedworth [22] and others have reported that the relationship between oxidation time and the thickness of the oxide layer is represented by a quadratic parabola, eq. 2. Their results, however, are based on experiments with oxide layers 10 to 1,000 times as thick as films corresponding to interference colors. As shown by the curves in figures 21 to 24 and figure 26, a quadratic parabola is not a generally correct representation of the variation of film thickness with time at constant temperature. The curves, however, do indicate approach to a quadratic relationship with increase in film thickness. At rapid rates of oxidation, the quadratic relationship is approached closely when the film thickness reaches a value corresponding to third-order blue. At slow rates of oxidation, this relationship is not nearly approached until the thickness of the oxide layer is much greater.

The range of oxygen concentration from the outer to the inner surface of the film, according to implication of the theory of Pilling and Bedworth [22], does not vary with film thickness. The curves in figures 21 to 24 and in figure 26, however, indicate that either the range of oxygen concentration or the diffusional conductivity is (or both are) greater for thin films than for relatively thick films. The thinnest possible film may have at first a layer of 100-percent oxygen adjacent to a layer of 100-percent iron; this would be the greatest possible range of oxygen concentration. With diffusion and with increase in film thickness, the range of concentration would decrease rapidly. Whether such variation in the oxygen concentration-range with film thickness would account for the course of curves such as those in figures 21 to 24, however, cannot be determined without additional evidence. The diffusional conductivity, as well as the concentration range, possibly decreases with the growth of the film throughout the range of interference colors.

4. COMPARISON OF TYPICAL DIAGRAMS

The ranges of coordinates are the same in all the diagrams of figures 21 to 24. The relative resistance to oxidation of the typical metals represented by these diagrams, therefore, may be studied by comparing the indicated ranges of temperature. In the diagrams for electrolytic iron, *A*, and 0.85-percent-carbon steel, *E* (fig. 21), and in the diagram for 5-percent-chromium steel, *N* (fig. 22), the temperatures represented by the highest and lowest curves are 350° and 100° C, respectively. In the diagrams for the 13.6-percent-chromium steel, *O* (fig. 22), for steel *Q* containing 8.8 percent of chromium and 2.8 percent of silicon (fig. 23), and for the stainless chromium-nickel alloys, *S*, *T*, and *U* (figs. 23 and 24), the temperatures represented by the highest and lowest curves are 900° and 300° C, respectively. In the diagram for 24.4-percent-chromium steel, *P* (fig. 23), the temperature range is from 900° to 400° C.

For closer comparison, typical curves from the diagrams of figures 21 to 24, and a curve for a steel (*R*) not represented in these figures, are assembled in figure 25. Considerable extrapolation was required in extending the diagram over this wide range of abscissas. At 300° C, comparison is made between electrolytic iron, *A;* 0.83-percent-carbon steel, *E;* 5-percent-chromium steel, *N;* and 13.6-percent-chromium

steel, *O*. A 400° C curve is used for steel *R*, because a 300° C curve would conflict with the group of curves representing 500° C. At 500° C, comparison is made between five steels with relatively high resistance to oxidation. A curve for the chromium-nickel-iron alloy, *U*, is not included in this group because it would follow closely the curve for chromium-nickel steel, *T*.

Curves *A* and *E*, representing electrolytic iron and 0.83-percent-carbon steel at 300° C, differ little in form and position. The relative positions, however, indicate that steel *E* is slightly superior in resistance to oxidation, especially at thicknesses greater than those corresponding to first-order colors. The relative positions of these two curves are in accordance with the relative positions of the corresponding graphs in the plan views, figures 16 to 19. The curve for 5-percent-chromium steel, *N*, diverges from curves *A* and *E* at a thickness corresponding to first-order straw color, and extends to the right of these curves, thus indicating increasing superiority for steel *N* with increase in film thickness. The relative positions of curves *R* and *N* indicate that a curve representing steel *R* at 300° C, instead of 400° C, would extend to the right of curve *N*. The superiority of steel *R*, thus indicated, probably is due chiefly to its larger percentage of chromium.

The curve representing 13.6-percent-chromium steel, *O*, at 300° C, if extended far enough to the left, probably would cross the curves representing electrolytic iron, carbon steel, and 5-percent chromium steel. To the left of the intersection, according to this evidence, carbon steel and 5-percent-chromium steel would be superior to the 13.6-percent-chromium steel. To the right of the intersection, the 13.6-percent-chromium steel is superior, and the superiority increases rapidly with increase in film thickness. The duration of heating required to reach first-order blue would be more than 10^7 times as great for the 13.6-percent-chromium steel as for carbon steels.

The curves of the group representing steels at 500° C differ little in position at very small film thicknesses. With increase in film thickness, the curves first diverge, then converge, and some of the curves intersect. Although the curves representing 13.6-percent-chromium steel, *O*, and 24.4-percent-chromium steel, *P*, intersect at about second-order straw color, they differ little in position to the right of the intersection. The accuracy of determination of the relative positions of these curves, however, is not great enough to justify the assumption that a steel containing 13.6 percent of chromium actually becomes superior to a steel containing 24.4 percent of chromium, when the film thickness exceeds a value corresponding to first-order blue. The evidence should rather be interpreted to mean that, at these film thicknesses, the two steels show practically no difference in resistance to oxidation. Throughout the range of film thickness corresponding to first-order colors, however, the 24.4-percent-chromium steel was found definitely superior to the 13.6-percent-chromium steel.

Curve *Q*, representing the steel containing 8.8 percent of chromium and 2.8 percent of silicon, coincides with curve *O* at interference colors beyond second-order brown. As they extend to the left, however, the two curves diverge. Throughout the range of first-order colors, curve *Q* is between curves *O* and *P*. Throughout this range of colors, therefore, the steel containing 8.8 percent of chromium and 2.8 percent of silicon was superior to the 13.6-percent-chromium steel, but inferior

to the 24.4-percent-chromium steel. With further extension to the left, the three curves again converge.

The curve for 18:8 chromium-nickel steel, *S*, differs little in position from the curve for 24.4-percent-chromium steel, *P*, until the film thickness exceeds a value corresponding to first-order brown. With further increase in film thickness, curve *S* extends to the right of curve *P*, thus indicating superiority of the chromium-nickel steel throughout a range of thicknesses corresponding to second- and third-order colors. The curve for 25:20 chromium-nickel steel, *T*, is above curves *P* and *S* throughout the range of first-order colors and part of the range of second-order colors. With further increase in film thickness, however, curve *T* extends to the right of curves *P* and *S*. A curve for chromium-nickel-iron alloy, *U*, if drawn in this diagram, would practically coincide with curve *T*.

The evidence obtained with the three chromium-nickel alloys, *S*, *T*, and *U*, therefore, indicates some superiority of these alloys over high-chromium steels for film thicknesses corresponding to second- and third-order colors, and possibly superior resistance to scaling at still greater thickness of the layer of oxide. For film thicknesses corresponding to first-order colors, the chromium-nickel alloys showed some superiority over the 13.6-percent-chromium steel, but no superiority over the 24.4-percent chromium steel.

At the left ends, the curves representing 500° C are much less steep than the curves representing electrolytic iron, carbon steel, and 5-percent-chromium steel at 300° C. This difference in slope would be even greater, if comparison were made at the same temperature; the curves representing carbon steels and 5-percent-chromium steel probably would cross all the curves representing the corrosion-resisting steels. (The evidence for this relationship is more clearly revealed in figs. 27 and 28, by comparison of entire diagrams of a different type, described in section VI.) For very thin films, therefore, resistance to oxidation at elevated temperatures evidently is less for corrosion-resisting steels than for carbon steels or for steels containing 5 percent (or less) of chromium.

Additional evidence that chromium and some other alloying elements first increase and then decrease the rate of oxidation, is given by Portevin, Prétet, and Jolivet [23, 24]. This effect is exhibited by elements, such as silicon, aluminum, and chromium, whose affinity for oxygen is greater than that of iron (as shown by the greater heats of formation of their oxides). These investigators reported that, because chromium tends to oxidize more rapidly than iron, the oxide of chromium eventually becomes concentrated in a thin layer at the inner surface of the oxide film. Through this layer, diffusion is less rapid than through oxide of iron. Until enough chromium has been oxidized to build up this thin layer of oxide of chromium with a superimposed layer consisting chiefly of oxide of iron, the rate of oxidation of chromium steel is greater than that of carbon steel. With increase in film thickness beyond this point, the rate of oxidation is less for chromium steel than for carbon steel. If the percentage of chromium in the steel is 13 percent or more, the protective effect of the chromium begins when the film is very thin.

VI. VARIATION OF FILM THICKNESS WITH TEMPERATURE, FOR CONSTANT OXIDATION TIME

1. GENERAL DESCRIPTION OF DIAGRAMS

Most of the reported results of investigation of oxidation of metals at elevated temperatures represent determinations of increase of weight during a fixed time at various temperatures. These results, therefore, give direct information about the variation of thickness of the oxide layer with temperature, for constant oxidation time. Diagrams representing the results, consequently, would be side elevations of three-dimensional diagrams, of the type that has been studied in plan and front views in sections IV and V. As the results were obtained with rapid rates of oxidation and with relatively thick oxide layers, however, they give no information as to the course of the curves throughout the side elevation, especially at film thicknesses corresponding to interference colors. To obtain information about the form of such curves, and to obtain complementary information about the forms of the three-dimensional diagrams, therefore, left-side elevations of typical diagrams have been assembled in figures 27 and 28.

The logarithmic coordinates in these diagrams represent the tenth powers of temperature and film thickness. The scale dimension, however, is twice as large for abscissas as for ordinates. The tenth power of each variable is used in these side elevations because the tenth powers of the same variables are used in the plan views and front views. A curve in such a diagram, however, is identical in form with the corresponding curve in a diagram with coordinates representing the first power of each variable. For correct representation of the left-side elevations, abscissas in figures 27 and 28 read from right to left.

The side elevation can be derived from either the plan view or the front view. The small circles and triangles in figures 27 and 28 were derived from corresponding points on graphs of the plan views. Each curve is based not only on the positions of the corresponding symbols, but also on the probable interrelationship between all the curves of the diagram, and on the proper interrelationship between the side elevation and the corresponding plan and front views.

2. FORM OF THE CURVES OF VARIATION OF FILM THICKNESS WITH TEMPERATURE, FOR CONSTANT OXIDATION TIME

The logarithmic curves in the side elevations (figs. 27 and 28) are qualitatively similar to the logarithmic curves in the front views (figs. 21 to 24). The slope increases with temperature and with film thickness. With approach to the upper boundary of the diagram, the curvature decreases continuously, and each curve apparently approaches a steeply sloping asymptote. The slope of a curve at any point is represented by the equation

$$\frac{d \log y}{d \log T} = dy/dT \cdot T/y = h \tag{12}$$

In this equation, y and T have the same significance as in previous equations, and h represents the tangent of the angle of slope at any point. Because of the difference in dimensions of the abscissa and ordinate scales in figures 27 and 28, h is one-half the tangent of the angle of slope of a curve (at any point).

From the range of values of h, represented by each logarithmic curve, may be deduced the probable form of a corresponding curve drawn with Cartesian coordinates. The extreme range of values of h for all the curves in figures 27 and 28, is between about 0.2 and 25. Throughout most of the represented extent of each curve (throughout the entire represented extent of some curves), however, h is greater than 1.0. Curves drawn with Cartesian coordinates, therefore, evidently should be qualitatively similar, except possibly in their lower portions, to the curves in figures 27 and 28. Curves actually plotted with Cartesian coordinates, but not here shown, give no evidence of reversal in the lower portions; the slope increases continuously with increase in temperature (and with increase in film thickness). The accelerating influence of rise of temperature, on the rate of oxidation, thus predominates over the retarding influence of increase of film thickness (for constant oxidation time).

The curves in the side elevation of a three-dimensional diagram, if drawn with Cartesian coordinates, are dissimilar in form to the curves so drawn in the front elevation (fig. 26). A three-dimensional diagram, when plotted with Cartesian coordinates, therefore, is complex in form; the graphs in the plan view as well as in the front view are strongly curved. This type of diagram will not be considered in detail.

The asymptotes of the curves in all the diagrams of Figures 27 and 28 apparently differ little in slope. The approximate slopes of these asymptotes may be deduced from the slopes of curves at corresponding points in the plan view and front view. The relationship between the tangent (h) of the angle of slope in the side elevation, the tangent (m) of the angle of slope in the front view, and the cotangent (n) of the angle of slope of the plan view, is given by the equation:

$$h=mn \tag{13}$$

By means of this equation and by use of the asymptotic values for m and n given in section V (3) and in table 2, corresponding values of h may be estimated. The tangent (m) of the angle of slope of the asymptote approached by each curve in a front elevation, as shown in section V (3) probably is about 0.5. The values of n corresponding to second-order blue, for steels *A*, *E*, *O*, and *P* (represented in figs. 27 and 28) are 38.5, 51.0, 32.8, and 35.7, respectively. By substituting these values for m and n in eq 13, the corresponding values obtained for h are 19, 25, 16.5, and 18. With allowance for the 2:1 ratio of scale dimensions in figures 27 and 28, corresponding tangents of the angles of slope of the asymptotes in these figures should be 9.5, 13, 8, and 9. These values are approximately in accordance with the slopes of the curves at the upper boundaries of the diagrams.

As shown in section II (3), results obtained by Dickenson [3] with steels at various temperatures, with constant oxidation time, led him to conclude that logarithmic plotting gives a linear relationship between temperature and the thickness of the oxide layer. Much thicker oxide layers, however, were obtained in his experiments than in experiments based on observation of interference colors. No graphs with logarithmic coordinates were published by Dickenson, and no values were given for the tangent of the angle of slope. From some of his published data, however, it is possible to plot such graphs. Although the graphs so plotted show wide scatter of experimental values, they conform approximately to a linear logarithmic relation-

ship. Values of h so obtained, for the six steels investigated by Dickenson, range from about 11 to 18. These values are generally smaller than the values (16.5 to 25) obtained from the upper ends of the curves in figures 27 and 28. As shown in these diagrams, moreover, the relationship between temperature and film thickness, for constant oxidation time, cannot be represented by any single equation. For constant oxidation time, the film thickness increases as an increasing power of the absolute temperature. With increase in film thickness, the exponent of the power increases from 1 or less to about 20 or 25.

As the logarithmic curves in the front and side elevations of a three-dimensional diagram apparently approach sloping asymptotes, the surface of the three-dimensional diagram (with increase in film thickness) probably approaches a steeply sloping asymptotic plane.

3. COMPARISON OF TYPICAL DIAGRAMS, REPRESENTING THE VARIATION OF FILM THICKNESS WITH TEMPERATURE

In each of figures 27 and 28 are two diagrams representing steels differing greatly in resistance to oxidation. One of the diagrams in each figure represents a carbon steel or iron, the other represents a high-chromium steel. Figure 28 contains also a diagram representing a steel with intermediate resistance to oxidation, a 5-percent-chromium steel. The range of oxidation time is the same in each diagram.

For film thicknesses beyond a value represented by a color between first-order straw color and brown, the temperature field traversed by the diagram representing the high-chromium steel (in each figure) is higher than that traversed by the diagram representing the carbon steel or iron. In the lower part of each figure, however, the diagram representing the high-chromium steel crosses the diagram representing the carbon steel or iron. The diagram representing the 5-percent-chromium steel (fig. 28) crosses both the diagram representing the carbon steel and the diagram representing the 24.4-percent-chromium steel. With increase in film thickness, the curves for the 5-percent-chromium steel extend to the left of the corresponding curves representing the carbon steel, but to the right of the curves representing the high-chromium steel.

The relative resistances to oxidation of these typical steels, revealed by comparison of side elevations of entire three-dimensional diagrams, are in accordance with those revealed by comparison of single curves in the front view, figure 25. The diagrams in figures 27 and 28 confirm the evidence in figure 25, that the resistance to oxidation of chromium steels is less than that of carbon steels until the film thickness exceeds a value corresponding to one of the interference colors of the first order. Probable reasons for this relationship have been given in section V (4).

VII. SUMMARY

By use of interference colors, an investigation has been made of the variation of the thickness of the oxide film on steels, with temperature and time. The relationship between temperature, time, and film thickness, for each of various steels, has been represented by three views of a three-dimensional diagram. From such diagrams, information may be obtained about the influence of temperature and film thickness on the rate of oxidation. The relation between temperature

and time (for constant film thickness), when plotted with logarithmic coordinates, is linear. The slope of the graph indicates that the mean rate of oxidation varies directly, and the oxidation time varies inversely, as a high power (23 to 60) of the absolute temperature.

The variation of film thickness with time at constant temperature, when plotted with logarithmic coordinates, gives a curved line. The slope of this line increases with film thickness, and the line approaches a sloping asymptote; the tangent of the angle of slope of the asymptote is about 0.5. If over short intervals the oxidation time is assumed to vary as a power of the film thickness, the exponent decreases from a high value (100 or more) for thin films, to about 2 for relatively thick films. When plotted with Cartesian coordinates, the form of the curve indicates that the instantaneous rate of oxidation decreases continuously with increase in film thickness.

For constant oxidation time, the relation between film thickness and absolute temperature, when plotted with logarithmic coordinates, also gives a curved line. If for short intervals the film thickness is assumed to vary as a power of the absolute temperature, the exponent increases from 1 or less for thin films to about 20 or 25 for relatively thick films. The accelerating influence of temperature on the rate of oxidation (for constant oxidation time) thus predominates over the retarding effect of increasing film thickness.

By means of views of the three-dimensional diagrams, comparison is made between steels of various compositions, and the influence of alloying elements is discussed.

A tentative discussion is given of the relationship between the rate of oxidation and the constitution and physical properties of the oxide film. The rate of oxidation depends on the oxygen concentration gradient in the film, and on the diffusional conductivity of the oxide. Consideration is given to the possible relationship between these two factors and various physical properties, and to the influence of film thickness on this relationship.

VIII. REFERENCES

[1] F. H. Constable, *Colors shown during oxidation of metallic copper.* Proc. Roy. Soc. (London) [A] **115,** 579 (1927).

[2] F. H. Constable, *Spectrophotometric observations on the growth of oxide films on iron, nickel, and copper.* Proc. Roy. Soc. (London) [A] **117,** 376 (1928).

[3] F. H. S. Dickenson, *Some experiments on the flow of steels at a low red heat, with a note on the scaling of heated steels.* J. Iron Steel Inst. **106,** 128 (1922).

[4] J. S. Dunn, *The low temperature oxidation of copper.* Proc. Roy. Soc. (London) [A] **111,** 210 (1926).

[5] J. S. Dunn, *High temperature oxidation of metals.* Proc. Roy. Soc. (London) [A] **111,** 203 (1926).

[6] U. R. Evans, Discussion of paper *"Oxidation of metals at high temperature"*—N. B. Pilling and R. E. Bedworth, J. Inst. Metals **29,** 585 (1923).

[7] U. R. Evans, *The colors due to thin films on metals.* Proc. Roy. Soc. (London) [A] **107,** 228 (1925).

[8] U. R. Evans, Metallic Corrosion, Passivity and Protection (Edward Arnold & Co. London, 1937).

[9] U. R. Evans and H. A. Miley, *Measurement of oxide films on copper and iron.* Nature **139,** 283 (1937).

[10] W. Feitknecht, *Über die Oxydation des Kupfers bei hohen Temperatur.* Z. Elektrochem. **35,** 142 (1929).

[11] H. Freundlich, G. Patscheke, and H. Zocher, *Über die Passivität von Eisenspiegeln.* Z. physik. Chem. **130,** 289 (1927).

[12] K. Heindlhofer and B. M. Larsen, *Rates of scale formation on iron and a few of its alloys.* Trans. Am. Soc. Steel Treating **21,** 865 (1933).

[13] J. C. Hudson and T. E. Rooney, Review of Oxidation and Scaling of Heated Solid Metals, Sec. 3. (His Majesty's Stationary Office, London, 1935).
[14] O. F. Hudson, T. M. Herbert, F. E. Ball, and E. H. Bucknall, *Properties of locomotive firebox stays and plates.—oxidation of arsenical copper and the effects of small quantities of added elements on the softening temperature and mechanical properties of copper.* J. Inst. Metals (London) **42,** 243 (1929).
[15] A. F. Joffé, The Physics of Crystals. (McGraw-Hill Book Co. Inc., New York, N. Y., 1928).
[16] A. Krupkowski and J. Jaszczurowski, *Vitesse d'oxydation des métaux à température élevée.* Congrès Int. Mines Métallurgie Géologie (Metallurgy) Paris, **2,** 329 (1935).
[17] R. F. Mehl and E. L. McCandless, *Oxide films on iron.* Metals Tech. **4,** Tech. Pap. 780 (1937).
[18] H. A. Miley, *The thickness of oxide films on iron.* Carnegie Scholarship Memoirs, Iron and Steel Inst. **25,** 197 (1936).
[19] H. A. Miley and U. R. Evans, Summary of Work at Cambridge on the Electrometric Study of the Growth of Oxide Films. Fifth Rep. Corrosion Comm. Iron and Steel Inst., Spec. Rep. No. 21, Sec. D 243 (1938).
[20] H. A. Miley and U. R. Evans, *The passivity of metals,* pt. 8. J. Chem. Soc. **1937,** 263.
[21] D. W. Murphy, W. P. Wood, and W. E. Jominy, *Scaling of steel at elevated temperatures by reaction with gases and the properties of the resulting oxides.* Trans. Am. Soc. Steel Treating **19,** 193 (1932).
[22] N. B. Pilling and R. E. Bedworth, *Oxidation of metals at high temperature.* J. Inst. Metals (London) **29,** 529 (1923).
[23] A. M. Portevin, E. Prétet, and H. Jolivet, *Contribution to the study of the chemical resistance of various special steels.* J. Iron Steel Inst. (London) **130,** 219 (1934).
[24] A. M. Portevin, E. Prétet, and H. Jolivet, *Méthodes d'étude de la corrosion des métaux et alliages par les gaz à température élevée et leurs applications.* Rev. met. **31,** 219 (1934).
[25] L. E. Price, *Recent German advances in the mechanism of oxidation and tarnishing of metals.* Chemistry & Industry **15,** 769 (1937).
[26] R. L. Rickett and W. P. Wood, *Action of oxygen and hydrogen sulphide upon iron-chromium alloys at high temperatures.* Trans. Am. Soc. Metals **22,** 347 (1934).
[27] E. Schröder and G. Tammann, *Die Geschwindigkeit der Einwirkung von Sauerstoff, Stickoxyd und Stickoxydul auf Metalle.* Z. anorg. Chem. **128,** 179 (1923).
[28] H. Schwarze, *Beitrag zur Kenntnis der Schutzwirkung der beim Zundern auf Stahl gebildeten Oxydschichten.* Mitt. Forsch-Inst. Ver. Stahlwerke A-G. Dortmund, **2,** 263 (1932).
[29] C. A. Siebert and C. Upthegrove, *Oxidation of a low carbon steel in the temperature range 1650 to 2100 degrees Fahrenheit.* Trans. Am. Soc. Metals **23,** 187 (1935).
[30] G. Tammann and K. Bochow, *Vergleich der Oxydschichtdicke, bestimmt durch Anlauffarben und durch Wägung.* Z. anorg. Chem. **169,** 42 (1928).
[31] G. Tammann and W. Koster, *Die Geschwindigkeit der Einwirkung von Sauerstoff, Schwefelwasserstoff und Halogenen auf Metalle.* Z. anorg. Chem. **123,** 216 (1922).
[32] G. Tammann and G. Siebel, *Die Anlauffarben auf Eisen-Kohlenstoffleigierungen und auf der Eisenmischkristallen.* Z. anorg. Chem. **148,** 297 (1925).
[33] L. Tronstad and J. Höverstad, *Optische Untersuchungen zur Frage der Passivität der Metalle.* Z. phys. Chem. [A] **170,** 172 (1934).
[34] C. Upthegrove. *Scaling of Steel at Heat-Treating Temperatures.* Eng. Res. Bul. Univ. Mich. No. 2[illegible] (1933).
[35] C. Upthegrove and D. W. Murphy, *Scaling of steel.* Trans. Am. Soc. Steel Treating **21,** 73 (1933).
[36] G. Valenski, *Introduction à la cinétique de l'oxydation des métaux donnant deux oxydes.* Compt. rend. **203,** 1252 (1936).
[37] W. H. J. Vernon, *First report to Atmospheric Corrosion Research Committee.* Trans. Faraday Soc. **19,** 839 (1923).
[38] W. H. J. Vernon, *Formation of protective oxide films on copper and brass by air exposure at various temperatures.* J. Chem. Soc. 2273 (1926).
[39] W. H. J. Vernon, *Laboratory study of atmospheric corrosion of metals, pt. 2.—Iron: Primary oxide film.* Trans. Faraday Soc. **31,**[2] 1668 (1935).
[40] C. Wagner, *Beitrag zur Theorie des Anlaufvorganges.* Z. physik. Chem. [B] **21,** 25 (1933).

[41] C. Wagner and K. Grünewald, *Beitrag zur Theorie des Anlaufvorganges III.* Z. physik. Chem. [B] **40,** 455 (1938).
[42] F. J. Wilkins, *Über die Oxydation des Kupfers bei hohen Temperatur.* Z. Elektrochem. **35,** 500 (1929).

TABLE 1.—*Chemical composition of steels*

Symbol	Material [1]	Element, percentage by weight							
		C	Mn	P	S	Si	Cr	Ni	Miscellaneous
A	Electrolytic iron [2]	0.008	0.003			0.001		0.018	0.030 Cu.; 0.006 Co.
B	Open-hearth iron [2]	.02	.03			.001			
C	0.09% C steel [2]	.09	.56			.01			
D	0.46% C steel	.46	.57	0.036	0.042	.20			
E	0.83% C steel	.83	.27	.017	.015	.16			
F	1.29% C steel	1.29	.23	.017	.017	.23	0.05		
G	Cr-W-Mn tool steel [2]	1.00	1.20				.50		0.50 W.
H	2.74% W tool steel [2]	1.34	0.25	.034	.054	.32	.14		2.74 W.
I	High-speed steel	0.66	.26	.027	.012	.09	3.90		18.25 W; 1.12 V.
J	3.35% Ni steel	.40	.67	.034	.039	.23		3.35	
K	31.95% Ni steel	.07	.81			.14	0.04	31.95	
L	1.38% Cr steel	1.06	.34	.016	.011	.19	1.38		
M	2.18% Cr steel	0.72	.49	.025	.008	.19	2.18		
N	5% Cr steel	.10 to 0.15	.50 max	.03	.03	.50	4.0 to 6.0		
O	13.6% Cr steel	.11	.55	.09	.066	.34	13.59		
P	24.4% Cr steel	.15	.42	.013	.030	.23	24.4	0.35	
Q	8.8:2.8 Cr-Si steel	.45	.26	.012	.006	2.80	8.75	.21	
R	8.8:46.8 Cr-Ni steel	.20	.02	.01	.04	1.53	8.85	46.8	3.60 Co; 0.055 Mg.
S	18.2:8.6 Cr-Ni steel	.07	.44	.012	.018	0.50	18.22	8.63	
T	25:20 Cr-Ni steel	.25 max				.7 to 1.5	24. to 26.	19. to 21.	
U	Cr-Ni-Fe alloy	.06	.53				13.4	78.6	

[1] Iron is the remainder constituent in each of these steels.
[2] Analysis by National Bureau of Standards; results not so designated are from mill analyses.

TABLE 2.—*Values for constant n, representing the variation of oxidation time with temperature, for constant film thickness*

Symbol	Material	First-order			Second-order			Third-order blue
		Straw	Brown	Blue	Straw	Brown	Blue	
A	Electrolytic iron	30.0	30.4	31.1	33.6	36.0	38.5	39.7
B	Open-hearth iron	30.5	31.2	31.7	33.6	35.6	38.5	
C	0.09% C steel	31.7	34.3	35.8	36.1	37.0	38.0	
D	0.46% C Steel	32.4	38.0	45.1	52.4	57.3	60.0	
E	0.83% C steel	30.3	35.6	42.7	44.7	48.4	51.0	
F	1.29% C steel	31.7	32.1	33.3	34.6	35.8	37.4	
G	Cr-W-Mn tool steel	31.7	32.1	32.9	33.1	33.2	33.3	
H	2.74% W tool steel	34.2	34.3	35.1	34.9	36.4	38.6	
I	High-speed steel	25.6	31.4	31.7	33.1	33.3	33.6	
J	3.35% Ni steel	31.5	35.9	43.2	45.1	46.6	47.3	
K	31.95% Ni steel	31.7	37.3	38.5	42.1	47.5	55.8	
L	1.38% Cr steel	28.8	31.6	34.1	35.8	38.1	41.0	
M	2.18% Cr steel	28.9	33.2	34.5	35.3	36.0	36.2	
N	5% Cr steel	25.5	29.7	36.4				
O	13.6% Cr steel	31.7	32.1	32.3	32.6	33.0	32.8	
P	24.4% Cr steel	23.0	33.1	34.3	34.7	35.5	35.7	36.1
Q	8.8% Cr, 2.8% Si steel	25.8	28.6	30.9	31.5	31.9	32.3	
R	8.8% Cr, 46.8% Ni steel	23.7	23.7	24.3				
S	18.2% Cr, 8.6% Ni steel	28.8	30.5	31.5	32.1	33.3	35.1	
T	25% Cr, 20% Ni steel	29.7	32.6	34.6	37.3	38.4	46.8	49.6
U	Cr-Ni-Fe alloy	30.8	31.9	33.7	34.0	33.9	33.9	
	AVERAGE VALUES							
A, B	Irons	30.2	30.8	31.4	33.6	35.8	38.5	
C, D, E, F	Carbon steels	31.1	33.6	36.6	39.2	41.7	43.9	
G, H, I	Alloy tool steels	30.5	32.6	33.2	33.7	34.3	35.2	
L, M	Low-Cr steels	28.9	32.4	34.3	35.5	37.1	38.6	
S, T, U	Cr-Ni stainless alloys	29.8	31.7	33.3	34.5	35.2	38.6	

GENERAL LEGEND

INTERFERENCE COLOR	DESIGNATION	FILM THICKNESS, ANGSTROM UNITS	EXPERIMENTAL POINTS, FIGURES 1—15	
FIRST ORDER STRAW	X	745	○	△ *
FIRST ORDER BROWN	Y	1025	⊘	◬
FIRST ORDER BLUE	Z	1580	●	▲
SECOND ORDER STRAW	X_2	2235	□	
SECOND ORDER BROWN	Y_2	3075	⊠	
SECOND ORDER BLUE	Z_2	4740	■	
THIRD ORDER BLUE	Z_3	7900	◆	

* TWO DIFFERENT SYMBOLS ARE USED WHEN TWO DIAGRAMS ARE SHOWN IN THE SAME FIGURE.

AN ARROW ATTACHED TO A SYMBOL INDICATES BY ITS DIRECTION THAT CORRECT TIME IS GREATER OR LESS THAN REPRESENTED.

NUMERALS ADJACENT TO A SYMBOL INDICATE THE NUMBER OF EXPERIMENTAL VALUES REPRESENTED BY THAT SYMBOL.

THICKNESS IS REPRESENTED IN CORRECTED AIR-EQUIVALENT VALUES.

IN FIGURES 21 TO 24, THE OPEN CIRCLES REPRESENT VALUES OBTAINED DIRECTLY FROM TEMPERATURE-TIME GRAPHS. THE CLOSED CIRCLES REPRESENT VALUES OBTAINED FROM EXTRAPOLATION OF THE TEMPERATURE-TIME GRAPHS.

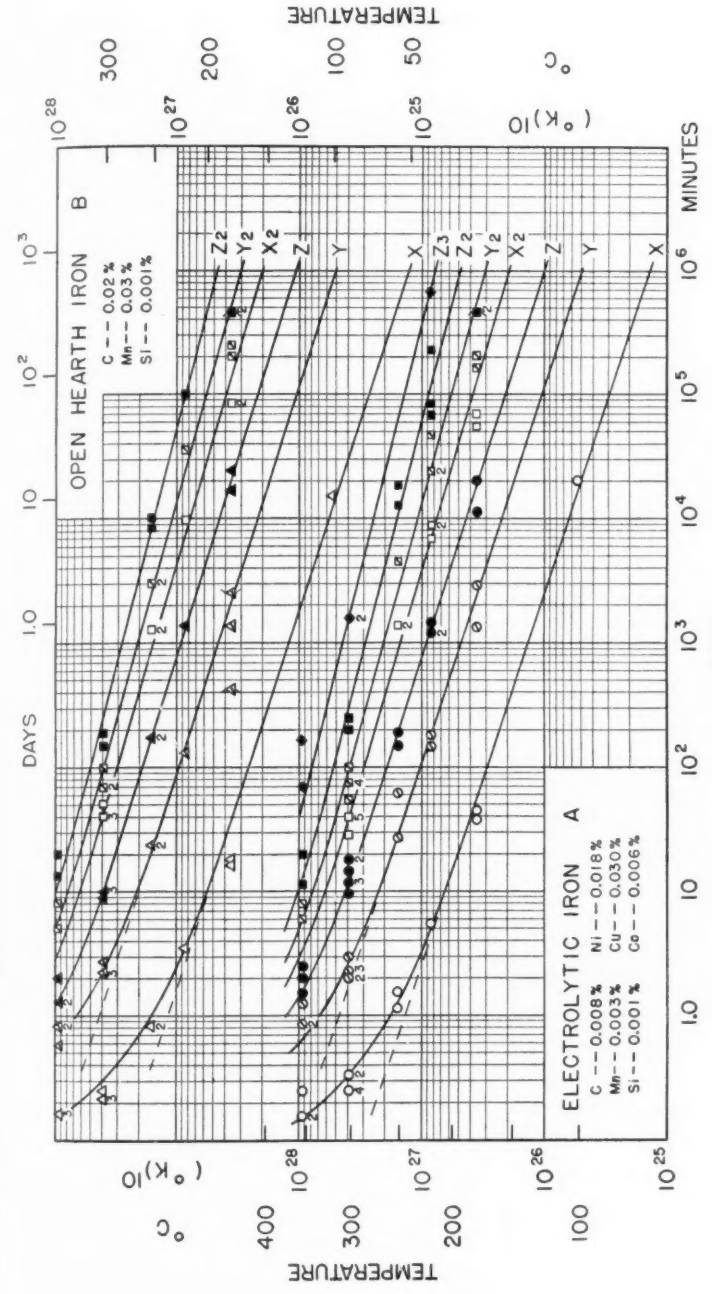

FIGURE 1.—*Influence of temperature on the oxidation time of electrolytic iron and open-hearth iron.*

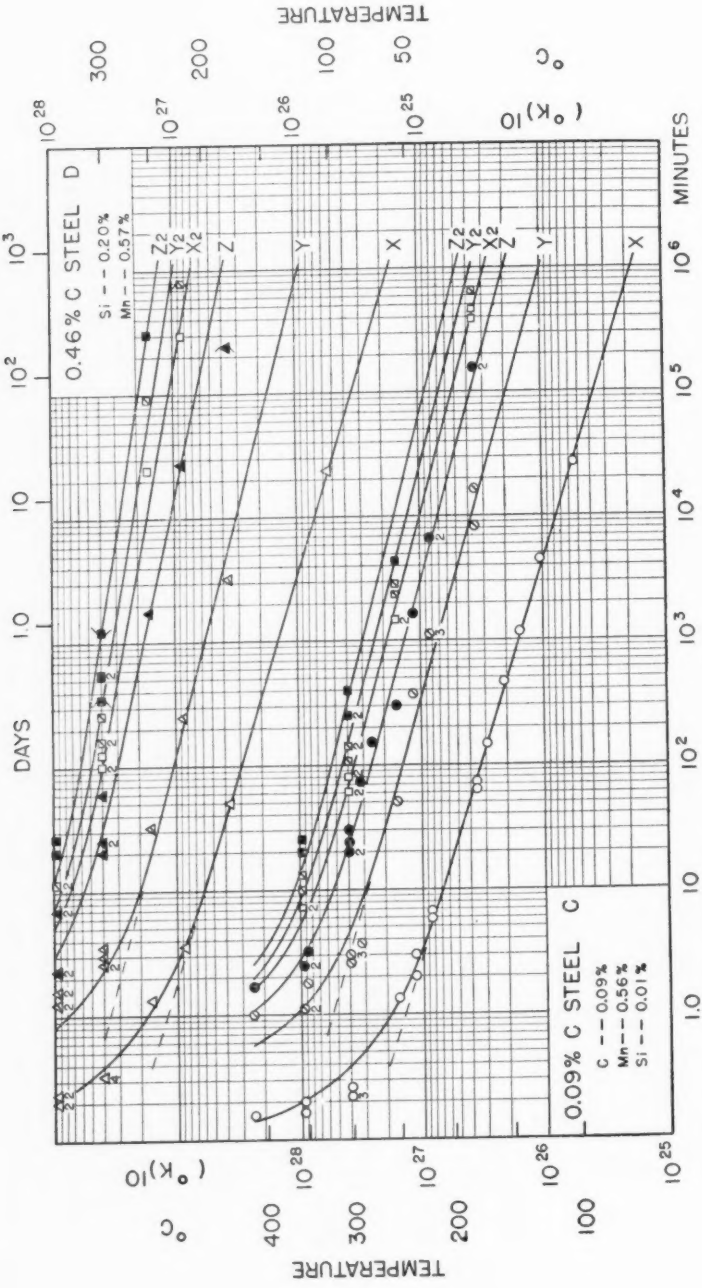

FIGURE 2.—*Influence of temperature on the oxidation time of carbon steels.*

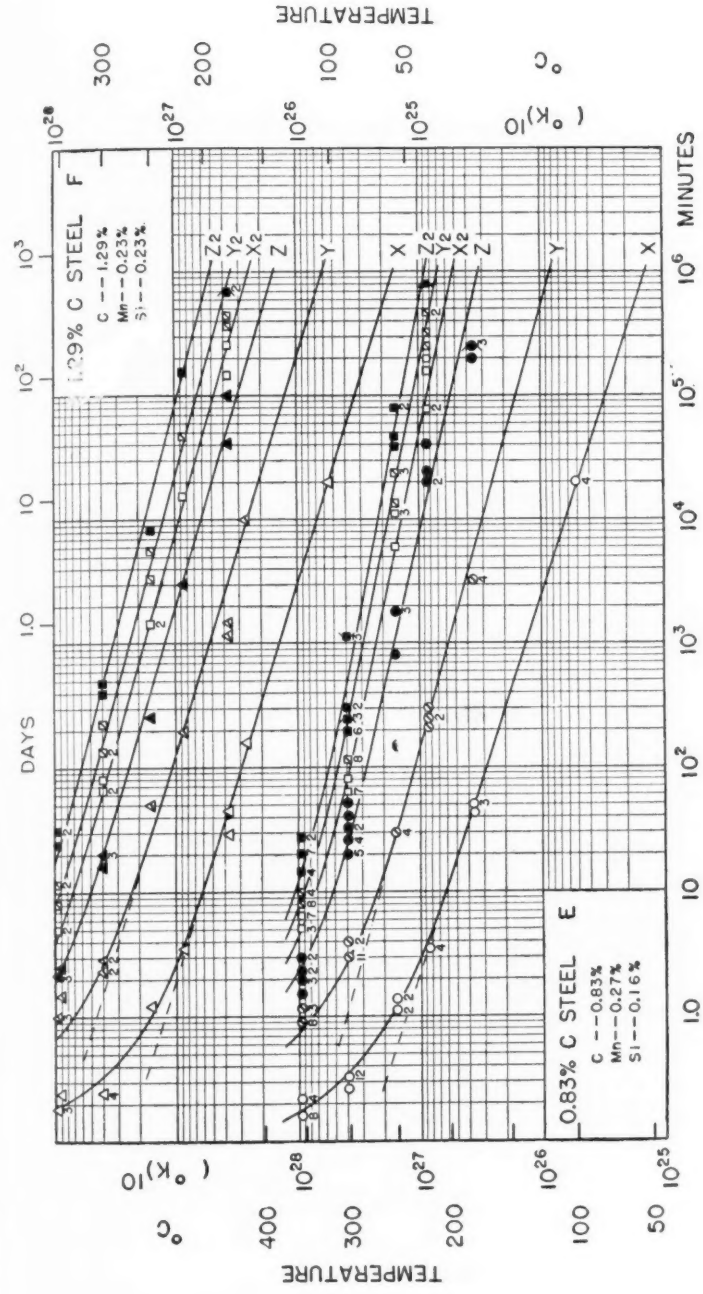

FIGURE 3.—*Influence of temperature on the oxidation time of carbon steels.*

FIGURE 2.—*Influence of temperature on the oxidation time of carbon steels.*

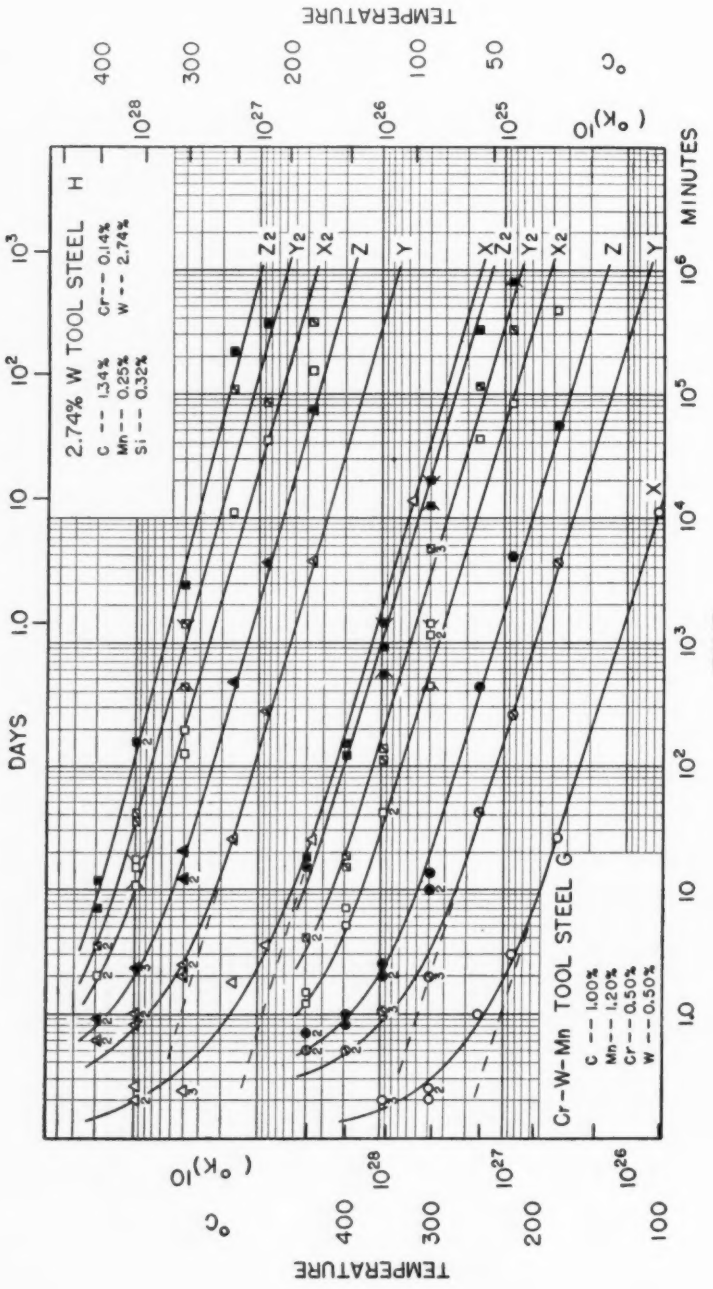

FIGURE 4.—*Influence of temperature on the oxidation time of tool steels.*

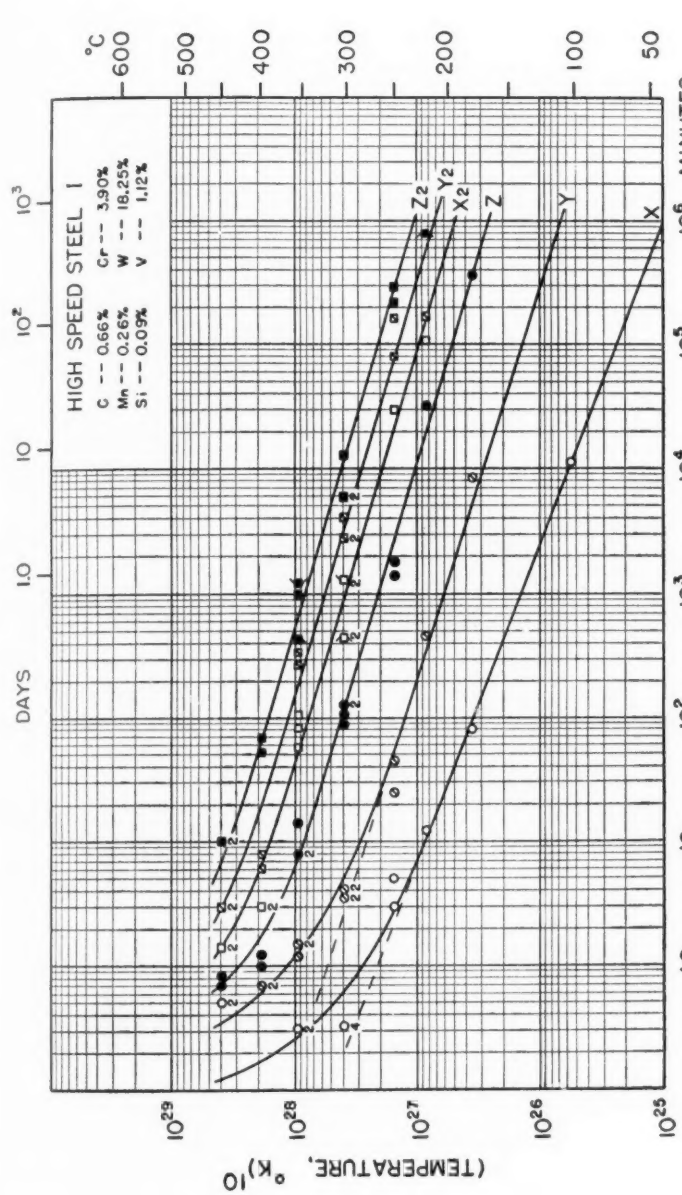

FIGURE 5.—*Influence of temperature on the oxidation time of high speed steel.*

FIGURE 4.—*Influence of temperature on the oxidation time of tool steels.*

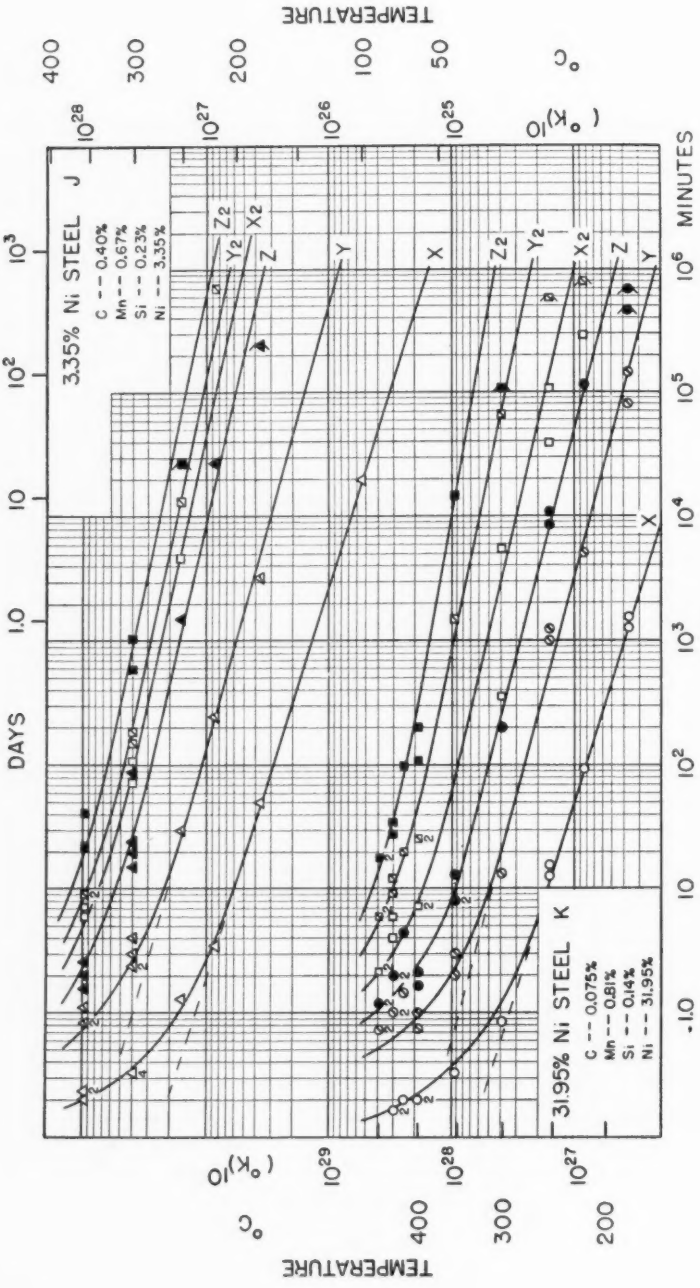

FIGURE 6.—*Influence of temperature on the oxidation time of nickel steels.*

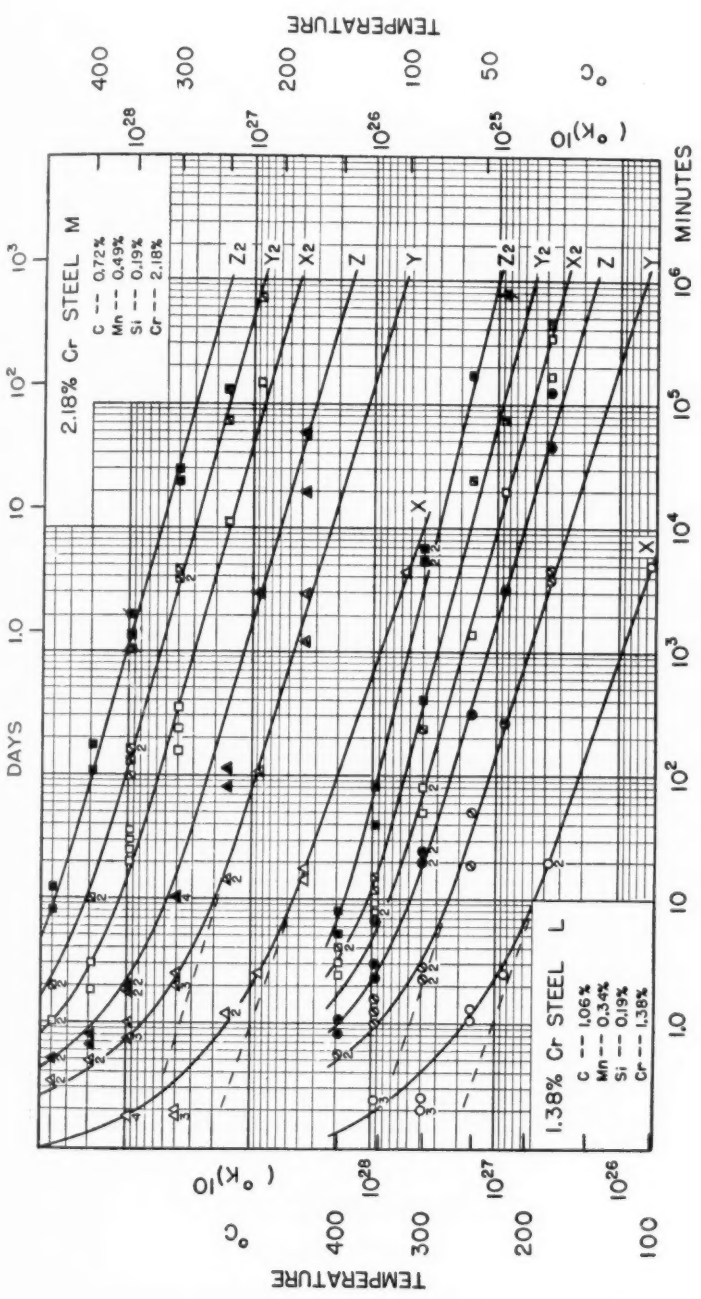

FIGURE 7.—*Influence of temperature on the oxidation time of low-chromium steels.*

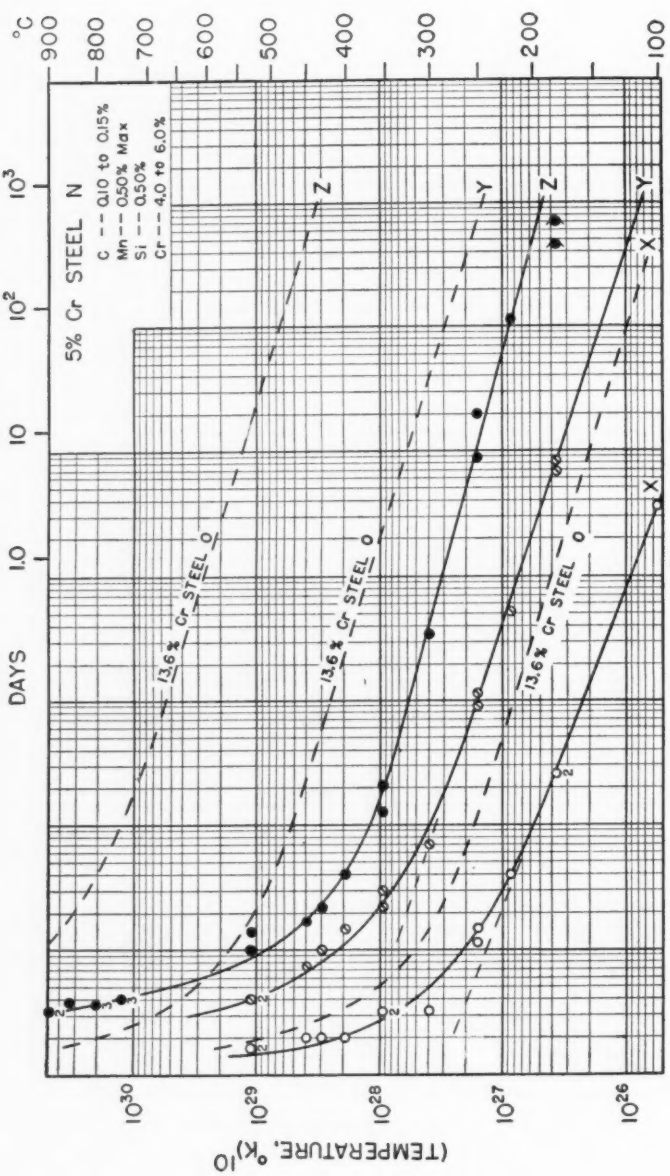

FIGURE 8.—*Influence of temperature on the oxidation time of 5 percent chromium steel.*

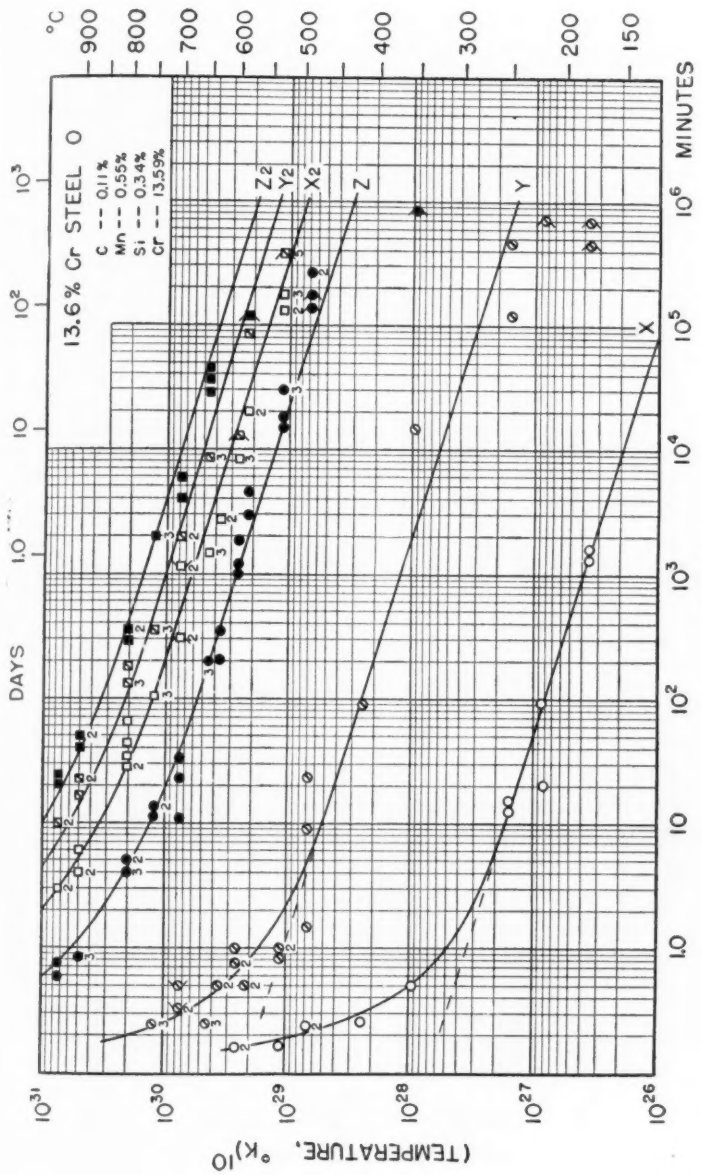

FIGURE 9.—*Influence of temperature on the oxidation time of 13.6 percent chromium steel.*

FIGURE 8.—*Influence of temperature on the oxidation time of 5 percent chromium steel.*

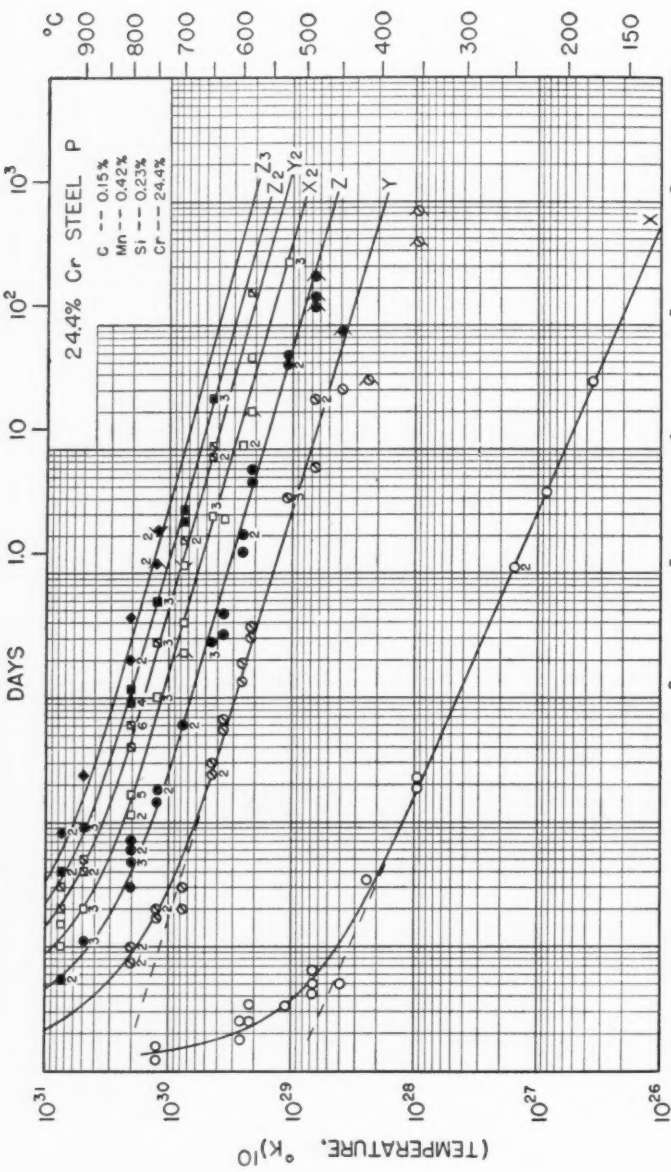

FIGURE 10.—*Influence of temperature on the oxidation time of 24.4 percent chromium steel.*

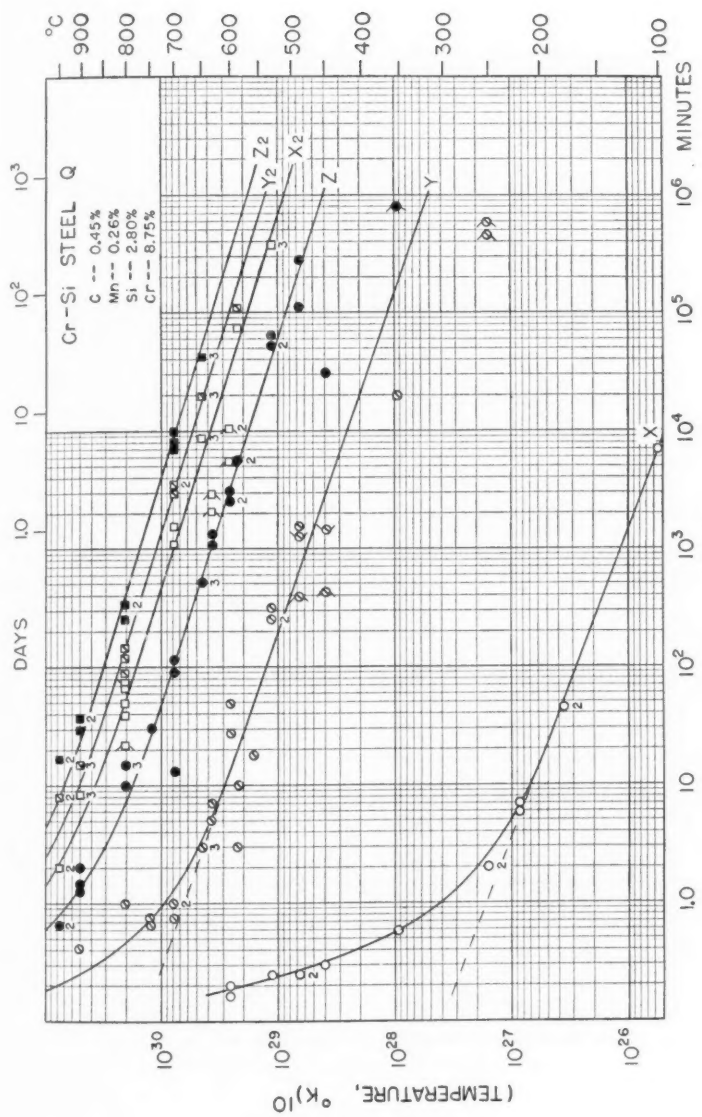

FIGURE 11.—*Influence of temperature on the oxidation time of chromium-silicon steel.*

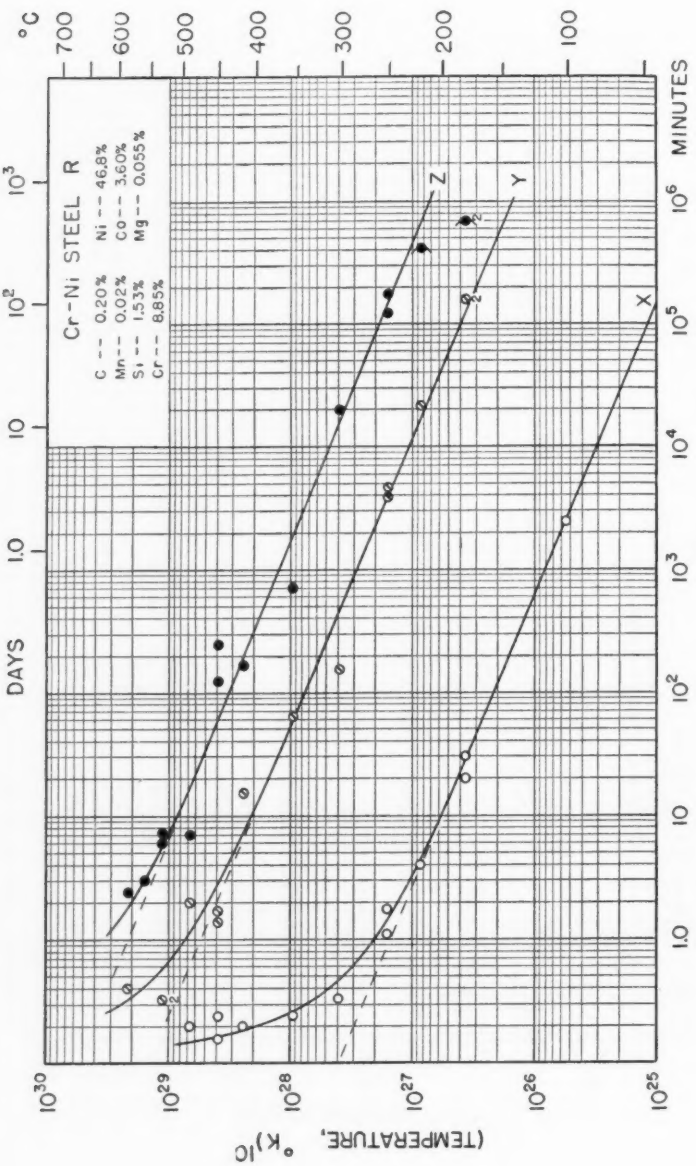

FIGURE 12.—*Influence of temperature on the oxidation time of chromium-nickel-cobalt steel.*

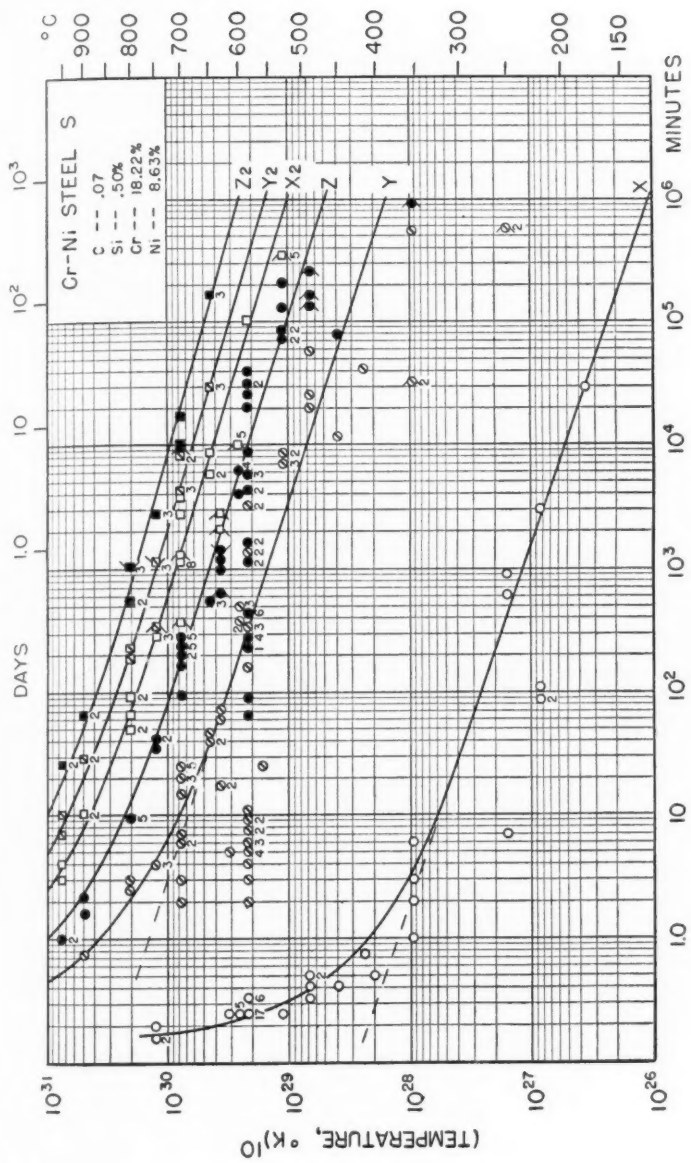

FIGURE 13.—*Influence of temperature on the oxidation time of 18:8 chromium-nickel steel.*

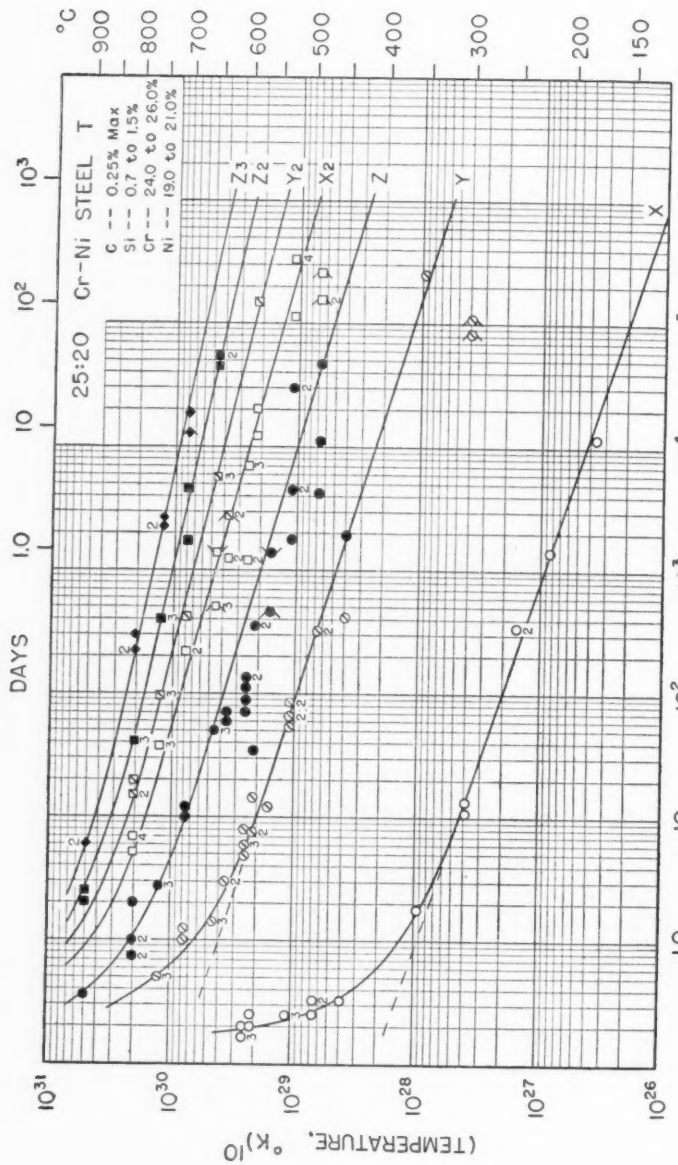

FIGURE 14.—*Influence of temperature on the oxidation time of 25:20 chromium-nickel steel.*

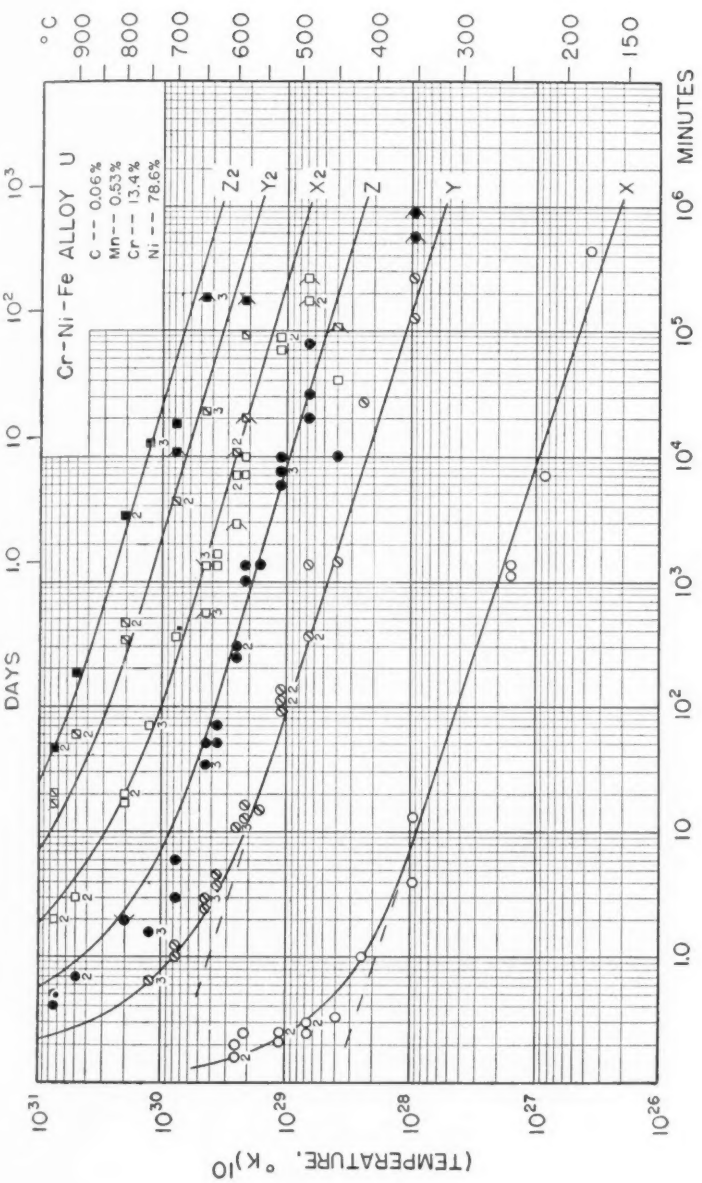

FIGURE 15.—*Influence of temperature on the oxidation time of chromium-nickel-iron alloy.*

FIGURE 14.—*Influence of temperature on the oxidation time of 25:20 chromium-nickel steel.*

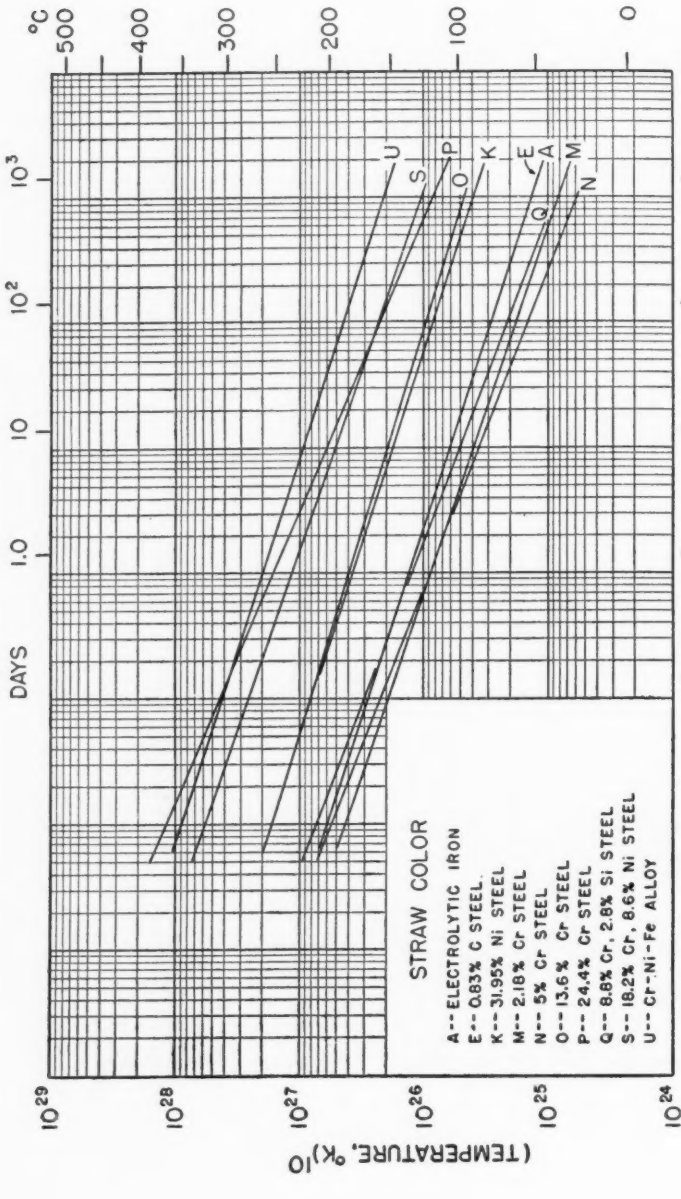

FIGURE 16.—*Influence of temperature on the oxidation time; comparison of graphs representing first-order straw color.*

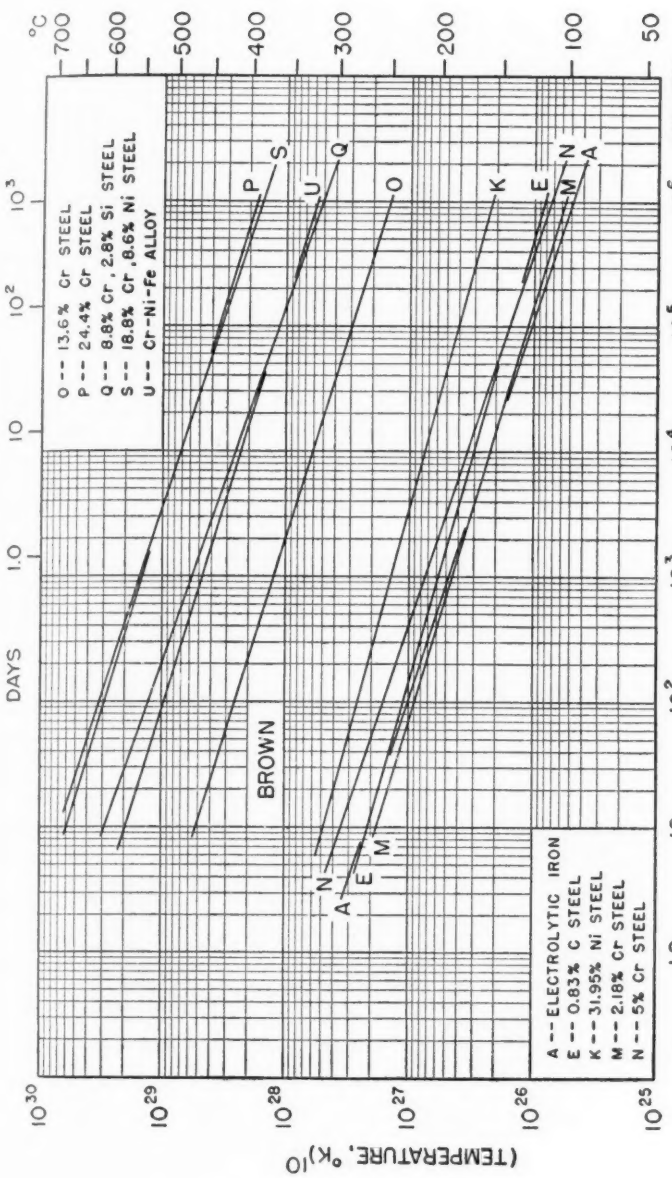

FIGURE 17.—*Influence of temperature on the oxidation time; comparison of graphs for first-order brown.*

FIGURE 16.—*Influence of temperature on the oxidation time; comparison of graphs representing first-order straw color.*

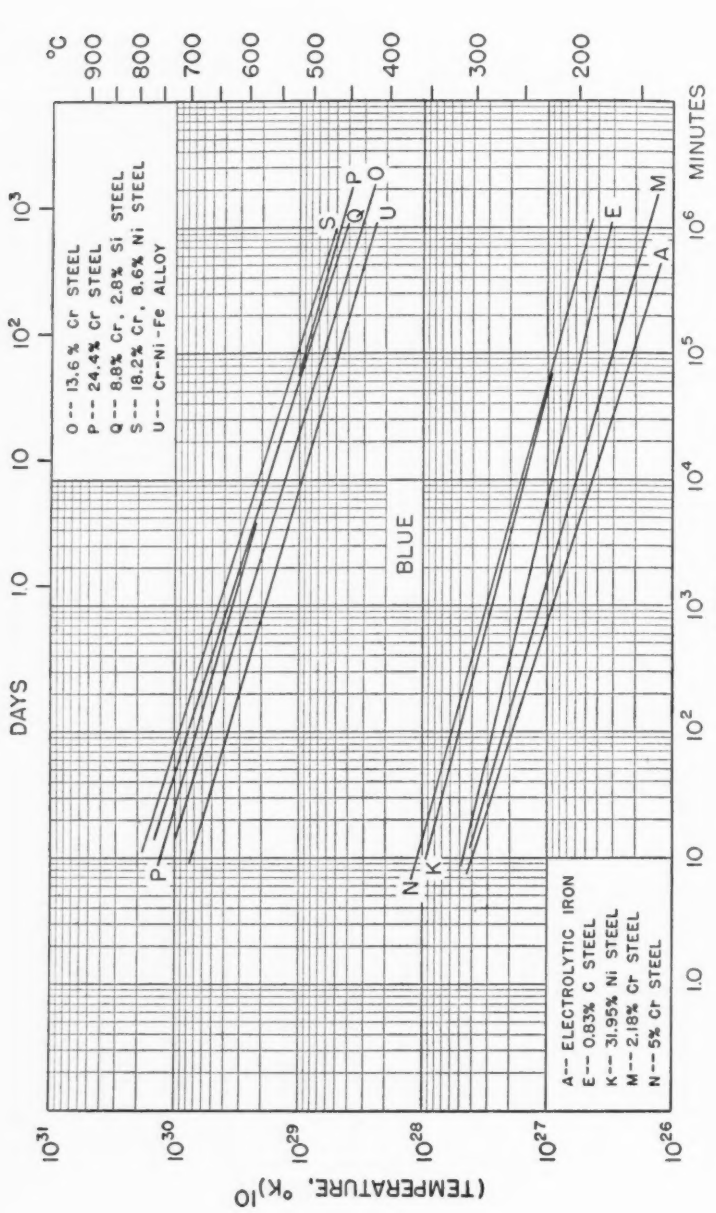

FIGURE 18.—*Influence of temperature on the oxidation time; comparison of graphs for first-order blue.*

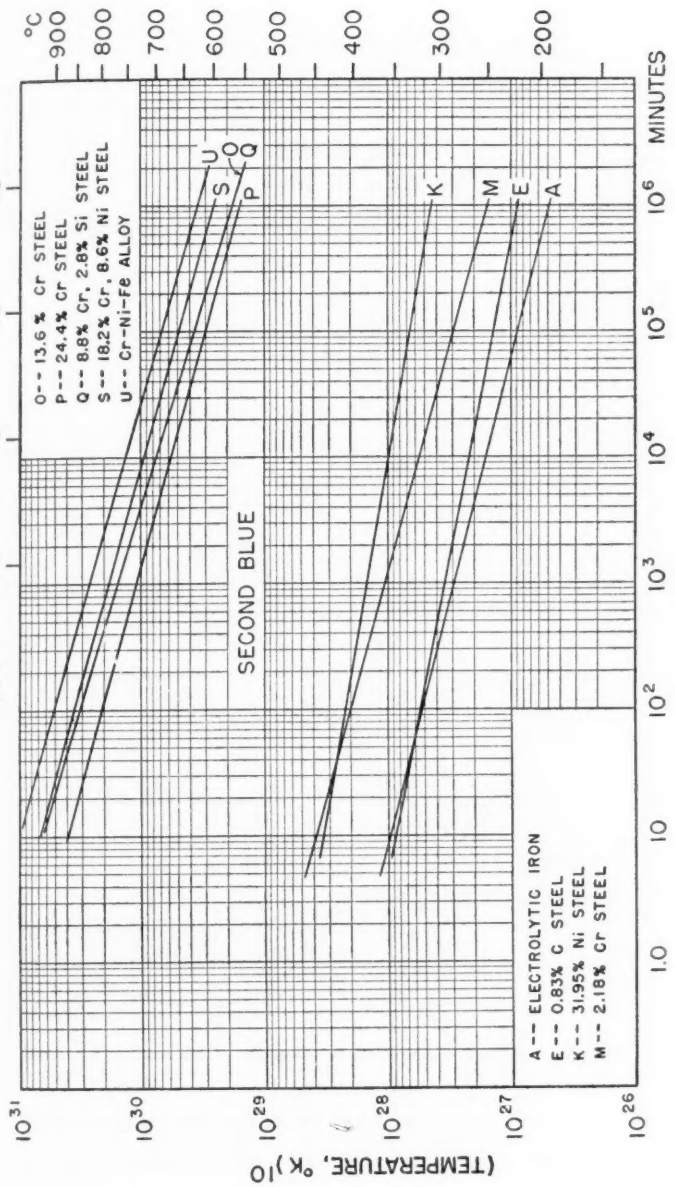

FIGURE 19.—*Influence of temperature on the oxidation time; comparison of graphs for second-order blue.*

FIGURE 18.—*Influence of temperature on the oxidation time; comparison of graphs for first-order blue.*

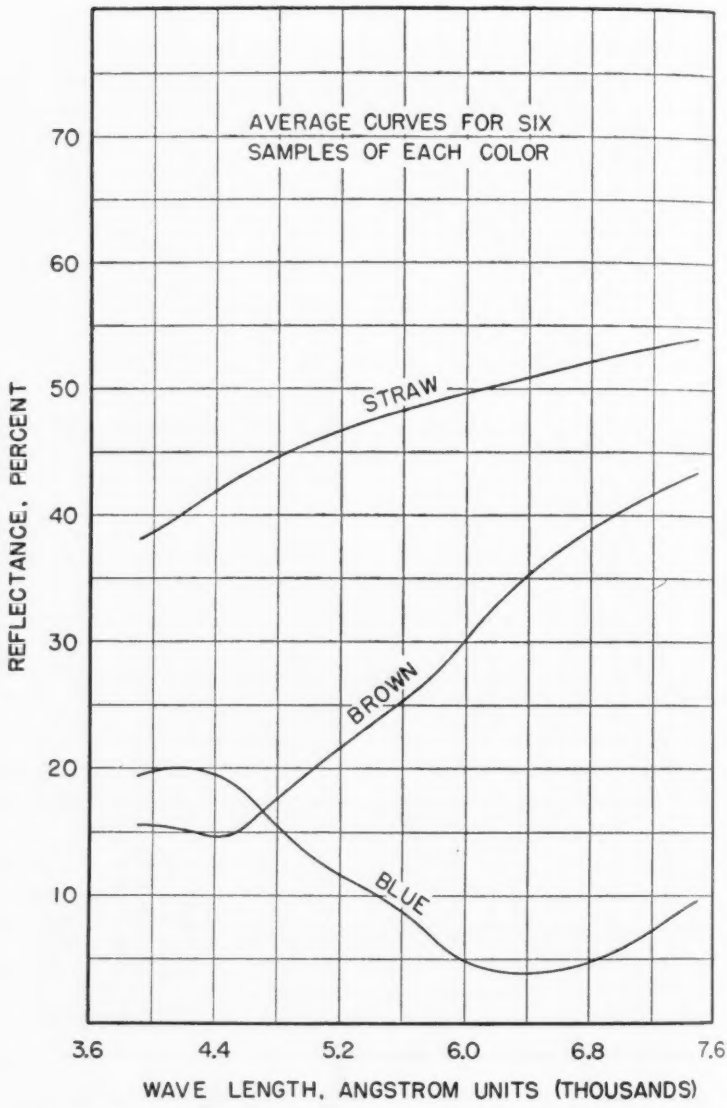

FIGURE 20.—*Variation of reflectance with wave length of incident light, for three interference colors.*

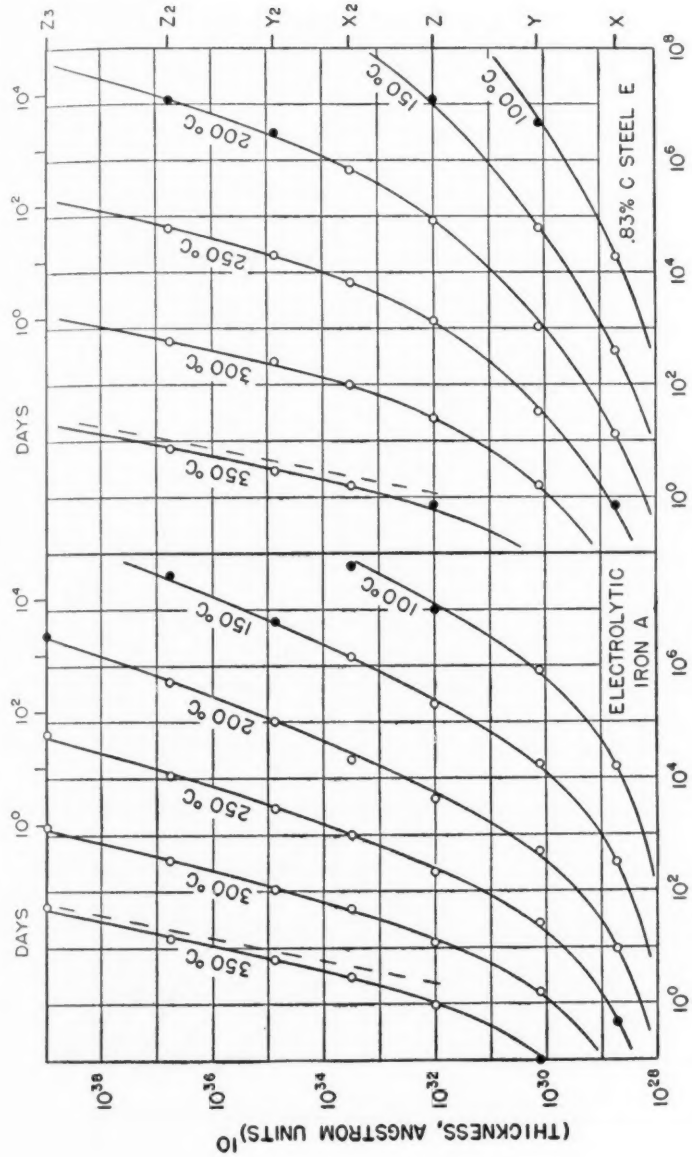

FIGURE 21.—*Variation of film thickness with time at constant temperature; electrolytic iron and 0.83-percent carbon steel.*

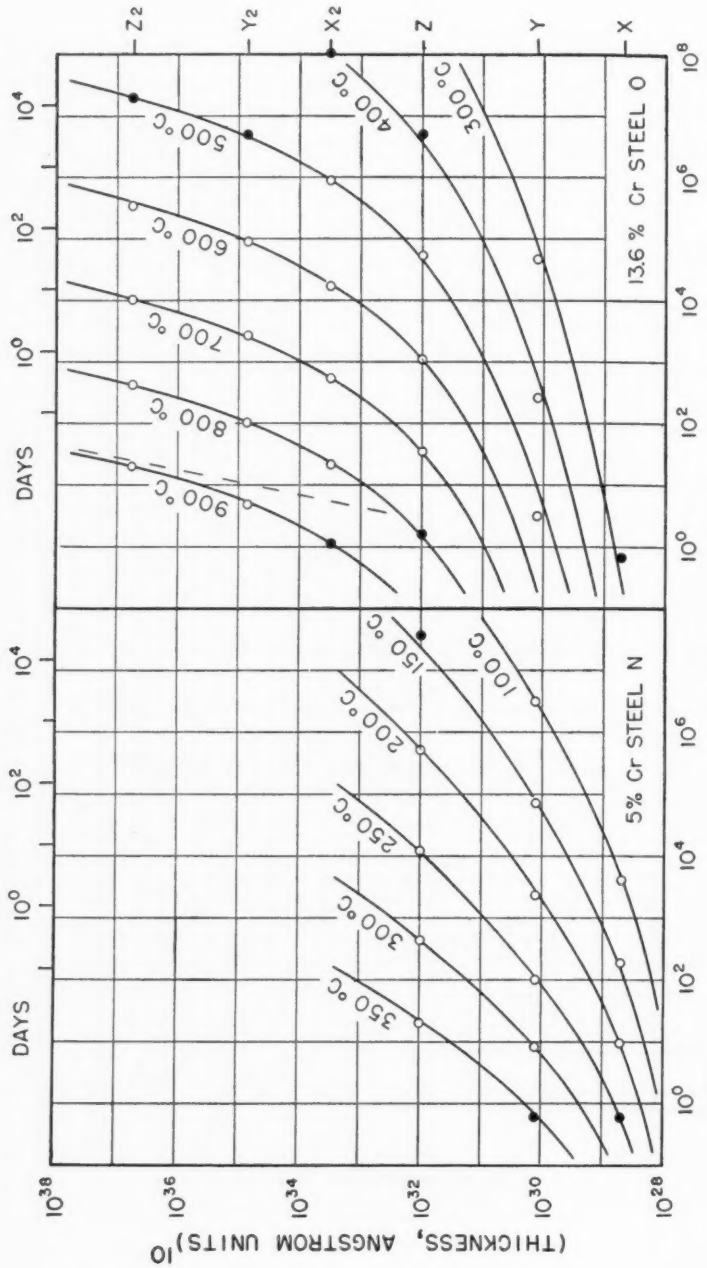

FIGURE 22.—*Variation of film thickness with time at constant temperature; chromium steels.*

FIGURE 22.—*Variation of film thickness with time at constant temperature; chromium steels.*

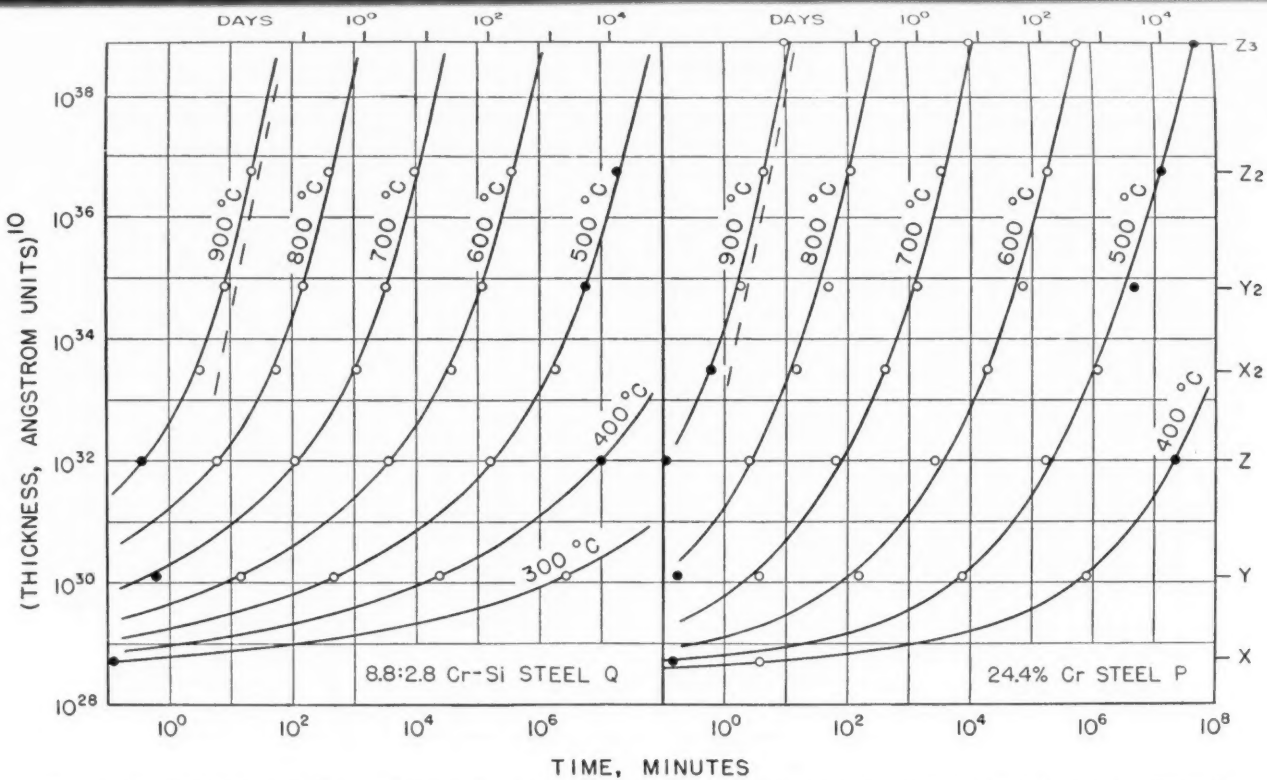

FIGURE 23.—*Variation of film thickness with time at constant temperature; chromium-silicon steel and high-chromium steel.*

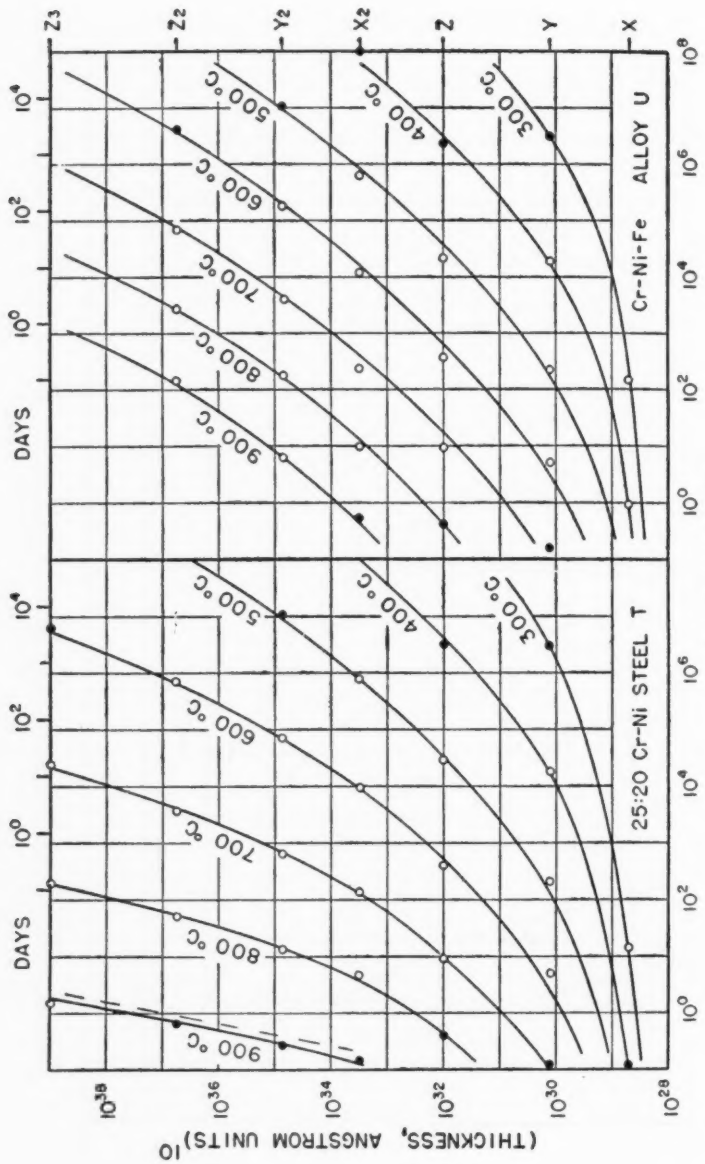

FIGURE 24.—*Variation of film thickness with time at constant temperature; chromium-nickel alloys.*

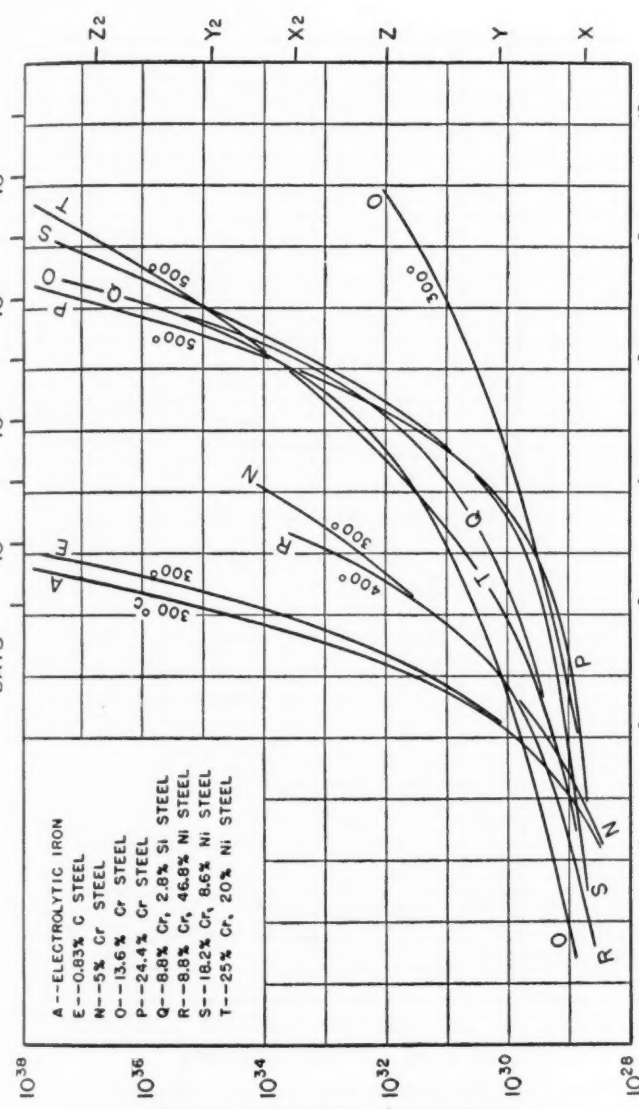

FIGURE 25.—*Variation of film thickness with time at constant temperature; comparison of curves for various steels.*

FIGURE 24.—*Variation of film thickness with time at constant temperature; chromium-nickel alloys.*

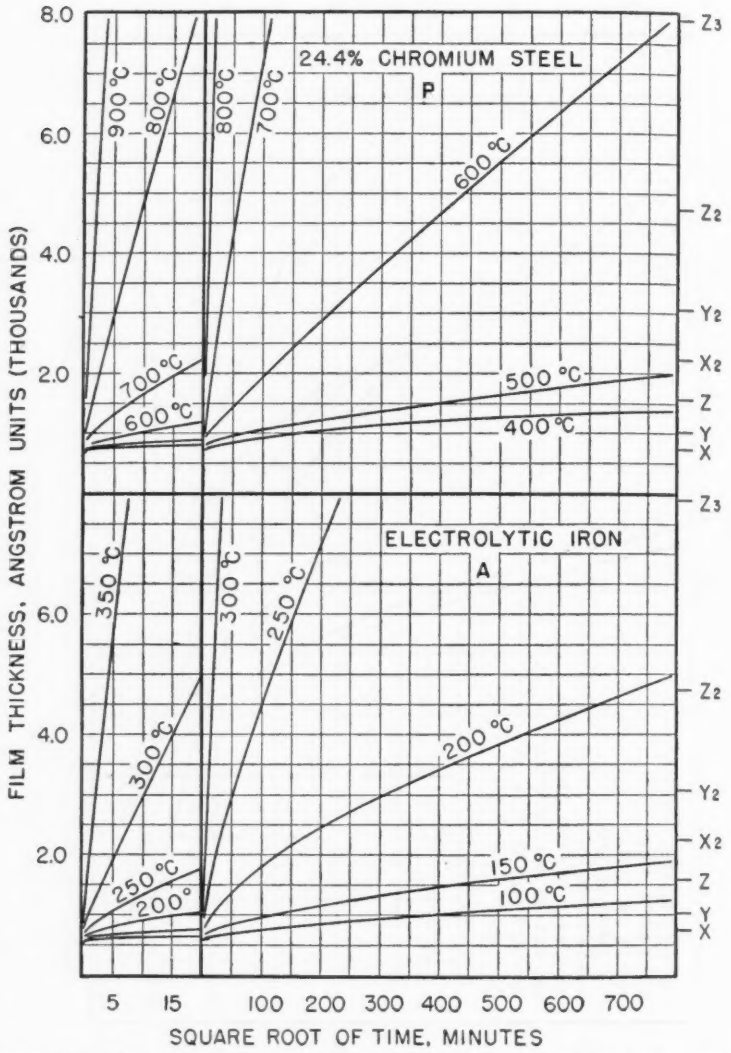

FIGURE 26.—*Variation of film thickness with the square root of the time at constant temperature; electrolytic iron and 24.4 percent chromium steel.*

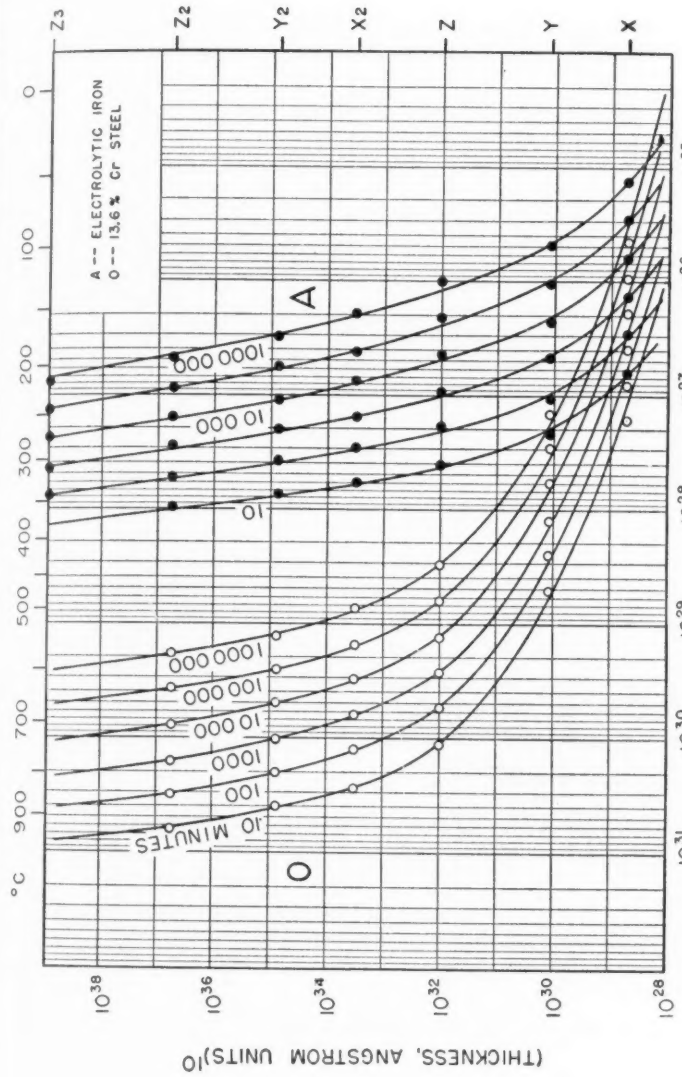

FIGURE 27.—*Variation of film thickness with temperature, for constant oxidation time; electrolytic iron and 13.6 percent chromium steel.*

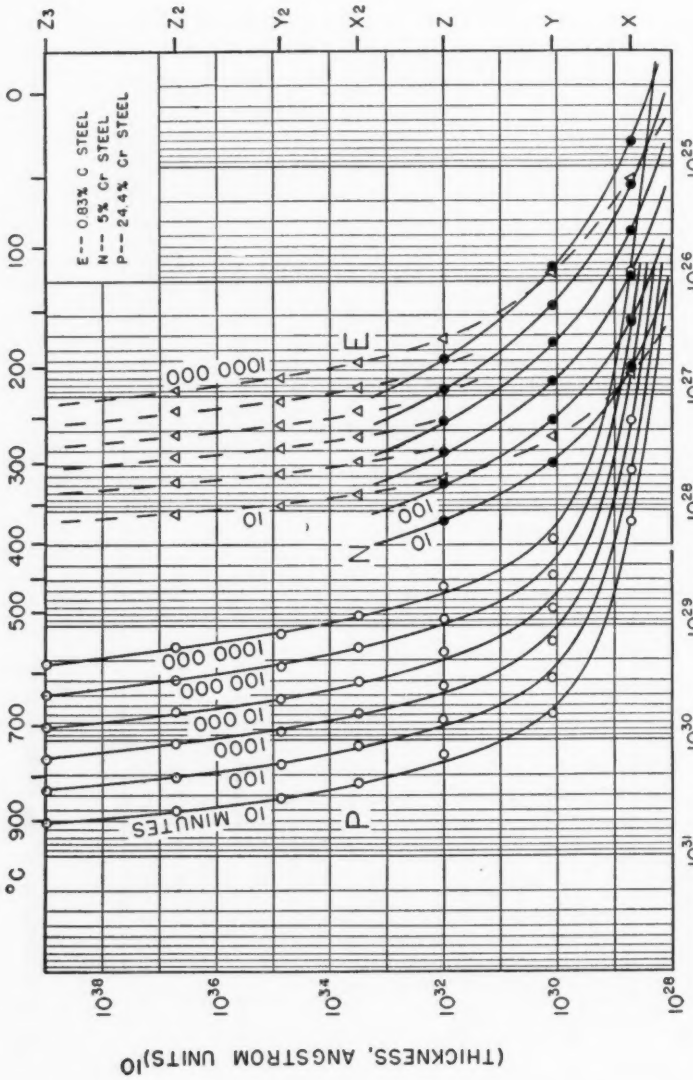

FIGURE 28.—*Variation of film thickness with temperature, for constant oxidation time; carbon steel and chromium steels.*

WASHINGTON, February 20, 1939.

U. S. DEPARTMENT OF COMMERCE NATIONAL BUREAU OF STANDARDS

RESEARCH PAPER RP1222

Part of Journal of Research of the National Bureau of Standards, Volume 23, July 1939

PRESSURE DISPLACEMENTS IN THE SECOND SPECTRUM OF IRON

By Curtis J. Humphreys

ABSTRACT

The changes in wave length of the intense ultraviolet lines in the second spectrum of iron, resulting from changes of pressure upon the source amounting to 1 or 2 atmospheres, have been measured with Fabry-Perot interferometers. The primary purpose of the experiments was to obtain data that would permit adjustment of the Fe II wave lengths of Burns and Walters, which were obtained by measurements of lines emitted by a vacuum arc, to equivalent arc-in-air values, thus furnishing an additional set of independently determined wave lengths for consideration as international secondary standards. These pressure effects are observed to be extremely small; of the order of 1 part in 6,000,000 for 1-atmosphere pressure change, sufficient to affect the seventh figure of proposed secondary standards in the case of only one of the observed term combinations.

CONTENTS

	Page
I. Present status of secondary standards of wave length in the ultraviolet region	125
II. General discussion of the pressure effect	127
1. Resumé of experimental investigations	127
2. Theory of the pressure effect	128
III. Experimental procedure	129
IV. Results	131
1. Classification of observed lines	131
2. Measured pressure displacements	131
3. Term depressions in Fe II	133
4. Conclusions	135
V. References	135

I. PRESENT STATUS OF SECONDARY STANDARDS OF WAVE LENGTH IN THE ULTRAVIOLET REGION

A large majority of spectral lines from laboratory sources which are used as standards of wave length are emitted by the iron arc. The International Astronomical Union,[1] which sponsors the specification and adoption of such standards, requires three independent and concordant determinations of the wave length of any spectral line before it may be considered for adoption as an international secondary standard. The IAU [1] has repeatedly stressed the need of additional independent observations particularly in the ultraviolet region. The list of secondaries in the iron spectrum adopted in 1928 terminated at 3370 A [1],[2] and no additional iron standards of wave length shorter than 3370 A were adopted until 1938 [2]. In the meanwhile, three new sets of measurements of iron wave lengths in the ultraviolet

[1] The complete title will be abbreviated to IAU elsewhere in the paper.
[2] Figures in brackets indicate the literature references at the end of this paper.

appeared. These were by Burns and Walters [3], by Jackson [4], and by Meggers and Humphreys [5]. These results are all quoted in the transactions of the IAU [2]. Jackson's measurements end at 2327 A in the ultraviolet. Those of Burns and Walters and of Meggers and Humphreys terminate at 2100 A. There can be no adoption of standards between 2327 and 2100 A until further observations are made.

The vacuum arc is regarded by some observers as superior to the Pfund arc, specified by the IAU [6], as a source of standard wave lengths. Consequently, Burns and Walters used the former in their wave-length determinations. Wave lengths from these two sources are not strictly comparable, since they differ slightly owing to the pressure displacement resulting from a pressure difference of about 1 atmosphere.

An interferometric investigation of the pressure effect in the iron arc arising from a pressure difference of 1 atmosphere was made by Babcock [7]. Using these observations, he was able to calculate the relative pressure displacements of a large number of Fe I terms. Of the lines observed by Burns and Walters, those which are classified lines of Fe I, involving terms for which the pressure displacements are known, have been adjusted to the equivalent arc-in-air values by use of Babcock's data. Such lines, having thus satisfied the prerequisite of three independent, concordant determinations, were adopted as secondaries by the IAU in 1938 [2].

The majority of the intense lines between 2755 and 2327 A in the spectra obtained with iron-arc sources belong, however, to the second spectrum. The adoption of additional standards in this wave-length interval has been delayed pending the investigation of the pressure effect in Fe II. It was the object of this investigation to measure the pressure displacements of such Fe II lines as were suitable for examination with interferometers. The subsequent calculation of the Fe II term depressions permitted the conversion of the vacuum-arc wave lengths observed by Burns and Walters to arc-in-air values. An additional set of independent observations was thus made available.

It may be stated at this point that the pressure displacements in Fe II appear to be considerably smaller than those obtained by Babcock for Fe I. The displacement for conspicuous lines involving the normal state are of the order of 1 part in 6,000,000, or about 0.0004 A at 2400 A. This is of the same order of magnitude as the random variation associated with repeated measurements using identical sources. It was necessary, therefore, to limit the measurements to very favorably placed lines and to those which appeared sharpest; also to make a sufficient number of observations to minimize the probable error in the final averages. The international secondary iron standards are given only to seven figures. Meggers and Humphreys retained eight figures in cases where the procedure seemed justified by evidence from the combination principle and calculation of the probable error. It is clear, however, that if the pressure effect in Fe II is insufficient to affect the seventh figure, it becomes of little practical importance whether a Pfund arc or vacuum arc is chosen as a comparison source in the ultraviolet between 2300 and 2700 A if Fe II lines are to be used as standards.

II. GENERAL DISCUSSION OF THE PRESSURE EFFECT

1. RESUMÉ OF EXPERIMENTAL INVESTIGATIONS

The pressure effect was discovered by W. J. Humphreys and J. F. Mohler more than 40 years ago. These observers carried out an extensive series of observations of the pressure displacements exhibited by a number of lines in the spectra of each of 48 metals, using pressures up to 15 atmospheres as well as pressures less than 1 atmosphere. The spectrograph contained a Rowland concave grating of 21-foot focus and ruled 20,000 lines per inch.

The results were published by these observers conjointly and separately in a series of articles in the Astrophysical Journal [8]. Among the conclusions drawn from these early experiments were the following: (1) Increase of pressure causes all lines to shift toward the red end of the spectrum. (2) This shift is directly proportional to the increase of pressure. (3) It does not depend upon the partial pressure of the gas or vapor, but upon the total pressure. Dependence of the effect upon various physical properties of the element such as melting point, coefficient of expansion, and atomic volume was indicated. The effect for similar lines appeared to be a periodic function of atomic weight. These experiments were performed many years before the Bohr theory of atomic structure and radiation appeared, and term analyses had been made in empirical fashion for only a few relatively simple spectra. Consequently, the conclusions of the first workers in this field, regarding the correlation of the pressure effect with different regions of the spectra and with various types of lines, must be regarded as superseded by those of later observers who had a previous knowledge of the complete term scheme of the spectrum under investigation. The first three conclusions enumerated above, however, remain essentially unchanged. Following the work of Humphreys and Mohler, little attention was given the pressure effect until comparatively recent times. One reason for this is the fact that the effect is small, often completely masked by other effects such as Doppler broadening, Stark effect in certain high-voltage discharges, or pole effect in arcs. It is always accompanied by a line broadening which increases with increase of pressure making the measurement of the actual shift difficult. The smallness of the effect renders it of little importance in practical spectroscopic measurements, except where precise interferometric wave-length determinations are being made, or in cases where pressure changes of several atmospheres are involved. Another reason why the pressure effect has received little attention is that unlike many other atomic-radiation phenomena such as Zeeman effect, for instance, it does not lend itself readily to a simple explanation in accordance with accepted theories of atomic mechanics.

Babcock's investigation of the pressure effect in Fe I [7], which was mentioned above, constitutes the most important contribution to our knowledge concerning the relation between the observed pressure displacements and the energy-level scheme. His results are in essential conformity with those of Catalán [9], who made a similar study 3 years earlier in 1924, using the pressure effect data of Gale and Adams [10] and the Fe I classifications of Walters [11]. Babcock examined 130 Fe I lines with Fabry-Perot interferometers and was

able to deduce relative pressure displacements for 44 terms. The wave lengths obtained from a vacuum arc were compared with those from a Pfund arc operated under conditions to eliminate any pole effect from the radiation utilized. In addition to substantiating earlier conclusions, that the effect of increased pressure was always a shift to the red, and that it was due to total rather than to partial pressure, Babcock showed that there was a relation between pressure effect on spectral terms of Fe I and their level in the atom. The results were presented in tabular and graphic form and showed an increasing term depression [3] for a given pressure change with elevation of the term. The graph indicated a slightly greater effect for the quintet and septet terms than for the triplets, although the evidence on this point can hardly be regarded as conclusive.

Grating measurements of the pressure displacements in two Fe I multiplets were reported by Beglinger [12] in 1934. His results indicated effects slightly larger than Babcock's, also a variation within the multiplets, dependent upon the wave lengths of the individual lines, which is in disagreement with the earlier findings.

2. THEORY OF THE PRESSURE EFFECT

It is not intended in this paper to give any detailed discussion of the theory of the pressure effect. There have been two distinct approaches to the problem. The first is an outgrowth of the theory of collision damping originally proposed by Lorentz [13] according to which, if an atom is emitting radiation, the phase and amplitude of the radiation may undergo considerable change during collision with another atom. The change of phase is associated with a change of frequency limited in time to the duration of the collision process. The other theoretical explanation of the effect is the statistical theory first proposed by Margenau in 1933 [14], according to which the phenomenon is explained by van der Waals forces between neighboring atoms which affect the magnitudes of the energy levels. The most complete development of this statistical theory has been given by Margenau and Watson [15]. Reference may be made to articles by Jablónski [16], by Kuhn [17], and to more recent papers by Margenau and his associates [18]. Very recently, Reinsberg [19] has derived both the Lorentz theory of collision damping and Margenau's statistical theory on a quantum-mechanical basis.

Observed pressure effects are explained as arising from unequal changes of elevation in the respective energy levels constituting the initial and final states involved in the production of any given line, these changes being caused by changes of pressure upon the emitting atoms. The effect invariably takes the form of an increase of wave length or, what amounts to the same thing, a decrease of frequency, with increase of pressure. Two alternative hypotheses as to the sense of the change of position of the energy levels are available, since only the indirect evidence of increased wave length is obtained by observation. The line displacement might be explained by an elevation of terms, the amount of elevation being relatively greater for the lower terms, or by a depression of terms, the amount of depression being relatively greater for the higher terms. Any reasonable theory of atomic mechanics would lead to the expectation that terms,

[3] The interpretation of the results obviously depends upon the choice between the elevation or depression hypotheses which is discussed below.

arising from electron configurations far removed from the core of the atom, would show an increasing sensitiveness to pressure effect with such removal. Consequently, universal acceptance of the term-depression hypothesis has resulted.

The amount of the pressure displacement is observed to be proportional to the relative density of the gas at the light source; that is, the ratio of the actual density to the density under normal atmospheric temperature and pressure conditions. It is not regarded as a partial pressure effect, in other words, not dependent upon an interaction between atoms of the same species, but rather a cumulative effect resulting from the total contribution of all particles present. The results obtained by surrounding a given source by different foreign gases indicate that the pressure shift depends to a slight extent upon the particular foreign gas introduced. This was demonstrated by Füchtbaur, Joos, and Dinkellacker [20], who studied the mercury resonance line, 2537 A, in absorption at pressures up to 50 atmospheres, using N_2 and CO_2, respectively, to maintain the desired pressures.

III. EXPERIMENTAL PROCEDURE

The experimental technique employed in this investigation was essentially the same as that described in several earlier publications reporting interferometric determinations of wave length, particularly the paper by Meggers and Humphreys [5] previously mentioned. Production of spectra under different conditions of pressure was effected by use of two sources, one, a Pfund arc conforming to the IAU specification [6] and described in the paper just referred to [5], the other an enclosed arc of the same design as that described and illustrated by Curtis [21], suitable for operation at either elevated or reduced pressures.

The same pair of crystal-quartz interferometer plates used in the earlier determination of iron wave lengths with the same evaporated aluminum coating were again used in these experiments. These were separated by invar etalons of 3, 5, and 7.5 mm in the various sets of observations.

A large Littrow mounting quartz spectrograph served to record the interference patterns. Optical accessories included two quartz-fluorite achromatic lenses, one of 25-cm and one of 50-cm focal length, employed to project the interference rings upon the spectrograph slit. The lens of longer focal length was used in making all the reported observations except one series with the 3-mm etalon. Images of the light sources were formed in the interferometer by means of a concave aluminized mirror of about 94-cm radius of curvature.

For the measurement of changes of wave length produced by a change of pressure, two possible methods are available. The first is the differential method by which the variation in ring diameters, occasioned by successive exposures to the respective sources, permits calculation of the change in fractional order of interference, and, consequently, the change of wave length. Attention is called to a method recently proposed by Williams and Gogate [22] for the simultaneous recording of the interference patterns from the two sources. The light from the respective sources would be polarized in mutually perpendicular planes. The overlapping sets of fringes which would appear with illumination of the interferometer by both sources at the

same time would be separated on the photographic plate by placing a double-image prism in the parallel beam of the spectrograph.

The second method may be called the absolute method. In practice the wave lengths from each source could be determined by comparison with the same standard of wave length, such as the primary standard or group of noble-gas lines. The differential method has the advantages of speed and simplicity, and the fact that no corrections are required which would be occasioned by location of source and standard in widely separated spectral regions. The differential method was chosen for these experiments not because it was regarded as inherently superior, but because in the vicinity of 2500 A, it is not possible to make comparisons simultaneously with the primary standard. Refocusing the spectrograph for alternate exposures to different spectral regions and different sources is a time-consuming procedure which always entails uncertainty as to whether the conditions of observation, accompanying the successive exposures, remain unchanged.

The most extensive series of experiments was performed to determine the change in wave length resulting from the operation of the source at atmospheric pressure, and at the lowest pressure at which the enclosed arc may be operated without serious loss of intensity. This low pressure amounted to an equivalent of 5 to 7 cm of mercury, so that the pressure difference in these experiments was somewhat less than 1 atmosphere. Five exposures were made on each plate, three with one source and two with the other, the exposures to the respective sources being alternated. A simple method was devised to permit rapid change from one source to the other. The light was always reflected from the spherical mirror along the same line coincident with the spectrograph axis. The mirror was mounted, however, so as to permit rotation about a vertical axis in order to receive as desired the light from whichever of the two sources was being used. In reducing the measurements from a single plate, the fractional orders corresponding to each source were averaged together, the differences between these averages being assumed to be accounted for by pressure displacement. This procedure is intended, of course, to lessen the effect of small fluctuations in the length of the interference path when not fully under experimental control.

Inasmuch as the pressure effect is proportional to the total pressure upon the source, it would seem desirable to make observations at high pressures amounting to several atmospheres in order to obtain larger displacements. Unfortunately the line broadening associated with increased pressures makes this procedure unsuitable for interferometric measurements if the total pressure exceeds 2 atmospheres.

A number of observations were made utilizing pressure differences of 2 atmospheres, realized by alternately reducing the pressure to the lowest optimum point and raising it to 1-atmosphere excess pressure by introducing compressed nitrogen from a cylinder and taking exposures at the respective pressures. The pressure estimates were somewhat uncertain at the high level, partly because of the unsteadiness resulting from the maintenance of a sufficient flow of gas through the arc chamber to sweep out the smoke and prevent fogging of the quartz window, and partly because the pressure was read from the dial gage on the low-pressure side of the reducing valve, which was recalibrated at the beginning of the experiments but was still regarded as

somewhat unreliable, because it was not very responsive to small pressure fluctuations. The low pressures were read from an aneroid gage which has been used in many previous investigations and gives entirely satisfactory performance.

IV. RESULTS

1. CLASSIFICATION OF OBSERVED LINES

The second spectrum of iron, Fe II, is strongly emitted in arcs along with the first spectrum. The lines are distributed throughout the spectrum, but the most intense multiplets occur in the ultraviolet. Almost all of the strong lines between 2413 and 2327 A, the region covered by the reported measurements, belong to the second spectrum. Fe II may now be ranked as one of the most completely analyzed spectra. Following the discovery of two multiplets by Meggers, Kiess, and Walters [23] in 1924, Russell [24] in 1926 published classifications of over 200 lines, comprising the conspicuous combinations of sextet and quartet terms. Later work by Dobbie [25] resulted in the discovery of most of the terms predicted by the Hund [26] theory, including the doublet system, and led to the classification of about 2,200 lines.

The term system of Fe II is discussed in this paper only to the extent necessary to indicate the quantum designations, origin, and relative positions of the terms which are involved in the production of lines that have been examined for pressure effect. The addition of an s electron to the $3d^6$ configuration of doubly ionized iron yields ^{6}D and ^{4}D terms of Fe II which are derived from ^{5}D of Fe III. The ^{6}D term is the lowest, or ground, term of Fe II and represents the normal state of singly ionized iron atoms. The $3d^7$ configuration yields ^{4}F and ^{4}P in addition to a large number of doublets. This ^{4}F term is located next to the lowest. The binding of a p-electron to the $3d^6$ configuration of Fe^{++} leads to the triads, ^{6}F, ^{6}D, ^{6}P, and ^{4}F, ^{4}D, ^{4}P, all derived from ^{5}D of Fe III. The lines for which pressure effects are reported here arise from combinations of two of these odd sextets, ^{6}F and ^{6}P with the ground term, and from combinations of two of the odd quartets, ^{4}F and ^{4}D with $3d^7$ ^{4}F. The results for these lines, designated by appropriate symbols, are assembled in table 1.

About 20 additional lines were examined, for which pressure effects either were not found, or could not be measured because of lack of sharpness or unfavorable location too near other lines. Most of these are between 2755 and 2562 A, and include combinations of $3d^6$ (^{5}D) $4p$ ^{6}D° with the ground term, also combinations of the odd quartets from the configuration $3d^6$ $4p$ with the moderately low $3d^6$ (^{5}D) $4s$ ^{4}D term. Many other lines in the region studied, including those of the multiplet $3d^7$ ^{4}F$-3d^6$ (^{5}D) $4p$ ^{4}P°, and numerous intersystem combinations, particularly transitions from the odd sextets to the low ^{4}F, are too faint for interferometric observations.

2. MEASURED PRESSURE DISPLACEMENTS

Pressure displacements of the lines for which measurable effects could be observed are reported in table 1. The wavelengths are quoted from the measurements of Meggers and Humphreys [5] except

2348.114 A, and 2348.301 A, which were determined relative to the other observed lines during this investigation. The lines are grouped by multiplets, since related lines are expected to show similar effects. Columns 4 and 5 contain the changes of wave length experienced by each line, corresponding to the pressure variation also noted at the top of the column. The same columns show the pressure displacements averaged for the respective multiplets.

TABLE 1.—*Pressure displacements of observed lines in the second spectrum of iron*

Term combination	Wave length (air)	Wave number (vac)	Change of wave length for 1-atmosphere pressure difference[1]	Change of wave length for 2-atmosphere pressure difference
	A	*cm*$^{-1}$	*A*	*A*
$a^6D_{5/2} - z^6F^\circ_{1/2}$	2413. 3087	41424. 284	0. 0004	0. 0013
$a^6D_{3/2} - z^6F^\circ_{1/2}$	2411. 0663	41462. 808	. 0003	. 0015
$a^6D_{1/2} - z^6F^\circ_{2/2}$	2410. 5172	41472. 250	. 0005	
$a^6D_{1/2} - z^6F^\circ_{1/2}$	2406. 6593	41538. 728	. 0004	. 0014
$a^6D_{1/2} - z^6F^\circ_{1/2}$	2404. 430	41577. 24	. 0006	. 0014
$a^6D_{2/2} - z^6F^\circ_{2/2}$	2399. 2396	41667. 176	. 0004	. 0010
$a^6D_{3/2} - z^6F^\circ_{3/2}$	2388. 6270	41852. 284	. 0003	. 0017
Average			0. 0004	0. 0014
$a^6D_{2/2} - z^6P^\circ_{3/2}$	2380. 7591	41990. 584	0. 0002	0. 0010
$a^6D_{3/2} - z^6P^\circ_{3/2}$	2364. 8269	42273. 457	. 0002	. 0008
$a^6D_{1/2} - z^6P^\circ_{2/2}$	2359. 1039	42376. 000	. 0004	. 0013
$a^6D_{2/2} - z^6P^\circ_{2/2}$	2348. 301	42570. 93	. 0003	
$a^6D_{5/2} - z^6P^\circ_{1/2}$	2344. 2802	42643. 934	. 0003	. 0015
$a^6D_{1/2} - z^6P^\circ_{1/2}$	2338. 0052	42758. 377	. 0002	. 0014
$a^6D_{3/2} - z^6P^\circ_{2/2}$	2332. 7972	42853. 827	. 0005	. 0015
$a^6D_{2/2} - z^6P^\circ_{1/2}$	2327. 3940	42953. 306	. 0001	. 0012
Average			0. 0003	0. 0012
$a^4F_{1/2} - z^4D^\circ_{1/2}$	2384. 386	41926. 72	0. 0005	0. 0018
$a^4F_{3/2} - z^4D^\circ_{3/2}$	2379. 2756	42016. 766	. 0005	. 0022
$a^4F_{1/2} - z^4D^\circ_{1/2}$	2375. 193	42088. 98	. 0006	. 0013
$a^4F_{2/2} - z^4D^\circ_{1/2}$	2368. 595	42206. 21	. 0008	. 0020
$a^4F_{3/2} - z^4D^\circ_{2/2}$	2360. 294	42354. 64	. 0004	. 0017
$a^4F_{4/2} - z^4D^\circ_{3/2}$	2348. 114	42574. 32	. 0008	
Average			0. 0006	0. 0018
$a^4F_{3/2} - z^4F^\circ_{3/2}$	2362. 019	42323. 71	0. 0007	0. 0021
$a^4F_{4/2} - z^4F^\circ_{4/2}$	2359. 997	42359. 96	. 0005	. 0020
$a^4F_{2/2} - z^4F^\circ_{1/2}$	2354. 8888	42451. 843	. 0004	. 0016
$a^4F_{4/2} - z^4F^\circ_{3/2}$	2331. 3067	42881. 222	. 0005	. 0016
Average			0. 0004	0. 0018

[1] The vacuum arc was operated at a pressure equivalent to a few centimeters of mercury to maintain satisfactory discharge conditions. Hence the pressure difference to which the effects in this column are attributed is somewhat less than 1 atmosphere.

The results for 1-atmosphere pressure difference represent the weighted mean of five sets of observations with the 3-mm etalon, nine with 5 mm, and five with 7.5 mm. By an observation is meant a set of five successive exposures on a single plate. The results for 2-atmosphere pressure difference are derived from five sets of observations all with the 5-mm etalon. This separation corresponds to the largest retardation permitting satisfactory resolution at this pressure.

The displacements for a 2-atmosphere pressure difference are considerably too large if the pressure effect is a linear function of pressure. The discrepancy may be partly accounted for by the necessity, previously noted, of operating the enclosed arc at low pressures of nearly one-tenth of an atmosphere rather than at negligibly low pressures. Hence, the results for 1-atmosphere pressure difference are actually obtained with pressure differences somewhat less than 1 atmosphere. On the other hand, the high-pressure observations were made with pressures slightly in excess of 1 atmosphere in order to obtain as nearly as possible a 2-atmosphere pressure difference. The measurements involving high-pressure observations are regarded as less reliable than the others, because, as mentioned previously, the pressure estimates may be in error. Furthermore, a slight underestimation of ring diameters in the measurement of poorly resolved interference fringes would lead to displacements apparently too large.

The general qualitative agreement of both sets of observations leaves no question of the genuinely positive character of the effect for the lines given in the table, a question which might possibly be raised if only the results for 1-atmosphere pressure difference were available.

3. TERM DEPRESSIONS IN Fe II

In order to apply the pressure-displacement correction to the wave length of any line in a spectrum, it is necessary to know the depressions for both levels involved in the transition. In practice we make the assumption that the ground level has no pressure displacement. The pressure displacements are then determined for lines involving transitions to the lowest state. We obtain in this manner the values of the pressure displacements of these combining levels relative to the lowest state. If these levels for which pressure displacements are known combine with a third set, the relative depressions of the latter become experimentally measurable. The method may be extended as far as intercombinations permit. Interferometric observations of the pressure displacements of the intersystem lines involving transitions between the odd sextets and the low ^4F term are lacking. The additional assumption is made that the latter term has negligible pressure displacement relative to the ground state, an assumption regarded as justifiable since the levels of this term lie from only 1,872 to 3,115 cm^{-1} above the ground level.

TABLE 2.—*Term depressions in* Fe II *resulting from a pressure increase of 1 atmosphere*

Designation	Term value	Depression
		cm^{-1}
$3d^6$ (^{5}D) 4s a $^6D_{4½}$	0. 06	
$^6D_{3½}$	384. 81	
$^6D_{2½}$	667. 66	0.
$^6D_{1½}$	862. 63	
$^6D_{½}$	977. 03	
$3d^7$ a $^4F_{4½}$	1872. 66	
$^4F_{3½}$	2430. 14	
$^4F_{2½}$	2837. 98	0.
$^4F_{1½}$	3117. 51	
$3d^6$ (^{5}D) 4s a $^4D_{3½}$	7955. 30	
$^4D_{2½}$	8391. 93	
$^4D_{1½}$	8680. 51	Not determined.
$^4D_{½}$	8846. 77	
$3d^7$ a $^4P_{2½}$	13474. 45	
$^4P_{1½}$	13673. 21	Not determined.
$^4P_{½}$	13904. 93	
$3d^6$ (^{5}D) 4p z $^6D°_{4½}$	38459. 07	
$^6D°_{3½}$	38660. 09	
$^6D°_{2½}$	38859. 01	Not determined.
$^6D°_{1½}$	39013. 23	
$^6D°_{½}$	39109. 34	
$3d^6$ (^{5}D) 4p z $^6F°_{5½}$	41968. 17	
$^6F°_{4½}$	42114. 85	
$^6F°_{3½}$	42237. 07	
$^6F°_{2½}$	42334. 85	0. 008.
$^6F°_{1½}$	42401. 35	
$^6F°_{½}$	42439. 90	
$3d^6$ (^{5}D) 4p z $^6P°_{3½}$	42658. 27	
$^6P°_{2½}$	43238. 63	0. 005.
$^6P°_{1½}$	43621. 01	
$3d^6$ (^{5}D) 4p z $^4F°_{4½}$	44232. 57	
$^4F°_{3½}$	44753. 84	
$^4F°_{2½}$	45079. 93	0. 008.
$^4F°_{1½}$	45289. 85	
$3d^6$ (^{5}D) 4p z $^4D°_{3½}$	44446. 95	
$^4D°_{2½}$	44784. 80	
$^4D°_{1½}$	45044. 23	0. 011.
$^4D°_{½}$	45206. 50	
$3d^6$ (^{5}D) 4p z $^4P°_{2½}$	46967. 47	
$^4P°_{1½}$	47389. 83	Not determined.
$^4P°_{½}$	47626. 17	

The average wave-number variation for each multiplet gives the relative depression of the upper term involved in the transition, assuming that all levels of a term are actually subject to the same displacements. These term depressions are indicated in table 2 to the extent permitted by the data. The level values and designations in this abridged Fe II term table are quoted from Dobble [25]. The results used in estimating term depressions were in all cases derived from observations with the respective sources operated at pressures differing by slightly less than 1 atmosphere.

4. CONCLUSIONS

The results indicate that a change of pressure of 1 atmosphere causes a shift of the Fe II lines in the neighborhood of 2400 A amounting to 0.0004 A on the average, or 1 part in 6,000,000. This is an extremely small effect. Except in case of the transitions, $a^4F - z^4D^\circ$, for which slightly larger effects were observed, the pressure displacements arising from a pressure difference of 1 atmosphere are insufficient to affect the values of vacuum-arc wave lengths, unless the probable error of the wave-length measurements is less than 0.0005 A. The Burns-Walters published wave lengths, which were determined by comparison with noble-gas standards, are given to seven figures although eight figures were retained for calculating wave numbers. In the list of proposed secondary standards [2] the following five wave lengths from the data of Burns and Walters need to be increased by 0.001 A to make them comparable with arc-in-air values on the basis of this investigation; 2384.385, 2379.275, 2375.191, 2368.594, and 2360.292.

V. REFERENCES

[1] Trans. Int. Astron. Union **3,** 77–102 (1928).
[2] Trans. Int. Astron. Union **6,** 85–108 (1938).
[3] K. Burns and F. M. Walters, Jr., Pub. Allegheny Observatory Univ. Pittsburgh **6,** 159–211 (1929); **8,** 39–64 (1931).
[4] C. V. Jackson, Proc. Roy. Soc. (London) [A] **130,** 395–410 (1931); [A] **133,** 553–564 (1931).
[5] William F. Meggers and Curtis J. Humphreys, J. Research NBS **18,** 543–557 (1937) RP992.
[6] Trans. Int. Astron. Union **2,** 36 (1925).
[7] Harold D. Babcock, Astrophys. J., **67,** 240–261 (1928).
[8] W. J. Humphreys and J. F. Mohler, Astrophys. J. **3,** 114–137 (1896); J. F. Mohler, Astrophys. J. **4,** 175–181 (1896); W. J. Humphreys, Astrophys. J. **4,** 249–262 (1896); **6,** 169–232 (1897); **23,** 233–247 (1906).
[9] M. A. Catalán, Nature **113,** 889–891 (1924).
[10] Henry G. Gale and Walter S. Adams, Astrophys. J. **35,** 10–47 (1912).
[11] F. M. Walters, Jr., J. Wash. Acad. Sci. **13,** 243–252 (1923); J. Opt. Soc. Am. **8,** 245 (1922).
[12] Erwin Beglinger, Helv. Phys. Acta **7,** 149–169 (1934).
[13] H. A. Lorentz, Koninkl. Akad. Wetenschappen Amsterdam **14,** 518, 577 (1905–1906).
[14] Henry Margenau, Phys. Rev. **43,** 129–134 (1933).
[15] Henry Margenau and W. W. Watson, Rev. Modern Phys. **8,** 22–53 (1936).
[16] A. Jablónski, Z. Physik **70,** 723–732 (1931).
[17] H. Kuhn, Phil. Mag. **18,** 987–1003 (1934).
[18] Henry Margenau, Phys. Rev. **48,** 755 (1935); Henry Margenau and W. W. Watson, Phys. Rev. **52,** 384 (1937); Henry Margenau and W. S. Wilson, Phys. Rev. **53,** 941 (1938).
[19] C. Reinsberg, Z. Physik **111,** 95–108 (1938).
[20] C. Füchtbaur, G. Joos, and O. Dinkellacker, Ann. Physik **71,** 204–227 (1923).
[21] H. D. Curtis, J. Opt. Soc. Am. **8,** 697 (1924).
[22] W. Ewart Williams and D. V. Gogate, Proc. Roy. Soc. (London) [A] **167,** 509–516 (1938).
[23] Wm. F. Meggers, C. C. Kiess, and F. M. Walters, Jr., J. Opt. Soc. Am. **9,** 371 (1924).
[24] Henry Norris Russell, Astrophys. J. **64,** 194–203 (1926).
[25] J. C. Dobbie, Proc. Roy. Soc. (London) [A] **151,** 703–726 (1935); Annals of the Solar Physics Observatory (Cambridge) **5,** 1–58 (1938).
[26] F. Hund, Linienspektren und periodisches System der Elemente (Julius Springer, Berlin, 1927).

Washington, March 9, 1939.

U. S. DEPARTMENT OF COMMERCE NATIONAL BUREAU OF STANDARDS

RESEARCH PAPER RP1223

Part of Journal of Research of the National Bureau of Standards, Volume 23, July 1939

DETECTION OF RADIOACTIVE CONTAMINATION, USING GEIGER-MÜLLER COUNTERS

By Leon F. Curtiss

ABSTRACT

Situations frequently arise in which it is desirable to determine the extent of accidental contamination by radioactive materials. Such contamination occurs in research laboratories where radioactive studies are in progress and also in commercial plants where radioactive materials are handled. An important example of the latter is the dial-painting plants, where self-luminous radium paint is applied.

This article describes a portable Geiger-Müller counter operated entirely from the alternating-current mains, which permits a rapid and accurate determination of such contamination wherever it exceeds the equivalent of about one-half microgram of radium per square meter. The device is also sufficiently sensitive to determine the presence of radium in amounts of micrograms in a living person and therefore may be used for routine test of workers, their garments, and objects habitually handled by them. The instrument is very rugged, readily portable, and silent in operation. Requiring no batteries of any kind, it is always ready for use. Commercial radio parts are used well within their ratings throughout, with the exception of the tube counter itself, so that there is little danger of failures, and the parts are easily replaced if they should fail. The indicator is a milliammeter, which is arranged to have a very steady deflection under constant conditions and is yet sufficiently sensitive to measure 1 microgram of radium at a distance of 1 meter. The device may therefore be used for intercomparison by gamma radiation of samples of radium of low activity. It has been tested under practical conditions and has been found well suited for surveys of contaminated locations. It also is a very sensitive detector for finding lost radium preparations and for testing radium ores for commercial value.

CONTENTS

	Page
I. Introduction	137
II. Power-supply unit	138
III. Amplifier unit	138
IV. Counter tube	139
V. Assembly and use of counter equipment	140
VI. Surveying for contamination	141

I. INTRODUCTION

Recently the writer has been called upon to determine the radioactive contamination present in several of the more important radium dial-painting plants, and also to design and construct 10 instruments for the Navy Department that would be suitable for similar surveys in their dial-painting plants. A sensitive portable Geiger-Müller counter seemed most suitable for this work. Equipment for such work should be capable of calibration and of maintaining its calibration over

periods of months or years. For most effective results, it should be entirely silent in operation. Furthermore, it should be rugged in construction. In the absence of any existing apparatus which entirely fulfilled these conditions, the writer undertook to design a counter unit which could be operated entirely from the alternating-current supply and would satisfy the above conditions. A description of the instrument is given below, with examples of its use in various parts of the country over a period of months, during which it has maintained its original calibration with surprising fidelity. Commercial radio parts, used well within their ratings, are employed throughout, except for the tube counter itself. Thus repairs, should they be required, may be quickly and simply made.

II. POWER-SUPPLY UNIT

For ease in handling, it was decided to build the equipment in two units, (1) a power supply to furnish the high voltage for the counter and the various plate and grid bias voltages for the amplifier, and (2)

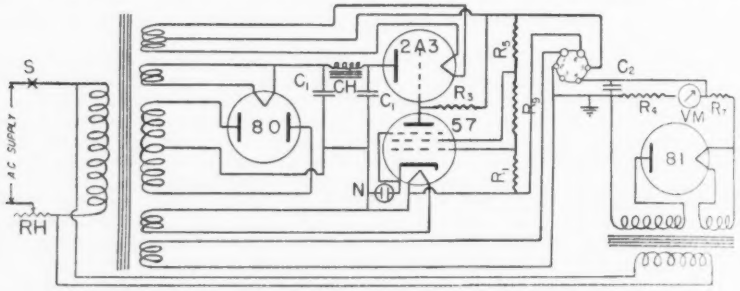

FIGURE 1.—*Wiring diagram of the power-supply unit.*

N, ¼-watt neon bulb; *CH*, 12-henry choke; R_1, 11,000 ohms; R_2, 0.5 megohm; R_4, 1 megohm; R_5, 10,000 ohms; R_7, 100,000 ohms; R_9, 27,000 ohms; C_1, 8 microfarads; and C_2, 4 microfarads.

an amplifier unit which contains the tube counter and an amplifier to make its indications visible by means of a milliammeter.

The wiring diagram of the power supply is shown in figure 1. The amplifier voltages are supplied by the self-regulating voltage supply, which contains the type 80, 2A3, and 57 vacuum tubes with a neon lamp, *N*, to provide a constant bias for the 57 tube. This type of voltage supply has been described by Grammer.[1] It is so arranged that the input-line voltage can fluctuate from about 85 to 135 volts without changing the plate voltage by more than 1 volt. The counter voltage is supplied by the simple rectifier circuit, using a type 81 rectifier and an 8-μf filter condenser. The voltage is read by a milliammeter with a megohm resistor, R_4, in series. The operating voltage for the counter is 600 volts and is controlled by the rheostat, *RH*. The power supply is built into a metal cabinet. Figure 2 shows this cabinet with its sides removed to show the arrangement of parts.

III. AMPLIFIER UNIT

The wiring diagram of the amplifier is shown in figure 3. The counter, *G–M*, is connected directly to the first 57 tube, which is arranged to form a Neher and Harper [2] circuit. This circuit is used

[1] G. Grammer, QST **21**, 14 (August 1937).
[2] Phys. Rev. **47**, 940 (1936).

FIGURE 2.—*Power-supply unit, with sides of cabinet removed.*

FIGURE 4.—*Tube counter.*

because of its high speed, being a much faster circuit than the Neher and Pickering circuit.[3] For a discussion of reasons for the relative speeds of these two circuits, see Kozodaev and Latyschev.[4] Since the pulses from a Neher and Harper circuit are not of uniform height, it is necessary to level them if an integrating circuit is to be used. This is accomplished by the second 57 tube. The levelled pulses are rectified by the 27 tube and charge the condenser C_4, connected to the plate of the 27 tube through a resistor, R_7, and also to the grid of the 56 tube. This tube is connected to serve as a vacuum-tube voltmeter to read the voltage on the condenser, C_4. The grid of the 56 tube is also connected to the cathode through resistors, as shown, so that for a given rate of charge the condenser acquires a steady negative voltage. This is indicated by a steady deflection of the meter, M, in the plate circuit of the 56 tube. To avoid excessive fluctuation of this potential

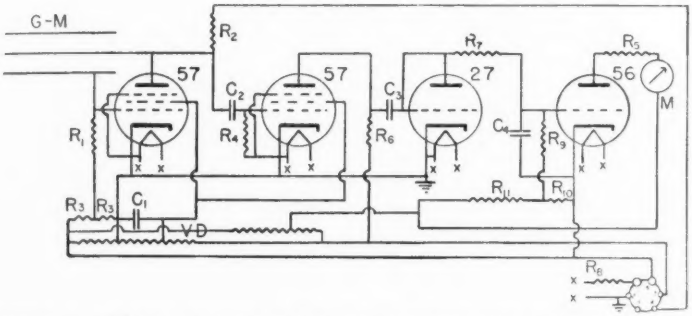

FIGURE 3.—*Wiring diagram of the amplifier used with the tube counter.*

GM, tube counter; *VD* voltage divider; R_1, R_7, 20 megohms; R_2, R_4, R_9, 5 megohms; R_3, 54,000 ohms; R_5, 10,000 ohms; R_6, 0.5 megohm; R_8, 1 ohm; R_{10}, 2,000 ohms; R_{11}, 0.25 ohm; C_1, 8 microfarads; C_2, 0.0001 microfarad and C_3, 0.0002 microfarad.

as a result of statistical fluctuations in the counting rate of the tube counter, a relatively large counter is used, so that its rate, even in the absence of a radioactive sample, is fast enough to give a sensibly steady reading. This stability is of course partly due to the large capacity, C_4, and relatively low resistance across it, R_9 plus R_{10}. For the complete range of the indicating meter, the actual counting rate of the tube counter changes from about 600 to 10,000 per minute.

IV. COUNTER TUBE

To secure the rapid counting rate required, the counter tube shown in figure 4 has been adopted. It is approximately 5 cm in diameter and 30 cm long, using a 100 by 100 mesh copper-gauze cylindrical electrode, as recommended by Evans.[5] The general construction, as can be seen from the photograph, is that described by Cosyns and de Bruyn,[6] using glass sleeves as guard rings on the wire electrode. Since it is desirable to operate the counter at a low voltage to reduce insulation problems and decrease the excess potential on the Neher and Harper circuit, these counters are filled with a mixture of argon and

[3] Phys. Rev. **53**, 316 (1938).
[4] M. Kozodaev and G. C. Latyschev, Compt. rend. (Doklady) acad. Sci. USSR **20**, 21, (1938).
[5] Rev. Sci. Inst. **7**, 444 (1936).
[6] Acad. roy. Belg. Sci. Bul. **20**, 371 (1934).

hydrogen at a pressure of approximately 6 cm of Hg. They require 600 volts to operate near the middle of their plateau. To secure a broad and sensibly level plateau, it has been found necessary to sputter the counters. This treatment is a modification of the method described by Diffenbach, Lifschutz, and Slawsky.[7] The electrodes are connected to a transformer adjusted to produce a steady glow between the electrodes in hydrogen at a pressure of a few millimeters. The hydrogen is changed frequently and the sputtering permitted to continue for from 12 to 24 hours. Care must be taken to prevent any actual sputtering of the metal which may be deposited on the interior surfaces of the glass and ruin the insulation. Counters prepared in this way have a characteristic voltage curve, as shown in the graph in figure 5. Within a range of about 200 volts their rate is

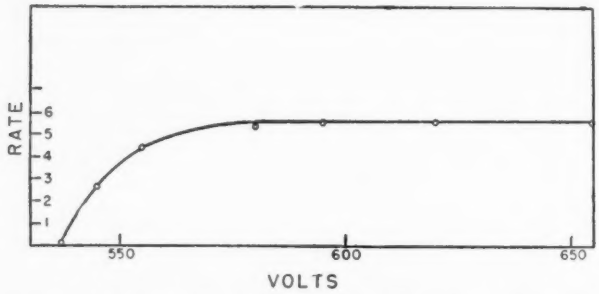

FIGURE 5.—*Curve showing operating characteristic of tube counter.*

practically independent of the voltage. This characteristic has been determined in integrating circuits of the type described above and also in scaling circuits where actual counts are scaled numerically. The curves obtained are nearly identical in shape, indicating that the integrating circuit delivers uniform pulses to the integrating condenser. This has also been checked with a cathode-ray oscillograph.

In actual use it is necessary to protect the tube counter from breakage, screen it from stray light, and provide an electrostatic shield. These are accomplished by mounting it inside a close-fitting Duralumin tube with walls about $\frac{1}{16}$ inch thick. Rubber supports are provided to act as shock absorbers. This metal tube acts as a filter to screen out most of the beta radiation. Figure 6 shows the interior parts of the amplifier and the method of supporting the tube counter within its tubular shield. The case is a rugged Duralumin box cast in one piece. Since surfaces, as tops of tables and floors, are most common objects for investigating contamination, the tube counter is mounted below the case, where it is well protected but also directly accessible from three sides. The asymmetrical position of the metal tube permits the mounting of the active volume of the counter in a symmetrical position with reference to the case.

V. ASSEMBLY AND USE OF COUNTER EQUIPMENT

Each of the two cabinets is provided with a socket into which a five-conductor cable, with suitable fittings, may be plugged. This cable is about 20 feet long, so that a considerable area may be surveyed without moving the power-supply cabinet. This cabinet is

[7] Phys. Rev. **52**, 1931 (1937).

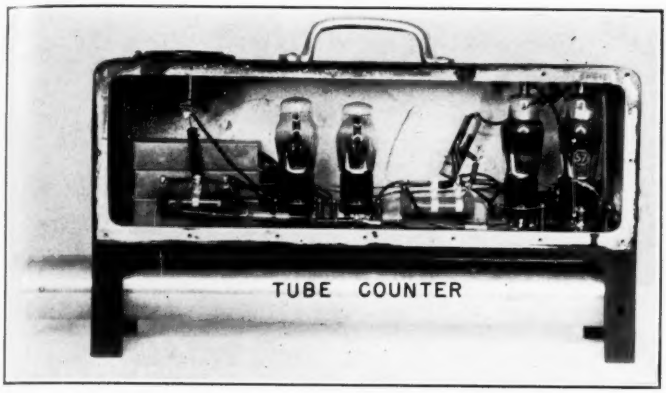

FIGURE 6.—*Amplifier unit with side removed and with tube counter in position.*

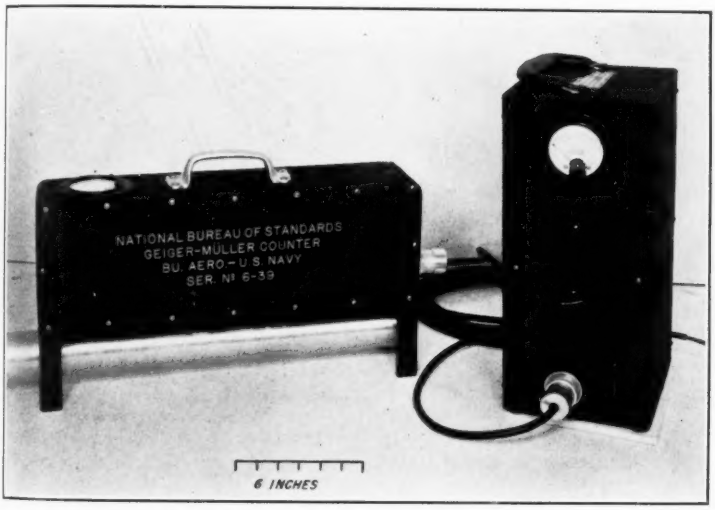

FIGURE 7.—*Complete apparatus assembly ready for use.*

UNIV. OF MICH.

somewhat heavy, inasmuch as all of the transformers are mounted in it.

Figure 7 is a photograph of the complete assembly, with the power supply on the right. The only control to adjust in the use of the instrument is the rheostat knob shown below the voltmeter, which is used to set the voltmeter to a reading of 600 volts. This also insures that tube filaments and heaters and bias voltages are the same as at the time of adjustment and calibration.

It has been found that this equipment can be calibrated and will hold its calibration to within better than 10 percent over a period of several months. A typical calibration curve is shown in figure 8,

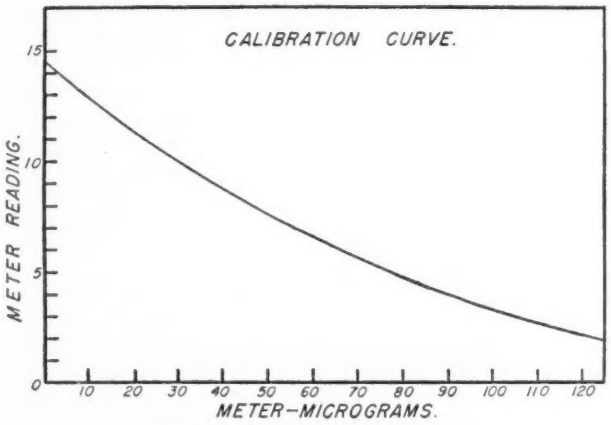

FIGURE 8.—*Calibration curve.*

where the reading of the meter is plotted against the intensity of gamma-radiation expressed in "meter-micrograms." Thus the numbers along the X-axis represent the number of micrograms of radium, at a distance of 1 meter, required to produce the corresponding reading on the milliammeter. The meter used has 75 divisions and can be read to the nearest division with certainty. A deflection of four divisions corresponds roughly to 2.5 meter-micrograms, so that 0.15 microgram will produce this deflection when placed at a distance of 25 cm.

It is possible to adjust this equipment to a greater sensitivity when desirable. In practical use, however, it has been found that an increased sensitivity makes it impossible to obtain readings in heavily contaminated areas. One convenient way to control the sensitivity is to change the size of the coupling condenser, C_2, shown in the wiring diagram, figure 3. In this way intensities up to 500 meter-micrograms can be measured. If a multirange instrument is desired this may be accomplished by inserting a switch which will change the coupling capacity by cutting various condensers in or out, so that the coupling is changed by fixed steps.

VI. SURVEYING FOR CONTAMINATION

The instrument described above has been used in several of the larger dial-painting plants. Measurements were made after all radioactive working materials had been removed. The general pro-

cedure in making these measurements was to take observations at about 10 to 15 different locations uniformly distributed over the plant and then explore the neighborhood of those showing the highest readings in order to locate definitely the areas or objects with heavy contamination. Typical results are shown in tables 1 and 2. The data in table 1 were obtained in a plant which had been in operation for about 5 years and employed about 25 painters. The data in table 2 were taken in a plant which had been in operation about 2 years and employed only four painters. The respective floor plans of these two plants are shown in figures 9 and 10.

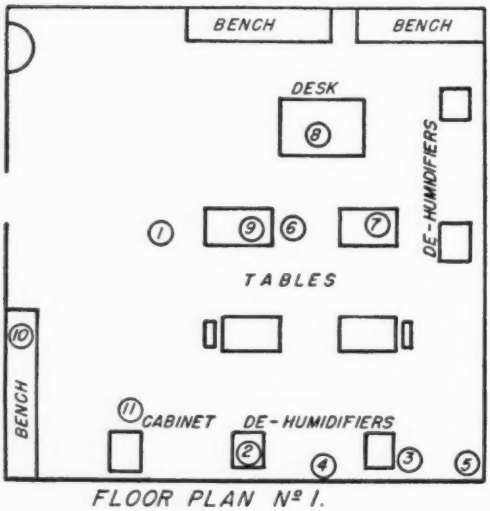

FIGURE 9.—*Floor plan to accompany table 1.*

The general result of the survey revealed that unpainted wooden-top tables, wooden floors, and wooden trays were most likely to accumulate contamination. Nonporous and metal surfaces were usually found to show only slight contamination. Also heaviest contamination was found near weighing tables and hoods in those plants where the dry luminous powder was weighed out and placed in small containers. This may be attributable to the use of wooden-top tables for this work. Wooden floors also showed much higher contamination than painted concrete floors. Where extreme care was used some wooden floors were cleaner than concrete floors where less care had apparently been exercised.

TABLE 1.—*Meter readings in plant 1*

Location number [1]	Location	Reading	Meter-micrograms
1	Center of workroom floor	1.6	250
2	On dehumidifier No. 1	2.7	200
2	On dehumidifier after removal of wastebasket containing wiping cloths.	4.3	145
3	On dehumidifier No. 2	5.1	120
4	On floor near west wall	6.9	70
5	On floor in southwest corner	8.0	37
6	On floor near small bench	4.1	150
6	On floor, bench removed	6.2	90
6	On floor, counter tube 5 cm from floor	5.0	120
7	Top of work table No. 1	1.8	240
8	Top of foreman's desk	1.7	245
9	On work table No. 2	1.3	265
10	On tray bench	2.3	217
11	Near metal cabinet	0.4	325

[1] See figure 9.

TABLE 2.—*Meter readings in plant 2*

Location number [1]	Location	Reading	Meter-micrograms
1	Center of floor	8.1	35
2	Floor under work table	8.0	35
3	Top of work table	9.0	10
4	Vertical branch of exhaust pipe	9.0	10
5	Horizontal branch of exhaust pipe	8.0	35
6	Close to main pipe at fan	8.5	25
7	Workers' locker room	9.3	0
8	Inside locker No. 1	9.3	0
9	Inside locker No. 2	9.3	0

[1] See figure 10.

With this equipment it was found that a plant could be completely surveyed in about 2 hours. Approximately 5 minutes is required to obtain a reading at any one point. This is a much shorter time than is usually required with tube counters and is a result of the use of a large counter with a high-speed counting circuit.

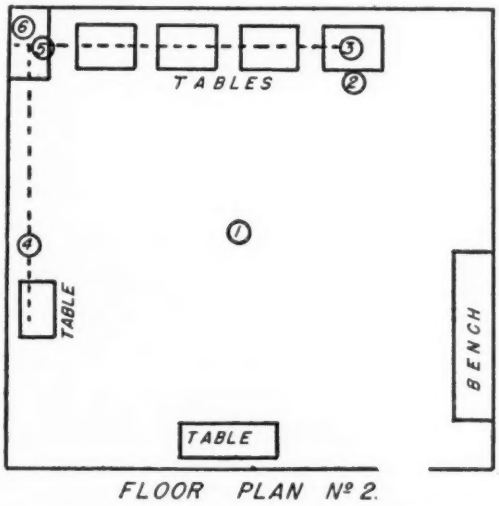

FIGURE 10.—*Floor plan to accompany table 2.*

Incidental to the tests made with this equipment, several small amounts of radium were discovered which had been misplaced by the owners. One milligram of radium can easily be detected at a distance of about 20 feet, even through intervening walls and other absorbing material. Wherever alternating current can be made available this equipment makes a very satisfactory detector for lost radium preparations. It is also sufficiently sensitive to test radium ores which contain sufficient radium to be of commercial value. In situations where alternating current is not available, a portable counter unit may be used operated entirely from dry batteries. Such a unit has been described by the author.[8]

Fifteen instruments have been made in this laboratory, and it was found necessary to make only minor adjustments to bring them all to about the same sensitivity. Calibration curves were then prepared which differed only slightly from each other. With microgram radium standards, such as are now being furnished by the National Bureau of Standards, the instruments may be used for more precise measurements by direct comparison of the unknown with a standard of suitable strength.

WASHINGTON, April 14, 1939.

[8] L. F. Curtiss, J. Research NBS **21**, 779 (1938) RP1154.

U. S. DEPARTMENT OF COMMERCE NATIONAL BUREAU OF STANDARDS

RESEARCH PAPER RP1224

Part of Journal of Research of the National Bureau of Standards, Volume 23, July 1939

STRENGTH OF A WELDED STEEL RIGID FRAME

By Ambrose H. Stang and Martin Greenspan

ABSTRACT

The distribution of stress in the knee of a welded steel rigid-frame specimen having straight flanges was determined from strain measurements. The maximum load also was determined.

CONTENTS

		Page
I.	Introduction	145
II.	Description of the specimen	145
III.	Testing procedure	145
IV.	Measured stresses	146
V.	Maximum load	147
VI.	Summary	150
VII.	References	150

I. INTRODUCTION

With the cooperation of the American Institute of Steel Construction, tests have been made on three steel rigid-frame specimens.

The results on a riveted specimen having straight flanges have been reported in RP1130 [1],[1] and on a riveted specimen having a curved inner flange in RP1161 [2]. The results on a welded specimen having straight flanges are reported here. This specimen was donated by Lukenweld, Inc.

II. DESCRIPTION OF THE SPECIMEN

The welded rigid-frame specimen is shown in figure 1. It was fabricated from steel plates and bars joined by welding. The weight as determined by Lukenweld, Inc., was 2,030 lb. The specimen was approximately symmetrical about the diagonal stiffeners through the knee.

III. TESTING PROCEDURE

The rigid-frame specimen was tested in a vertical, screw-driven, beam-and-poise testing machine having a capacity of 600 kips. The load was not applied through pin-connected shoes as in previous tests [1, 2]. The end flanges of the specimen were in direct contact with the platens of the testing machine.

Strain-gage readings were taken on 252 rosettes located as shown in figure 1 with Whittemore strain gages, 2-in. gage length. One division on the dial of the strain gage corresponds to a strain of 0.00005. Readings were estimated to 0.1 division. Each rosette consisted of

[1] Figures in brackets indicate the literature references at the end of this paper.

four gage lines intersecting at a point and inclined at 45° to one another.

Each rosette location shown in figure 1 represents two rosettes, one on each side of the specimen.

The specimen in the testing machine is shown in figure 2. Before strain-gage readings were taken, a compressive load of 57 kips was applied and released five times. Strain-gage readings were taken at compressive loads of 4 kips and 54 kips.

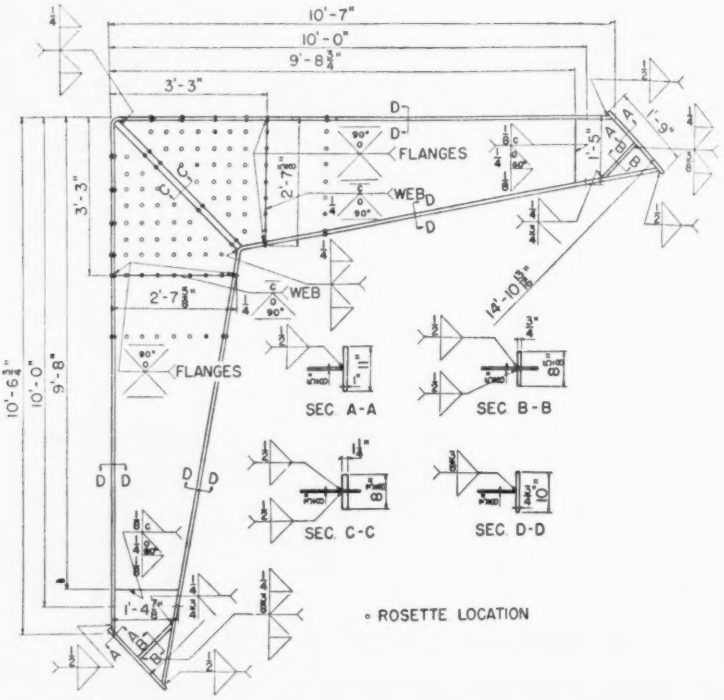

FIGURE 1.—*Welded rigid-frame specimen.*

The welding symbols are those of the American Welding Society [3].

IV. MEASURED STRESSES

Stresses computed from the strain-gage readings will be called measured stresses. These stresses were computed from the strains due to the 50-kip increase in load by the methods outlined in RP1130 [1] using an assumed [2] Young's modulus of elasticity of 29,000 kips/in.[2] For the web the strains in corresponding gage lines of rosettes on opposite sides were averaged and the average values used in the computations. For the flanges the strains in corresponding gage lines of the four rosettes were averaged and the average values used in the computations. The magnitudes and directions of the principal stresses and of the maximum shearing stress for each set of rosettes were computed.

[2] No material for test coupons was submitted with the specimen.

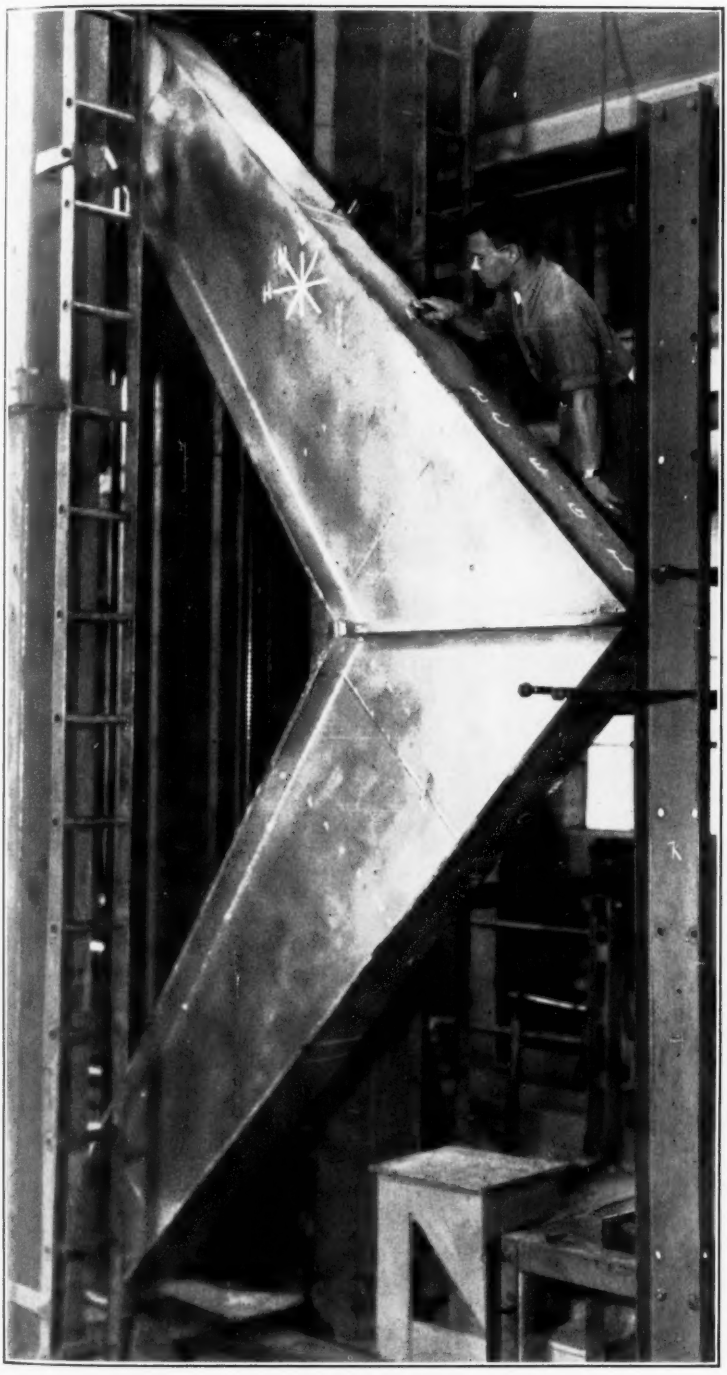

FIGURE 2.—*Rigid-frame specimen in the testing machine.*

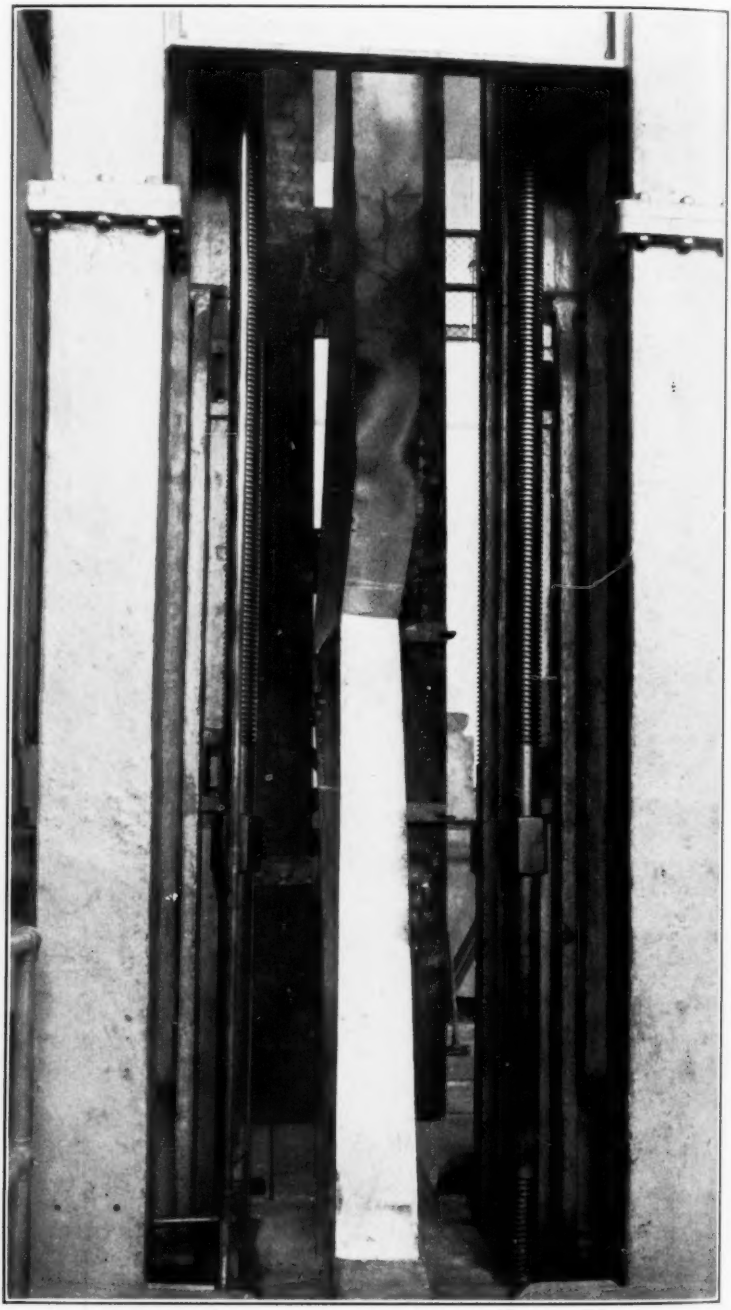

FIGURE 8.—*Rigid-frame specimen after the maximum load of 153.6 kips had been passed.*

FIGURE 9.—*Inner portion of the rigid-frame specimen after failure.*

UNIV. OF MICH.

The results of these computations are shown in figures 3 to 7, inclusive. Figure 3 is a contour chart of the maximum principal stress. Each contour line is a locus of points of equal maximum principal stress in the plane of stress. The contour lines show only the magnitudes of the stress. The directions of the contour lines are not the directions of the maximum principal stresses. The contour lines do not give the values of the stresses in the diagonal stiffener. Similar contour charts of the minimum principal stress and of the maximum shearing stress are shown in figures 4 and 5, respectively, except that the contour lines of maximum shearing stress in figure 5 were drawn for the three-dimensional state of stress. At any point at which the principal stresses in the plane of stress are of the same sign, the maximum shearing stress occurs in planes at 45° to the plane of stress and is equal to one-half the numerically larger of these principal stresses.

The magnitudes and directions of the principal stresses in the plane of stress are shown in figure 6. The normal and shearing stresses on sections perpendicular to the outer flanges are shown in figure 7. The dotted lines in figure 7 show the bending stresses on the assumption that the direct compressive stress is uniform over the cross section.

The largest normal stresses occur at the inner corner of the frame, where the diagonal stiffener joins the inner flanges. The largest shearing stress occurs in this neighborhood also. These large stresses are local effects due to the action of the stiffener.

An analytical solution for the stresses in the knee was not obtained.

Because the load was applied to the flat end flanges of the specimen, the position of the load line is indefinite. If the flanges were initially parallel, the load line would pass through the center of the flanges at low loads. As the load increased, the load line would move toward the knee of the frame. The effective position of the load line may be computed as follows. On a cross section of a leg remote from the knee the normal-stress distribution is linear and presumably follows that of the ordinary beam theory. Assuming the direct compressive stress due to the normal component of the load to be distributed uniformly over the cross section, the moment arm of the load may be computed from the measured stresses. It was computed that for this test the effective load line moved about 7.4 in. from the center of the loading flanges toward the knee of the frame.

V. MAXIMUM LOAD

The rigid-frame specimen arranged for the determination of the maximum load is shown in figure 8. The conditions for this test were the same as for the stress-distribution determination, except that the outer corner was restrained laterally.

The maximum load was 153.6 kips. Failure occurred by buckling of the web and flange on the compression side of the upper leg, as shown in figure 8. The buckle in the flange is shown more clearly in figure 9. The welds did not fail. Lüders' lines were not observed, as the mill scale had been removed from the specimen by the fabricators.

For the stress-distribution determination, the ratio of the load to the greatest measured stress was 2.91 kips per kip/in.^{2} Assuming a linear variation of stress with load up to failure, the greatest stress in the frame would be 52.8 kips/in.^{2} Since this is probably higher than the compressive yield point of the material, it is probable that the full compressive strength of the material was utilized.

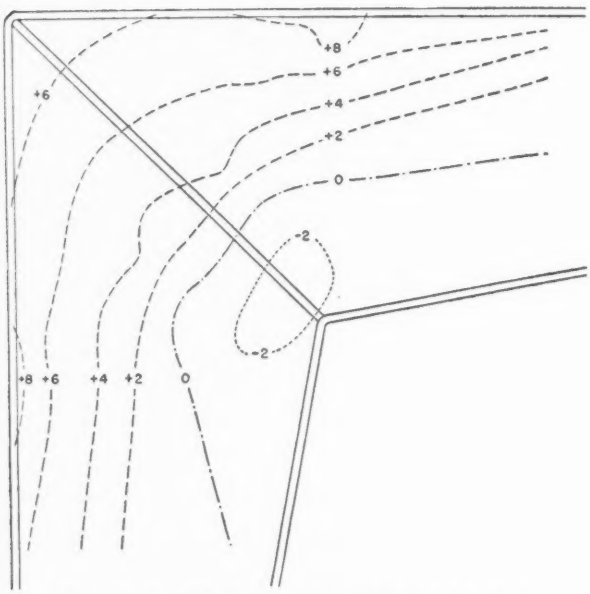

FIGURE 3.—*Maximum principal stress, kips/in.*^{2}.

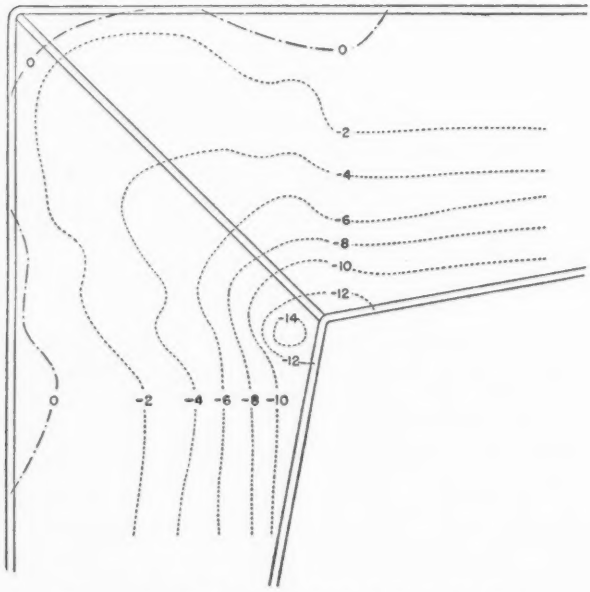

FIGURE 4.—*Minimum principal stress, kips/in.*^{2}.

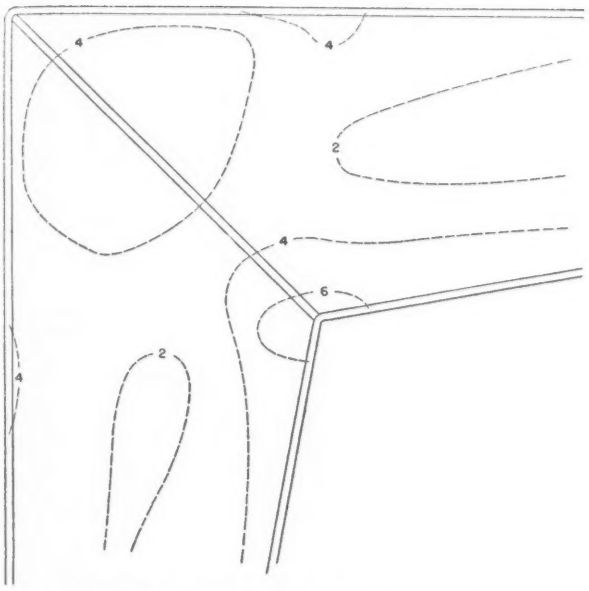

FIGURE 5.—*Maximum shearing stress, kips/in.²*.

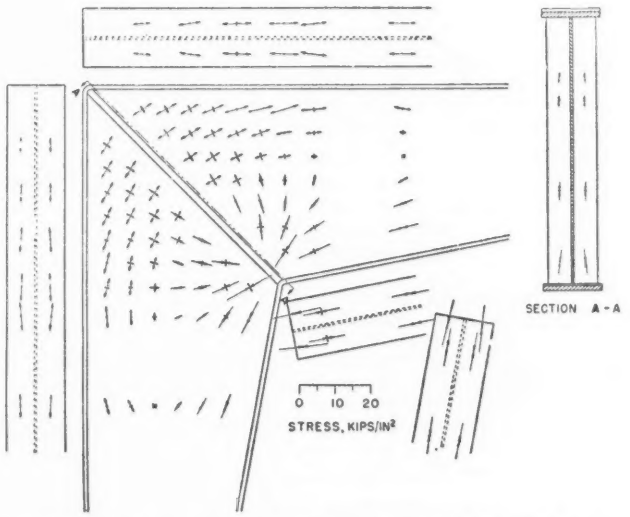

FIGURE 6.—*Magnitude and direction of the maximum and of the minimum principal stresses.*

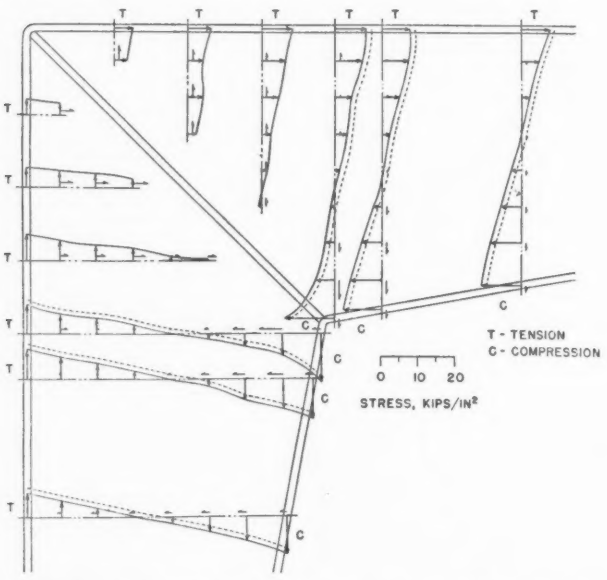

FIGURE 7.—*Normal and shearing stresses on twelve sections.*

VI. SUMMARY

The stress distribution in a welded steel rigid frame having straight flanges was determined experimentally. It was found that on cross sections of the legs remote from the inner corner of the frame, the distribution of normal stress followed that of the ordinary beam theory. The largest stresses occurred at the inner corner of the frame, and appeared to be a local effect due to the presence of the diagonal stiffener. No analytical solution for the stresses in the knee was obtained.

The maximum load was 153.6 kips. Failure occurred by buckling, but it is probable that the full compressive strength of the material was utilized. The welds did not fail.

VII. REFERENCES

[1] Ambrose H. Stang, Martin Greenspan, and William R. Osgood, *Strength of a riveted steel rigid frame having straight flanges*, J. Research NBS **21,** 269 (1938) RP1130.

[2] Ambrose H. Stang, Martin Greenspan, and William R. Osgood, *Strength of a riveted steel rigid frame having a curved inner flange*, J. Research NBS **21,** 853 (1938) RP1161.

[3] Welding Handbook, p. 7 (American Welding Society, New York, N. Y., 1938).

WASHINGTON, March 29, 1939.

U. S. Department of Commerce National Bureau of Standards

RESEARCH PAPER RP1225

Part of Journal of Research of the National Bureau of Standards, Volume 23, July 1939

TRANSFORMATION OF AUSTENITE ON QUENCHING HIGH-PURITY IRON-CARBON ALLOYS

By Thomas G. Digges

ABSTRACT

The tests described in this report were made primarily to show the influence of variation of distribution and solution of carbon in austenite on the mode and rate of transformation of austenite in high-purity iron-carbon alloys. The transformation of a nonuniform grain of austenite often proceeds at various rates in different regions within the grain, and its initial transformation to troostite is not always confined solely to its grain boundaries. These facts are illustrated by a representative case in which an individual grain of austenite transformed to cementite, ferrite, lamellar pearlite, nodular troostite, and martensite. The results of microhardness tests made on the decomposition products of this same grain of austenite, the influence of grain size on the transformation rate of austenite, and the occurrence of cracks in quenched specimens of the hypereutectoid alloys are also discussed.

CONTENTS

	Page
I. Introduction	151
II. Preparation of alloys	152
III. Experimental procedure	152
IV. Transformation of austenite on quenching the alloy	153
1. Uniform austenite—mode of transformation and influence of grain size on transformation rate	153
2. Nonuniform austenite—mode of transformation and influence of carbon distribution and grain size on transformation rate	155
3. Influence of carbon content of austenite on temperature of the Ar'' transformation	160
V. Summary	161

I. INTRODUCTION

The cooling rate required to prevent austenite from transforming to troostite (fine pearlite) is influenced by the composition, grain size, and chemical homogeneity of the austenite at the time of quenching. The important influence of the carbon content on the rate of transformation of austenite of both high-purity iron-carbon alloys and plain carbon steels was discussed in a previous publication.[1] The previous study included the determination of the critical cooling rates of the alloys and steels quenched directly from temperatures establishing an average constant austenitic grain size and complete solution of the carbon, and in addition, the critical cooling rates of the plain carbon steels quenched from the usually recommended hardening temperature range. In carrying out the latter experiments, it was observed that

[1] Thomas G. Digges, *Effect of carbon on the critical cooling rate of high-purity iron-carbon alloys and plain carbon steels*, J. Research NBS **20**, 571–587 (1938) RP1092.

some of the rapidly quenched specimens of the 0.20-percent-carbon steels contained areas of free ferrite. At the time of quenching these specimens, the carbon was nonuniformly distributed in the austenite, and regardless of the high cooling rates, the specimens were not completely hardened.

The present study was made to show the influence of distribution and solution of the carbon in austenite on the mode and rate of transformation of austenite on quenching high-purity iron-carbon alloys. Determinations were also made to show the influence of the grain size of austenite on its rate of transformation in these alloys. The qualitative results of the latter experiments will be supplemented by quantitative data in a subsequent report.

II. PREPARATION OF ALLOYS

The high-purity iron-carbon alloys used in the present investigation were the same as those described in detail in a previous report.[2] Essentially, the procedure for preparing these alloys consisted in carburizing hot- and cold-worked specimens of high-purity iron in a mixture of hydrogen and benzene vapor, and subsequently homogenizing by heating in vacuo at 1,700° F. The method used in preparing the alloys eliminated the quality factor and variables other than carbon in the composition.

Results of spectrochemical and chemical analyses, and determinations of gas content by the vacuum-fusion method, made on specimens of the iron-carbon alloys after treatment for homogeneity, showed that sulfur, nickel, cobalt, and oxygen were the major impurities contained in the alloys. These elements amounted to about 0.021 percent, whereas the total percentage (by weight) of all impurities determined was about 0.030.

III. EXPERIMENTAL PROCEDURE

All specimens used in the present study were approximately $\frac{1}{10}$ inch square by 0.040 inch thick. One wire of a 32-gage Chromel-Alumel thermocouple was spot-welded to the center of the flat face of the specimen, and the other wire was spot-welded to the center of the opposite face. The specimens were heated rapidly in vacuo within a Chromel coil, approximately 1 minute being required to reach the desired temperature, and held at that temperature for 15 minutes before quenching in hydrogen. Depending upon the purpose of the test, the specimens were either quenched directly from the high temperature or were cooled from this temperature to a temperature in the vicinity of A_1 before quenching. The assembly of the apparatus used for heating the specimens in vacuo and quenching directly in hydrogen is shown in figure 1.[3] The chamber (*E*) containing the heating coil and the specimen is evacuated before heating the specimen. On quenching the specimen, the stopcock (*D*) to the vacuum pump is closed, the switch (*B*) opened, and the stopcock (*F*) turned to permit passage of hydrogen into the heating chamber. The hydrogen, after passing around the specimen, is exhausted into the air through the mercury seal (*C*). The desired cooling rates are

[2] See footnote 1.
[3] This apparatus will be described in more detail in a subsequent report.

obtained by regulating the flow of gas with reducing and needle valves attached to the hydrogen tank.

IV. TRANSFORMATION OF AUSTENITE ON QUENCHING THE ALLOYS

1. UNIFORM AUSTENITE[4]—MODE OF TRANSFORMATION AND INFLUENCE OF GRAIN SIZE ON TRANSFORMATION RATE

The manner in which austenite transforms on quenching high-purity iron-carbon alloys and the influence of grain size on its rate of decomposition are shown in figure 2. These structures were produced in alloys containing 0.73 percent of carbon (fig. 2, *A*) and 0.85

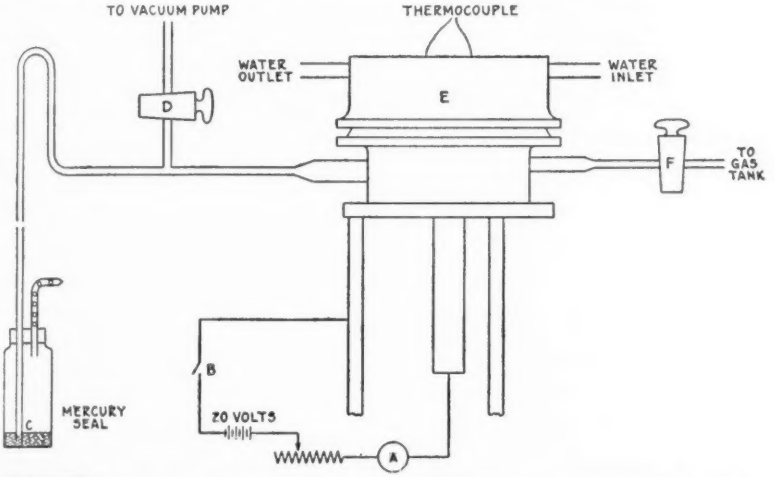

FIGURE 1.—*Diagram of the apparatus used for heating the specimens in vacuo and quenching directly in hydrogen.*

A, ammeter; *B*, switch; *C*, mercury seal; *D* and *F*, stopcocks; *E*, heating chamber.

percent of carbon (fig. 2, *B*) by heating in vacuo to 1,800° F and quenching directly in hydrogen at rates slower than the critical cooling rate. At the start of the quench, all carbon was in solution and uniformly distributed in austenite of mixed grain size.

It is evident that the initial transformation of each grain of austenite occurred at its boundary and that the interior of the austenitic grain was cooled unchanged to a temperature favorable for its transformation to martensite. That is, the austenite in the vicinity of the grain boundary was the least stable, and, on quenching, transformed at a higher temperature than the more stable austenite in the interior of the grains.

The grain boundaries of the uniform austenite contained the nuclei that were effective in the formation of nodular troostite during the quench. These nodules of troostite appear to have grown radially from the nuclei. The fact that a large proportion of these nodules is located symmetrically with respect to the grain boundaries of both

[4] The term "uniform austenite" as used in this report denotes complete solution and uniform distribution of carbon in gamma iron. Conversely, "nonuniform austenite" denotes incomplete solution or nonuniform distribution of carbon, or both, in gamma iron.

the uniform austenite (fig. 2) and nonuniform austenite (fig. 5) indicates that a nucleus may be so located as to start transformation simultaneously in more than one grain of austenite. Possibly the majority of the nuclei, however, were located in such a manner as to restrict the activity of each nucleus to a particular austenitic grain.

Mehl [5] has discussed the decomposition of austenite of eutectoid composition. He expresses the opinion that the nuclei grow to approximately half spheroids, by a radial fanlike extension until adjacent nodules come into contact, whence they continue to grow by radial and columnar extension toward the center of the grain. He further states that nodules of pearlite (troostite) extend only into the grains in which the nucleus forms, and do not cross the austenitic grain boundary during growth. He considers that the process of the formation of martensite is definitely not one of nucleation and growth.

The relative stability of small and large grains of austenite is shown by comparing the decomposition products of these grains. The smaller grains, after quenching, obviously contained larger proportions of troostite than did the similarly cooled large grains. With all other factors which affect the transformation rates remaining constant, the larger the grain size the more stable is the austenite or the deeper the hardening of the alloy. This is in agreement with the general concept of the relationship between austenitic grain size and hardenability. Quantitative data on the influence of austenitic grain size on the transformation rates of these alloys will be presented in a subsequent report.

The type of structure produced in the 0.23-percent-carbon alloy by quenching directly from 1,800° F in hydrogen at a rate in excess of the critical cooling rate is shown in figure 3 (*A*). The austenite started to transform at about 890° F (fig. 14), and its decomposition product consisted entirely of low-carbon martensite. Figure 3 (*B*) shows the structure produced in the same alloy by quenching directly from 2,100° F in hydrogen at a rate slower than the critical cooling rate. The austenite transformed to proeutectoid ferrite at its grain boundaries and to martensite in the interior of the grains. This shows that when transformation of the 0.23-percent-carbon austenite occurred at temperatures above the range where martensite was formed, the transformation product was ferrite, not troostite as was the case in higher-carbon alloys.

Figure 3 (*C*) shows the structure produced in the 1.21-percent-carbon alloy by quenching directly from 1,800° F in hydrogen at about the critical cooling rate. This specimen contained a large number of fine quenching cracks in the martensite. These cracks were located not only in the original austenitic grain boundaries but also in the interior of the grains. This condition was characteristic of the hypereutectoid alloys on quenching from high temperatures at rates which completely hardened the alloys. However, when sufficient external stress was applied to these martensitic specimens to cause rupture, the fractures were intergranular with respect to the parent austenitic grains. This is illustrated in figure 4, representing specimens of the hypereutectoid alloys quenched directly from 1,800° F in hydrogen, by the appearance of cracks after Rockwell hardness determinations were made. Figure 4 (*A*) shows the grain size (at 1,800° F) of the

[5] Robert F. Mehl, The physics of hardenability. The mechanism and rate of the decomposition of austenite. Preprint No. 25. Paper presented at Twentieth Annual Convention of the Am. Soc. Metals, October 17-21, 1938.

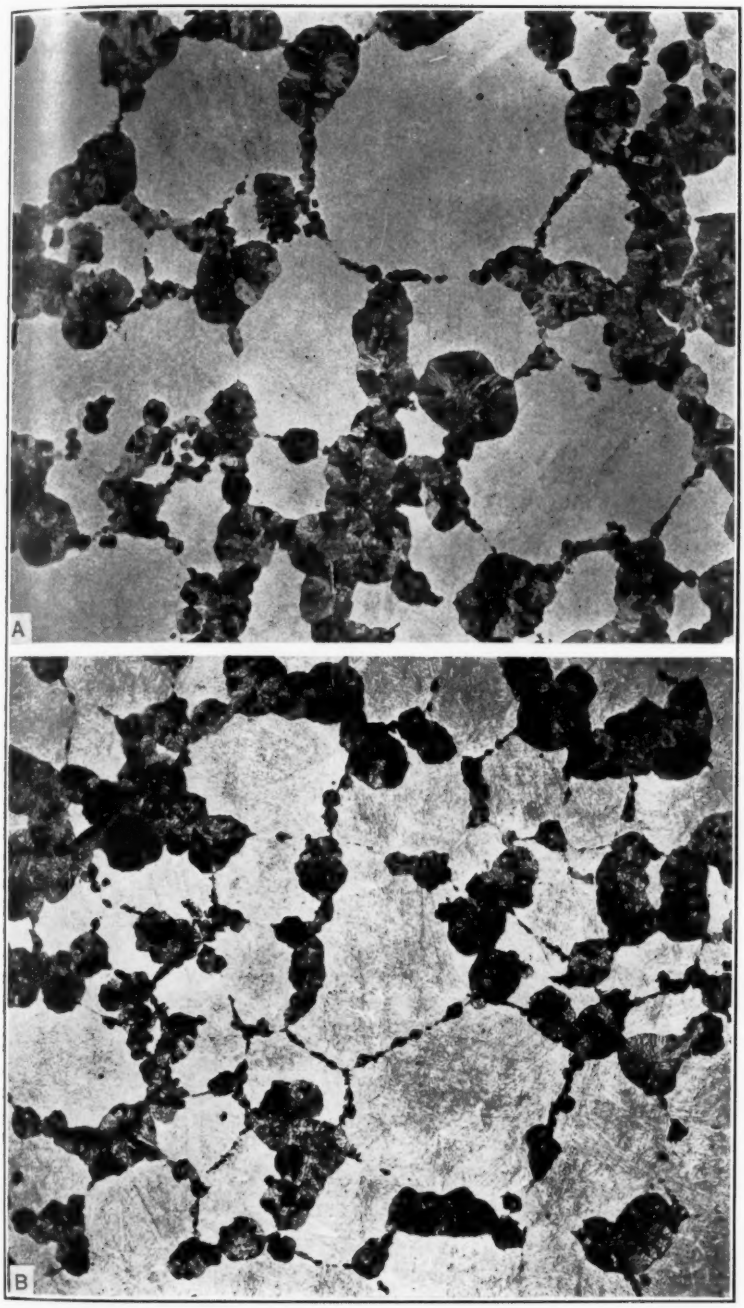

FIGURE 2.—*Grain size at 1,800° F and structure of quenched iron-carbon alloys.*

Specimens were quenched directly from 1,800° F in hydrogen. The uniform austenite of mixed grain size, on quenching, transformed to troostite at the grain boundaries, and to martensite in the interior of the grains. Relative stability of small and large grains of austenite is shown by the decomposition products of these grains. The small unstable grains contained a higher percentage of troostite than the more stable large grains. *A*, 0.73 percent of carbon; *B*, 0.85 percent of carbon. Etched with 1-percent nitric acid in alcohol. ×100.

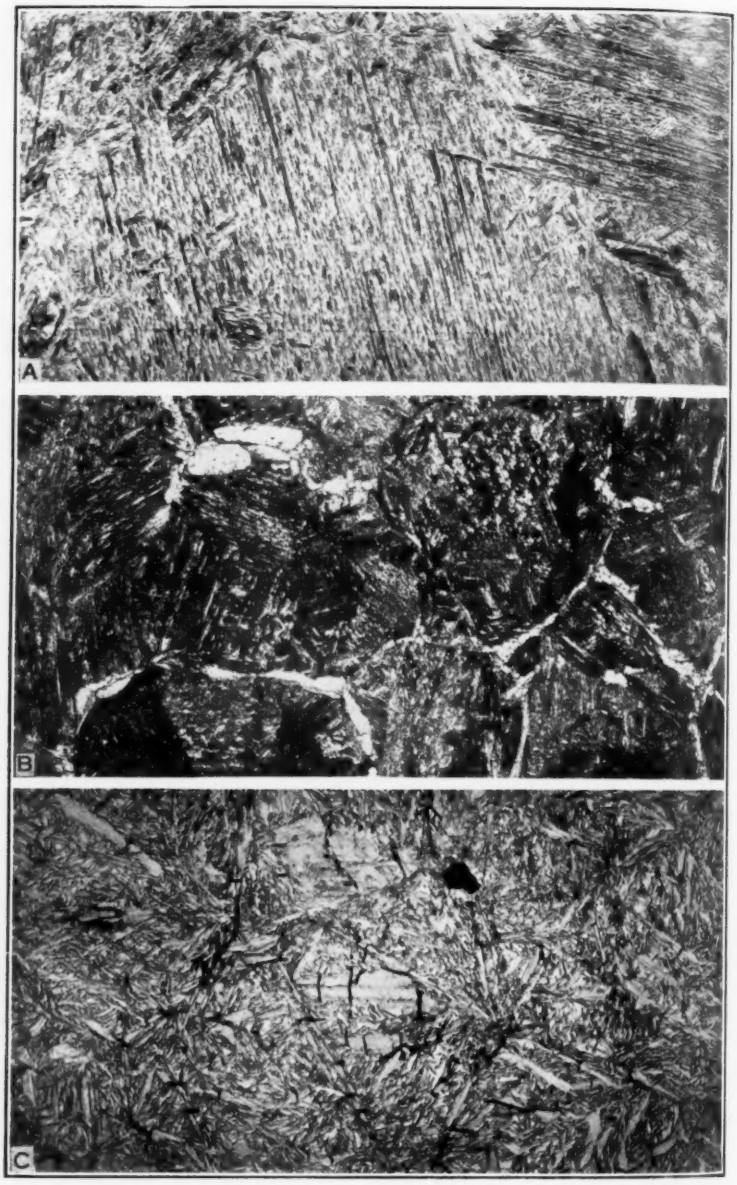

FIGURE 3.—*Structure of quenched iron-carbon alloys.*

A, martensite produced in alloy containing 0.23 percent of carbon by quenching directly from 1,800° F in hydrogen at a rate in excess of the critical cooling rate. ×250. *B*, martensitic matrix and ferritic network produced in alloy containing 0.23 percent of carbon by quenching directly from 2,100° F in hydrogen at a rate slower than the critical cooling rate. ×100. *C*, martensitic matrix with trace of nodular troostite produced in alloy containing 1.21 percent of carbon by quenching directly from 1,800° F in hydrogen at about the critical cooling rate. Quenching cracks formed in boundaries and interior of original austenite grains. ×250. Etched with 1-percent nitric acid in alcohol.

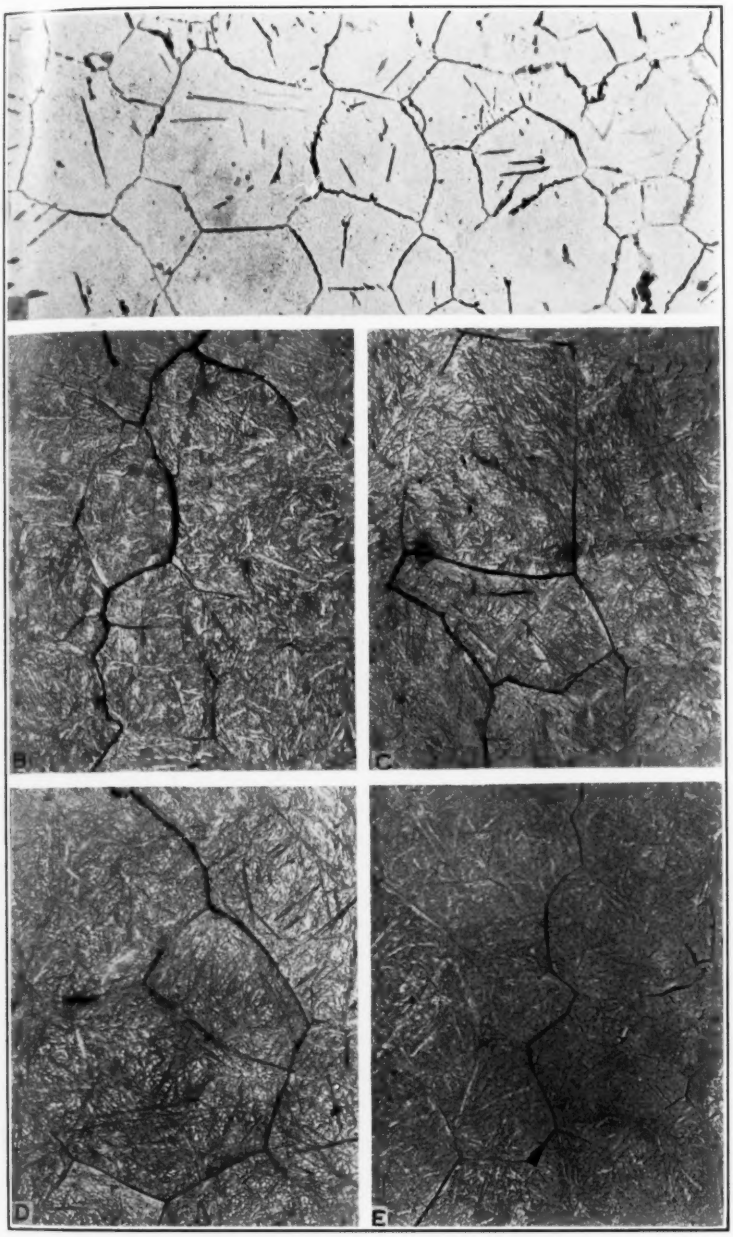

FIGURE 4.—*Intergranular cracks in martensite of iron-carbon alloys.*

A, austenitic grain size at 1,800° F of the 1.21-percent-carbon alloy. All the alloys had the same average grain size at 1,800° F. Etched with boiling sodium picrate. ×100. *B*, intergranular cracks in martensite of 1.01-percent-carbon alloy. ×100. *C*, intergranular cracks in martensite and quenching cracks in interior of original austenitic grains of 1.01-percent-carbon alloy. ×250. *D*, intergranular cracks in martensite and quenching cracks in interior of original austenitic grains of 1.14-percent-carbon alloy. ×100. *E*, intergranular cracks in martensite of 1.21-percent-carbon alloy. ×100. *B*, *C*, *D*, and *E* structures produced by quenching the specimens directly from 1,800° F in hydrogen. The intergranular cracks, with respect to the parent austenitic grains, appeared after applying external stress in making determinations for hardness. Etched with 1-percent nitric acid in alcohol.

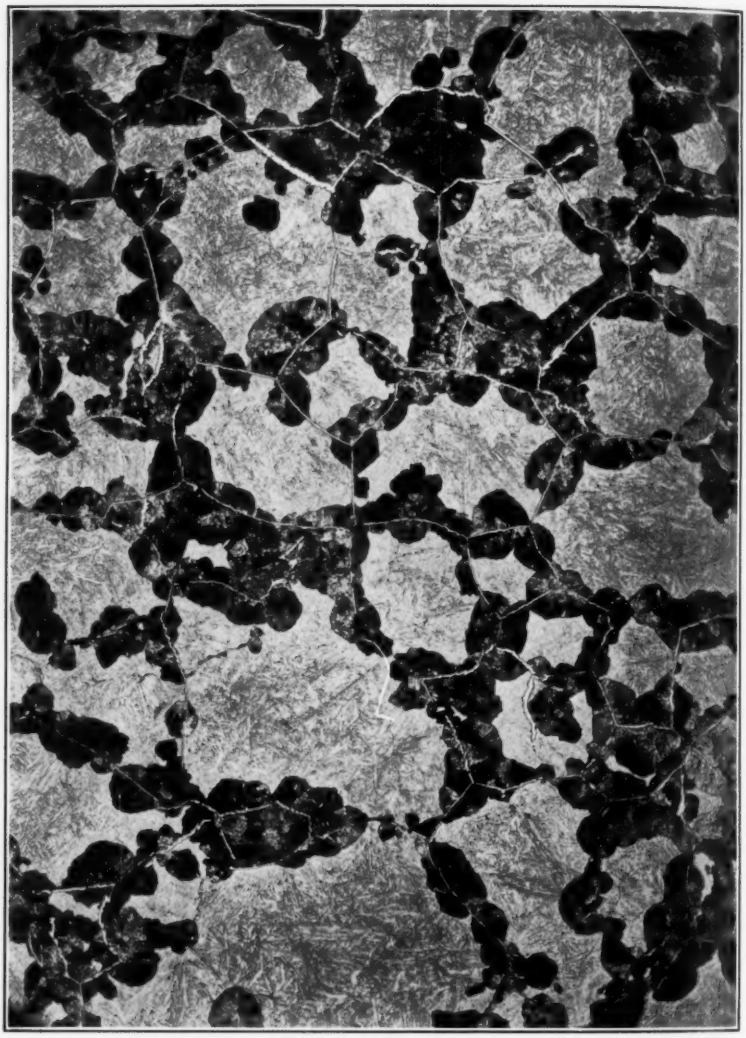

FIGURE 5.—*Grain size at 2,000° F and structure of quenched iron-carbon alloy containing 1.14 percent of carbon.*

Specimen was cooled from 2,000° F to 1,330° F and held at the latter temperature for 5 minutes before quenching in hydrogen. The grain size at 2,000° F is shown by the cementite precipitated at the austenitic grain boundaries by the treatment prior to quenching and also by the troostite formed at the grain boundaries during the quench. Except for several of the small austenitic grains that transformed entirely to troostite, the same austenitic grains were revealed by each of its decomposition products consisting of cementite and troostite. Etched with 1-percent nitric acid in alcohol. ×100.

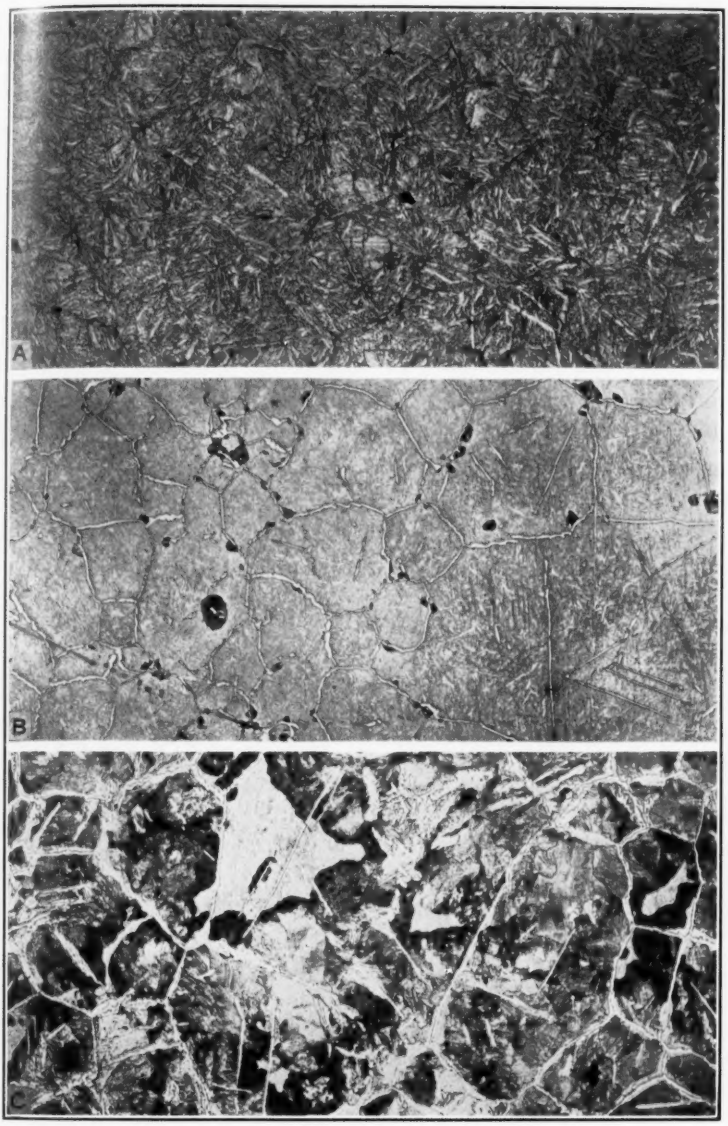

FIGURE 6.—*Structure of quenched iron-carbon alloy containing 1.21 percent of carbon.*

Specimens were 0.10 inch square by 0.040 inch thick, cooled through the temperature range 1,110° to 930° F, at the average rate of approximately 520° F per second. *A*, specimen quenched directly from 1,800° F in hydrogen. Quenched specimen had a Rockwell hardness of C 62. *B*, specimen cooled from 1,800° F to about 1,380° F and held at this temperature for 5 minutes before quenching in hydrogen. Quenched specimen had a Rockwell hardness of C 65. Note troostite formed in the interior of the parent austenitic grains. *C*, specimen cooled from 1,800° F to the temperature range 1,330° to 1,310° F and held for 8 minutes before quenching in hydrogen. The average hardness value obtained on the quenched specimen was Rockwell C 27. Etched with 1-percent nitric acid in alcohol. ×100.

UNIV. OF MICH.

alloy containing 1.21 percent of carbon; this grain size is the same as that of the other alloys at this temperature.

2. NONUNIFORM AUSTENITE—MODE OF TRANSFORMATION AND INFLUENCE OF CARBON DISTRIBUTION AND GRAIN SIZE ON TRANSFORMATION RATE

The effect of incomplete solution of carbon in austenite of varying grain size on the rate of transformation of the 1.14-percent-carbon alloy is shown in figure 5. The structure illustrated was obtained in a specimen that was heated in vacuo to 2,000° F, then cooled to about 1,330° F and held at the latter temperature for about 5 minutes before quenching in hydrogen.

The parent austenitic grains at 2,000° F were outlined not only with the cementite network precipitated by the treatment prior to quenching but also with the nodular troostite formed during the time of quenching. With the exception of a few of the grains of smaller size, each grain of austenite was identified by each of its decomposition products, cementite and troostite. On quenching, several of the smaller grains transformed completely to troostite, whereas the larger grains transformed predominantly to martensite. It should be noted, however, that at the time of quenching, approximately eutectoid proportion of carbon only was in solution, and the manner in which the specimen was cooled did not necessarily insure the same distribution of the carbon in the small as in the large grains.

With this specimen, the mode of transformation of the austenite on quenching was similar to that already described for uniform austenite. The nuclei effective in the decomposition of the austenite to troostite were located in the boundaries of the grains. However, the initial transformation of nonuniform austenite to troostite does not necessarily occur solely in the grain boundaries.

The influence of variations of distribution and solution of carbon on the mode and rate of transformation of austenite of the high-purity iron-carbon alloys is illustrated by the structures in figure 6 produced in specimens of the 1.21-percent-carbon alloy. The structure shown in figure 6 (*A*) is that of a specimen quenched directly from 1,800° F in hydrogen; the structure shown in figure 6 (*B*) is that of a specimen heated to 1,800° F and cooled to 1,380° F (a temperature above A_1) and held at this temperature for 5 minutes before quenching in hydrogen; and the structure shown in figure 6 (*C*) is that of a specimen heated to 1,800° F and cooled about 1,330° to 1,310° F (within the temperature range of Ar_1) and held in this temperature range for about 8 minutes before quenching in hydrogen. All these specimens, therefore, had the same average grain size of the parent austenite and the same total carbon content. Each specimen was cooled through the temperature range 1,110° to 930° F (the upper range in which the austenite is least stable) at an average rate of approximately 520° F per second. The specimen quenched directly from 1,800° F evidently cooled practically unchanged to the low temperature favorable for the decomposition of austenite to martensite. The average hardness value of this specimen was Rockwell *C 62*. The specimen quenched from 1,380° F had a structure consisting of proeutectoid cementite and a small amount of nodular troostite in a matrix of martensite. The average hardness of this specimen was Rockwell *C 65*. The

specimen quenched from 1,330° to 1,310° F transformed over a wide range of temperature to ferrite, carbide, and martensite, resulting in an average hardness value of Rockwell *C 27*. Although the specimen which was cooled to 1,380° F before quenching contained more troostite than the one quenched directly from 1,800° F, it is noteworthy that the former specimen had the higher average hardness value (Rockwell *C 65* and *62*, respectively). The lower hardness value of the latter specimen is believed to be due to the retention of some austenite after the quench.

At the time of quenching the specimens, variations existed in the distribution and amounts of dissolved and undissolved carbon, as is shown schematically in figure 7. All carbon was in solution and uniformly distributed in the specimen quenched directly from 1,800° F (fig. 6). On cooling the other specimens from 1,800° F through the A_{cm} temperature range, proeutectoid cementite precipitated at

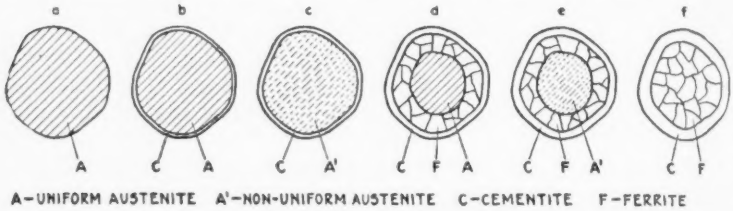

FIGURE 7.—*Sketch illustrating the solution and distribution of carbon in the hypereutectoid alloys at the time of quenching.*

the boundaries of the parent austenitic grains. At the time of quenching the specimen from 1,380° F, approximately eutectoid proportion of the carbon was in solution and the remaining undissolved carbon existed principally as grain-boundary network. At the time of quenching the specimen from 1,330° to 1,310° F, partial transformation of the austenite evidently had already taken place, and there existed an aggregate of austenite, carbide, and ferrite.

The stability of the parent austenite decreases (hardenability decreases) progressively as the conditions represented in figure 7 change consecutively from *a* to *f*. Obviously, complete hardening of the alloy cannot be obtained by quenching the parent austenite when conditions represented by *d*, *e*, and *f* exist.

Quenching the specimens, referred to in figure 6, from different temperatures influenced the stability of the austenite, on cooling through the temperature range 1,110° to 930° F, only to the extent of varying the amount and distribution of the carbon in solution at the time of quenching. This fact was confirmed by determinations of the critical cooling rate made on specimens of the 0.80- and 0.85-percent-carbon alloys. Specimens from each of these alloys were quenched directly from 1,800° F, while similar specimens were cooled from 1,800° to 1,400° F before quenching in hydrogen. Each specimen had the same average austenitic grain size and all carbon was in solution at the quenching temperatures of 1,800° and 1,400° F. The critical cooling rate for each alloy quenched directly from 1,800° F was the same as that for the corresponding alloy heated to 1,800° F and cooled to 1,400° F before quenching.

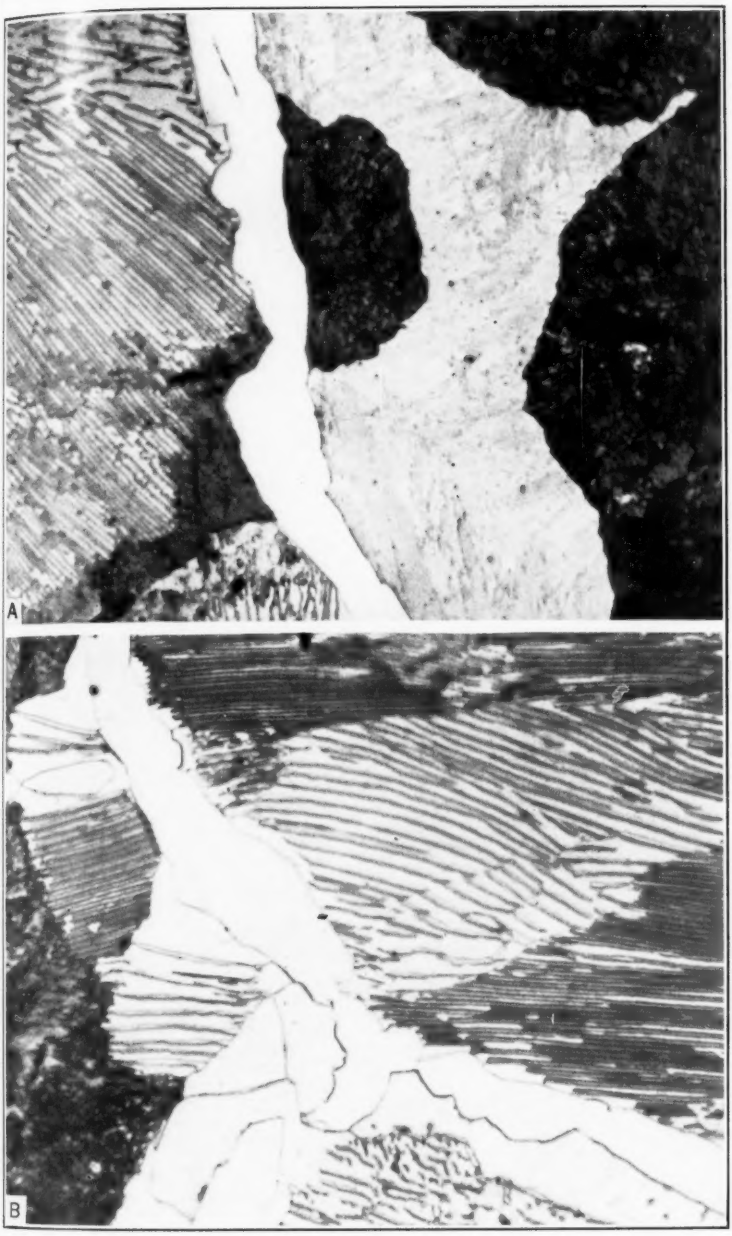

FIGURE 8.—*Structure of quenched iron-carbon alloy containing 1.21 percent of carbon. The structure of this same specimen is also shown in figure 6 (C).*

A, transformation products in portions of two adjacent grains of austenite. Along the common cementite boundary, the smaller grain transformed to martensite and nodular troostite, whereas the larger grain transformed to lamellar pearlite. Relative grain size of the austenite is shown in figure 6 (*C*). Note the continuity of the pearlite and the absence of a ferritic layer adjacent to cementite. *B*, this structure shows the feature of abnormality consisting of coalesced masses of cementite and ferrite. Etched with 1-percent nitric acid in alcohol. ×2,000.

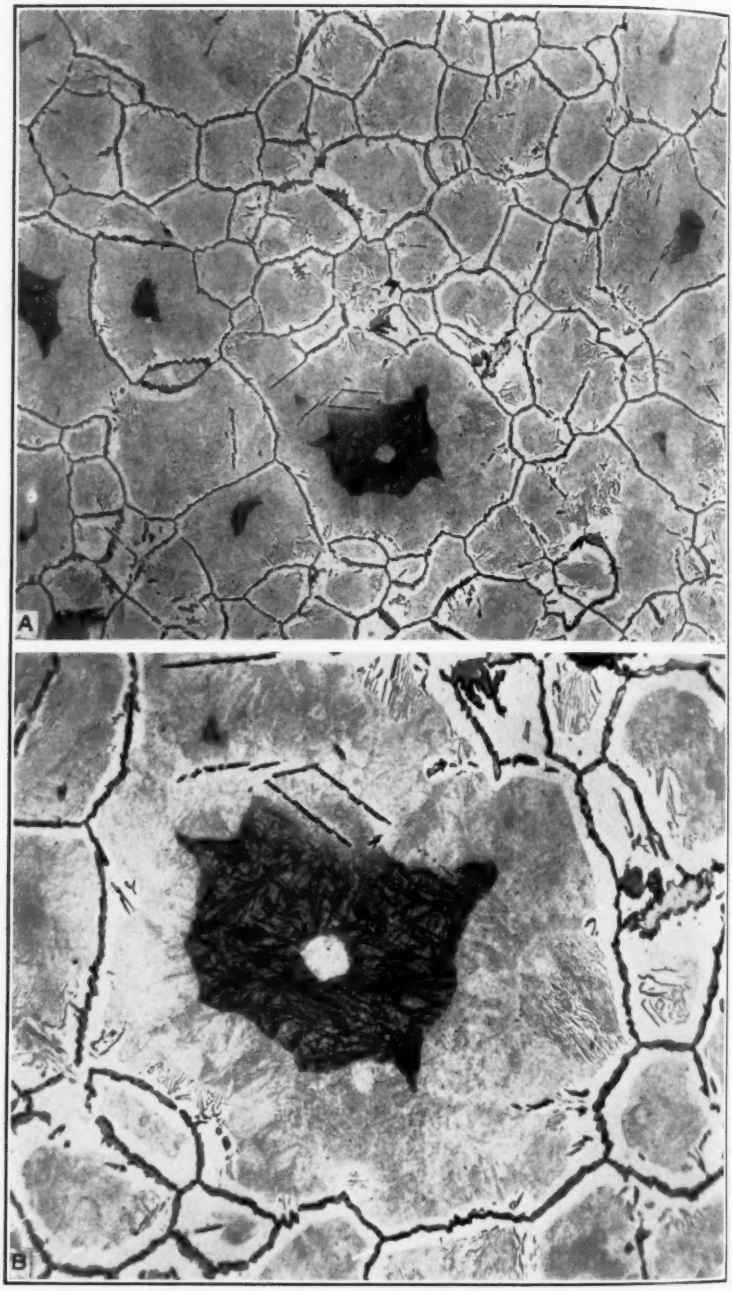

FIGURE 9.—*Grain size at 1,700° F and structure of quenched iron-carbon alloy containing 1.14 percent of carbon.*

Specimen was cooled from 1,700° F to 1,330° to 1,310° F and held in the latter temperature range 5 minutes before quenching in hydrogen. The austenitic grains are outlined with cementite. On quenching only portions of the large grains of austenite transformed to martensite. Etched with boiling sodium picrate. *A*, ×100; *B*, ×250.

As shown in figure 6 (*B*), the initial transformation of nonuniform austenite to nodular troostite is not confined to the grain-boundary region, but often occurs in the interior of the parent grains.

The mode of transformation of austenite in high-purity iron-carbon alloys also may be followed readily by allowing partial transformation of the austenite before quenching. Transformation products obtained in portions of two adjacent grains of nonuniform austenite (grains indicated by arrow at right of figure 6, *C*) of such a specimen of the alloy containing 1.21 percent of carbon are reproduced in figure 8 (*A*). At the time of quenching, these two grains were separated from each other by cementite. Along this common boundary, the smaller austenite grain transformed to martensite and nodular troostite, whereas the larger grain transformed to lamellar pearlite (see fig. 6, *C*, for relative size of these two grains). Martensite is the transformation product of the relatively stable austenite, troostite is that of the less stable austenite, and lamellar pearlite is that of the least stable austenite.

Similar distribution of the transformation products of austenite were observed not only in other parts of this same specimen but also in another specimen of the 1.21-percent-carbon alloy similarly treated. Indeed, an area of lamellar pearlite entirely surrounded by troostite (fine pearlite) was found in the interior of one of the parent austenitic grains. It is surprising to find martensite at the grain boundary and troostite in the interior of a relatively small grain of the parent austenite and lamellar pearlite in the adjacent large grain, the pearlite being separated from the martensite only by the common grain boundary constituent of cementite. The actual cause of such a mode of transformation of austenite cannot be definitely stated at this time. It is recognized that the conditions were favorable for carbon segregation prior to quenching, and this is believed to have been a contributing factor. These results show that the initial transformation of austenite does not always take place only at its grain boundary and that the grain size of the austenite is not always a true index to its stability.

The hypereutectoid alloys had a high degree of abnormality in structure as shown by coalesced masses of cementite and ferrite.[6] This abnormality was observed not only in the annealed alloys but also in some of the quenched structures (figs. 10 and 12). An interesting feature, therefore, was the absence of abnormality in the structure shown in figure 8 (*A*). That abnormality did exist in portions of this same specimen is shown by the structure of figure 8 (*B*).

A specimen of the alloy containing 1.14 percent of carbon was heated to 1,700° F, cooled to 1,330° to 1,310° F, and held in the latter temperature range for 5 minutes before quenching in hydrogen. Figure 9 (*A*) shows the grain size of the alloy at 1,700° F. With the boiling sodium picrate etching reagent, the cementite in the grain boundaries was attacked and the martensite was darkened. Only the large grains contained the dark massive constituent (martensite), thus illustrating the relationship between grain size and hardenability. However, the large grain shown in figure 9 (*B*), behaved as though grain size was not the only factor influencing its stability. The parent austenitic grain is outlined by a cementite envelope. Adjacent to the cementite is a layer of ferrite. Lamellar pearlite and

[6] H. K. Herschman, *Microstructures of high-purity iron-carbon alloys*, Metal Progress, **32**, 781 (Dec. 1937); also **32**, 689 (Dec. 1938).

varying degrees of fine pearlite extend from the ferrite to the large area of martensite (see also figure 10). Enclosed by the martensite is a light constituent that appears to be only mildly attacked with boiling sodium picrate. If the center of the original austenitic grain was the most stable part of the grain, then this constituent should be retained austenite. That it is nodular troostite and not retained austenite will be shown later. Another interesting feature shown in the decomposition products of this large grain of austenite is the small area of martensite formed a short distance from the grain boundary. This result is contrary to the generally accepted idea that the transformation of an austenitic grain occurs initially at its boundary and proceeds progressively toward its center.

To identify the constituent formed in the interior of the large area of martensite, the specimen was lightly repolished and subsequently etched in 1-percent nital. The resulting structure is shown in figure 10. With the nitric acid etch, this particular constituent was darkened, thus showing that it was nodular troostite. This finding was further confirmed by the results of microhardness tests made on the etched specimen as shown in figure 11.

The microhardness tests were made with an instrument using a diamond indenter of a special shape which was developed and described by Knoop, Peters, and Emerson.[7] The microhardness number, H, was computed from the formula

$$H=\frac{\text{Load (kg)}}{\text{Projected Area (mm}^2\text{)}}.$$

Impressions designated 1 to 9 in figure 11 were made with a load of 100 g, while those shown near the left of the original austenitic grain were made with a load of 50 g. For the range in hardness shown, the microhardness and Brinell numbers agree sufficiently closely to permit consideration of the present values in terms of the more familiar Brinell numbers. The nodule of troostite, 25 to 30 microns in diameter (position 4), had a hardness number of 570, whereas the surrounding martensite (positions 3, 5, and 6) had a value of about 700. Determinations of hardness were also made on the coarse grain of lamellar pearlite both transversely (position 8) and in the direction of the laminations (position 9). The result showed that the pearlite grain was appreciably softer in the direction of the laminations.

An interesting feature brought out by the microhardness tests was the wide variations in values obtained for the decomposition products of one grain of austenite, although the cooling rate must have been uniform throughout the entire grain. The hardness values determined ranged from about 190 for the soft pearlite to about 720 for the fully hardened martensite. Determinations of hardness were not made in areas consisting entirely of ferrite or of cementite.

There remains no doubt as to the identification of the transformation products of this quenched grain of austenite. However, there is need for further discussion of the factor believed to have been primarily responsible for the wide variations in its reaction rates. These variations obviously cannot be attributed to either differences in rates of cooling from the boundary to the center of the grain or to grain size. Furthermore, spectrochemical analysis made on an adjacent specimen

[7] F. Knoop, C. G. Peters, and W. B. Emerson, *A sensitive pyramidal-diamond tool for indentation measurements*, J. Research NBS **23**, 39 (1939) RP1220.

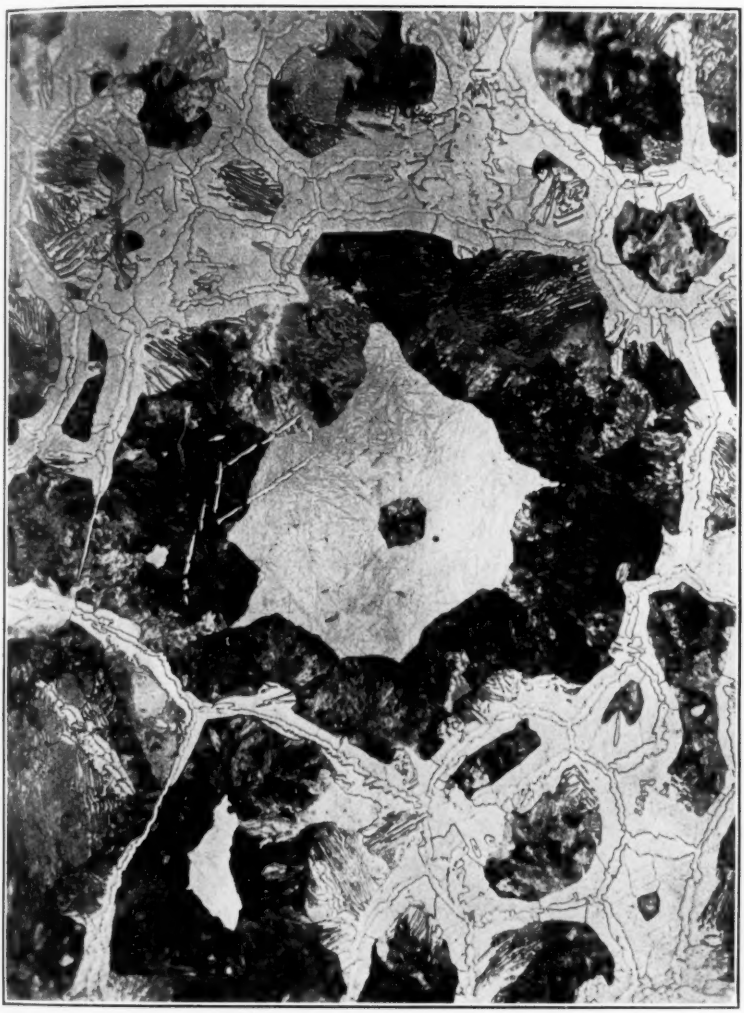

FIGURE 10.—*Transformation of austenite in iron-carbon alloy containing 1.14 percent of carbon.*

Decomposition products of the same large grain of austenite as shown in Figure 9 (*B*). The large grain of austenite transformed to cementite, ferrite, lamellar pearlite, troostite, and martensite. Stability within this grain of nonuniform austenite did not increase uniformly with the distance from the grain boundary. At the time of quenching, some of the small grains consisted essentially of coalesced cementite and ferrite. Regardless of the rate of cooling, these grains cannot be completely hardened. Etched with 1-percent nitric acid in alcohol. ×250.

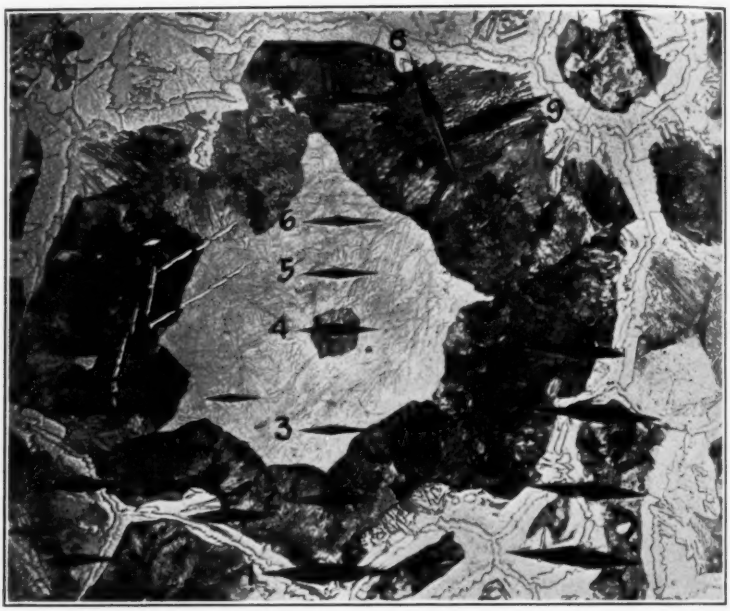

FIGURE 11.—*Microhardness of decomposition products of a grain of austenite of iron-carbon alloy containing 1.14 percent of carbon.*

Transformation products of the same large grain of austenite as shown in figures 9 (*B*) and 10. Etched with 1-percent nitric acid in alcohol. ×250.

Position	Microhardness number[1]	Position	Microhardness number[1]
1	260	6	725
2	475	7	425
3	690	8	300
4	570	9	190
5	720		

[1] For the range of hardness shown, the microhardness and Brinell numbers agree sufficiently closely to permit consideration of the present values in terms of the more familiar Brinell numbers.

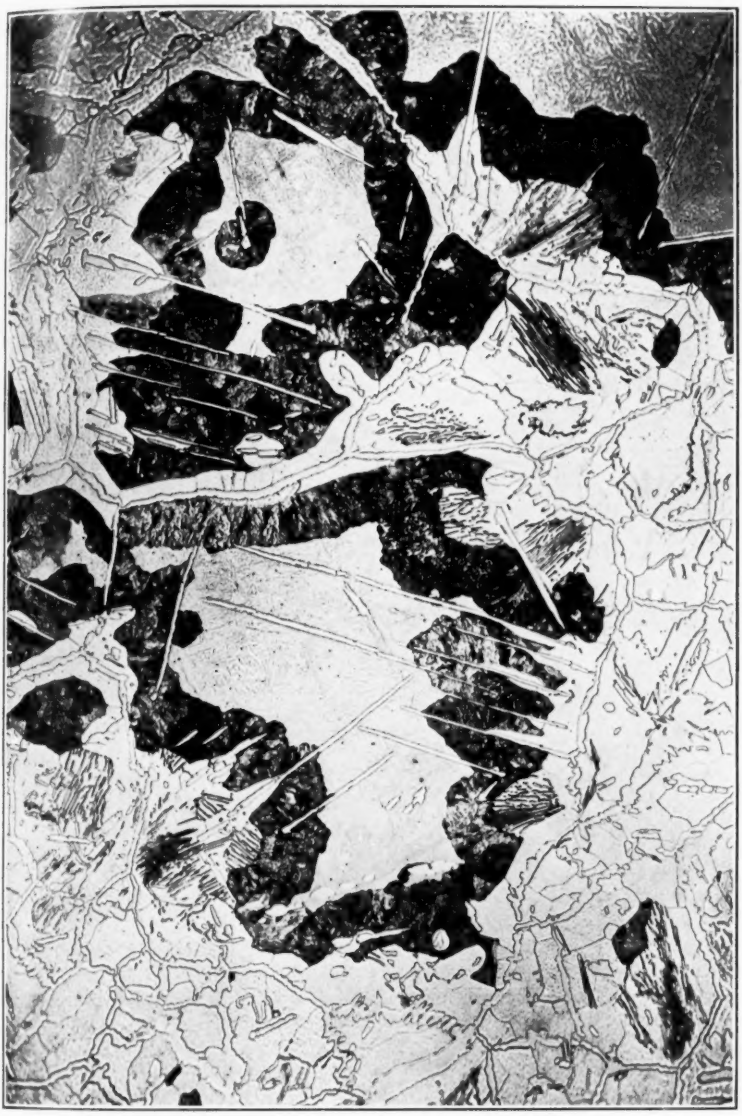

FIGURE 12.—*Structure of quenched iron-carbon alloy containing 1.21 percent of carbon.*

Specimen was cooled from 1,700° F to about 1,330° F and held at the latter temperature for 5 minutes before quenching in hydrogen. A nodule of troostite was formed around the free carbide in the large grain of austenite shown in the top portion of the micrograph, whereas in the large adjacent grain directly below there were several free carbide particles without the presence of troostite in the martensitic matrix. At the time of quenching, some of the small grains consisted essentially of coalesced cementite and ferrite. Etched with 1-percent nitric acid in alcohol. ×250.

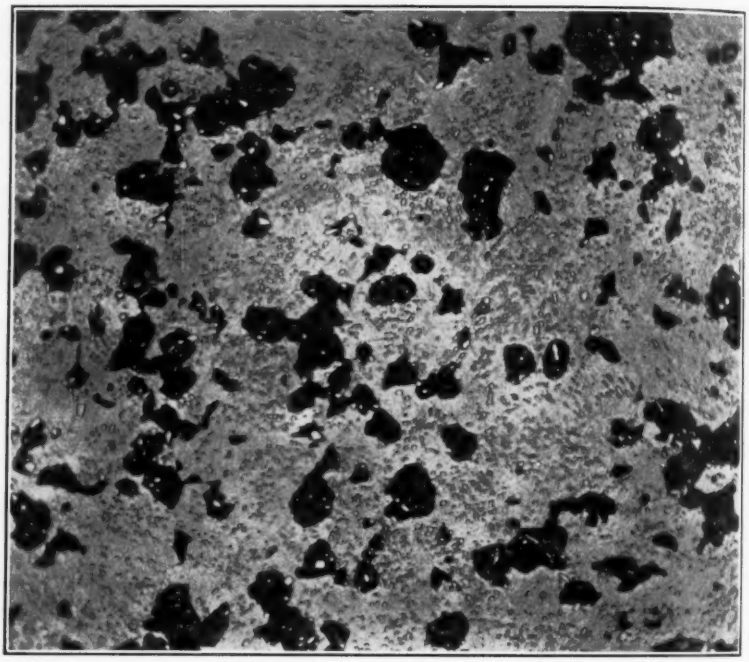

FIGURE 13.—*Structure of quenched iron-carbon alloy containing 1.01 percent of carbon.*

Specimen was quenched directly from 1,425° F in hydrogen. The transformation rate of the austenite on quenching was influenced by the presence of free carbide particles. Etched with 1-percent nitric acid in alcohol. ×750.

of this 1.14-percent-carbon alloy showed no indication of the presence of aluminum. Evidently alumina inclusions, to act as nuclei for its transformation, were not present in the austenite. However, the manner in which the austenite was cooled was very favorable for segregation of carbide in the grain at the time of quenching. It seems probable, therefore, that carbon gradients were largely responsible for the wide range in decomposition products of this uniformly quenched grain of austenite.

In a previous report [8] it was shown that with constant austenitic grain size and with all carbon in solution in the austenite, the critical cooling rate decreases (stability of austenite increases) continuously with increase in carbon for both these high-purity iron-carbon alloys and plain carbon steels.

Under certain conditions, the particles of free carbides at the time of quenching tend to accelerate the decomposition of the austenite by serving as centers for its transformation during cooling. Under other conditions, the free carbides apparently have but little influence on the transformation rate of quenched austenite. These facts are illustrated in figure 12 by the structures produced in a specimen of the 1.21-percent-carbon alloy heated to 1,700° F and then cooled to about 1,330° F before quenching in hydrogen. A nodule of troostite was formed around the free carbide in the large austenitic grain, shown in the top portion of the micrograph, whereas in the large adjacent grain directly below there were several free carbide particles, without the presence of troostite, in the martensitic matrix. Furthermore, the carbide needles or plates that formed along certain planes within the original austenitic grain apparently did not influence the rate of decomposition of the austenite.

That the presence of free carbide in the austenite at the time of quenching influences its transformation rate is also shown in figure 13 by the structure obtained in a specimen of the 1.01-percent-carbon alloy heated to 1,425° F and quenched directly in hydrogen. It is apparent that some of the undissolved carbide particles or free carbides acted as nuclei for transformation during cooling, and thus increased materially the reaction rates of the austenite. In figure 13 the martensitic matrix also contains numerous free carbide particles which did not act as transformation centers for austenite. This suggests that the reaction rate of the austenite increases with increase in the number of free carbides until a value is finally reached beyond which further increase in number has no effect on its transformation rate or hardenability. The transformation rate of austenite is believed to be influenced not only by the number and size but also by the distribution of the free carbides.

Morris and McQuaid [9] expressed the opinion that the actual differences in transformation rates or hardenability between fine- and coarse-grained austenite may well consist in low-carbon or carbonless boundaries. That is, the relation between the physical size of the austenitic grain at the time of quenching and hardenability was thought to be less important than low-carbon austenitic areas present because of nonuniform carbon solution and diffusion.

[8] See footnote 1.

[9] N. J. R. Morris and H. W. McQuaid, The effect of the silicon and aluminum addition on the hardenability of commercial steels. Preprint No. 27. Paper presented at the Twentieth Annual Convention, Am. Soc. Metals October 17-21, 1938.

It has been shown that nonuniform distribution of carbon and the presence of free carbides in the austenite at the time of quenching materially influence the transformation rates of high-purity iron-carbon alloys. These factors may have an effect equal to or even greater than that of grain size in controlling the reaction rates of the quenched austenite.

3. INFLUENCE OF CARBON CONTENT OF AUSTENITE ON TEMPERATURE OF THE *Ar''* TRANSFORMATION

Specimens of the alloys ranging in carbon from 0.23 to 1.21 percent were heated in vacuo to 1,800° F and quenched directly in hydrogen. Each of the alloys had an average austenitic grain size of 1½ to 3 grains per square inch at 100 diameters (ASTM grain number 2) at 1,800° F, and all carbon was in solution at the time of quenching. The specimens were quenched at various rates, which were sufficiently fast

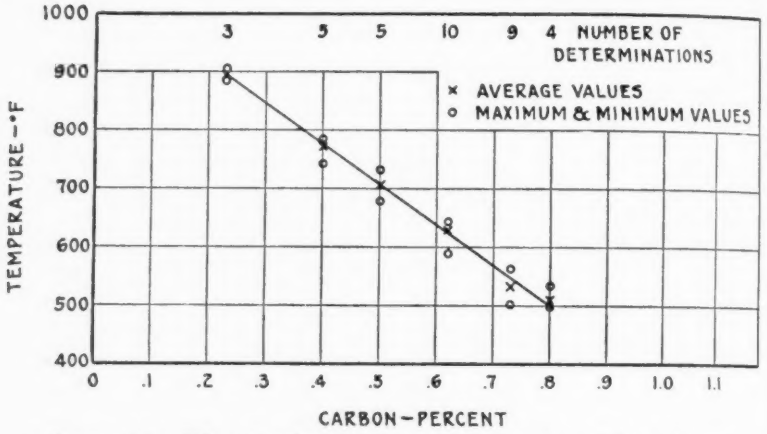

FIGURE 14.—*Effect of carbon content on the temperature of the Ar'' transformation of quenched iron-carbon alloys.*

Specimens 0.10 inch square by 0.040 inch thick were quenched in hydrogen at various rates directly from 1,800° F. At 1,800° F, all the alloys had the same average grain size of 1½ to 3 grains per square inch at 100×, and all carbon was in solution.

to cool the austenite unchanged to the temperature range favorable for its transformation to martensite (*Ar''*). A photographic time-temperature cooling curve was obtained during the quench by means of a string-galvanometer apparatus.

The photographic records show clearly the arrest in the cooling curves at the *Ar''* transformation of the hypoeutectoid and eutectoid alloys. With the type of cooling curves obtained in the present experiments, no arrest was observed at the *Ar''* transformation for the relatively stable austenite of the hypereutectoid alloys.

As shown in figure 14, the temperature at the start of the *Ar''* transformation progressively decreased with increase in carbon content of the alloys from about 900° F for the 0.23-percent-carbon to about 500° F for the 0.80-percent-carbon alloy.

Esser, Ellender, and Spenle [10] found that the temperature range of the *Ar''* transformation was influenced both by the rate of cooling and

[10] H. Esser, W. Ellender, and E. Spenle, *Quenching diagrams of the iron-carbon alloys*, Arch. Eisenhüttenw. **6**, 389–393 (1933).

by the carbon content of high-purity iron-carbon alloys. Their results showed that the temperature of the *Ar''* was lowered, with increase in carbon content, from 750° F for the 0.20-percent-carbon to 170° F for the 1.8-percent-carbon alloy. For plain carbon steels, French and Klopsch [11] showed that the temperature of *Ar''* was lowered, with increase in carbon content, from about 1,080° F for the 0.20-percent-carbon to about 710° F for the 0.60- to 0.70-percent-carbon steels and remained at about 710° F for steels containing about 0.70 to 1.25 percent of carbon.

Davenport, Bain,[12] and coworkers,[13] in their studies of the process and results of the transformation of austenite at constant temperatures, found that the general form of the transformation temperature-time curve was the same for all steels investigated, but that there were significant differences in the position of the *S*-curve on the time scale and minor differences on the temperature scale. The hardenability of a steel thus depends on the stability of its austenite on cooling through the temperature range of about 1,110° to 930° F., and the position of this range is not appreciably altered by variation in such factors as composition and grain size of the austenite. In the present investigation, the *Ar''* transformation commenced at temperatures appreciably higher than in the interrupted quench experiments of Davenport and Bain. Indeed, the *Ar''* for the high-purity iron-carbon alloy containing 0.23 percent of carbon began at about 900° F., a temperature only slightly below the upper range, as shown in the *S* curve, where the austenite is unstable and in which its decomposition products are relatively soft.

Data on the transformation of austenite at constant temperature levels in high-purity iron-carbon alloys would be of value in removing the existing confusion. This information would also aid in the determination of the critical cooling rates by definitely establishing the upper range in which the quenched austenite is most likely to decompose. However, accurate data on this subject would be difficult to obtain because of the relatively high rate of transformation of austenite in the high-purity iron-carbon alloys, especially those of the lower carbon contents.

V. SUMMARY

Specimens of high-purity iron-carbon alloys were heated in vacuo to various temperatures and either quenched directly from these temperatures or cooled to the temperature range in the vicinity of A_1 before quenching in hydrogen. The preparation and analyses of the alloys were described in a previous report.[14]

Examination of the microstructures of the quenched specimens showed (1) the mode of transformation of austenite of varying grain size with both uniform and nonuniform distribution of the carbon, and (2) the effects of these factors on the rate of transformation of the austenite.

[11] H. J. French and O. Z. Klopsch, *Quenching diagrams for carbon steels in relation to some quenching media for heat treatment*, Trans. Am. Soc. Steel Treating **6**, 251–294 (1924).

[12] E. S. Davenport and E. C. Bain, *Transformation of austenite at constant sub-critical temperatures*, Trans. Am. Inst. Mining Met. Engrs., Iron and Steel Div. **90**, 117–154 (1930).

[13] A contribution from the Research Laboratory, United States Steel Corporation, *The process and results of austenite transformation at constant temperatures*, Metals & Alloys **8**, 22–24 (Jan. 1937).

[14] See footnote 1.

With all carbon in solution and uniformly distributed in austenite of mixed grain size, the initial transformation occurred at the grain boundaries. This austenite was least stable in the vicinity of its grain boundaries, where transformation occurred at a higher temperature than in the interior of the grains.

With incomplete solution and nonuniform distribution of carbon in austenite of relatively large grain size, the transformation often proceeded at various rates within the grains. This was illustrated in an alloy containing 1.14 percent of carbon by the transformation products of one large grain of austenite. This grain of austenite transformed to cementite, ferrite, coarse lamellar pearlite, varying degrees of fine pearlite (troostite), and martensite. Microhardness tests made on this decomposed grain of austenite showed how the hardness varied with the transformation products. The microhardness values determined ranged from about 190 for the soft pearlite to about 720 for the fully hardened martensite.

Under certain conditions, free carbide particles in the austenite at the time of quenching act as nuclei for transformation and thus increase materially the reaction rate of the austenite. The reaction rate of the austenite apparently increases with increase in the number of free carbide particles per unit volume up to a point beyond which further increase in number has no effect on its transformation rate or hardenability.

The transformation rate of the alloys was influenced by the grain size of both uniform and nonuniform austenite with respect to carbon. With austenite of constant carbon content, uniformly distributed, the larger the grain size the more stable is the austenite (the slower is its transformation rate on quenching). With nonuniform distribution and solution of carbon in austenite, the grain size is not always a true index to its stability. The high rate of transformation of small grains of nonuniform austenite may be attributed principally to depletion in carbon of the austenite at the instant of quenching rather than to the actual size of the austenitic grains.

With the exception of a few of the grains of smaller size whose transformation on quenching was completed at a high temperature, each grain of austenite was revealed by each of its decomposition products, cementite and troostite.

The temperature at the start of the Ar'' transformation progressively decreased with increase in carbon content of the alloys from about 900° F for the 0.23-percent-carbon to about 500° F for the 0.80-percent-carbon alloy.

Specimens of the hypereutectoid alloys, quenched from high temperatures at rates resulting in complete hardening, often showed numerous fine cracks located not only in the original austenitic grain boundaries but also in the interior of these grains. Intergranular cracks with respect to the original austenite were produced in these martensitic specimens by applying sufficient external stress to the quenched specimen to cause rupture.

WASHINGTON, April 14, 1939.

U. S. DEPARTMENT OF COMMERCE NATIONAL BUREAU OF STANDARDS

RESEARCH PAPER RP1226

Part of Journal of Research of the National Bureau of Standards, Volume 23, July 1939

PREPARATION OF HIGH-PURITY IRON

By John G. Thompson and Harold E. Cleaves

ABSTRACT

Iron of high purity, in the form of 1-lb ingots, has been prepared by reducing purified iron oxide to sponge iron, melting the sponge iron, and remelting under hydrogen and in vacuo. The ingots were examined by spectroscopic and chemical methods for the presence of 55 possible impurities; the number of impurities that could be identified in individual ingots ranges from 6 to 9. The total of impurities in each ingot in most cases is less than 0.010 percent. The major impurities are nonmetallic, chiefly oxygen and sulfur, with traces of carbon, phosphorus, nitrogen, and hydrogen. Copper is the only metallic impurity in seven of the ingots; others contain small amounts of silicon and occasional traces of aluminum or beryllium from the refractories.

CONTENTS

	Page
I. Introduction	163
II. Materials	164
III. Conversion of purified oxide to sponge iron	165
IV. Removal of silica from sponge iron	167
V. Removal of oxygen from melted sponge iron	169
VI. High-purity iron	171
VII. References	174
VIII. Appendix. Analytical methods employed in the analysis of high-purity iron	174
1. Spectrochemical analysis (by Bourdon F. Scribner)	174
2. Determinations of carbon, sulfur, phosphorus, and copper (by Harry A. Bright)	175
3. Determination of oxygen, nitrogen, and hydrogen (by Vernon C. F. Holm)	176

I. INTRODUCTION

The preparation of metals of the utmost possible purity has ever been a matter of interest to metallurgists, primarily because the fundamental properties of a metal can be ascertained with accuracy only by direct determinations made on samples that are free from significant amounts of impurities. What constitutes a significant amount of an impurity depends both on the nature of the impurity and on the metal which it contaminates, as well as on the purpose for which the metal is to be used. It has been known for a long time that some properties of certain metals, for example, the ductility of gold and the electric conductivity of copper, are seriously affected by the presence of very small amounts of impurities. Consequently, a high degree of purity with respect to particular impurities has been demanded in such metals when they are to be used for special purposes. On the other hand, mechanical properties such as strength, hardness, and load-carrying capacity, for which the common metals are valued, are

less sensitive to the presence of impurities; in fact these properties in iron are improved by increasing the amount of certain constituents, such as carbon, which are normally present in small amounts as "impurities." For these reasons, the definition of "purity" in metals has varied with the metal and with the intended use; in general the requirements of purity were more rigid for the noble and precious metals than for the common ones. However, in recent years the preparation of common metals such as aluminum and zinc, in higher states of purity than had been previously obtained, has shown that certain properties of common metals may be materially affected by amounts of impurities so small that they were formerly considered insignificant. Furthermore, intensive investigation of the magnetic properties of iron revealed outstanding examples of the significance of minute amounts, 0.001 or 0.002 percent, of impurities such as carbon, oxygen, and sulfur. Such observations naturally lead to speculation regarding the effect of small amounts of these and other impurities on the properties of iron, and the degree of purity with respect to various constituents which must be attained to permit measurements of properties that will not be significantly affected by the inevitably remaining traces of contaminating substances.

Attempts to prepare metallic iron of the utmost possible purity have been made from time to time throughout the past one hundred years, but the elimination of impurities with which iron is associated in its ores and the avoidance of contamination from other sources are matters of extreme difficulty. Previous investigations of the preparation of high-purity iron and the varying properties that have been observed in the products of these investigations were reviewed in previous publications [1, 2],[1] the preparation of which constituted the first phase of the current investigation. A critical review of the previous work led to the conclusion that the best possibilities for the preparation of iron of very high purity lay in the chemical methods, that is, in the preparation of a purified compound of iron and its subsequent conversion to metallic iron. Experimental work indicated that recrystallization of ferric nitrate offered promise for the production of a purified compound of iron, and a description of the preparation of a quantity of recrystallized nitrate and the conversion of this material to high-purity iron oxide has been published [3]. The present paper describes attempts to convert the purified iron oxide to metallic iron of equally high or superior purity.

II. MATERIALS

Four lots of purified iron oxide were available, representing two purification processes applied to each of two lots of ferric nitrate. The only impurities that could be identified by spectroscopic and chemical methods are listed in table 1. The presence of silicon, aluminum, calcium, magnesium, and copper was revealed by spectrochemical examination, and the numerical values for the silicon contents were determined by chemical analysis. Sulfur and phosphorus could not be detected in any of the oxide samples, using chemical methods that were sensitive to 0.001 percent of sulfur and 0.0005 percent of phosphorus. Examination of the spectra failed to reveal the presence of sensitive lines of any of the following elements: Antimony, arsenic, barium, beryllium, bismuth, boron, cadmium, cerium, chro-

[1] Numbers in brackets indicate the literature references at the end of this paper.

mium, cobalt, columbium, gallium, germanium, gold, hafnium, indium, iridium, lead, lithium, manganese, mercury, molybdenum, nickel, osmium, palladium, platinum, potassium, rhodium, ruthenium, scandium, silver, sodium, strontium, tantalum, thallium, thorium, tin, titanium, tungsten, uranium, vanadium, yttrium, zinc, and zirconium.

TABLE 1.—*Impurities in purified iron oxide*

Elements	Oxide			
	A	*B*	*C*	*D*
Silicon	0.016%	0.009%	0.006%	0.005%.
Aluminum	Trace	Faint trace	Faint trace	Faint trace.
Calcium	do	do	do	Do.
Magnesium	do	do	do	Do.
Copper	Faint trace	do	do	Do.

III. CONVERSION OF PURIFIED OXIDE TO SPONGE IRON

Iron oxide may be converted to metallic iron by several means. In commercial operations iron ores are reduced with carbon or carbonaceous compounds, but the iron thus produced is always contaminated by carbon. Metallic reducing agents—calcium [4], aluminum [5], zinc [6], and sodium [7]—have been suggested for the production of carbon-free iron, but these reagents also are open to the objection of contamination of the iron by the products of deoxidation and by the excess of reducing agent that is necessary to insure complete reduction. Reduction by hydrogen offers the least possibility of contaminating the reduced iron, either by the products of the reduction reaction or by an excess of the reducing agent. The product of the reduction reaction is water vapor which is removed by the stream of hydrogen. Contamination by an excess of the reducing agent is minimized because the solubility of hydrogen in iron is only 0.0005 percent [8, 9] at 1,000° C and atmospheric pressure, and is even less at lower temperatures.

The reduction of iron oxide by hydrogen begins at low temperatures, about 370° C according to Tammann and Nikitin [10] and only a little above 300° C according to Kamura [11], but at these temperatures the reaction proceeds slowly and is difficult to carry to completion. The rate of the reaction increases with increasing temperature until an optimum temperature for rapid and complete reduction is reached, between 500° and 600° C [11, 12, 13]. With increasing temperature above the optimum range there is an increasing tendency to sinter the surface of the particles of partially reduced oxide, which hinders the penetration of hydrogen to the center of the particles and thus increases the time required to complete the reduction.

Another factor to be considered, in addition to the speed and completeness of the reduction, is that iron reduced at low temperatures is pyrophoric, that is, subject to spontaneous reoxidation upon exposure to the air. Pyrophoric iron results from reduction at any temperature below 530° C, according to Tammann and Nikitin [10], and even up to 710° C, according to Smits and Wallagh [14]; but the tendency towards pyrophoric behavior can be overcome by heating the reduced iron to still higher temperatures.

The procedure adopted for the reduction of iron oxide to sponge iron in the present investigation comprised two steps, (a) maintenance

of the material at about 500° C until the reduction was practically complete, followed by (b) raising the temperature to about 1,000° C to sinter the surface of the particles and destroy the tendency towards pyrophoricity. This procedure is similar to the one successfully employed on a small scale by Baxter and Hoover [13] in their classic determination of the atomic weight of iron.

The hydrogen used in the reduction was a commercial product, compressed in cylinders and containing up to 0.5 percent of oxygen as the principal impurity. The hydrogen was purified by passing it through Ascarite to remove any hydrogen sulfide and carbon dioxide that might be present, then through platinized silica at 750° C to convert the oxygen to water, which was absorbed by anhydrous magnesium perchlorate.

Preliminary experiments indicated that a charge of iron oxide could be reduced, sintered, and cooled in the furnace within 7 hours. Under these conditions of operation, only about 10 percent of the hydrogen was utilized in the reduction of the iron oxide, the remainder serving merely to flush the reaction product (water vapor) out of the furnace and thus permit the reaction to go to completion within the allotted time. However, the use of two furnaces in series, with provision for repurifying the gas between furnaces, doubled both the rate of production of sponge iron and the efficiency of the utilization of hydrogen. The reaction chamber in each furnace was the central portion, about 40 cm in length, of a fused silica tube 5 cm in inside diameter. Each reaction chamber was lined with a sheet of electrolytic iron to protect the iron oxide and sponge iron from contamination during the reduction. The inlet end of each silica tube was sealed to the hydrogen supply line; the outlet ends were closed by removable stoppers, to facilitate charging and discharging the furnaces. Perforated porcelain disks near the ends of the silica tubes served as radiation shields, and the extreme ends of the tubes were further protected by water cooling.

The schedule of operation of the apparatus shown in figure 1 was as follows: Reduction furnaces *A* and *B* were each loaded with 300 g of iron oxide, equivalent to 200 g of sponge iron, contained in a boat that was made from a thin sheet of electrolytic iron. The apparatus was flushed with purified hydrogen from one of two cylinders connected in parallel, the furnaces were heated to 500° C, and the rate of flow of the hydrogen was adjusted to about 2 liters per minute. These conditions were maintained for about 3½ hours, until the reduction was practically completed as indicated by the disappearance of condensed water in the outlet tubes of the furnaces. The hydrogen flow was then reduced to about 300 ml per minute; the temperature was raised to 1,000° C and maintained there for 1 hour, after which the power was cut off, the rate of flow of the hydrogen was further reduced to 100 ml or less per minute, the split furnaces were opened, and the silica tubes and contents were cooled with streams of air from electric fans. The catalyst furnace in the hydrogen purification train was then allowed to cool, after which the hydrogen flow was stopped. The following morning the condensate was drained from the water and vapor traps located between the two furnaces, the boats were removed from the furnaces, the sponge iron was transferred to storage containers, the boats were refilled with iron oxide and replaced in the furnaces, and another run was started.

The sponge iron was easily removed from the boats and was readily granulated, but the boats frequently stuck to the electrolytic-iron sleeve. The oxygen content of the sponge iron was not determined, in fact an oxygen-free sponge iron was not desired because, as described in the ensuing paragraphs, the presence of FeO was found to facilitate the removal of silica. Examination of the sponge iron indicated that no new impurities had been introduced and that the impurities other than oxygen were the same as in the four lots of iron oxide. However, because of the decrease in weight that accompanied the reduction, the concentration of each impurity in the sponge iron was about one-third greater than it had been in the oxide. Silicon or silica was still the principal impurity, ranging from 0.024 percent of Si in sponge iron *A* to 0.008 percent of Si in sponge iron *D*.

IV. REMOVAL OF SILICA FROM SPONGE IRON

Two processes, (a) sintering and (b) melting, were considered for converting the sponge iron to solid metal. Sintering at temperatures below the melting point of iron is, perhaps, less apt to introduce new impurities but offers no possibility of reducing the content of impurities already present in the sponge iron. On the other hand, previous work in this laboratory has demonstrated the feasibility of melting, without contamination, high-purity metals, such as platinum and its alloys, which melt at temperatures appreciably higher than the melting point of iron. Furthermore, there was a possibility that the content of silica, and perhaps of other impurities in the sponge iron, could be reduced by slagging during a melting operation, as was indicated by the work of Adcock and Bristow [15]. Also, a dense, coherent structure is more readily obtained by melting than by sintering. For these reasons a melting process was preferred for the conversion of the sponge iron to solid metal.

The sponge iron, prepared as described in the preceding section of this report, was granular and bulky, with an apparent density of about 2 g/cm^3. This material was compressed under approximately 2,000 lb/in.^{2} in a steel mold, to form briquettes 4 cm in diameter and 2 to 3 cm thick, with densities slightly less than 6 g/cm^3. Briquetted sponge iron was melted in alumina, magnesia, and beryllia crucibles to determine the relative merits of the three refractories with respect to contamination of the melt as well as to elimination of silica. The alumina was purified oxide prepared commercially for the production of metallic aluminum and contained sodium salts as its principal impurities. The magnesia and beryllia were of "chemically pure" grades. Crucibles were formed by the methods of pressing or tamping that had been previously used for the preparation of small crucibles [16], but difficulty was encountered in preparing crucibles, in the larger sizes desired in this work, with satisfactorily smooth walls and bottoms. Better crucibles were obtained by a slip-casting process, based on the results of Turner [17] and of Partridge and Lait [18]. The slip-cast crucibles had excellent inner surfaces, and, consequently, there was a minimum possibility of contaminating the melt with particles or flakes of the refractory. Ingots melted in slip-cast crucibles were smooth surfaced and seldom required cleaning, in contrast to the rough-surfaced, refractory-contaminated ingots from the tamped crucibles. For these reasons, slip-cast crucibles were used in most of this work, particularly in the later stages.

Spectrochemical examination of ingots melted in alumina and magnesia revealed contamination from the refractories either by inclusions of minute particles of refractory oxides or by partial reduction of the refractory and solution of the reduced metal in the molten iron. However, ingots melted in beryllia, in these preliminary experiments, were not contaminated. From the point of view of possible contamination of high-purity iron by the refractory, beryllia was preferable to magnesia or alumina.

Beryllia was also found to be preferable to the other two in the removal of silica during melting. The silicon content of some sponge iron was reduced from 0.027 to 0.007 percent by melting in a beryllia crucible, but similar melts in magnesia and alumina retained respectively 0.010 and 0.016 percent of silicon. These figures were further reduced by holding the metal quietly molten for long periods of time, but the silicon was never eliminated completely in any of these simple melts, even in beryllia crucibles. The removal of silicon (or silica) apparently was accomplished through the formation of an iron silicate slag that was absorbed by the crucible. There was little if any evidence of slag on the upper surface of the melt, but the inner walls of the crucible were noticeably discolored. If the silicon content of the sponge iron could be reduced 50 percent or more by slagging in the presence of a small amount of oxygen or FeO, it appeared probable that further reduction of the silicon content could be obtained if more slag, that is, more FeO, were present. Accordingly, mixtures of sponge iron and purified iron oxide were briquetted, melted in beryllia crucibles, and held quietly molten for 30 minutes. A melt without added oxide contained 0.004 percent of silicon; addition of 0.5 and 1.0 g of iron oxide to 100 g of sponge iron decreased the silicon content progressively, and a minimum silicon content of about 0.001 percent was obtained with an addition of 2 percent by weight of iron oxide. Larger amounts of iron oxide, up to 8 percent by weight of the sponge iron, showed no further improvement, and incorporation of 2 percent of iron oxide in the briquettes was therefore adopted as regular practice in melting the sponge iron.

Considerable difficulty was encountered in melting the briquetted sponge iron in vacuo in a high-frequency induction furnace, because of the poor conductivity of the briquettes and their high shrinkage during melting. The usual result was that the lower portions of the charge melted, but the upper portions only softened enough to adhere to the crucible, and remained suspended above and not in contact with the pool of the molten metal. Melting of the bridged material required the application of so much power that the pool of molten metal was heated to a high temperature, and there was danger of failure of the crucible and loss of the melt. These difficulties were not encountered when the sponge iron was melted in a resistance furnace of the Arsem type, heated by a graphite spiral resistor. In this furnace a crucible full of briquettes melted smoothly and completely, without overheating any portion of the charge. The atmosphere in this furnace was chiefly carbon monoxide, at a pressure of 3 or 4 mm of mercury. There was a possibility, therefore, of contaminating the iron by absorption of carbon or CO; but this possibility appeared to be slight, particularly in view of the high oxygen contents of the briquettes and of the molten iron.

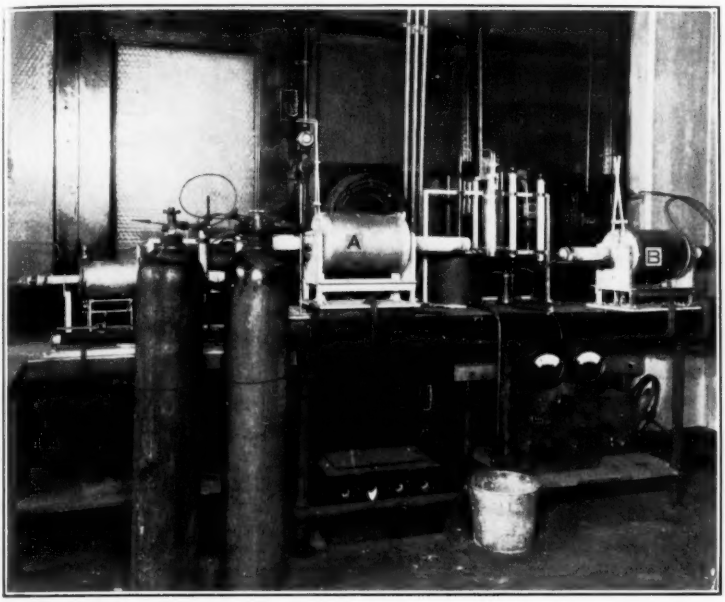

FIGURE 1.—*Apparatus for the reduction of iron oxide to sponge iron.*

Hydrogen from the cylinders is passed successively through a purification train, over iron oxide in furnace *A*, through a water trap and drying train, and over a second portion of iron oxide in furnace *B*

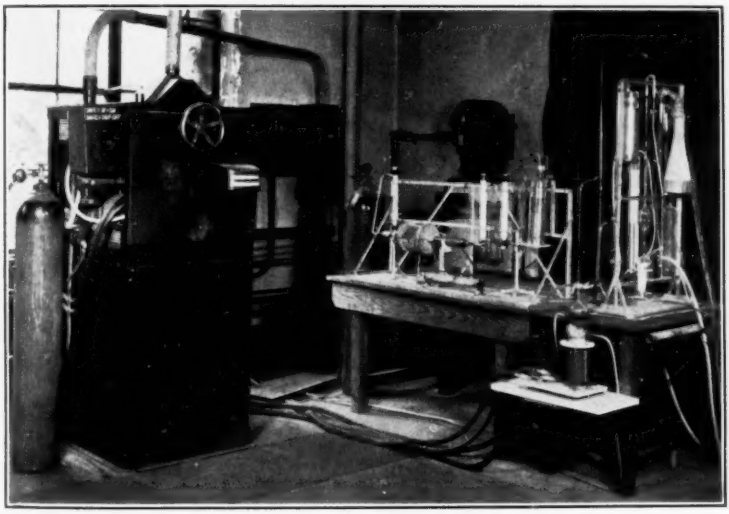

FIGURE 2.—*Apparatus for melting oxygen-rich ingots under hydrogen and in vacuo.*

The furnace is heated by a high-frequency induction coil and is connected with a source of purified hydrogen or with vacuum pumps.

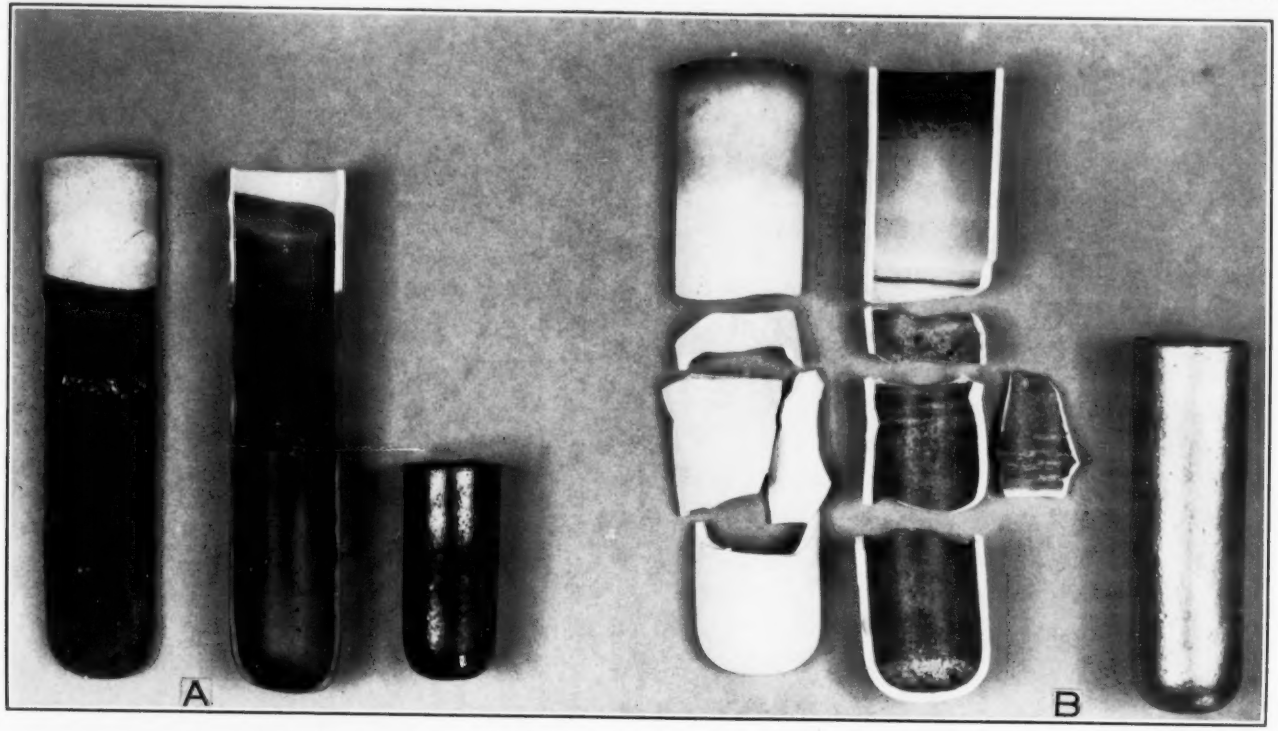

FIGURE 3.—*Steps in the conversion of sponge iron to high-purity solid iron.*

A, ingot prepared by melting a crucible full of briquetted sponge iron with added iron oxide to facilitate removal of silica by slagging; *B*, ingot prepared by remelting, under hydrogen and in vacuo, two ingots from operation *A*.

The melts of briquetted sponge iron, with 2 percent of iron oxide to assist in removal of silica, therefore were made in the Arsem furnace. Beryllia crucibles approximately 3 cm in inside diameter by 18 cm long were used. The crucible, supported in a graphite shell, was filled with approximately 350 g of briquetted sponge iron. The briquettes were melted slowly and maintained molten for 30 minutes. The power was then shut off and the ingot allowed to cool in the furnace. Ingots so prepared contained about 0.2 percent of oxygen. The appearance of the ingot, the shrinkage of the sponge iron on melting as indicated by the relative volumes of ingot and crucible, and the discoloration of the slip-cast crucible by absorption of iron oxide and silica, are illustrated at the left of figure 3.

V. REMOVAL OF OXYGEN FROM MELTED SPONGE IRON

The logical procedure to deoxidize the oxygen-rich ingots was to hold the iron molten under hydrogen for a sufficient length of time, with subsequent evacuation of the molten metal to remove dissolved hydrogen. Heating by induction was desirable for these operations because the deoxidation and subsequent evacuation would be expedited by stirring the molten metal, and further, because the crucible remains colder than the metal, which decreases the possibility of contamination of the melt by the refractory.

In contrast to the sponge-iron briquettes, the oxygen-rich ingots were readily melted in an induction furnace, particularly in an evacuated furnace. Melting under hydrogen required more power and was more susceptible of bridging of the charge, because of cooling of the exposed top of the ingot. If the cold ingot fits too snugly in the crucible, the latter may be cracked by thermal expansion of the ingot before it melts, but this difficulty was avoided by using a slightly larger crucible, with an internal diameter about 3 mm greater than that of the ingot.

The apparatus used for the final deoxidation of the oxygen-rich ingots is shown in figure 2. The hydrogen purification train, mounted on the table at the left of the furnace, was similar to the one used in the reduction of iron oxide to sponge iron. It contained a tube of Ascarite, to remove hydrogen sulfide and carbon dioxide, a platinized silica catalyst maintained at 750° C, a tube of anhydrous magnesium perchlorate to remove water, and a trap cooled with a mixture of solid carbon dioxide, chloroform, and acetone, to remove the last of the water vapor. The furnace chamber was a silica tube, 40 cm long and 6 cm in inside diameter, mounted vertically in an induction coil that was 7.5 cm in diameter. The upper end of the furnace tube was sealed with Picene wax to a Pyrex dome equipped with an inlet connection to the hydrogen purification train and with outlet connections to a vent and to the vacuum pumps. A small silica tube was attached to the inlet tube, inside the glass dome, to conduct the incoming stream of hydrogen directly onto the surface of the melt. The apparatus for evacuating the furnace, shown in figure 2 behind and to the right of the induction furnace, consisted of a rotary oil pump, mercury diffusion pump, McLeod gage, and a trap to prevent back diffusion of mercury vapor.

The procedure of melting, deoxidation, and evacuation was as follows: Two oxygen-rich ingots, weighing about 300 g each, were placed in a beryllia crucible, the second ingot being inverted on the

first, so that the flat tops of the two ingots were in contact and the rounded bottom of the second ingot was uppermost and free from contact with the crucible walls. This arrangement materially reduced the danger of bridging. The crucible was packed for about three-fourths of its length in granular beryllia in a slip-cast shell that fitted loosely in the silica furnace tube. The glass dome was sealed in place, the furnace was evacuated, and power was applied to the induction coil slowly, to minimize the thermal shock to the crucible. The initial 3 kva of power was increased by 1 kva each 5 minutes until the first signs of melting were noted, usually at about 10 kva. At this point the power was increased to about 20 kva to hasten the melting and to avoid bridging. As soon as melting was completed, the power was reduced to about 6 kva, just sufficient to keep the iron molten.

In the meantime the flow of hydrogen through the purification train and out the vent had been adjusted to 2.5 liters per minute. When the iron was completely molten, the furnace was disconnected from the vacuum pumps and hydrogen was introduced slowly into the evacuated furnace. When the pressure in the furnace reached 1 atmosphere, indicated by the escape of hydrogen through a safety trap, the exit connection of the furnace was turned to permit release of the hydrogen to the vent, and the inlet connection was opened to divert the full stream of hydrogen into the furnace. The power input was adjusted until the temperature of the metal was slightly higher than the melting point, just enough to render the metal fluid and inductively stirred, to facilitate the reduction. Overheating of the metal was avoided because of the attendant possibility of reduction of the refractory at high temperatures and consequent contamination of the melt. About 12 kva was required to maintain 600 g of iron molten under hydrogen, in contrast to the 6 kva that kept the same metal molten in vacuo.

The iron was maintained in the molten condition under hydrogen for periods that varied from 45 minutes for a 600-g melt to 60 minutes for an 800-g melt. Most of the oxygen was removed from the iron rapidly, as was indicated by the formation of drops of water on the cooler portions of the furnace tube and in the outlet tube. These drops disappeared within a few minutes and thereafter there was no more condensation. Preliminary experiments had indicated that 30 minutes' exposure to hydrogen under these conditions reduced the oxygen content of a 600-g melt from about 0.2 percent to 0.001 or 0.002 percent, which values were not improved by longer treatments. Treatment for 45 minutes therefore should insure complete deoxidation with a reasonable margin of safety.

At the expiration of the allotted time for the deoxidation, the hydrogen inlet to the furnace was closed and the furnace outlet was connected to the vacuum pumps. During evacuation of the furnace the temperature of the molten metal was maintained approximately constant by gradually decreasing the power input, to 5 or 6 kva. When the pressure in the furnace was reduced to 0.02 mm or less, the power was cut off and the metal was allowed to solidify and cool to room temperature in the evacuated furnace.

Ingots prepared in the manner just described had clean, bright surfaces in contrast to the dark-colored, oxidized surfaces of the oxygen-rich ingots. As is shown in figure 3, the final ingots required practi-

cally no cleaning or grinding after removal from the crucible. The inner surface of the slip-cast beryllia crucible was slightly discolored by iron oxide, presumably absorbed during the first melting of the oxygen-rich ingots. The black band at the top of the crucible was a metallic deposit, apparently of vaporized iron.

VI. HIGH-PURITY IRON

Nineteen ingots, with an average weight of about 1 lb each, were prepared. The top surface of each ingot was flat and solid, but the interior contained a concealed pipe that frequently extended for half the length of the ingot as is shown in figure 4. The structures were coarsely crystalline, and some evidence of porosity was noted, particularly in the vicinity of the lower portions of the pipes. Better structures would have been obtained from chill-cast ingots, but equipment for melting and casting in vacuo was not available at this time.

In preparing the specimens shown in figure 4, the ingots were sawed in two and one-half was ground flat and smooth on a surface grinder. The parallel striations running lengthwise of each ingot are evidence that the surface grinding work-hardened the metal to an appreciable depth. The striations persisted through several repolishings and etchings.

The data from analyses of the ingots are summarized in table 2. Copper, silicon, beryllium, and aluminum were determined by spectrochemical methods; carbon, sulfur, and phosphorus by chemical methods; and oxygen, nitrogen, and hydrogen by vacuum-fusion methods. Because many of these determinations approach the limits of uncertainty of available analytical methods, brief descriptions of the procedures by means of which these numerical values were obtained are given in an appendix to this report.

The data of table 2 show that the elimination of metallic impurities has been quite successful, except for copper. This element was practically unaffected by the purification process to which the material was subjected, and the copper contents of the final ingots are essentially the same as those of the iron oxide and sponge iron. A trace of copper is present in all of the ingots, but in seven of them copper is the only metallic impurity whose presence could be detected. The calibration of the spectrochemical procedure did not permit a more precise statement of the copper contents than that they are all less than 0.002 percent. Direct determinations of the copper content of each ingot, by chemical methods, has not been practicable because of the amount of sample material consumed in the multiple determinations necessary to establish with precision copper contents of this magnitude. Four direct determinations of copper have been made, two on samples of the sponge iron from which the ingots were made and two on composite samples of the ingots themselves. The results of these four determinations range from 0.0018 to 0.0006 percent of copper, which indicates that the figure 0.002 percent is an adequate and in some cases perhaps a liberal estimate of the amount of copper.

TABLE 2.—*Composition of ingots of high-purity iron*

Element	Ingot number [1]																		
	1	2	3	4	5	6	7	8	9	10	11	12	13	14	15	16	17	18	19
Cu[2]	<0.002	<0.002	<0.002	<0.002	<0.002	<0.002	<0.002	<0.002	<0.002	<0.002	<0.002	<0.002	<0.002	<0.002	<0.002	<0.002	<0.002	<0.002	<0.002
Si[2]	.001	.001	.003	.001	.003	.001	.001	.001	nil	nil	nil	.002	nil	.002	nil	nil	<.001	nil	nil
Be[2]	<.001	<.001	<.001	nil	nil	<.001	nil	nil	nil	nil	nil	nil	nil	nil	nil	nil	nil	nil	nil
Al[2]	nil	nil	nil	nil	<.001	nil	nil	nil	nil	nil	nil	nil	nil	nil	<.001	nil	nil	nil	nil
C	<.001	.001	.001	.001		<.001	<.001					<.001	<.001	.001				.001	<.001
S	$.002_8$	$.002_8$	$.002_6$	$.001_0$	$.001_0$	$.001_8$	$.002_1$	$.001_0$	$.002_2$	$.002_3$	$.001_8$	$.001_2$	$.002_4$	$.001_1$	$.001_3$	$.004_1$	$.002_5$	$.001_1$	$.002_3$
P		<.0005															<.0005		
O_2	$.001_8$	$.000_2$	$.000_8$	$.003_8$	$.004_0$	$.004_8$	$.002_0$	$.003_2$	$.003_5$	$.001_9$	$.004_5$	$.001_4$	$.004_0$	$.002_0$	$.001_0$	$.001_3$	$.003_0$	$.003_4$	$.004_2$
N_2	$.000_1$	$.000_2$	$.000_4$	$.000_4$	$.000_2$	$.000_2$	$.000_1$	$.000_0$	$.000_0$	$.000_1$	$.000_2$	$.000_5$	$.000_2$	$.000_2$	$.000_6$	$.000_1$	$.000_2$	$.000_1$	$.000_2$
H_2	$.000_1$	$.000_2$	$.000_1$	$.000_2$	$.000_2$	$.000_2$	$.000_2$	$.000_2$	$.000_1$	$.000_1$	$.000_1$	$.000_2$	$.000_1$	$.000_1$	$.000_2$	$.000_1$	$.000_2$	$.000_2$	$.000_2$
Total of identified impurities	$<.009_2$	$<.008_4$	$<.011_1$	$<.009_8$	$<.012_0$	$<.011_7$	$<.008_8$	$<.008_8$	$<.009_3$	$<.008_4$	$<.009_3$	$<.008_8$	$<.010_2$	$<.008_9$	$<008_8$	$<.009_0$	$<.010_8$	$<.008_2$	$<.010_2$

[1] Ingots 1 to 6, inclusive, were made from sponge iron from oxide *A*; ingots 7 to 12, inclusive, from oxide *B*; ingots 13 to 15 from oxide *C*; and ingots 16 to 19 from oxide *D*.

[2] The arc spectrum of each ingot was examined for the presence of sensitive lines of 49 elements. Determinations of Cu, Si, Be, and Al are recorded above, the expression "nil" meaning that the amount of the impurity if present at all, was less than the sensitivity of the analytical method. None of the following 45 elements could be identified in any of the ingots: Ag, As, Au, B, Ba, Bi, Ca, Cb, Cd, Ce, Co, Cr, Ga, Ge, Hf, Hg, In, Ir, K, Li, Mg, Mn, Mo, Na, Ni, Os, Pb, Pd, Pt, Rh, Ru, Sb, Sc, Sn, Sr, Ta, Th, Ti Tl, U, V, W, Y, Zn, and Zr.

FIGURE 4.—*Macrosections of two ingots of high-purity iron, showing the concealed pipes and the coarsely crystalline structure.*

Etched with 1-percent nital.

UNIV. OF MICH.

Silicon was the chief impurity in each of the lots of purified iron oxide (see table 1) and sponge iron, but the silicon contents of the ingots are, in general, satisfactorily low. As much as 0.024 percent of silicon was present in some of the sponge iron, but the maximum silicon content in any of the ingots is only 0.003 percent, and in 8 of the ingots silicon could not be detected. The silicon contents of ingots 1 to 6, inclusive, that were prepared from the high-silicon sponge iron *A* are perhaps a trifle higher than those of other groups; but, in general, the uniformity of the silicon contents of the ingots, irrespective of the silicon contents of the sponge iron from which they were made, attests the effectiveness of the removal of silicon by slagging. The slagging operation likewise was efficient in removing the "dust elements," calcium and magnesium, that were present in or on the purified oxides.

Traces of beryllium in four of the ingots undoubtedly represent contamination from the beryllia crucibles. The trace of aluminum that was detected in two ingots probably also originated in the refractory. It has not been possible to determine whether these traces of beryllium and aluminum represent random inclusions or material in solution in the iron. Inclusions of BeO or Al_2O_3 have not been identified in the course of microscopic examinations.

Nonmetallic elements, particularly oxygen and sulfur, constitute the bulk of the impurities in most of the ingots. The oxygen contents range from 0.0003 to 0.0045 percent. The lower values are close approximations of the irreducible minimum content of oxygen in iron, as determined by the vacuum-fusion method. The higher values presumably represent incomplete deoxidation in the final stages because, in attempting to avoid overheating of the molten metal with attendant danger of contamination from the refractories, the temperature may have dropped enough to cause the molten metal to become viscous, and thereby to retard the progress of the deoxidation. The oxygen contents presumably represent FeO; oxide inclusions have not been identified in microscopic studies, and there is no correlation between the oxygen and silicon contents.

Sulfur contents ranging from 0.001 to 0.0041 percent cause this impurity to rank second to oxygen. The presence of sulfur could not be detected in the purified oxide; its presence in the final ingots represents contamination during melting, probably from refractories, although the beryllia was precalcined and washed with acid to remove sulfur compounds. The presence of 0.001 percent or less of carbon in 11 of the ingots likewise is ascribed to contamination from the crucibles, which were fired in an Arsem furnace. Because the carbon determinations consumed large quantities of material, and further, because a uniform carbon content was indicated in 11 determinations, the carbon contents of the other eight ingots were not determined.

The remaining impurities—nitrogen, hydrogen, and phosphorus, whose presence was determined in some or all of the ingots—are present only in amounts that approach the limits of uncertainty of the analytical methods. The nitrogen contents range from undetectable amounts to a maximum of 0.0006 percent; hydrogen in all cases is either 0.0001 or 0.0002 percent; phosphorus was not expected to be a serious contaminant in the iron, and analyses of two ingots showed that only a faint trace of phosphorus was present. Additional deter-

minations of phosphorus were not made because of the quantity of sample material required.

The totals of identified impurities, out of the 55 elements that were sought, as listed in table 2, include the maximum values for all determinations that were reported as "less than" a maximum value. It was further assumed that the carbon and phosphorus contents of each ingot were, respectively, 0.001 and 0.0005 percent. These totals of identified impurities range from 0.0083 percent for ingot 18 to 0.0129 percent for ingot 5, with 13 of the 19 ingots having contents of less than 0.010 percent of total impurities. Such figures are comparable with the best available analyses of other pure irons [15, 19], and the compositions given in table 2 are noteworthy in the limited number of impurities whose presence could be detected. This is particularly true of metallic impurities; in seven of the ingots, only one metallic impurity, copper, could be identified.

The material remaining after analysis of the ingots will be used for determinations of the properties of high-purity iron and to observe the effect on these properties of the variations in composition of the different ingots.

VII. REFERENCES

[1] H. E. Cleaves and J. G. Thompson, The Metal—Iron (McGraw-Hill Book Co., Inc., New York, N. Y., 1935).
[2] J. G. Thompson and H. E. Cleaves, J. Research NBS **16,** 105 (1936), RP860.
[3] H. E. Cleaves and J. G. Thompson, J. Research NBS **18,** 595 (1937), RP996.
[4] F. M. Perkin and L. Pratt, Trans. Faraday Soc. **3,** 179 (1908).
[5] H. Goldschmidt, Z. Elektrochem. **4,** 494 (1898).
[6] J. A. Poumarede, Compt. rend. **29,** 518 (1849).
[7] A. Hiorth, Norwegian Patent 18,750 (1908).
[8] C. J. Smithells, Gases and Metals (John Wiley & Sons, Inc., New York, N. Y., 1937).
[9] L. Luckemeyer-Hasse and H. Schenck, Tech. Mitt. Krupp **1,** 121 (1933); Arch. Eisenhüttenw. **6,** 209 (1932–33).
[10] G. Tammann and N. Nikitin, Z. anorg. allgem. Chem. **135,** 201 (1924).
[11] H. Kamura, J. Iron Steel Inst. **112,** 278 (1925).
[12] K. Hoffmann, Z. angew. Chem. **38,** 715 (1925).
[13] G. P. Baxter and C. R. Hoover, J. Am. Chem. Soc. **34,** 1657 (1912).
[14] A. Smits and G. Wallagh, Rec. trav. chim. **44,** 130 (1925).
[15] F. Adcock and C. H. Bristow, Proc. Roy. Soc. (London) **153,** 172 (1935–36).
[16] W. H. Swanger and F. R. Caldwell, BS J. Research **6,** 1131 (1931), RP327.
[17] D. Turner, Trans. Ceram. Soc. **33,** 33 (1933–34).
[18] J. H. Partridge and J. R. Lait, J. Soc. Glass Tech. **20,** 200 (1936).
[19] C. Wells, R. A. Ackley, and R. F. Mehl, Trans. Am. Soc. Metals **24,** 46 (1936).

VIII. APPENDIX. ANALYTICAL METHODS EMPLOYED IN THE ANALYSIS OF HIGH-PURITY IRON

1. Spectrochemical Analysis

By Bourdon F. Scribner

The samples of high-purity iron consisted of rods approximately ¼ in. in diameter and 1 in. long, sawed from the ingots and rounded by filing. Tests showed that a few of the rods were contaminated on the surface, probably by handling, and, to avoid errors, all samples were cleaned in dilute acid. The rods were used directly as electrodes for spectrochemical analysis in which the spectra were excited by a direct current arc of 6 amperes. The spectra were photographed in the region 2450 to 5000 A, using a Bausch & Lomb large Littrow spectrograph and a stigmatic concave grating spectrograph built in this laboratory. The dispersion obtained in the spectrograms was 5 A (or less) per millimeter, so that the complex iron spectrum was sufficiently well resolved for the identification of impurities.

The photographed spectra were examined on a micrometer comparator for the sensitive lines of the following elements: Ag, Al, As, Au, B, Ba, Be, Bi, Ca, Cb, Cd, Ce, Co, Cr, Cu, Fe, Ga, Ge, Hf, Hg, In, Ir, K, Li, Mg, Mn, Mo, Na, Ni, Os, Pb, Pd, Pt, Rh, Ru, Sb, Sc, Si, Sn, Sr, Ta, Th, Ti, Tl, U, V, W, Y, Zn, and Zr. The sensitivity of the test is indicated by data, for several elements, obtained chiefly from National Bureau of Standards Standard Samples of iron and steel. Concentrations, in percentage by weight, which have been detected with certainty are as follows:

Al	0. 0005	Ge	0. 0002	Si	0. 001
Co	0. 001	Mn	0. 0005	Sn	0. 0003
Cr	0. 0001	Mo	0. 001	Ti	0. 0005
Cu	0. 0001	Ni	0. 001	V	0. 0005

Although the sensitivity of the test is known to be well below 0.001 percent for a number of elements, the quantitative interpretation of spectrochemical data for concentrations of the order of 0.001 percent frequently is uncertain because of a lack of reference standards. Estimations of the concentration of aluminum, copper, and silicon in the iron samples were made by comparison with the spectra of available standards.

2. Determinations of Carbon, Sulfur, Phosphorus, and Copper

By Harry A. Bright

The carbon content of high-purity iron was determined by direct combustion in oxygen. The porcelain combustion tube (⅞-in. internal diameter) was maintained at 1,050° to 1,100° C. The oxygen was passed through a preheater and through a tower containing Ascarite (asbestos impregnated with sodium hydroxide) and Anhydrone (anhydrous magnesium perchlorate) before entering the combustion tube. The purification train at the exit end of the combustion tube consisted of a U-tube filled with platinized silica-gel maintained at 450° C., and a tube containing ironized asbestos and Anhydrone. The absorbing tubes were glass-stoppered 4-in. U-tubes, containing 20- to 30-mesh Ascarite and a layer of Anhydrone, about 1½ in. deep, at the exit end. A platinum boat approximately 4 in. by ¾ in. by ½ in., and a well-burned cover of nickel were used. The bedding material was R. R. Alundum, specially prepared for carbon determinations. The boat and contents were heated in oxygen at 1,050° to 1,100° C. until the blank correction for a 10-minute run, including removal and reinsertion of the boat in the furnace, was uniform and less than 0.2 mg of carbon dioxide.

Three grams of iron was placed on the bedding material so that the particles were in intimate contact. The covered boat was placed in the hot combustion tube and preheated for 1½ to 2 minutes. Oxygen was admitted at a rate sufficient to maintain a flow of 300 to 350 ml per minute through the exit end of the tube during the combustion period. When combustion was complete, the flow of oxygen was reduced to about 150 ml per minute and maintained at this rate for about 10 minutes. The absorption tube filled with oxygen was disconnected, placed in the balance, and weighed, using the same procedure and time intervals as in the blank determination.

The percentage of carbon was calculated from the increase in weight of the absorbing tube minus the weight of carbon dioxide obtained in the "blank" run. Before burning another sample of iron, the sequence of preburning the boat, cover, and alundum, to obtain a small and uniform "blank," was repeated.

Sulfur in high-purity iron was determined by the evolution method. A 5-g sample was placed in a 500-ml Florence flask which had a ground-glass stopper with an inlet thistle tube and an outlet tube to the absorption vessel. The latter was a 25- by 200-mm test tube containing 50 ml of water and 20 ml of an ammonical solution of cadmium chloride.[2] 100 ml of diluted hydrochloric acid (1+1) was added to the sample in the Florence flask, and a slow stream of hydrogen was passed through the inlet tube and through the solution. The flask was heated gently until the sample dissolved, after which the solution was boiled for 3 to 4 minutes. The delivery tube was disconnected, and the ammoniacal cadmium chloride solution was filtered through a small, close-textured paper without

[2] Ammoniacal cadmium chloride: Dissolve 10 g in 400 ml of water and add 600 ml of ammonium hydroxide (sp gr 0.90).

washing. The paper was transferred to a beaker containing 150 ml of water, 2 to 3 ml of starch solution,[3] and 25 ml of diluted hydrochloric acid (1+1) were added, and the solution was titrated immediately, with 0.03 *N* iodate solution,[4] to a permanent blue color. The receiver (test tube) was washed with the titrated solution. If the color was bleached, it was restored by a further addition of iodate solution. The percentage of sulfur was calculated after deducting the volume of iodate solution used in a "blank" determination.

The phosphorus content of high-purity iron was determined in 3- to 4-g samples by the conventional alkali-molybdate method.

For the determination of copper, a 25-g sample was placed in an 800-ml beaker, 300 ml of diluted sulfuric acid (1+5) was added, and the mixture was heated gently until the action ceased. The solution was diluted to 500 to 600 ml with water, heated to boiling, and a stream of hydrogen sulfide was passed in for 1½ to 2 hours. After it stood for about 30 minutes, the solution was filtered through a close-textured paper, which was washed with diluted sulfuric acid (1+99) that had been saturated with hydrogen sulfide.

The residue and paper were transferred to a 25-ml tall-form porcelain crucible, ignited at a temperature below 550° C, and fused with 2 g of alkali pyrosulfate. The cooled fusion was dissolved in 15 ml of diluted sulfuric acid (1+2), and the solution was diluted with water to a volume of 70 to 75 ml.[5] 2 ml of nitric acid (sp gr 1.42) was added, and the copper was determined by electrolysis, with small (1 to 1.25 g) platinum electrodes made from 50 to 60 mesh gauze. Electrolysis, in a beaker covered with split watch glasses, was continued for 15 to 17 hours (overnight), with a current of about 0.1 ampere at 2 to 2.2 volts. When the deposition was completed and with current still flowing through the solution, the cathode was quickly removed and washed with a stream of water to remove electrolyte. The cathode was then dipped in alcohol, the excess alcohol was shaken off, and the cathode was dried for 1 minute at 100° C. After being cooled in a desiccator, it was weighed,[6] preferably on a microbalance.

The results of some of the electrolytic determinations of copper in high-purity irons were confirmed by colorimetric determinations[7] made on 30 to 50-g samples, using a solution of 0.1 g of copper per liter for the comparison. The electrolytic method was preferred, however, because of susceptibility of the colorimetric determination to interference by minute amounts of iron.

3. Determination of Oxygen, Nitrogen, and Hydrogen

By Vernon C. F. Holm

Oxygen, nitrogen, and hydrogen in samples of high-purity iron were determined by the vacuum-fusion method. The procedure was essentially as described by Vacher and Jordan,[8] although some modifications in the apparatus have been made. Mullite radiation screens have been replaced by slotted graphite screens, as described by Chipman and Fontana.[9] To facilitate removal of the gases from the furnace, the outlet connections have been increased in diameter and decreased in length, and a three-stage high-capacity diffusion pump has been installed. Determinations were made by observing the pressure in a closed system before and after absorption of one of the components of the gaseous mixture.

---

[3] Starch solution: Suspend 5 g of soluble starch in 25 ml of water, add to 500 ml of boiling water, cool, add a cool solution of 5 g of sodium hydroxide in 50 ml of water, then add 5 g of potassium iodide and mix thoroughly.

[4] Iodate solution: Dissolve 1.12 g of potassium iodate and 12 g of potassium iodide in 1,000 ml of water. Standardize by means of sodium oxalate through potassium permanganate and sodium thiosulphate. (See Lundell, Hoffman, and Bright, Chemical Analysis of Iron and Steel, John Wiley & Sons, Inc., New York, N. Y., p. 242, (1931)).

[5] If a small residue of siliceous material remained, the solution was filtered.

[6] Traces of silver, if present in the sample, will accompany the copper. Likewise, if molybdenum and tin are present, a small proportion of these elements may be deposited. None of these three elements was detected in the samples of high-purity iron.

[7] Lundell, Hoffman, and Bright, Chemical Analysis of Iron and Steel, John Wiley & Sons, Inc., New York, N. Y., p. 274 (1931).

[8] BS J. Research **7**, 375 (1931) RP346.

[9] Ind. Eng. Chem., Anal. Ed., **7**, 391 (1935).

Samples usually weighed about 12 g, although samples as small as 9 g and as large as 18 g were used. The samples were prepared for analysis by lightly grinding the entire surface, rinsing with ether, and drying in the air until the ether had evaporated. The samples were then placed in the sample holder and evacuation of the apparatus was begun. Redeterminations of the gas content of completely outgassed residues from previous vacuum-fusion determinations have shown that oxygen and nitrogen equivalent, respectively, to about 0.0009 and 0.0002 percent by weight, are present in a surface film on samples thus prepared for vacuum-fusion analyses. Consequently, these corrections for surface gases, in addition to the customary blank correction for the apparatus, were applied to determinations of the gas content of high-purity irons.

The determinations of oxygen and nitrogen in these samples are believed to be accurate to within ± 0.001 percent. The maximum amount of hydrogen determined in any of the samples of high-purity iron was 0.0002 percent.

WASHINGTON, March 28, 1939.

U. S. DEPARTMENT OF COMMERCE NATIONAL BUREAU OF STANDARDS

RESEARCH PAPER RP1227

Part of Journal of Research of the National Bureau of Standards, Volume 23, July 1939

IMPROVED INTERFEROMETRIC PROCEDURE WITH APPLICATION TO EXPANSION MEASUREMENTS

By James B. Saunders

ABSTRACT

The Fizeau interferometric method, as applied to thermal expansion measurements, has been studied in order to determine the source of some very serious errors and to find means of reducing such errors. Two types of errors were found to predominate. These may be termed (1) error caused by tilting of the spacers under mechanical forces, and (2) error caused by variations in air-film thickness at the contact points. Such errors often amount to 10 percent and may, under certain conditions, exceed in magnitude 50 percent of the value sought.

In this paper the two types of errors are considered in detail, and a modified procedure is given whereby the errors are reduced to a magnitude comparable to other unavoidable errors, such as those in reading the fringes and in determining the actual temperature of the specimens.

CONTENTS

	Page
I. Introduction	179
II. Indications of errors	180
III. Demonstration of tilting as a source of error	181
IV. Modified procedures	186
1. Correction of data	186
2. Elimination of tilting and surface-film effects	186
3. Weighting of spacer	187
V. Results showing the value of the weighted spacer procedure	188
VI. Necessary precautions	192

I. INTRODUCTION

A study of the variations in expansivity caused by differences in heat treatments or by minor differences in composition requires the measurement of small differences in the expansion of materials. Various differential methods are in use, but most of these require larger samples than are suitable for many types of investigations. When it is necessary to use very small samples, the Fizeau interferometric method [1] is the only one available. The accuracy usually claimed for results [2] obtained by this method is more than adequate; however, when the method is applied in the usual manner,[3] the required accuracy cannot always be assured. A modification of the Fizeau method used by Peters [4] would seem ideal, but it too has proved unsatisfactory for the purpose now in view.

When the interferometer is applied in the form mentioned above, a progressive change is usually observed in the width and orientation

[1] L. Fizeau. Ann. phys. **128,** 564 (1866).
[2] H. G. Dorsey, Phys. Rev. **25,** 88 (1907); H. M. Randall, Phys. Rev. **20,** 10 (1905); H. D. Ayers, Phys. Rev. **20,** 38 (1905); J. B. Austin, Physics **3,** 250 (1932).
[3] C. G. Peters and C. S. Cragoe, BS Sci. Pap. **16,** 449 (1920) S393.
[4] C. G. Peters, J. Wash. Acad. Sci. **9,** 281 (1919).

of the fringes. This change can only be caused by a tilting of one interferometer plate with respect to the other. Such a tilting normally occurs if three spacers of different thermal expansivities are used to separate the plates, but it also often occurs in the absence of differential expansions and indicates, therefore, the presence of spurious displacements.

The present study was undertaken in order to determine the source of these spurious displacements and also to find means of eliminating them. The causes of these displacements were found to be twofold: (1) Changes in surface-film thicknesses at the points of contact between the plates and spacers, and (2) tilting of the individual spacers when not rigidly attached to each other. In some cases the magnitude of the resulting errors was found to exceed 50 percent of the true value of the expansion; but it was also found that either they can be eliminated from the initial observations by certain precautions, or their magnitude can be determined for the purpose of applying corrections to the observations. By following either procedure, the precision claimed for the interferometric method of expansion measurements can be fully attained.

II. INDICATIONS OF ERRORS

Before it was realized that the errors could be effectively eliminated from results furnished by the interferometric method, it was always found necessary to take many sets of data on each sample in order to make sure that the results were fairly representative of the values sought. Although changes in the fringe pattern were quite obvious, it has not been generally realized, heretofore, that these erratic fringe shifts were indicative of spurious displacements which resulted in large errors in the observed data. In fact, errors of this type are prevalent in many of the published data where the interferometric method has been used.

In the course of a test, the number of fringes between 2 supporting spacers of the same material is frequently observed to change by as much as 10. In previous procedures this has been assumed to be unimportant. This change indicates, however, that for the temperature interval used, 1 spacer increases the separation of the interferometer plates by an amount equivalent to 10 fringes more than the increase caused by the other spacer. If the spacers expand equally, some spurious change must have taken place which produces a difference in plate separation equivalent to 10 fringes. Usually, on repeating the test without disturbing the specimens (spacers), this observed difference is closely duplicated. However, when the setup is removed from the furnace and reassembled, this apparent differential expansion of the spacers is usually appreciably different.

In many cases a fringe configuration that has been changing more or less slowly with the temperature will suddenly take on a new form which is usually more like the initial configuration. When this occurs, the shift of the fringes past any point represents a corresponding jump in the average separation of the interferometer plates. Other observers [4] have noted such changes, but apparently they have failed to realize the magnitude of the associated errors.

[4] See, for example, H. G. Dorsey, Phys. Rev. **25**, 88 (1907).

III. DEMONSTRATION OF TILTING AS A SOURCE OF ERROR

A warping of the spacers, caused possibly by their failure to slide on the lower plate, which usually expands differently, was first believed to be the cause of the errors mentioned above. The action of the fringes agrees very well with such an assumption. They change slowly in width and orientation as the spacers expand; then, as if some constraining force suddenly disappeared, they return approximately to their original configuration.

To test this possibility of warping, three specially shaped spacers were made from a specimen of optically homogeneous glass (dense barium crown, NBS melt 480; $n_D=1.6225$, $\nu=56.7$). The expansivity of each spacer was then determined separately (by a procedure described in section IV–3 of this paper) and the results showed the thermal expansions of the spacers to be equal within the required limits of accuracy. Each of these spacers (fig. 1, *A*) was made from two parts (fig. 1, *B*) by cementing the base of a small conical part on top of a relatively broad, low, stool-like tripod part. The three feet of each tripod were equally spaced, the top was polished flat, and the legs were made almost equal in length so that when the tripod was standing on the flat surface of an interferometer plate the top was almost parallel to it. The height of each spacer was then adjusted almost to equality with that of the others by grinding off the conical tips. The tip of each spacer was vertically above the center (median point) of the equilateral triangle formed by the three feet of the tripod. The four supporting areas (three feet and conical tip) of each spacer were made small by pointing.

On mounting the three spacers between two fused-quartz interferometer plates, easily readable fringes were obtained between the quartz plates and also between the top of each stool and the upper quartz plate. The primary fringe system is represented as set *D* in figure 2, and the three secondary sets, formed by the stool tops and the upper plate, by *A*, *B*, and *C*. On heating this assembly from 25° to 250° C, the fringes changed gradually from the numbered configuration represented by figure 2 (*A*) to that by 2 (*B*), and all fringes remained straight regardless of changes in width and orientation. If the changes in the fringe system had been caused by a warping of the tripod part of any spacer, the fringes over this spacer would have become curved. Consequently, it is concluded that no warping occurred.

Since the construction of these particular spacers is such that the air-film errors cannot be large, the only other cause to which one can attribute the gross errors under discussion is a tilting of one or more of the spacers, where the tilting is the result of one or two feet of a spacer being lifted from the base plate. As will be seen, this action was definitely established as causing most of the errors.

When viewing an interferometer fringe system with collimated light, the number of fringes between any two points is a direct indication of the difference in the distance between the interferometer plates at those points. If the separation is known at one point, it may easily be determined at any other by adding or subtracting the difference in separation of the plates at the two points. The magnitude of this difference is known from the number of fringes observed between

the points, and its sign is determined by noting the direction of fringe motion when the plate separation is increased or decreased.

Since it has now been shown that the spacers do not warp or expand differentially, any relative rotation of the interferometer plates must result from a changed separation between the spacers and plates at some of their contact points. Such changes in the separation between the spacers and the top plate will always be comparatively small, since there is only one contact point for each of the three spacers; nevertheless, this change at any spacer will produce an equal change in the separation of the plates at that point. Since there are three contacts between a spacer and the lower plate, any change in separation at one of these contact points produces (for the type of separators used) only one-third as much change in the total separation of the interferometer plates at the fiducial point over the center of the spacer. The changes at some of the lower points are, however, much larger than at the upper points. This is because the spacer can tilt up on one or two of its feet, causing at least one foot to leave the base plate entirely. The cause of this tilting is assumed to be as follows: In general, one spacer is more stable than either of the others, due to either a greater load, a greater spread of its feet, or both. Also, one foot of the most stable spacer will usually bear a greater load than either of its other two feet. However, a differential expansion between this spacer and the lower plate will force two of its feet to slip. This results in a sidewise motion of the spacer which, in turn, causes a horizontal motion of the top plate. This action on the top plate generally causes the other two spacers to tilt and the motion is usually in such a direction as to force two feet of each of these spacers to be lifted from the base plate. As soon as this condition develops, the top plate usually begins to rotate horizontally about the contact point with the stable spacer, while the unstable spacers rotate similarly about their own contacts with the base plate. This combination of motions continues until a third foot of the unstable spacers comes into contact with the base plate. The motions are now arrested until differential expansion causes further tilting.

To study the action and magnitude of the tilting, reference marks (fig. 2) were placed on the top surface of each stool vertically above the contacts of its three feet with the lower plate. These marks, which correspond to the points of contact between spacers and lower plate, are designated by the trios: 11, 12, and 13 for spacer *A;* 21, 22, and 23 for spacer *B;* and 31, 32, and 33 for spacer *C.* The three supporting points of the top plate, indicated by 10, 20, and 30 for spacers *A*, *B*, and *C*, respectively, were marked on the upper surface of the top interferometer plate and are at the median points of the triangles formed by the above three sets of points. Thus, there are 4 reference points in each of the fields *A*, *B*, and *C;* and all 12 points may be considered as being within field *D*. The *D*-fringes are obscured at the reference marks by the spacers, as are also the *A*, *B*, and *C*-fringes at the points 10, 20, and 30, respectively. The fringe positions with respect to these points, however, can be read very accurately with the aid of a straight filament which lies in the focal plane of the observing instrument and is rotatable about the optic axis. The instrument employed could be moved horizontally as a whole so as to bring such a filament over the image of any point in the field of view.

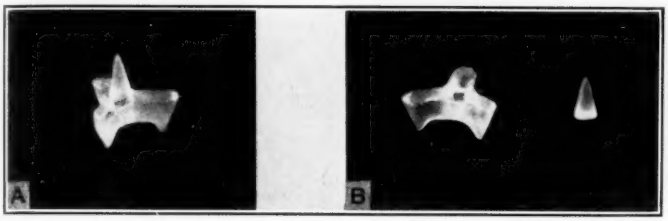

FIGURE 1.—*A form of specimen used for the demonstration of tilting.*

A, complete specimen after assembly, and *B*, tripod (or stool) with flat and polished top, and cone-shaped piece, the base of which was sealed to top of tripod.

UNIV. OF MICH.

The interferometer system shown in figure 2 was properly adjusted in an electric furnace,[6] and data were taken at the points 10, 20, and 30 as the furnace was heated from room temperature (25° C) to about 250° C. These data were used to compute the apparent expansion of the three spacers for this interval, and the results shown in table 1, column 2, indicate that the three spacers have different apparent expansivities. The test was repeated a second, third, and fourth time without disturbing the interferometer, and columns 3, 4, and 5 of table 1 show that the results obtained by these three tests for the expansion of spacer *A* were practically identical. However, the results for the same spacer on the first or preliminary test (column 2) differ somewhat from them.

TABLE 1.—*Expansivity of a glass at 100° C*[1]

Spacer	Observed expansivity $\times 10^6$ (at 100° C)			
	1st run	2d run	3d run	4th run
A	7.37	7.34	7.34	7.33
B	7.87	8.00	7.97	7.97
C	7.50	7.68	7.72	7.70

[1] This table illustrates the necessity of making a preliminary run (1st run, column 2) before consistent data can be obtained. The results for *B* and *C* after the first run are fairly consistent but not so consistent or accurate as those of *A*, for reasons described later.

While the results for spacers *B* and *C* are fairly consistent for the four runs, yet they are much less so than for spacer *A*. Furthermore, the results for the three spacers differ greatly among themselves. These data indicate that spacer *A* was the most stable and that its greater stability caused it to remain fixed in position, whereas the others were forced to tilt by differential expansion. Any tilt of the spacers will necessarily cause their apparent expansivities to be too great. Since the tilt would, in general, be different for different spacers, the computed expansions could not be expected to agree. The slight difference between the results of the first test and those of the later tests suggests also that there was an initial surface film trapped between the contact points, and that this film disappeared during the first heating, or at least was reduced to a minimum and remained constant throughout the remaining tests.[7] The differences between the second, third, and fourth runs then appear to be caused almost entirely by tilting.

After the tests described above, a fifth heating was given the furnace. The initial fringe configuration (at room temperature) was observed to be that shown in figure 2 (*A*). After completing the observations at room temperature, the interferometer assembly was heated and the changing order of the fringes at each of the spacers was recorded at frequent intervals. When the temperature reached 250° C, another set of readings was taken, and the observed fringe configuration is indicated in figure 2 (*B*). The temperature was held constant while the data (table 2) for each of these two drawings were taken. The differences in the various fringe systems allow a computation of the change in separation of the interferometer surfaces at each of the several reference points.

[6] Similar to that used by G. E. Merritt, BS J. Research **10**, 59 (1933) RP515.
[7] This film may be absorbed air, moisture, or some other contamination on the surfaces.

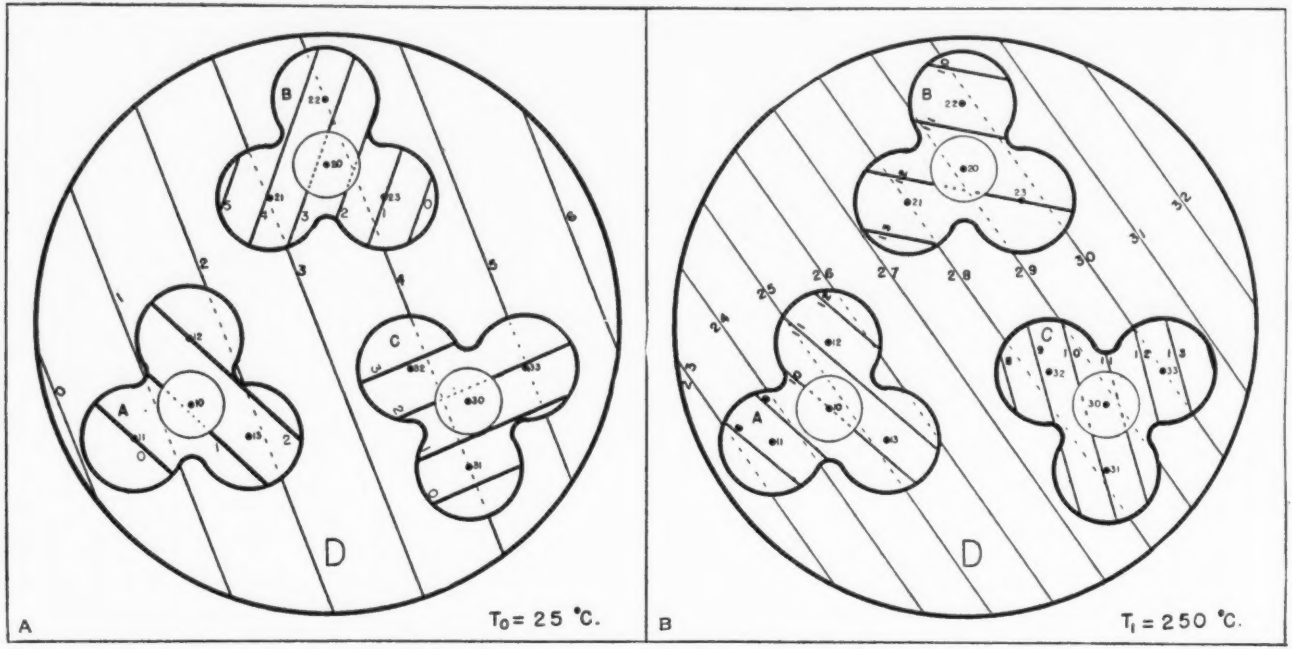

FIGURE 2.—*Diagrammatic representation of the fringes observed in the multiple interferometer field before and after a change in temperature.*

The straight lines represent the observed fringes and are identified by the associated numbers. These numbers indicate the fringe count in relation to the fringes, which were designated by 0, because they were found to have the lowest order appearing in their respective fields previous to heating.
The small dots represent the reference points over the various contact points. These points are designated by the associated numbers. The curved lines represent the outlines of the various fields.

TABLE 2.—*Fringe readings*

[Data taken from figure 2]

Temperature		25° C		250° C	
Spacer	Reference point	Primary field	Secondary field	Primary field	Secondary field
A	10	1.35	1.10	24.70	10.00
	11	0.65	0.	23.50	8.40
	12	1.65	2.00	25.35	11.25
	13	1.80	1.40	25.20	10.35
B	20	3.75	2.75	29.15	11.65
	21	3.05	3.90	28.00	12.40
	22	4.00	3.35	29.80	10.55
	23	4.20	1.00	29.65	12.00
C	30	4.25	1.75	28.80	10.65
	31	4.00	0.45	28.15	10.15
	32	3.80	2.85	28.25	9.25
	33	4.95	1.90	30.00	12.50

If it is assumed that all spacers expand equally, that all feet contact the base plate at the initial reading, and that each spacer contacts each plate at one or more points at all times during a test, the magnitude of all tilts may be computed from the data of table 2. The change in the number of fringes between any two points in a secondary fringe field over any stool gives the rotation of the top plate with respect to that stool top about a horizontal axis perpendicular to a line joining the two points; similarly, the corresponding change in field D, between the same two points, gives the rotation of the top plate with respect to the lower interferometer plate. The difference between these two rotations is the rotation of the stool with respect to the bottom plate; and this rotation is, in turn, proportional to the difference in the separation between the feet of the spacer (stool) and the lower plate at these points. If we consider the set of fringes marked A in figure 2, and let T_{11}, T_{12}, and T_{13} represent the changes in separation between this spacer and the lower plate at the points 11, 12, and 13, respectively, we have the following relationships:

$$\left.\begin{aligned} T_{12}-T_{11}&=\Delta_{12,\,11},\\ T_{13}-T_{11}&=\Delta_{13,\,11},\end{aligned}\right\} \tag{1}$$

where the Δ's represent the difference between the change in number of fringes between the points, indicated by the subscripts, in field A and the corresponding fringe change in field D. Since one of the T's in eq 1 must be zero, according to the above assumptions, these equations are easily solved by placing the smallest T equal to zero. The magnitude of the two Δ's gives the order in magnitude of tilts T_{12} and T_{13}, and the magnitude of either Δ gives the order in magnitude of the two T's appearing in the same equation as the Δ considered.

In this manner all tilts were determined (see table 3), and the results of several such sets of data indicated that at least one spacer does not tilt and that the others usually do. All results agreed perfectly with the assumption as to the nature of the tilting.

TABLE 3.—*Computed tilts (in fringe equivalents)*

	Spacer		
	A	*B*	*C*
The three feet	$T_{11}=0.00$ $T_{12}=.00$ $T_{13}=.00$	$T_{21}=2.00$ $T_{22}=4.15$ $T_{23}=.00$	$T_{31}=0.00$ $T_{32}=3.75$ $T_{33}=.00$
Median point	$T_{10}=0.00$	$T_{20}=2.05$	$T_{30}=1.25$

IV. MODIFIED PROCEDURES

1. CORRECTION OF DATA

It has been found that when an interferometer (of the type mentioned above) is heated, at least one of the three spacers does not tilt, and that a preliminary heating practically frees this spacer from the effects of surface film changes. Under these conditions the error caused by tilting and by changing surface films at the contacts of the other spacers may be evaluated and used as a correction to data taken at any chosen reference point.

In presenting this method of corrections, which has been used successfully, it will be assumed that the observations requiring the corrections are taken at the median point of an equilateral triangle formed by the contact points on which the top interferometer plate rests. The method is not restricted to cases meeting this condition. It has been introduced merely to simplify the discussion and to facilitate the computations of the corrections. If all spacers properly contact the interferometer plates in the beginning, and if at least one spacer does so at each later observation, the corrections for the observations at the median point may be obtained from the change in the number of fringes between the contact point of the most stable spacer with the top plate and the corresponding points of the other two spacers. If we represent these points by 10, 20, and 30 (see fig. 2) and assume point 10 to be over the most stable spacer, then the correction to be supplied is $1/3\ (\delta_{10,20}+\delta_{10,30})$ where $(\delta_{10,20})$ represents the change in the number of D-fringes between points 10 and 20, and where $(\delta_{10,30})$ represents the corresponding change between points 10 and 30. This correction is to be subtracted from the observed order of the fringes read at the median reference point, and the result is what would have been observed at this point had there been no tilting or changes in the films between the spacers and the plates. The most stable spacer is easily identified as the one giving the least apparent expansion. If there are two such spacers, either one may be chosen with no difference in the results.

2. ELIMINATION OF TILTING AND SURFACE-FILM EFFECTS

In order to eliminate tilting, the spacers supporting the top plate must be bound together in one rigid unit. To produce this type of support, a spacer was made in the form of a ring,[8] which was so cut that it rested with three feet on the lower plate and supported the top plate at three points, one over each of the feet. The use of this

[8] BS J. Research **11**, 799 (1933) RP626.

type of specimen greatly reduces the change in fringe configuration during a test, although small but troublesome changes still remained.

In adjusting these rings so that readable fringes were produced, the ring was finished on a flat stone, increased pressure being applied to the points where the height was too great. This treatment gave the spacers appreciable supporting areas which were relatively flat. To check the supposition that the small troublesome changes in fringe configuration were caused by variations in the thickness of the surface films in these areas between the spacers and plates, the three surfaces supporting the top plate (each having an area of approximately 1 mm^2) were polished sufficiently flat to produce distinguishable fringes between them and the top plate. This added three small but sharp sets of fringes to the primary field between the plates, which could be easily observed although they were usually very far from being straight and uniform in width. On heating this interferometer system to 220° C, the thickness of the films in the contact areas was observed to decrease by as much as 16 fringes (8 wave lengths of yellow helium light). Heating to higher temperatures, followed by cooling to room temperatures, always failed to produce further appreciable changes at one of the contact points. Even repeated heatings and coolings failed to produce further changes. At the other two points, however, fluctuations in the film thickness were always present after the first heating to 220° C. The use of plates having the same expansivity as the specimens themselves greatly reduces this fluctuation but does not eliminate it. A further reduction is obtained by decreasing the temperature gradients between the plates and specimens and also by pointing the supports. This suggests that slippage at the contact points causes much of the change in surface film thickness after the first heating.

In accounting for these differences in stability, it was assumed that the first heating developed a condition in which the friction at one of the points was sufficient to force all of the slippage to take place at the other two points. No doubt similar variations occur in the film thicknesses at some of the contacts between the ring and the lower plate.

With the unit type of specimen (all three supporters of the top plate, bound rigidly together) none of the tilting mentioned in section III is observed, but the surface film effects are greater if the supporting areas of this spacer are relatively large. The correction method of the previous section is still applicable and in general the correction is smaller for this type of specimen.

If the reference point can be chosen over the contact point which is free from both tilting and surface film effects, then there is no such correction to be applied, and the resultant data are practically free from these errors.

3. WEIGHTING OF SPACER

Even though the errors mentioned above can be determined with fair accuracy, their direct elimination is always desirable. This elimination is accomplished by choosing the reference point at the proper place, which is easily located during the test as shown in the previous section. For practical application it becomes necessary to predetermine this point. This is done by increasing the stability of one spacer or support, in the case of a unit-type spacer. This favoring is accom-

plished by shifting the center of the top interferometer plate towards the chosen spacer until it bears most of the weight of the top plate, or an auxiliary weight may be placed on the top plate near this spacer. A U-shaped weight is convenient since it may be so placed as to add load to the chosen spacer only, without obscuring the fringes there.

In using this procedure, it was found that the chosen spacer should carry several times the load of either of the other two, and that under this condition the data obtained at an observation point over the weighted spacer appeared to be practically free from errors caused by tilting and by changing surface films. That is, after the preliminary heating of the specimens, the data seemed to be as reliable as an interferometric method is capable of yielding.

Obviously, the instability of the other spacers still produces changes in the fringe configuration, but as long as the fringes are broad enough for observation such changes do not affect the data obtained at the weighted spacer. To aid in maintaining the required fringe breadth, it is found advisable to weight the tallest spacer, since in that case any tilt usually leaves the fringes broader than they would have been with the same tilt if one of the shorter spacers had been weighted. Even then the fringes often get too narrow and the observer will have to rap gently on the furnace (a procedure which usually restores the fringes to their original width without introducing error in the data) in order to proceed with the observations. As stated before, the use of interferometer plates that have nearly the same expansion as that of the specimens greatly reduces such changes in the width of the fringes.

If, when three individual spacers are used, the triangular base of the weighted spacer is small compared to those of the other two, or if the contact point of this spacer with the top plate is not sufficiently near the center of the base triangle, the stability of the spacer is then relatively low, and the pull of the other two spacers may ultimately overcome it. To insure stability of the weighted spacer, its base should be at least as large as that of either of the other two. It should, however, not be too large, since increasing its size also increases the slippage of its feet produced by differential expansion and the tilt imposed on the other spacers.

V. RESULTS SHOWING THE VALUE OF THE WEIGHTED SPACER PROCEDURE

To illustrate the improvements obtained by using the weighted spacer procedure instead of the customary one, 12 samples were taken from a piece of optically homogeneous glass (medium flint, NBS melt 457; $n_D=1.6264$; $\nu=36.7$) and tested as follows: From this set of samples three were selected as spacers and shaped so as to give good broad fringes when placed between two interferometer plates. Of these spacers the one designated by n_1 bore approximately three-fourths of the total weight of the top plate. This interferometer assembly was placed in the furnace and expansion data were taken on three successive runs from room temperature to 250° C. The three contact points of the spacers with the top plate were selected as reference points, at each of which expansion data were taken as described by Peters.[9]

[9] J. Wash. Acad. Sci. 9 [10], 281 (1919).

The interferometer was then removed from the furnace, and the load of the top plate shifted to another spacer, designated by n_2. Data for three runs were again taken at the three reference points. For a third set of similar data, spacer n_3 bore most of the weight of the top plate. From the data of these tests the expansivity at 100° C was computed for each run and for each spacer, as shown in table 4. In computing the accepted expansion, only the results obtained at a weighted reference point and after a preliminary heating were found to meet the desired precision. The accepted values are italicized and are averaged in the bottom row. The results show the expansion of each spacer to be very near 8.28×10^{-6}, and that the expansions of the three spacers differ very little, if any, from each other. The various values obtained by the different tests on the unweighted specimens are seen to differ broadly among themselves, and the same is also true for the results obtained by the first or preliminary tests on all specimens.

TABLE 4.—*Expansivity of a glass (medium flint) at 100° C* [1]

Spacer weighted	Runs for each arrangement of spacers	Expansivity×10⁶ of spacers (n_1, n_2, and n_3) as determined from observations taken directly over each of them			
		n_1	n_2	n_3	Average
n_1	1st	8.26	8.44	8.25	8.32
	2d	*8.29*	8.54	8.42	8.42
	3d	*8.27*	8.45	8.46	8.39
n_2	1st	8.31	8.29	8.26	8.29
	2d	8.25	*8.28*	8.66	8.40
	3d	8.26	*8.27*	8.72	8.42
n_3	1st	7.95	8.22	8.30	8.16
	2d	8.22	8.26	*8.27*	8.25
	3d	8.26	8.25	*8.29*	8.27
Average of values in italic		8.280	8.275	8.280	8.278

[1] The figures in italic are those procured on weighted spacers after the preliminary (1st) runs.

After finding that the expansivities of the three spacers were so nearly identical that the changing fringe configurations, together with the resultant erratic apparent expansions of the unweighted spacers, could not be the result of actual differences in expansion, similar tests were then extended at the usual heating rate to the range of rapid expansion. However, instead of reading at three points, as above, the top point of the weighted spacer and the median point of the triangle formed by the three spacers were chosen as reference points. These points were selected for the purpose of comparing the results obtained by the weighted spacer procedure with those by the usual method, where the reference point is generally chosen near the center of the triangle formed by the three supports of the top plate. The results are represented in figure 3 by solid dots. Curve A was computed from data taken at the point over the weighted spacer. The other dotted curves (A', A'', and A''') represent the data taken at the median point and show the effects of three possible interpretations of a sudden jump observed in the fringe configuration.

During this heating to the rapid expansion range, there were, at the beginning, 2.9 fringes crossing the triangle formed by the three spacers and 1.6 fringes between the two reference points. As the heating progressed, the fringes broadened until at 91° C there was only 0.2

fringe between the reference points. Just before reaching this temperature, the fringes began to vibrate and change width as they rotated back and forth about the point where the top plate was supported by the weighted spacer. This signified that the rising of the top plate at this point was caused only by the uniform expansion of the weighted spacer, whereas it was bobbing erratically at other points. After a few moments the vibration stopped, leaving the fringe configuration as it was at the beginning of the heating; that is, with 2.9 fringes crossing the triangle and 1.6 fringes between the two reference points. Obviously, there had been an abrupt shift of 1.4 fringes at the median reference point as the result of one or both unweighted spacers having changed from a tilted to a relatively stable position.

The fringe reading at the median point was 9.3 just before the vibration started and $n+0.9$ (n being some integer) immediately after it stopped. If observations had been made only at the median point, the value for n would not have been known, and the observer would probably have chosen either 8 or 9 as its value. If $n=9$, then the plate jumped up 0.3 of a wave length (0.6 fringe), and A''' is the proper course of the curve. If $n=8$, the plate fell 0.2 of a wave length (0.4 fringe) and the proper curve follows A''. The slope of the curve before, and the position of the next point after the jump, would seem to favor curve A''' as being the proper one to choose. On the other hand, the value $n=8$, and consequently curve A'', might seem the more probable because of a belief that such jumps are almost invariably caused by a sudden sinking of the top plate. By having taken observations simultaneously at a point where the fringes did not jump, in addition to the readings at the median point, one can be certain of the corrections for the readings taken at the median point both before and after such a jump. These corrections are obtained from a consideration of the change in the number of fringes between the two reference points. Thus the correct value to be assigned to n was found to be neither 9 nor 8, but 7, giving curve A' as the real curve for the change in distance between the interferometer plates at the median reference point. That is, the jump at this point was from 9.3 down to 7.9, a jump of 1.4 fringes, which was the sudden change observed in the number of fringes between the two reference points.

After these tests the remaining nine samples were similarly tested, three at a time, to the rapid expansion range of this glass. In each case the samples were given a preheating to 250° C and allowed to cool back to room temperature. The furnace was then given a slight shock to rectify any remaining tilt that might have developed during the preliminary treatment. As before, two curves were obtained from each test, one giving the real expansion of the weighted spacer, and the other giving the average apparent expansion of all three spacers. The real expansion values [10] for these three sets of spacers are plotted in figure 3 as curves B, C, and D. Obviously, these curves practically coincide with curve A.

The curves for the apparent expansions, as obtained from the data taken at the median points, showed certain peculiarities which are similar to those often appearing in curves procured by other investigators [11] who have used the median point between three individual

[10] Because of crowding, only every fourth point is plotted in curves A, B, C, and D of figure 3; all points are, however, indicated in figure 4.

[11] This knowledge was gained through private communications.

spacers in procuring expansion data. That is, one or more rather definite changes in slope [12] have often appeared at certain points in the range between 100° and 400° C, and abrupt irregularities or slight jumps in the trend of the observations have also been noted occasionally. These changes in slope probably develop from a progressive tilting of one or two of the spacers followed by a slow readjustment. The readjustment may be caused either by a gradual slippage at one or more of the contact points or by a slow rotation of the tilted spacers

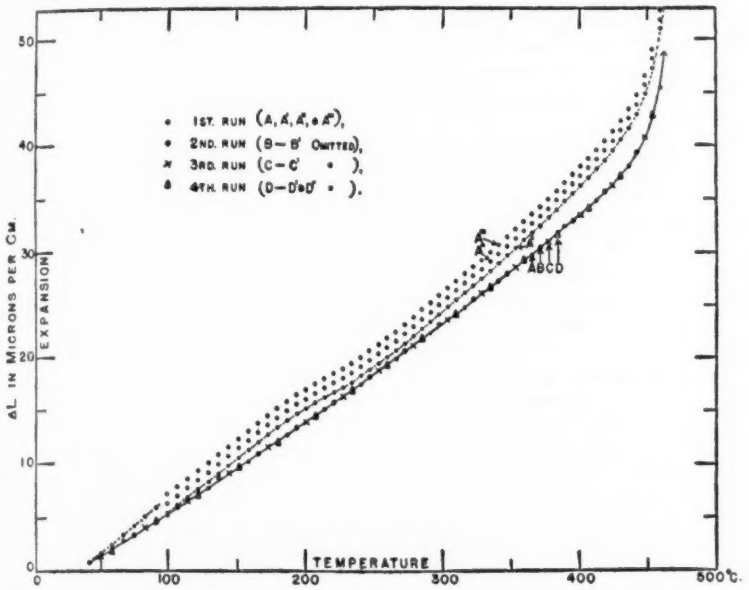

FIGURE 3.—*Expansion curves, showing uncertainty in data taken at median reference point.*

The curves A'' and A''', represented throughout by solid dots, indicate the different results obtained by a failure to apply proper corrections for tilting. The curve represented by solid dots and dashes indicates the result of applying the proper correction at one temperature (near 90° C) and not elsewhere. The composite curve is based on every fourth observation of four tests, each on different sets (*A*, *B*, *C*, and *D*) of separators. These observations were all so obtained that corrections for tilting were unnecessary, as shown in the text.

about these points. Such changes in slope are particularly evident in curve A', figure 3, between 200° and 300° C. The more abrupt irregularities noted (indicated by discontinuities at vertical arrows in the curves of fig. 4) are caused by sudden readjustments after a progressive tilting.

In figure 4 the residuals are plotted for all curves obtained from the four sets of spacers. In obtaining these residuals, the proper ordinate of the best curve obtainable for fitting the preferred data (that taken at the points over the weighted spacers) was subtracted from the data observed at all reference points and the difference plotted on an enlarged scale. In this plot the ordinates of the various curves correspond very closely to the errors in the data. Curves *A*, *B*, *C*,

[12] The same type of discontinuities were also obtained by Klemm and Berger, Glastech. Ber. 5, 405 (927), and by Turner and Winks, J. Soc. Glass Tech. 14, 84 (1930), using entirely different methods of measurements.

and D are the residuals for the data taken at the reference point over the weighted spacers. As seen, the deviations in these curves are small compared to those in A', B', C', and D', which are the residual curves for the data taken at the median points. There are no sudden breaks in curves B' and C' such as that in A' at 91° C. These curves were smooth and the data appeared good, but when compared to the companion curves B and C, they are obviously quite erroneous. Curve D' has an abrupt break at or near 360° C and another at 440° C. At these points the fringes had grown so narrow that reading was difficult at both reference points. To improve this condition, the furnace was given a slight rap which in both cases caused the fringes to broaden out to their original width and orientation. This means that the proper curve returns (within the error of reading) to the base line.

Just before causing the first jump in D', the fringe count at the median reference point was 46.5, and just afterwards, 40.6. The amount of this jump was determined as in the case of curve A'. Had the readings been taken at the median reference point only, the amount of the jumps could not have been determined, and an observer would probably have chosen 46.6 instead of 40.6 as the reading. This would have given uniform data, and the resultant curve would have been D'' from 360° C upward. After each of these jumps the fringes grew narrow very rapidly. This indicated a rapid deviation of the data taken at the median reference point from the true expansion, which is represented by the data taken at the reference point over the weighted spacer.

It is seen that the largest ordinates (residuals) in curve D fall at temperatures where there are jumps in the corresponding primed curve. At these points the fringes were narrow and difficult to read, and relatively large deviations are therefore to be expected. If the fringes remain fairly broad and the reference point is properly situated over the weighted spacer, this deviation will always be small in spite of jumps and rotations.

VI. NECESSARY PRECAUTIONS

In taking precise expansion data, temperature gradients play a large role in the reproducibility of the results. With the interferometer method the specimens can be made small and this greatly reduces gradients. Even so, the temperature indicator and specimens must be in different places and are usually so different in shape, conductivity, and heat capacity that the temperature of the specimens can be appreciably different from that of the indicator. During a uniform heating at only moderate rates, the difference may be unexpectedly large and change considerably with increasing temperature. Holding the furnace for some time at a constant temperature before each reading lowers these differences, but in actual operation does not wholly eliminate them.

For making tests to determine the amount of these gradients, an aluminum cup 5 cm in height, 4½ cm in diameter, 6 mm in wall thickness, and with a 2-cm opening in the top, was used. The opening in the top was closed with a fused-quartz window. Within the cup, a porcelain plate 3 mm in thickness covered the bottom. A fused-

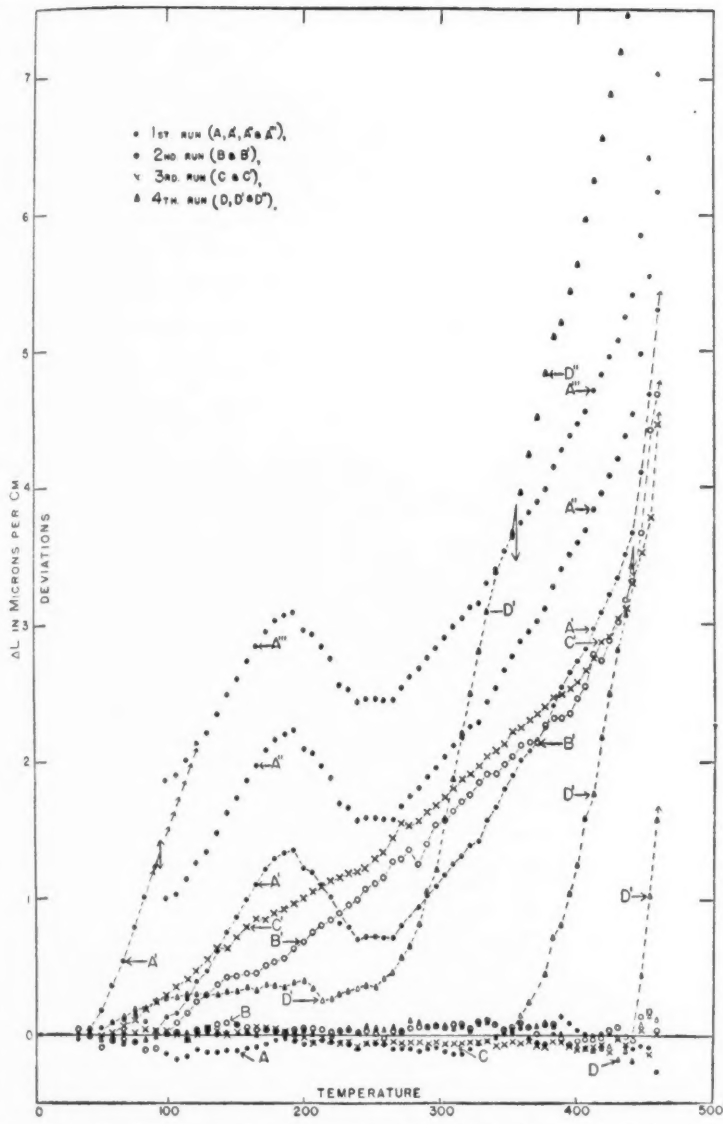

FIGURE 4.—*Residual curves for expansion data obtained on four different sets of separators from the same glass.*

These residuals are the differences between observed results and the probable values for the expansion as determined from the average or preferred data (continuous curve in fig. 3).

Curves *A*, *B*, *C*, and *D* are the residuals in the preferred data obtained at reference points over weighted spacers. Curves designated by primed symbols represent deviations of results obtained at median reference points.

quartz "refraction thermometer" [13] (3 mm thick) was placed on the center of this plate. A similar thermometer resting on the first was shifted to one side just enough to allow the fringes of the bottom thermometer to be read. The reference points of the two thermometers were placed close together and near the edges of the plates. The cup with the two thermometers was placed in the center of an electric furnace and heated at a rate of 3 degrees per minute to 400° C. After they were cooled back to room temperature, the relative positions of the two thermometers were reversed and the heating was repeated. The two runs were made for the purpose of eliminating, as far as possible, errors that might arise from differences in the calibrations of the thermometers. The average difference between the readings on the two plates, at any temperature, for two such runs gives a good indication of the temperature difference which may be introduced by changes in the position of a specimen and in the manner of its mounting. Assuming that each thermometer indicated approximately the average temperature between its faces at the reference point, the difference in temperature for a vertical distance of 3 mm was found to vary from approximately 10° at 100° C to about 4° at 400° C. A change in the rate of heating gives a corresponding change in this difference.

When, as was the usual practice in this work, the bottom thermometer plate is separated from the porcelain plate by a thin-walled fused-quartz ring 8 mm in diameter and 3 mm high, the observed differences between the indicated temperatures of the two thermometers were all less than 1 degree. By this method of mounting, the thermometers were practically suspended in the middle of the cup and received most of their heat from the air and by radiation. Consequently, each plate receive heat at about the same rate.

Since it is impossible to eliminate temperature gradients, even when only moderate rates of heating and cooling are used, it becomes necessary (especially when comparative tests of considerable accuracy are required) to duplicate as nearly as possible the following factors: The rates of heating and cooling; the height and mass of the specimens (or at least those of the weighted spacer); the size, shape, and material of the cup and of the interferometer and thermometer plates; the position of these plates with respect to the cup walls and specimens; and finally, the position of the cup in the furnace. Moreover, the top plate should not be too heavy, and a large part of its weight should be borne by the weighted spacer so as to insure no sliding on this spacer. The reference point should be directly over the top contact point of the weighted spacer, if the pin-type is used, and also over the lower contact point in the case of the ring or unit-type spacer.

Several types of spacers used in this laboratory are illustrated in figure 5. There are two views of each: *A* and *B*, the pyramidal or pin types; *C* and *D*, the ring type mentioned in a previous paper,[14] and the Y- and T-types, represented by *E* and *F*, respectively. The T- and Y-types are recommended for ease in making observations. They are easily constructed and mounted and also are free from tilting. When used between plates having the proper expansivity, these types are also free from surface-film effects after a preheating to 250° C.

[13] Sci. Pap. BS **19**, 357 (1924) S485.
[14] BS J Research **11** 799 (1933) RP626.

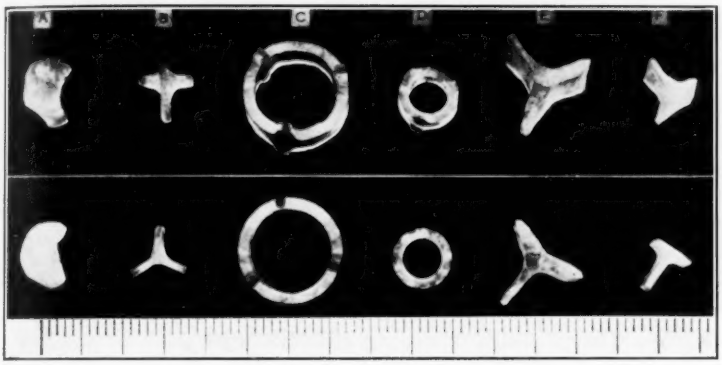

FIGURE 5.—*Several forms of specimens.*

For the types *A* and *B* three such tripods are required to support the top interferometer plate, whereas one of the other types is sufficient. The scale is in millimeters.

By taking all of the precautions mentioned, results on the expansivity of glass can be duplicated by using the interferometer method and any of the above types of spacers to within ⅓ percent, if the expansions exceed 10 fringes and the temperature range of the test is of the order of 100° C or more. Of these precautions, properly weighting one spacer and choosing the position of the fiducial point have proved to be most important and have permitted the precision, and also the accuracy, to be increased at least tenfold over that obtainable by most of the previous interferometric procedures. This has been accomplished by the almost complete elimination of the effects caused by the lateral expansions of spacers and plates and by changes in air films. Some of the residual uncertainty is the result of temperature gradients and errors in the temperature determinations. If these sources of error which are also present in all similar procedures, could be eliminated, the precision would be sensibly increased, and the accuracy of the results for the expansivity should closely approach that indicated by the precision.

With all the precautions taken, it is considered possible that the determinations of the temperature range may be in error by as much as 1 degree, even for slow rates of heating. Where rates of 3 or 5 degrees per minute are used, the errors may approach 2 or 3 degrees for a range of 200° C. In measuring differences between the expansitivity of two or more materials, these errors are to a great extent eliminated, especially if the same apparatus and test conditions are used. Also, they tend to be eliminated in the expansivity results if the thermometer plate is calibrated in the same apparatus and under the same conditions used in the expansion measurements.

WASHINGTON, April 29, 1939.

○